MOLECULAR STUDIES OF GRIF-1 AND GRIF-1 INTERACTING PROTEINS

By

Karine Pozo

A Thesis Submitted for the Degree of Doctor of Philosophy of the University of London

School of Pharmacy, University of London
29/39 Brunswick Square
London WC1N 1AX

This thesis describes research conducted in the School of Pharmacy, University of London between February 2003 and January 2006 under the supervision of Professor F. Anne Stephenson. I certify that the research described is original and that any parts of the work that have been conducted by collaboration are clearly indicated. I also certify that I have written all the text herein and have clearly indicated by a suitable citation any part of this dissertation that has already appeared in publication.

Signature Date

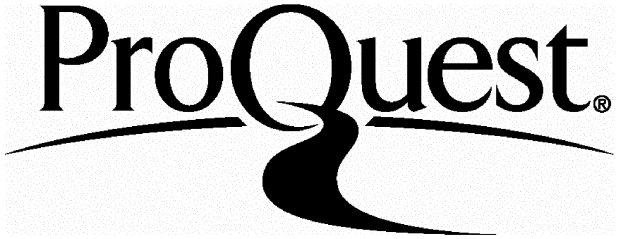

ABSTRACT

Communication between neurones in brain occurs at specialised zones, the synapses. The transport of proteins and organelles to these active regions relies on motor proteins. Motors associate with their cargoes either directly or via adaptor proteins. $GABA_A$ receptor interacting factor-1, GRIF-1, is thought to function as a scaffold linking kinesin-1 to mitochondria and/or vesicle-enclosed $GABA_A$ receptors for transportation to synapses.

A confocal microscopy approach was used to investigate the association between GRIF-1 and the prototypic kinesin-1, KIF5C, GRIF-1 and the $GABA_A$ receptor and GRIF-1 and the enzyme, β-*O*-linked *N*-acetylglucosamine transferase (OGT). Enhanced yellow or cyan fluorescent (EYFP, ECFP respectively) fusion proteins of GRIF-1, KIF5C, the motor domain of KIF5C, the non-motor domain of KIF5C, the $GABA_A$ receptor β2 subunit and OGT were generated. The fusion proteins were characterised and their distribution in mammalian cell lines was examined. To characterise further GRIF-1/KIF5C interactions, fluorescence resonance energy transfer analyses were carried out. These studies showed that ECFP-GRIF-1 was associated directly with the carboxyl-terminal, non-motor domain of EYFP-KIF5C. Cellular organelles in cells overexpressing ECFP-GRIF-1 and EYFP-KIF5C were fluorescently labelled. In these cells, mitochondria were found re-distributed to GRIF-1 enriched regions.

Searching for novel GRIF-1 associated proteins, a yeast two-hybrid cDNA library screen using the bait, GRIF-1 (545-913), was carried out and a partial cDNA encoding an interactor was isolated. Characterisation of this cDNA revealed that it encoded a mitochondrial isoform of OGT.

The potential use of the CytoTrap® yeast two-hybrid system to identify new GRIF-1 interactors was investigated. A full length GRIF-1 bait fusion protein was generated, characterised and the CytoTrap® yeast two-hybrid system evaluated.

To conclude, the analysis of GRIF-1 and its associated proteins indicates a role for GRIF-1 as an adaptor linking kinesin-1 to its cargoes, i.e. mitochondria and vesicle-enclosed $GABA_A$ receptors. This association may be regulated by the enzyme OGT.

TABLE OF CONTENT

Chapter 3: Molecular characterisation of GRIF-1 and kinesin-1 heavy chains interactions by confocal microscopy imaging studies

Chapter 4: Fluorescence resonance energy transfer (FRET) study of GRIF-1/kinesin-1 and GRIF-1/$GABA_A$ receptor interactions: establishment of a protocol for the determination of FRET efficiencies by acceptor photobleaching

Appendices

List of Figures

List of Tables

ABBREVIATIONS

AD	Activation domain
Ade	Adenine
ADH	Antidiuretic hormone
AKAP	A-kinase anchoring protein
AMPA	α-Amino-3-hydroxy-5-methyl-isoxazole-4-propionic acid
AMP-PNP	Adenylyl imidophosphate
AMP	Ampicillin resistance
AP	Action potential
AP2	Adaptor protein 2 complex
APP	Amyloid precursor protein
APLIP-1	Amyloid precursor like protein-1
APS	Ammonium persulphate
APOER2	Apolipoprotein E receptor 2
ATP	Adenosine triphosphate
BD	Binding domain
BDNF	Brain-derived neurotrophic transport
BIG2	Brefeldin A-inhibited guanosine diphosphate/guanosine triphosphate exchange factor 2
bp	Base pairs
BP	Band pass filter
BSA	Bovine serum albumine
CaMKII	Ca^{2+}-calmodulin type 2 dependent protein kinase
CAM	Chloramphenicol resistance
CDK5	Cyclin-dependent kinase 5
cDNA	Complementary deoxyribonucleic acid
cfu	Colony forming unit
COS	Transformed African green monkey kidney fibroblasts
ddH20	Bi-distilled water
Dlg	*Drosophila* discs large tumor suppressor gene
DMF	Dimethylformamide
DMEM	Dulbecco's modified Eagle medium
DMSO	Dimethylsulphoxide
DNA	Deoxyribonucleic acid
DNA-BD	DNA-binding domain

dNTPs	Deoxyribonucleotide triphosphates
DTT	Dithiothreitol
ECFP	Enhanced cyan fluorescent protein
EGFP	Enhanced green fluorescent protein
EGFR	Epithelial growth factor receptor
EPSP	Excitatory postsynaptic potential
EYFP	Enhanced yellow fluorescent protein
EDTA	Ethylenediaminetetraacetic acid
EGTA	Ethylene glycol bis(2-aminoethyl ether)-N,N,N'N'-tetraacetic acid
ER	Endoplasmic reticulum
FRET	Fluorescence resonance energy transfer
γ2L	γ2 Subunit long form
γ2S	γ2 Subunit short form
GABA	γ-Amino butyric acid
$GABA_A$	γ-Amino butyric acid receptor type A
GABARAP	GABA receptor associated protein
GAD	Glutamic acid decarboxylase
GAT	GABA transporters
GDP	Guanosine diphosphate
GEF	Guanyl nucleotide exchange factor
GFP	Green fluorescence protein
GTP	Guanosine triphosphate
GluR2	Glutamate receptor subunit type 2
GRIF-1	GABA receptor interacting factor 1
GRIP	Glutamate receptor interacting protein
GSK3	Glycogene synthase kinase 3
GODZ	Golgi apparatus-specific protein with a DHHC zing finger domain
h	Hour
HAP1	Huntingtin-associated protein 1
HBSS	Hank's buffered salt solution
HC	Heavy chain
HEK 293	Human embryonic kidney 293 cells
HEPES	4-(2-hydroxyethyl)-1-piperazineethanesulfonic acid
$5\text{-}HT_3$	5-Hydroxytryptophan type 3
HRP	Horseradish peroxidise
Hrs	Hepatocyte-growth-factor-regulated tyrosine kinase substrate

htt	Huntingtin
IC	Intermediate chain
IgG	Immunoglobulin G
IL	Intracellular loop
IPSP	Inhibitory postsynaptic potential
IPTG	Isopropyl-β-D-thiogalactopyranoside
JNK	c-Jun NH_2-terminal kinase
JIP1	c-Jun NH_2-terminal kinase interacting protein 1
KAN	Kanamycin resistance
Kb	Kilobase
kDa	Kilodalton
KHC	Kinesin heavy chain
KIF	Kinesin family
KIF5A, B, C	Kinesin heavy chain protein types A, B and C
KLC	Kinesin light chain
λ	Wavelenght
LB	Luria-Bertani
LC	Light chain
LGIC	Ligand gated ion channel
LIC	Light intermediate chain
LP	Long pass filter
MAP	Microtubule associated protein
MD	Motor domain
MDCK	Madin-Darby canine kidney
min	Minute
M_r	Molecular weight
MCS	Multiple cloning site
MVB	Multi-vesicular bodies
mOGT	β-*O*-linked *N*-acetylglucosamine transferase mitochondrial isoform
MOPS	3-*N*-morpholino propane-sulphonic acid
mRNA	Messenger ribonucleic acid
nACh	Nicotinic acetylcholine
nOGT	β-*O*-linked *N*-acetylglucosamine transferase nucleocytoplasmic isoform
NF-H	Neuronal intermediate filament subunit of high molecular weight
NF-L	Neuronal intermediate filament subunit of low molecular weight
NF-M	Neuronal intermediate filament subunit of medium molecular weight

NGF	Neuronal growth factor
NMD	Non-motor domain
NSF	N-ethylmaleimide-sensitive factor
nm	Nanometer
NMDA	*N*-methyl-D-aspartate
NR1	NMDA receptor subunit type 1
NR2B	NMDA receptor subunit type 2B
NSF	N-ethylmaleimide-sensitive fusion protein
OD	Optical density
ORF	Open reading frame
OGT	β-*O*-linked *N*-acetylglucosamine transferase
OIP98	OGT interacting protein of 98 kilodaltons
OIP106	OGT interacting protein of 106 kilodaltons
O-GlcNAc	N-acetylglucosamine
PC12	Pheochromocytoma 12
PCR	Polymerase chain reaction
PDI	Protein disulphide isomerase
PDZ	Postsynaptic density-95, *Drosophila* discs large tumor suppressor gene A, zonula occludens-1
PEG	Polyethylene glycol
PICK	Protein interacting with C Kinase
PKA	Protein kinase A
PKC	Protein kinase C
Plic-1	Ubiquitine-like protein 1
PMSF	Phenylmethylsulphonylfluoride
PP1, 2A	Protein phosphatase types 1 and 2A
PSD	Post-synaptic density
PRIP-1, 2	Phospholipase-C related inactive protein types 1 and 2
RACK-1	Receptor for activated C kinase-1
RNA	Ribonucleic acid
RT	Room temperature
SAP	Shrimp alkaline phosphate
SD	Selection dropout
SD	standard deviation
SDS	Sodium dodecyl sulphate
SDS-PAGE	Sodium dodecyl sulphate-polyacrylamide gel electrophoresis
SEM	Standard error of the mean

SMART	Simple Modular Architecture Research Tool
SNAP25	Synaptosomal-associated protein of 25 kDa
SNARE	Soluble N-ethylmaleimide-sensitive factor attachment protein receptor
Sos	Son of sevenless
TBE	Tris-buffered EDTA
TBPS	t-Butylbicyclophosphorothionate
TEMED	N,N,N',N'-tetramethylethylenediamine
TGN	Trans-golgi network
TM	Transmembrane
TPR	Tetratricopeptide repeat
TRAK1, 2	Trafficking protein kinesin binding types 1 and 2
UDP	Uridine diphosphate
U	Unit
UV	Ultra violet
v/v	volume/volume
w/v	weight/volume
X-GAL	5-Bromo-4-chloro-3-indolyl-β-D-galactopyranoside
YPAD	Yeast peptone adenine dextrose
ZO-1	Zonula occludens-1

ACKNOWLEDGEMENTS

Firstly, I would like to thank Prof. F. Anne Stephenson for giving me the opportunity to carry out my PhD in her laboratory at the School of Pharmacy and for her supervision throughout my PhD and especially during writing of this thesis.

A big thank you to Dr. Kieran Brickley for his technical help throughout my PhD and particularly during the revision of this thesis. Additionally, a thank you for all the preparation of the in-house antibodies that I actively used. I am also grateful to Dr. Jeff McIlhinney for his initial help with the FRET studies.

I would like to thank Sarah Cousins for the scientific and philosophical discussions and her encouragement throughout my PhD. Thank you also to Dr. Miriam Smith for her useful and wise advice. I would like to thank all the previous and current lab-members I worked with, Linda, Michaelis, Ojla, Anna and Blaise and the project students, Assana and Ana.

I would also like to acknowledge my new colleagues in the Goda Lab at the LMCB. Thank you especially to Drs. Kevin Staras, Lorenzo Cingolani and Andrew Vaughan for their critical reading of parts of my thesis and to Dr. Yukiko Goda for having patience in me obtaining my PhD. Thank you also to Lily Yu and Maz to liven the place.

Finally, I would like to thank my parents and grand-parents for their permanent support during all my studies. A big thank you goes also to Dr. Florian Plattner for his valuable support throughout the last few years.

The work presented in Chapter 4 was partially funded by an award to me from the University of London Central Research Fund

CHAPTER 1

INTRODUCTION

1.1. KINESINS AND FAST TRANSPORT MECHANISMS IN NEURONES

Neurones are asymetric, polarised cells formed by a cell body, numerous dendrites and a single, long axon (Figure 1.1). Dendrites and axon terminals are specialised cellular extensions that connect adjacent neurones. The contact zones or synapses underly synaptic transmission (section 1.2). Axon terminals form the presynapse and they send synaptic signals to other neurones. Dendrites form the postsynapse and they receive synaptic inputs from surrounding neurones.

Maintenance of neuronal function relies on the presence of specific proteins and organelles in a given neuronal location, e.g. postsynaptic receptors in dendritic membranes or mitochondria in axon terminal. Synaptic proteins and organelles are generally synthesized in the cell body although some local protein synthesis also occurs in the dendrites. They are targeted to the synapses by fast axonal/dendritic transport processes performed by molecular motors. Motor proteins transport various cargoes to their destination by travelling via the neuronal cytoskeleton network. These trafficking mechanisms are highly regulated. The role of the protein, $GABA_A$ receptor interacting factor-1, GRIF-1, in these transport processes is addressed in this PhD-thesis.

1.1.1. The neuronal cytoskeleton

The cytoskeleton network consists of microtubules, actin microfilaments and neurofilaments (Baas and Ahmad, 2001).

Microtubules- Microtubules are polymers of α- and β-tubulin. They are polarised structures with a fast growing- or plus-end and an opposite slow growing- or minus-end. In the axon and distal dendrites, microtubules are oriented with their plus-end radiating either from the cell body to the synapse, or from the cell body to the dendrites respectively. In proximal dendrites, microtubules have mixed orientations (Baas *et al.*, 1988). Microtubules are highly unstable structures that assemble and disassemble constantly. They are stabilised by microtubule-associated-proteins (MAPs) that differ according to their axonal or dendritic location. For example, tau is a MAP found in axons whereas MAP2 is localised in dendrites (Dotti *et al.*, 1987).

Actin microfilaments- Actin microfilaments result from the polymerisation of actin subunits and they are polarised similarly to the microtubules (Baas and Ahmad, 2001). Actin microfilaments are found underneath the plasma membrane. They are particularly enriched within dendritic spines at post-synaptic sites and at axon termini.

Microtubules and actin microfilaments serve as tracks for molecular motors in fast axonal/dendritic transport processes.

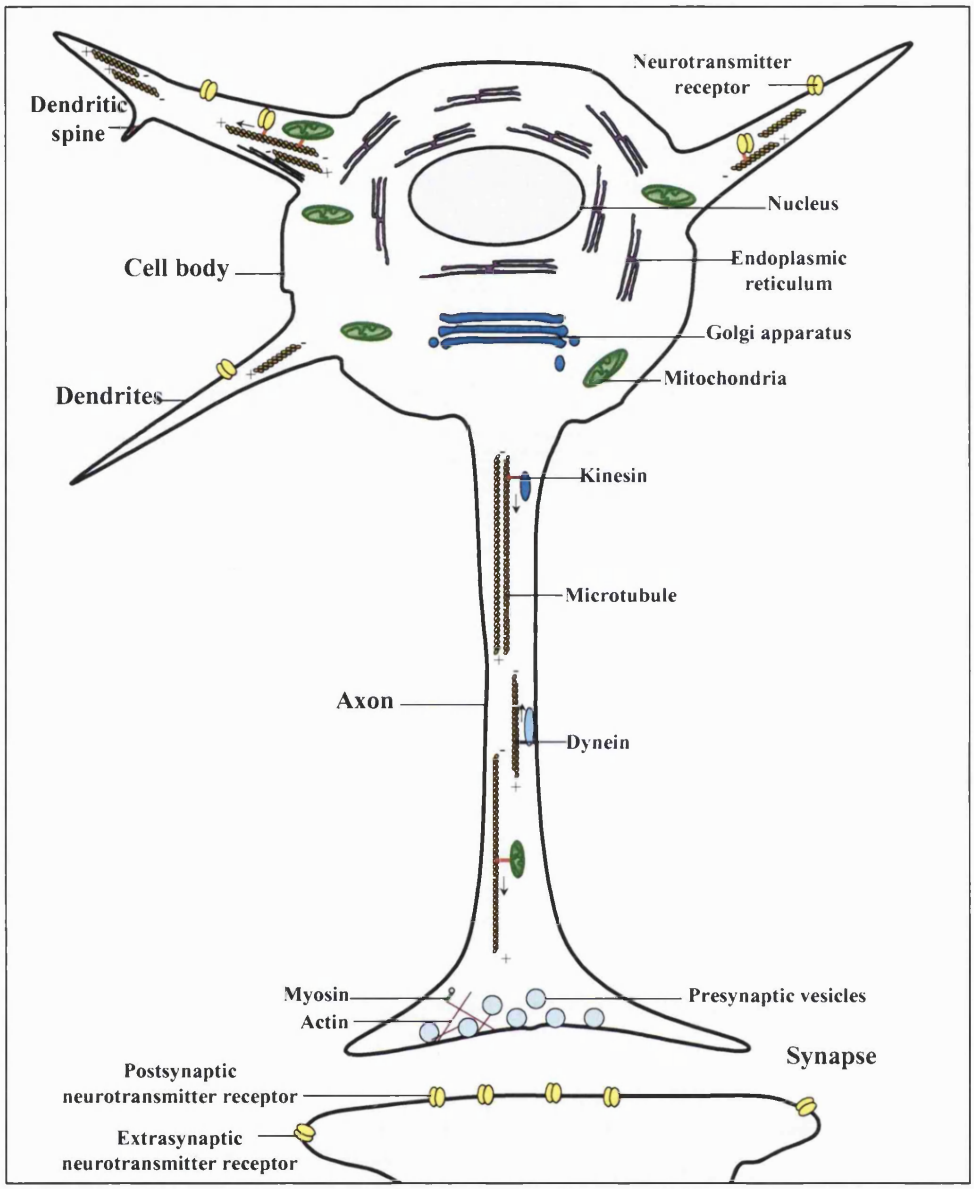

Figure 1.1. A schematic diagram depicting the general organisation of a neurone. A neurone is an asymetric cell composed of a cell body, dendrites and a long axon. Neuronal components such as organelles, neurotransmitter receptors and other synaptic proteins are transported to and from the dendrites and to and from axonal terminals by molecular motor proteins. Those are kinesins, dyneins and myosins. Molecular motors move their cargoes along the neuronal cytoskeleton. Kinesins move anterogradely towards the microtubule plus-end. Dyneins move retrogradely towards the microtubule minus-end. Myosins can move in both directions along actin filaments in areas devoided of microtubules such as the dendritic spines or axon terminals.

Neurofilaments- Neurofilaments (NF) are formed of 3 subunits with low (L), medium (M) and high (H) molecular weights, i.e. NF-L, NF-M and NF-H (Baas and Ahmad,

2001). Neurofilaments are mostly found within the axon where they help to maintain the axon structure.

1.1.2. The molecular motors

Motor proteins are ATPases. They move along microtubules or actin microfilaments by hydrolysing ATP (reviewed in Vale, 2003). They are composed of 2 functional domains: a cargo binding domain and a motor domain that contains the ATPase activity and the microtubule/actin binding site. Three molecular motor superfamilies have been identified: kinesin, cytoplasmic dynein and unconventional myosin. Kinesins and dyneins are microtubule-based motors whereas myosins are actin-based motors. Kinesins and dyneins are responsible for long-distance vesicular transport whereas myosins carry out short range vesicular transport.

Kinesins- This thesis focuses on kinesins and they are described in detail in section 1.1.3.

Dyneins- Cytoplasmic dyneins, referred to hereafter as dyneins, transport vesicular cargoes and organelles towards the minus-end of the microtubules. They are protein complexes composed of 2 heavy chains (HC), 2 intermediate chains (IC), 4 light intermediate chains (LIC) and several light chains (LC) (Kamal and Goldstein, 2002) (Figure 1.2 A). The HCs form a motor domain that contains a microtubule binding site and several ATP binding sites. LCs and LICs are involved in cargo attachment. Dynein is always associated with the dynactin complex via the interaction of the LICs with the $p150^{Glued}$ subunit of the dynactin complex (Kamal and Goldstein, 2002; Vale, 2003). The dynactin complex is necessary for the attachment of dynein to its different cargoes and for the regulation of dynein motility.

Myosins- Unconventional myosins, referred to hereafter as myosins, ensure short range anterograde and retrograde transport of vesicular cargoes and organelles along actin microfilaments (Mermall *et al.*, 1998). Among the 18 classes of myosin motor identified, myosin-Vs are the most studied (reviewed in Langford, 2002). They carry out actin-based transport of the endoplasmic reticulum (ER), synaptic vesicles and neurotransmitter receptors in neurones (Langford, 2002; Lisé *et al*, 2006). Myosin-Vs transport also pigment granules, i.e. melanophores, in melanocytes. Myosin-Vs are heteromers composed of 2 HCs and 12 calmodulin-like LCs (6 LCs per HCs) (Figure 1.2 B). The HCs contain 3 functional domains: (i) an N-terminal motor domain with actin, ATP and LC binding sites, (ii) a medial tail domain serving for the dimerisation of the 2 HCs and containing regulation sites and (iii) a C-terminal cargo binding

domain. Attachment of myosin-Vs to their cargoes is mediated by vesicle-specific Rab proteins. Additional adaptor proteins can be necessary to bridge myosin-V to Rab proteins. For example, the protein melanophilin interacts with both myosin-V and Rab27, a Rab-protein found in the membrane of melanophores, thus linking motor and cargo (Langford, 2002). Myosin-V is associated with microtubule motors. This is discussed in section 1.1.3.4.

1.1.3 Kinesins

1.1.3.1. Identification, structure and function

The kinesin superfamily (KIF) of molecular motors are ATPases that mediate anterograde transport of organelles along microtubules. More than 40 different kinesin proteins have been identified in human and mouse and classified into 14 phylogenetic kinesin families (kinesin-1 to kinesin-14) (Lawrence *et al.*, 2004). The nucleotide and amino acid sequences encoding the motor domain are highly conserved across families whereas the nucleotide and amino acid sequences encoding the remaining region show little similarities (Hirokawa and Takemura, 2005). The position of the motor domain can vary across families. For example, kinesin-1 proteins have an N-terminal motor domain whereas kinesin-13 members have a middle motor domain and kinesin-14 proteins a C-terminal motor domain (Hirokawa and Takemura, 2005).

The conventional kinesin (kinesin-1) was initially isolated from squid axoplasm, bovine and chick brains, searching for a "translocator", i.e. a protein responsible for fast microtubule-based organelle transport (Vale *et al.*, 1985; Brady, 1985). Kinesin was co-purified with microtubules in the presence of the non-hydrolysable ATP analogue, adenylyl imidodiphosphate (AMP-PNP), as it was known that the "translocator" could not dissociate from microtubules under this condition. The purified kinesin was a 130 kDa protein with a microtubule-dependent ATPase activity (Brady, 1985; Vale *et al.*, 1985; Kuznetsov and Gelfand, 1986). Further, the isolated protein could mediate microtubules, beads and organelles movements in *in vitro* motility assays (Brady, 1985, Vale *et al.*, 1985). The purified kinesin was found associated with membranous organelles and it was shown to be involved in their anterograde transport (Hollenbeck *et al.*, 1989; Hirokawa *et al.*, 1991).

The human conventional kinesin was identified, cloned and characterised by Navone *et al.* (1992). It was isolated from a human placenta complementary DNA (cDNA) library using a probe based on the sequence of the *Drosophila* kinesin C-terminal domain. Most of the mouse kinesin genes were discovered by Hirokawa's group (Aizawa *et al.*,

1992; Nagawa *et al.*, 1997). This was done using polymerase chain reaction method with degenerate primers designed according to the nucleotide sequence of kinesin motor domains already identified using as template, mouse brain cDNA libraries.

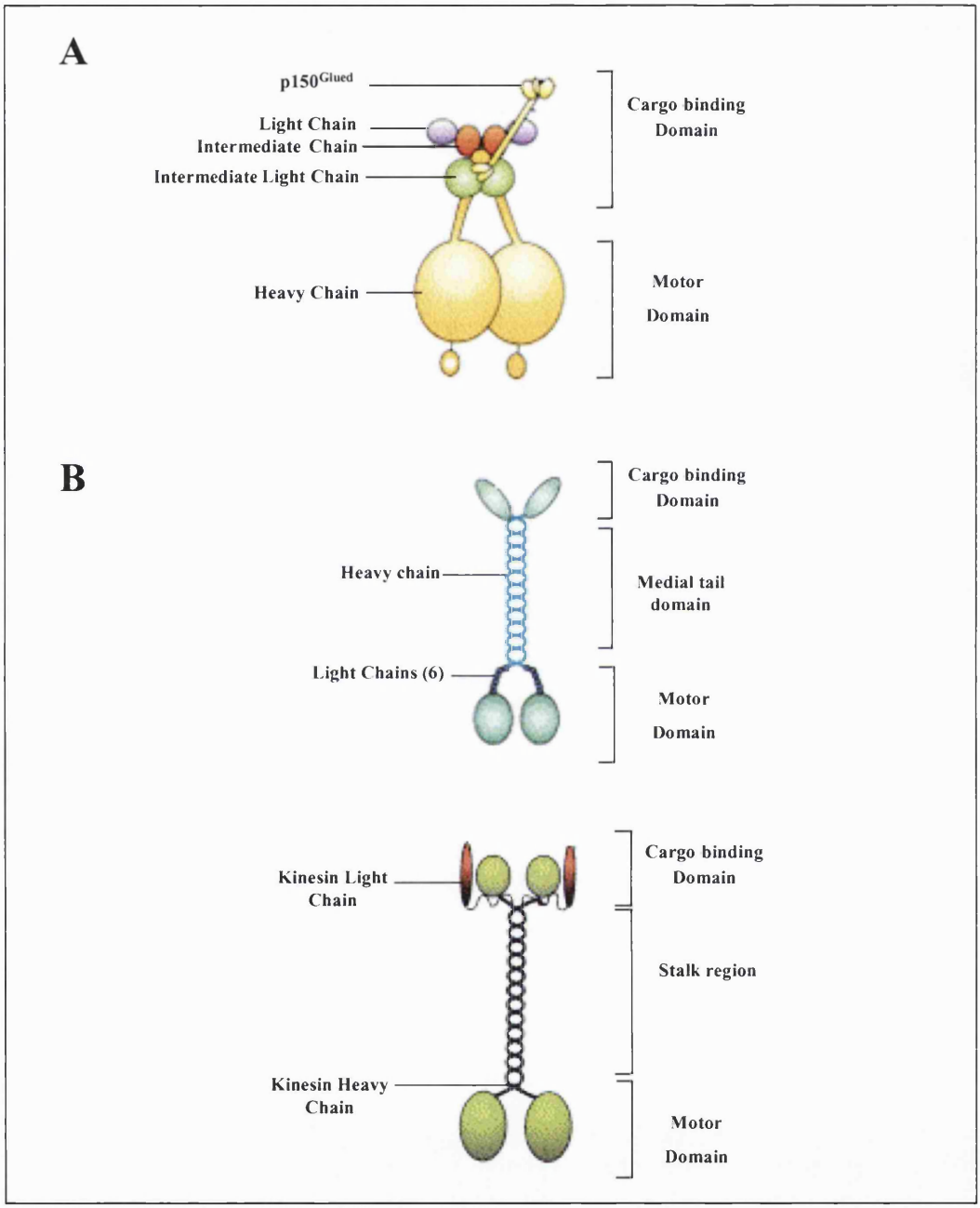

Figure 1.2. A schematic representation of the molecular motors dynein, myosin and kinesin. A, dynein; B, myosin-V; C, kinesin-1. Taken from Karcher *et al.*, 2002.

The structure of the conventional kinesin (kinesin-1) was first determined using purified bovine brain kinesin (Kuznetsov *et al.*, 1988). Kinesin is a heterotetramer consisting of 2 kinesin heavy chains (KHCs), or KIF5s, with a molecular weight (M_r) of 120 kDa and

2 kinesin light chains (KLCs) with $M_r \sim 62$ kDa (Figure 1.2 C). Each KHC consists of (i) an N-terminal motor domain containing a microtubule binding site and the ATPase activity (Kuznetsov *et al.*, 1989), (ii) a C-terminal domain with a membrane binding site (Skoufias *et al.*, 1994) and for the interaction of KHC with KLCs (Diefenbach *et al.*, 1998) (iii) a central coiled-coil region serving for dimerisation of KHCs. The KLCs are formed of 15 N-terminal hepta repeats for the interaction with KHC and 7 C-terminal tetratricopeptide repeats (TPRs) (Cyr *et al.*, 1991; Gauger *et al.*, 1993). TPRs are 34 amino acid repeats that mediate protein-protein interactions (Lamb *et al.*, 1995). In mouse, 3 KHC isoforms, KIF5A, KIF5B and KIF5C, and 3 KLC isoforms, KLC1, KLC2 and KLC3, have been identified (Aizawa *et al.*, 1992; Nagawa *et al.*, 1997; Rahman *et al.*, 1998). KIF5A, KIF5C and KLC1 are found in neurones whereas KIF5B and KLC2 are distributed ubiquitously. The localisation of KLC3 is not known.

As mentioned earlier, many different kinesin molecules have been identified. The diversity of existing kinesins accounts for the importance of their function: kinesins are involved in fast intracellular transport, cell cycle processes and neuronal development (Hirokawa and Takemura, 2005). This thesis focuses on the role of kinesin in fast axonal/dendritic transport mechanisms.

In neurones, kinesin-driven anterograde transport ensures the correct localisation of neurotransmitter receptors, ion channels, organelles and dendritic mRNAs. For example the kinesin-1 protein, KIF5B, trafficks the α-amino-3-hydroxy-5-methylisoxazole-4-propionate (AMPA) receptor GluR2 subunit to dendrites (Setou *et al.*, 2002; sections 1.1.3.2-1.1.3.3). Kinesin-1 molecules, KIF5A, KIF5B and KIF5C are also involved in mRNA granule transport to the dendrites for local protein synthesis (Kanai *et al.*, 2004). The kinesin-2 protein, KIF17, transports *N*-methyl-D-aspartate (NMDA) receptors (Setou *et al.*, 2000; sections 1.1.3.2-1.1.3.3) and potassium channels Kv4.2 (Chu *et al.*, 2005; section 1.1.3.3) to the dendrites. Kinesins also play an important role in mitochondrial transport in neurones (section 1.1.4).

1.1.3.2. Kinesin/cargo interactions

A given kinesin can transport various cargoes along microtubules as described above for KIF5B (section 1.1.3.1). The specific attachment of kinesin to a cargo is mediated by adaptor proteins. These molecules provide a physical link between the motor and its cargo. Recently, several adaptors have been identified (Hirokawa and Takemura, 2005). Known kinesin/adaptor complexes are summarised in Table 1.1. Some examples are described hereafter.

Cargo	Adaptor	Kinesin isoform*	Reference
AMPA receptors	GRIP1	KIF5A$_{807-934}$, B, C	Setou *et al.*, 2002
NMDA receptors	mLin-10/mLin-2/mLin-7	KIF17$_{839-1039}$	Setou *et al.*, 2000
Mitochondria	Milton Syntabulin	KIF5B$_{810-891}$ KIF5B$_{814-963}$	Stowers *et al.*, 2002 Cai *et al.*, 2005
Syntaxin1	Syntabulin	KIF5B$_{814-963}$	Su *et al.*, 2004
Synaptic vesicles precursor	APLIP-1 Liprin-α	KLC KIF5, KIF1A	Horiuchi *et al.*, 2005 Miller *et al.*, 2005
APP	JIP 1	KLC	Matsuda *et al.*, 2003
APOER2	JIP 1-2	KLC	Verhey *et al.*, 2001
mRNA	Protein complex	KIF5A, B, C$_{865-923}$	Kanai *et al.*, 2004
Dystrophin associated protein complex	Dystrobrevin	KIF5A$_{804-934}$	Macioce *et al.*, 2003
Nuclear export complex	Ran binding protein 2	KIF5	Cai *et al.*, 2001
Vesicles	Kinectin	Kinesin-1	Toyoshima *et al.*, 1992
Unknown	YETI	KLC (TPRs) KIF5$_{850-975}$	Wisniewski *et al.*, 2003

Table 1.1. A summary of the known adaptor proteins linking kinesin motors to their cargoes. * The adaptor protein binding site on kinesin is indicated as subscript when known. The full length KIF5A, KIF5B, KIF5C and KIF17 are 1027, 963, 957 and 1039 amino acid long respectively.

The glutamate receptor interacting protein 1, GRIP1, links GluR2-containing AMPA receptors to the kinesin-1 heavy chains, KIF5 (Dong *et al.*, 1997; Setou *et al.*, 2002). GRIP1 is a cytoplasmic protein found at the synapse. It contains 7 PDZ (postsynaptic density-95 (PSD-95), *Drosophila* discs large tumor suppressor gene A (DlgA), zonula occludens-1 (ZO-1)) domains. The PDZ domains 4-5 bind to the AMPA receptor GluR2 subunit (Dong *et al.*, 1997). The region between PDZ domains 6-7 mediates the interaction with the KIF5B C-terminal domain (KIF5B residues 807-1027) (Setou *et al.*,

2002). The KIF5/GRIP1/AMPA receptor complex is targeted to the dendrites following the interaction between KIF5 and GRIP1 (section 1.1.3.3).

Kinesin-1 is also involved in amyloid precursor protein (APP) transport processes. The APP interaction with KLC is mediated by the adaptor protein, c-Jun NH_2-terminal kinase (JNK)-interacting protein 1 (JIP1). This protein, JIP1, serves as an anchor point for MAP kinases that activate the JNK signaling pathway. JIP-1 associates with the TPRs of KLC by its C-terminal domain (Matsuda *et al.*, 2003).

The kinesin-2 protein, KIF17, association with NR2B subunit-containing NMDA receptors is indirect. KIF17 interacts with the PDZ domain-containing protein complex, mLin-10/mLin-2/mLin-7, that in turn binds the NMDA receptor NR2B subunit (Setou *et al.*, 2000). The KIF17 C-terminal region (residues 939-1038) interacts with a C-terminal PDZ domain of mLin-10 as shown by yeast two-hybrid studies. Co-immunoprecipitation analyses confirmed that KIF17 was associated with the mLin-10/mLin-2/mLin-7/NR2B subunit-containing NMDA receptor complex in brain. Association of KIF17 with mLin-10 is essential for NMDA receptor NR2B subunit trafficking as shown by *in vitro* motility assays.

1.1.3.3. Axonal versus dendritic anterograde transport

Kinesin motors selectively deliver their cargoes either to the dendrites or to the axon. For example, kinesin-1 (KIF5) targets AMPA receptors to dendrites and apolipoprotein E receptor 2 (APOER2) receptors to axon terminals (Setou *et al.*, 2002; Verhey *et al.*, 2001), kinesin-2 (KIF17) transports NMDA receptors and Kv4.2 potassium channels to dendrites (Setou *et al.*, 2000; Chu *et al.*, 2005, section 1.1.3.1). It is still not clear how selective axonal/dendritic transport is achieved but recent findings suggest that the ability of the molecular motor to recognise axonal versus dendritic microtubules and/or targeting signals within the cargo could target the molecular motor to the correct compartment.

Kinesins can distinguish axonal from dendritic microtubules. This is because microtubules in these regions have different biochemical properties that may affect motor-microtubule interactions (Nakata and Hirokawa, 2003; Jacobson *et al.*, 2006). In hippocampal neuronal cultures, KIF5 motor domains recognise the axon initial segment and move preferentially to axon terminals (Nakata and Hirokawa, 2003; Jacobson *et al.*, 2006). This selectivity is lost following application of paclitaxel, a chemical that inhibits microtubule dynamics by modifying tubulin and MAP phosphorylation

patterns. This suggests that selective accumulation of KIF5 in the axon is dependent on microtubule properties.

However targeting of KIF5/GRIP1 complexes to dendrites (Setou *et al.*, 2002) is in contrast with the previous observations and it indicates that additional signals direct the direction of kinesin movements. As mentioned earlier (section 1.1.3.2), GRIP1 consists of 7 PDZ domains with PDZ domains 4-7 involved in the attachment to kinesin-1 and to the AMPA receptor GluR2 subunit. Thus, it could be possible that PDZ domains 1-3 interact with another protein containing a dendritic targeting sequence. Alternatively, the GluR2 subunit could carry this targeting signal itself thereby enabling the specific dendritic localisation. Thus the ability of the motor to recognise axonal from dendritic microtubules is not sufficient for the correct targeting of motor/cargo complexes.

This is supported by recent studies on the trafficking of the potassium channel Kv4.2 (Rivera *et al.*, 2003; Chu *et al.*, 2005). KIF17 transports Kv4.2 channels to the dendrites (Chu *et al.*, 2005). However a Kv4.2 dileucine motif within Kv4.2 is essential for dendritic targeting (Rivera *et al.*, 2003). Thus, in this example correct dendritic localisation of Kv4.2 channels requires both the motor protein, KIF17, and the cargo targeting sequence.

1.1.3.4. Regulation of kinesin function

Kinesin function can be regulated by conformational changes and by post-translational modifications.

In cells, kinesin is found as both a soluble form and an organelle-associated form (Hollenbeck, 1989). Soluble kinesin is in a folded conformation that prevents kinesin from binding to microtubules (Hackney *et al.*, 1992; Friedman and Vale, 1999; Coy *et al.*, 1999). In contrast, organelle-associated kinesin is an extended, motile microtubule-bound form. The inactive folded conformation results from the interaction of the KHC tail domain with the KHC motor domain (Friedman and Vale, 1999; Coy *et al.*, 1999). This conformation is stabilised by KLCs (Verhey *et al.*, 1998). In *in vitro* assays, kinesin motility can be restored by binding to a cargo (Coy *et al.*, 1999). This suggests that association of kinesin to its cargo mediates the transition from the folded to the unfolded form thereby enabling movement along microtubules.

In addition to these conformational changes, kinesin motor activity and kinesin cargo attachment can be modulated by post-translational modifications. Kinesin is phosphorylated on serine residues *in vivo* within its non-motor region (Hollenbeck, 1993). The level of kinesin phosphorylation is increased in cells with intense

anterograde trafficking (Lee and Hollenbeck, 1995). Further, organelle-associated kinesin is more phosphorylated than the soluble form of kinesin (Lee and Hollenbeck, 1995). Therefore it was proposed that phosphorylation could regulate kinesin motor activities and/or its association with organelles. Another study showed that, *in vivo*, KLC was specifically phosphorylated by the serine/threonine kinase, glycogen synthase kinase 3 (GSK3), which resulted in cargo detachment and inhibition of kinesin-based transport (Morfini *et al.*, 2002). Since GSK3 is expressed in specific neuronal locations such as the growth cone, it was proposed that GSK3 phosphorylation could regulate the cargo delivery at specific sites within the neurone.

1.1.3.5. Coordination of molecular motor activities

Cargoes such as mitochondria and synaptic vesicle precursors are moved along microtubules anterogradely by kinesins and retrogradely by dyneins (Hollenbeck and Saxton, 2005; Pilling *et al.*, 2006; Miller *et al.*, 2005). Subsequently, their delivery to specific actin-rich neuronal areas lacking microtubules such as dendrites or axon terminals is achieved by myosins (Dillon and Goda, 2006; Hollenbeck and Saxton, 2005). Thus, transport and targeting of cargoes involve both microtubule- and actin-based motors. Several motors can be present on the same cargo, e.g. both dynein and kinesin are found on mitochondria (Pilling *et al.*, 2006). Therefore motor activities must be tightly coordinated so that the cargo can switch from the microtubule to the actin track for a successful delivery (Welte, 2004). It has been proposed that motor activities could be coordinated by turning-off one motor and turning-on another one (Gross *et al.*, 2002; Kural *et al.*, 2005). This may be achieved via motor-motor interactions as kinesin-1 KHCs (residues 763–856) were found to associate with myosin-V in mouse brain (Huang *et al.*, 1999).

A direct interaction of dynein with kinesin-1 KLCs was revealed by yeast two-hybrid studies (Ligon *et al.*, 2004). Dynein was mainly found associated with KLC in the soluble pool of inactive kinesin isolated from rat brain. It was proposed that binding of dynein to KLC could activate kinesin motility (section 1.1.3.3). Immunocytochemistry analyses showed that kinesin and dynein were co-localised on some vesicles transported along microtubules. It was suggested that kinesin could transport newly synthetised inactive dynein molecules to the microtubule minus-end (Ligon *et al.*, 2004).

Additional studies from the Saxton laboratory also suggested that kinesin and dynein-based transports were inter-dependent. Work from Martin *et al.* (1999) showed that a mutation in dynein heavy chain and in the dynein-associated protein, dynactin, impaired

both anterograde and retrograde transport processes (Martin *et al.*, 1999). It was also shown that kinesin-1 was necessary for the dynein-based retrograde transport of mitochondria in neurones (Pilling *et al.*, 2006). Indeed disruption of KHC expression in flies affected both anterograde and retrograde transport of mitochondria. Another study showed that the *Drosophila* adaptor protein, APP like protein-1, (APLIP-1) was important for both anterograde and retrograde transport of synaptic vesicles (Horiuchi *et al.*, 2005). APLIP-1 is the *Drosophila* homologue of the JNK signalling pathway scaffold protein, JIP1. Since APLIP1 binds to both kinesin-1 (KLC) and dynein, it was proposed that kinesin-1 and dynein activities were coordinated by the JNK-signalling pathway.

1.1.4. Mechanisms of mitochondrial transport in neurones

In neurones, mitochondria are found at energy-demanding sites where they provide the ATP necessary for metabolic reactions and they buffer cytosolic calcium. Transport of mitochondria to these regions is stimulated by synaptic activity (Li *et al.*, 2004) and extracellular molecules such as neuronal growth factor (NGF) (Chada and Hollenbeck, 2004). Mitochondrial transport is performed by molecular motors. Dyneins and kinesins move mitochondria along microtubules and in areas devoided of microtubules, myosins transport these organelles along actin filaments (Morris and Hollenbeck, 1995). Kinesin-1 and kinesin-3 motor proteins, i.e. KIF5B and KIF1Bα, transport mitochondria anterogradely to the axon terminal and to dendrites (Elluru *et al.*, 1995; Tanaka *et al.*, 1998; Hirokawa and Takemura, 2005). Dyneins transport mitochondria retrogradely to the cell body in a kinesin-1-dependent manner (Hollenbeck and Saxton, 2005; Pilling *et al.*, 2006). The minus-end-directed kinesin-14 motor, KIFC2, could also be involved in retrograde transport processes (Hirokawa and Takemura, 2005).

Targeting of mitochondria to kinesin can be mediated via the KLC and/or adaptor proteins. In contrast with mouse brain where 2 KLC isoforms co-exists (section 1.1.3.1), 5 KLC isoforms have been identified by phage-display in chinese hamster ovary cells (Khodjakov *et al.*, 1998). They all interact with KHC but only one of them co-localises with mitochondria. Therefore it has been proposed that this isoform could target mitochondria to KHC.

Scaffolding proteins essential for microtubule-based mitochondrial transport, have been recently identified in rat and in *Drosophila* (Table 1.1). In rat hippocampal neurones the protein, syntabulin, facilitates mitochondrial anterograde axonal transport (Cai *et al.*,

2005). Depletion of syntabulin expression results in impairment of this transport. The *Drosophila* protein, Milton, is a kinesin-1-associated protein necessary for the proper distribution of mitochondria at the synaptic terminal (Stowers *et al.*, 2002; section 1.3.2). In Milton mutants, mitochondria are not trafficked to the axon terminals and they accumulate in the cell body (Stowers *et al.*, 2002; Gorska-Andrzejak *et al.*, 2003; Glater *et al.*, 2006). Another *Drosophila* protein, APLIP-1, is required for the retrograde transport of mitochondria (Horiuchi *et al.*, 2005). As noticed earlier, APLIP-1 is the *Drosophila* homologue of JIP1 and it associates with both kinesin-1 and dynein (section 1.1.3.4). In APLIP-1 mutants, retrograde transport of mitochondria is significantly reduced thus suggesting an important role for APLIP-1 in this process.

The importance of APLIP-1 in mitochondrial retrograde transport suggests that trafficking of mitochondria could be regulated by the JNK signalling pathway (Horiuchi *et al.*, 2005).Mitochondrial transport may also be regulated by small GTPases as suggested by the identification of the *Drosophila* GTPase, dmiro (Guo *et al.*, 2005). This protein consists of a mitochondrial transmembrane domain for mitochondrial targeting, 2 EF hand motifs for calcium binding and 2 GTPase domains. In dmiro mutant flies, mitochondria accumulate in the cell soma as seen in Milton mutants. Further, dmiro and Milton were shown recently to interact, thereby providing a link between Milton and mitochondria (Glater *et al.*, 2006).

1.1.5. Molecular motors and neurodegenerative diseases

Defects in axonal/dendritic transport have been linked to neurodegenerative diseases. These defects can be caused by mutations of the molecular motor, misregulation of the cargo attachment/release processes or interference with the formation of the transport machinery.

A mutation in KIF1B, a kinesin transporting synaptic precursors and mitochondria to axon terminals, is found in Charcot-Marie-Tooth disease type 2 (Zhao *et al.*, 2001). A mutation in KIF5A is found in hereditary spastic paraplegia, a disease characterised by lower-limb weakness (Reid *et al.*, 2002). A mutation in dynein or its associated protein, dynactin/p150^{Glued}, has been found in patients with motor neurone disease (Hafezparast *et al.*, 2003). Finally, a mutation in myosin-V has been found in Griscelli syndrome type 2 patients, a disease characterised by pigmentation defects and neurologic dysfunctions (Pastural *et al.*, 1997).

Recent studies suggest that misregulating kinesin/cargo attachment could be involved in Alzheimer's disease pathology (Morfini *et al.*, 2002; Morfini *et al.*, 2004). As

mentioned earlier (section 1.1.3.4), the protein kinase, GSK3, regulates the attachment of kinesin-1 to membranous organelles by phosphorylating KLC. Activation of GSK3 is dependent on another enzyme, cyclin dependent kinase 5 (CDK5). Since CDK5 and GSK3 activities are changed in Alzheimer's disease, it has been suggested that these alterations could account for axonal transport deficiencies seen in this disease.

Another neurodegenerative disease, Huntington's disease has also been linked to defects in both anterograde and retrograde transport. This disease is characterised by the addition of glutamine repeats (polyQ) to the protein huntingtin (htt), a protein involved in brain-derived neurotrophic factor (BDNF) transport via its association with huntingtin-associated protein, HAP1 (Gauthier *et al.*, 2004; sections 1.2.2.2.6, 1.3.2.4). The affinity of htt for HAP1 increases in a polyQ-dependent manner. Thus, it has been suggested that this stronger polyQ-htt/HAP1 interaction could affect fast axonal transport by preventing HAP1 from binding efficiently to molecular motors.

1.2. GENERAL MECHANISMS OF FAST SYNAPTIC TRANSMISSION AT CHEMICAL SYNAPSES

Communication between adjacent neurones occurs at the synapses where synaptic information is transmitted as an electrical signal, the action potential (AP). Synapses are specialised zones of contact between the axon terminal of a neurone, i.e. the presynapse, and the dendrite of an adjacent neurone, i.e. the postsynapse. There are 2 distinct classes of synapses: electrical and chemical synapses. At electrical synapses, pre- and postsynaptic compartments are connected by gap junctions through which the AP flows. At chemical synapses, pre- and postsynaptic compartments are separated by an extracellular space, the synaptic cleft. The AP is converted into a chemical signal via the presynaptic release of neurotransmitter molecules which diffuse across the synaptic cleft and subsequently bind to postsynaptic receptors located in the dendritic membrane (Figure 1.3). Based on structure/function properties, neurotransmitter receptors can be broadly classified into 2 types, ionotropic or metabotropic receptors. Ionotropic receptors are usually ligand-gated ion channels. They mediate fast synaptic transmission. Metabotropic receptors are coupled to G-proteins. Their activation results in slow synaptic transmission. Depending on the nature of the neurotransmitter released,

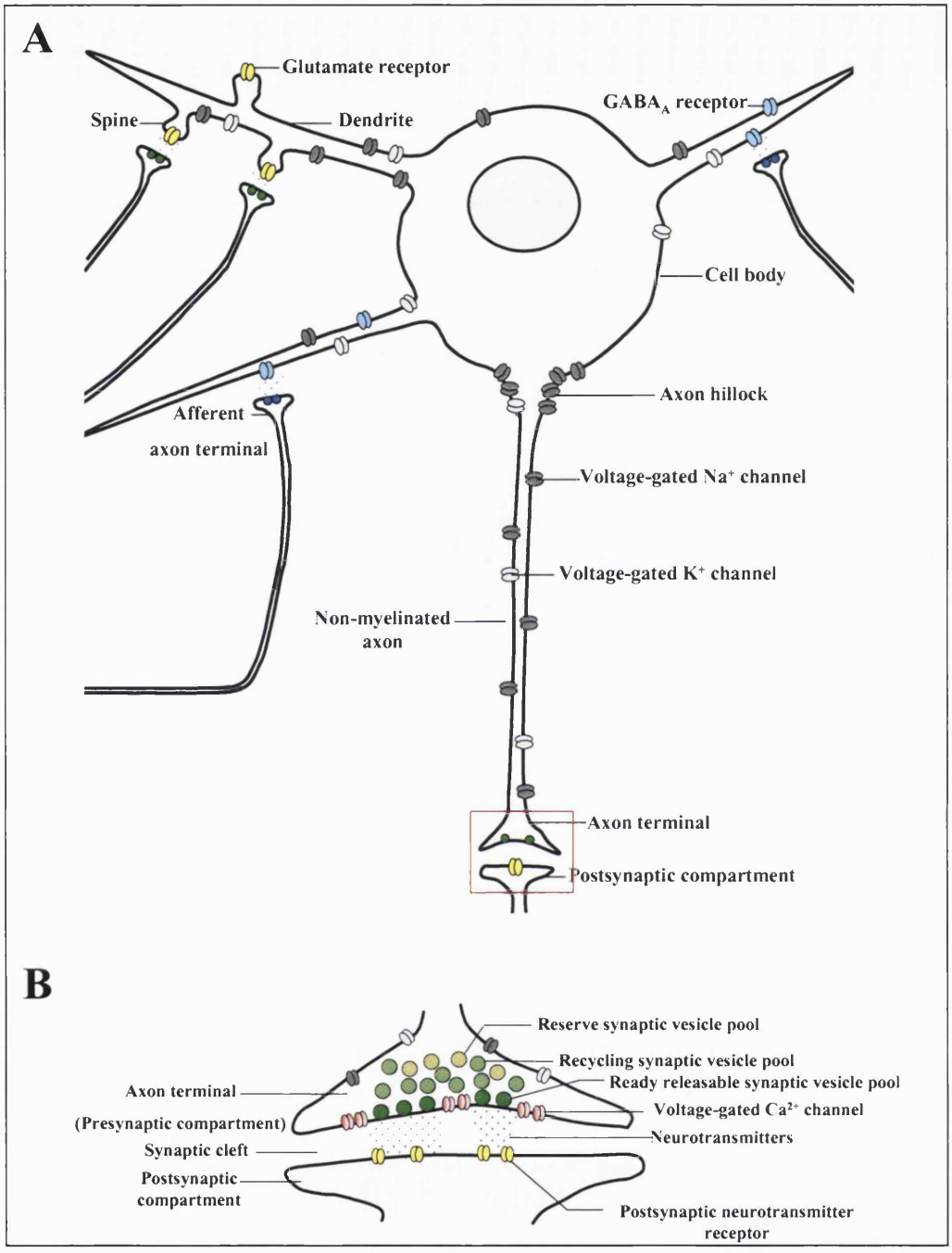

Figure 1.3. A schematic representation of a neurone during fast synaptic transmission at chemical synapses. The Figure shows the structure/function relationship of a neurone within a neuronal network. A, Dendrites make connections with axon terminals of neighbouring neurones. Neurotransmitters are released by the axon terminals, i.e. the presynapse, and they bind to their receptors located in the dendritic membrane, i.e. postsynapse. Activated neurotransmitter receptors open allowing ions to enter the cell. The resulting depolarisation activates voltage-gated Na^+ and K^+ channels resulting in an enhancement of the initial depolarisation. If the depolarisation reaches a threshold, an AP is generated. The AP propagates down the axon by depolarising the axonal membrane and activating voltage-gated Na^+ and K^+ ion channels. B, Enlargement of the boxed region in A. Arrival of the AP at the axon terminal activates voltage-gated Ca^{2+} channels leading to neurotransmitter release in the synaptic cleft and their binding to postsynaptic neurotransmitter receptors.

synaptic transmission is excitatory or inhibitory. Only fast synaptic neurotransmission at chemical synapses will be considered in this section.

1.2.1. Ion movements across neuronal membrane

Neurones can actively change their membrane potential in response to extracellular stimuli. At rest the intracellular space is relatively more negatively charged than the extracellular space. Upon stimulation, with electrodes for example, the membrane is depolarised, i.e. the intracellular space becomes relatively more positively charged than the extracellular space. Depolarisation of the neuronal membrane above a critical threshold leads to an AP (reviewed in Elmslie, 2001).

Neurones contain specific concentrations of several ions, i.e. potassium (K^+), sodium (Na^+), chloride (Cl^-) and calcium (Ca^{2+}). Higher K^+ concentrations are found in the intracellular space than in the extracellular space but the converse is true for Na^+, Cl^- and Ca^{2+}. Ion movements between intracellular and extracellular sides across the impermeable neuronal membrane occur through ion channels. These form selective pores that are either constitutively opened, e.g. leakage channels, or opened in response to a stimulus, e.g. voltage-gated or ligand-gated ion channels. Ion movements are driven by the ion concentration and electrical gradients. For example, K^+ flows towards the extracellular side and Na^+, Cl^-, Ca^{2+} flow intracellularly. At rest the membrane is relatively more permeable to K^+ through K^+ leakage channels and this contributes largely to the negative resting potential. In depolarised neurones, the membrane becomes more permeable to Na^+.

1.2.2. Generation and propagation of the action potential

At chemical synapses, the neuronal membrane is depolarised following ion movements through activated ligand-gated ionotropic ion channels such as AMPA receptors (see section 1.2.4). Membrane depolarisation results in activation of voltage-gated Na^+ and K^+ channels. Na^+ channels have faster activation and inactivation kinetics and thus they open first. K^+ channels open later during the closing phase of Na^+ channels. Following opening of voltage-gated Na^+ channels, Na^+ enters the cell. The increase in intracellular Na^+ concentration further enhances the initial depolarisation and additional voltage-gated Na^+ channels open (Figure 1.4). This positive feedback process goes on until a threshold depolarisation is reached leading to the AP (Figure 1.4). If the threshold potential is not reached, no AP is generated. This is the "all-or-nothing" principle. APs are usually generated at the axon hillock, also called, the initial segment. This region connects the cell body of a neurone to the axon. It is highly enriched in voltage-gated

Na^+ channels and it has a membrane potential close to threshold. Na^+ channels are closed and inactivated within milliseconds after their opening. At the same time, voltage-gated K^+ channels activated by the initial depolarisation open. This allows the exit of K^+ towards the extracellular side and the repolarisation of the neuronal membrane to the resting potential (Figure 1.4). The entry of Na^+ into the cell corresponds to the rising phase of the AP and the K^+ exit to its falling phase (Figure 1.4).

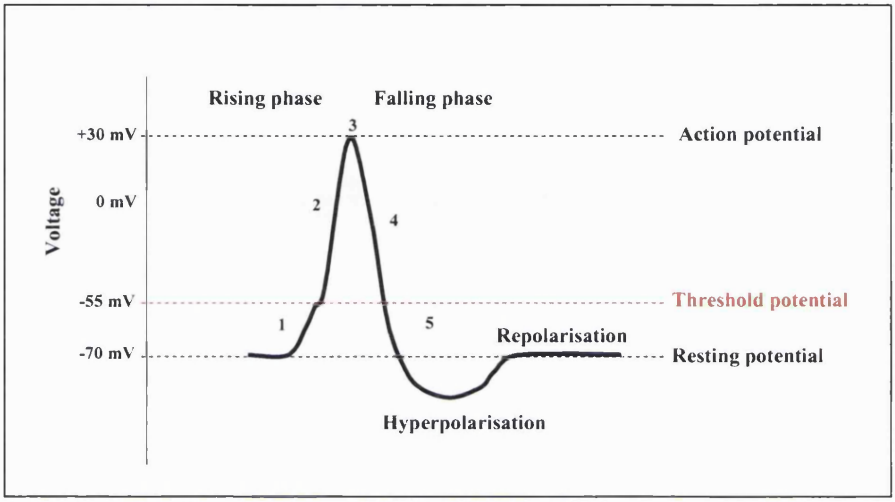

Figure 1.4. A schematic representation of an action potential. An action potential occurs when the neuronal membrane reaches a threshold potential. The Figure shows the 3 phases that characterise an action potential, i.e. rising phase, falling phase and hyperpolarisation. The numbers correspond to the opening state of voltage-gated Na^+ and K^+ channels during each of these phases as described hereafter. 1, Na^+ channels are opened, K^+ channels are closed; 2, more Na^+ channels are opened, K^+ channels are closed; 3, Na^+ channels are closed and K^+ channels are opened; 4, more K^+ channels are opened, Na^+ channels are closed; 5, Na^+ and K^+ channels are closed. Adapted from Elmslie, 2001.

APs propagate from the axon hillock down to the axon terminal by depolarising the axonal membrane and activating axonal voltage-gated Na^+ and K^+ channels in a positive feedback cycle similar to that described above. In the brain, many axons are covered by an insulating phospholipid layer, the myelin sheath, interrupted by myelin-free areas, the Ranvier nodes. Voltage-gated Na^+ channels are enriched in the Ranvier nodes, while voltage-gated K^+ channels are thought to be in the internodal regions (Elmslie, 2001). APs propagate by depolarising the membrane and activating voltage-gated Na^+ channels in the Ranvier nodes. This is known as saltatory propagation. In non-myelinated axons, the AP is conducted continuously via activation of voltage-dependent ion channels distributed uniformly along the membrane. Backward propagation of the AP from the axon to the cell body is prevented by the inability of inactivated Na^+ channels to re-

open immediately (refractory period). Arrival of the AP in the axon terminal, i.e. the presynaptic compartment, results in depolarisation of the presynaptic membrane and activation of voltage-gated Ca^{2+} channels. The subsequent entry of Ca^{2+} into the terminal triggers synaptic vesicle fusion with the presynaptic membrane and release of their contents, the neurotransmitters, into the synaptic cleft (reviewed in Martin, 2002).

1.2.3. Mechanisms of neurotransmitter release

Neurotransmitters are stored as packets or quanta inside synaptic vesicles. These are broadly divided into 2 different pools: a recycling pool which participates in synaptic transmission and a non-releasable pool which does not. The recycling pool contains a subset of vesicles forming the ready releasable pool docked at electron-dense regions, the active zones, close to voltage-gated Ca^{2+} channels (Figure 1.3) (reviewed in Zhai and Bellen, 2004). Docking and fusion of neurotransmitter-containing synaptic vesicles with the presynaptic membrane is mediated by proteins from the SNARE (soluble N-ethylmaleimide-sensitive factor attachment protein receptor) complex, i.e. synaptobrevin, SNAP25 (synaptosomal-associated protein of 25 kDa) and syntaxin. Synaptobrevin is localised to synaptic vesicles and it interacts with the plasma membrane proteins, syntaxin and SNAP25. Another protein, synaptotagmin I, is thought to behave as the Ca^{2+} sensor in the Ca^{2+}-dependent exocytosis of neurotransmitters. It is a transmembrane protein composed of 2 C2 Ca^{2+} binding domains and it is found on synaptic vesicles. It associates with syntaxin and SNAP25 in a Ca^{2+}-dependent manner (Martin, 2002) forming a complex that might be involved in the formation of the fusion pore for neurotransmitter secretion (Zhai and Bellen, 2004). Following exocytosis and diffusion into the synaptic cleft, neurotransmitters bind to and activate specific receptors in the postsynaptic membrane. Unbound transmitters are quickly removed from the synaptic cleft either by enzymatic degradation (acetylcholine) or by reuptake into the presynaptic compartment and into neighbouring glial cells.

1.2.4. Basic mechanisms of excitatory and inhibitory neurotransmissions

Neurotransmitters can be either excitatory or inhibitory. In the central nervous system, the main excitatory transmitter is glutamate while the major inhibitory transmitter is γ-aminobutyric acid (GABA). Glutamate binds to the ionotropic AMPA, NMDA or kainate receptors that are usually located at the surface of dendritic spines (Figure 1.3). Binding of glutamate to AMPA or kainate receptors results in the opening of the receptors. Subsequently Ca^{2+} and Na^{+} enter the cell whereas K^{+} moves towards the extracellular space. These ion movements result in depolarisation of the neuronal

membrane and in the generation of an excitatory postsynaptic potential (EPSP). This leads to the activation of voltage-gated Na^+ and K^+ channels as described in section 1.2.2. GABA binds to $GABA_A$ receptors located on dendritic or somatic membranes (Fritschy and Brunig, 2003). As described in section 1.3, $GABA_A$ receptors are Cl^--permeable. Activation of $GABA_A$ receptors by GABA results in entry of Cl^- into neurones. This leads to a hyperpolarisation of the postsynaptic membrane and to the generation of an inhibitory postsynaptic potential (IPSP). EPSPs and IPSPs are spatially and temporally summated by the postsynaptic neurone. If the summated PSP is above threshold an AP will be generated (section 1.2.2). This is the basis for excitatory neurotransmission. In contrast, in inhibitory neurotransmission, the summated PSP does not reach the threshold and no AP occurs.

1.3. MECHANISMS OF $GABA_A$ RECEPTOR TRAFFICKING IN NEURONES

As mentioned earlier, efficient synaptic transmission relies on the presence of neurotransmitter receptors at the surface of neurones. Multi-subunit neurotransmitter receptors are assembled in the endoplasmic reticulum (ER), modified in the Golgi apparatus and transported to the neuronal cell surface. This section describes the molecular mechanisms underlying the trafficking of γ-aminobutyric acid type A ($GABA_A$) receptors to and from the synapse, focussing on the role of $GABA_A$ receptor interacting proteins in the regulation of these events.

1.3.1. The $GABA_A$ receptors

$GABA_A$ receptors are belong to the Cys-Cys loop family of ligand-gated ion channels (LGIC). The LGIC superfamily also includes nicotinic acetylcholine (nACh) receptors, the 5-hydroxytryptamine 3 ($5\text{-}HT_3$) subclass of serotonin receptors, and the glycine receptors. Amino acid sequence comparisons showed that the LGIC superfamily was derived from a common ancestor (Ortells and Lunt, 1995). The $GABA_A$ and glycine receptors are inhibitory neurotransmitter receptors whereas the nACh and $5\text{-}HT_3$ receptors are excitatory receptors.

$GABA_A$ receptors mediate fast synaptic inhibition in the brain (for review, see Stephenson, 2001). They are chloride permeable channels activated by the binding of the neurotransmitter, GABA. $GABA_A$ receptors are of medical interest because of their sensitivity to benzodiazepines, barbiturates, neurosteroid and anaesthetics.

$GABA_A$ receptors are hetero-pentamers assembled from the combination of different subunits. A total of 7 $GABA_A$ receptor subunit classes, α, β, γ, δ, ε, θ and π, encoded by 16 different genes, have been identified in human brain (Schofield *et al.*, 1987; Lüscher and Keller, 2004). Each class contains several isoforms: α (1-6), β (1-3), γ (1-3). Additional β and γ isoforms (β4 and γ4) are found in chick brain (Lüscher and Keller, 2004). Further diversity is generated by alternative splicing. For example, the γ2 subunit is expressed as a short (γ2S) and as a long (γ2L) isoform, with γ2S lacking 8 amino acids in the intracellular loop (Whiting *et al.*, 1990). Amino acid sequences are conserved across subunit classes (30-40% amino acid identity) and within subunit classes (70% amino acid identity).

The $GABA_A$ receptor subunits have a similar structure: a large ~220 amino acid N-terminal domain, 4 transmembrane domains (TM1-TM4), a large intracellular loop between TM3-TM4 and a short extracellular C-terminal domain (Figure 1.5 A). The TM2 forms the lining of the pore. The N-terminal region contains consensus sequences for N-glycosylation and a 15 amino-acid Cys-Cys loop that is conserved within the LGIC superfamily. The intracellular loop contains consensus sequences for protein kinase A (PKA), protein kinase C (PKC) and tyrosine kinase. It is the most divergent region within subunit classes (Stephenson, 2001).

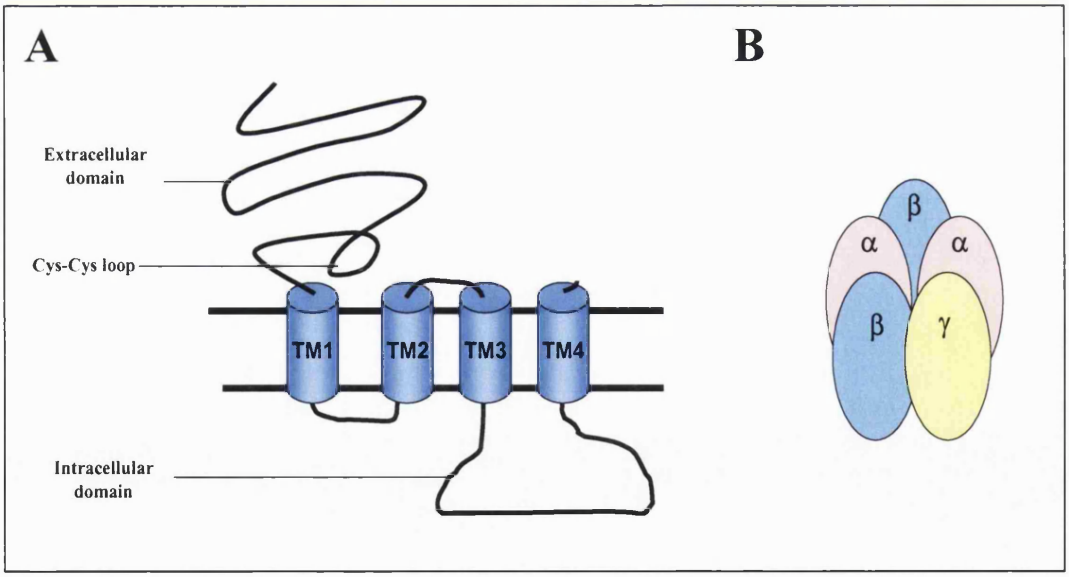

Figure 1.5. A schematic representation of a prototypic $GABA_A$ receptor subunit. A, a $GABA_A$ receptor subunit contains a large extracellular domain with a Cys-Cys loop, 4 TM domains and a short extracellular C-terminal domain. The large intracellular loop between TM3 and TM4 is the target of protein phosphorylation and it interacts with several cytoplasmic proteins. B, $GABA_A$ receptors are hetero-pentamers composed of 2 α, 2 β and 1 γ subunit.

The subunits are assembled as pentameric integral membrane receptors with pharmacological and electrophysiological properties differing according to the subunit composition (Sieghart, 2000). Further, the receptor distribution in the brain varies depending on the subunit subtypes (reviewed in Fritschy and Brünig, 2003). Immunofluorescence analysis using antibodies raised against the different $GABA_A$ receptor subunit isoforms and *in situ* hybridisation studies demonstrated that the β (1/2/3) subunits in combination with α (1/2/5) and/or γ2 are widely distributed throughout the brain (Fritschy *et al.*, 1992; Wisden *et al.*, 1992; Pirker *et al.*, 2000). Particularly, the α1β(2/3)γ2 combination is the most common $GABA_A$ receptor subtype found in brain. The $GABA_A$ receptor stoichiometry was determined as 2 α subunits, 2 β subunits and 1 γ subunit (Figure 1.5 B) (Tretter *et al.*, 1997; Farrar *et al.*, 1999). The GABA binding site is located at the interface between α and β subunits and the benzodiazepine binding site at the interface between the α and γ subunits (Stephenson, 2001).

1.3.2. Regulation of $GABA_A$ receptor cell surface expression by $GABA_A$ receptor associated proteins

Transport of $GABA_A$ receptors to synaptic sites and maintenance of inserted receptors at the neuronal cell surface are crucial for efficient synaptic inhibition. $GABA_A$ receptor associated proteins are thought to play an important role in the regulation of trafficking and clustering of $GABA_A$ receptors to the synapse (Kittler and Moss, 2003). Known $GABA_A$ receptor associated proteins are summarised in Table 1.2. Some of them are described in more detail below.

1.3.2.1. $GABA_A$ receptor clustering proteins

Maintenance of $GABA_A$ receptors at the postsynaptic membrane is thought to be mediated by the scaffolding proteins, gephyrin and dystrophin.

Gephyrin was initially co-purified with glycine receptors. It is a 93-kDa protein essential for glycine receptor postsynaptic localisation (reviewed in Lüscher and Keller, 2004). It also associates with the cytoskeletal protein tubulin and forms oligomers, thus gephyrin was proposed to function as a postsynaptic scaffold for glycine receptors. Gephyrin is also co-localised with $GABA_A$ receptors in brain (Craig *et al.*, 1996). Gephyrin was suggested to play a similar anchoring function for $GABA_A$ receptors. This was supported by the observation that $GABA_A$ receptor γ2 subunit knock-out mice showed a reduction in gephyrin expression at GABAergic synapses (Essrich *et al.*,

Interacting protein	Subunit specificity	Function	Reference
Gephyrin	Indirect interaction with γ2	Clustering of $GABA_A$ receptors at the synapse	Essrich *et al.*, 1998
Dystrophin associated complex	Not known	Stabilisation of $GABA_A$ receptors at the synapse	Knuesel *et al.*, 1999
GABARAP	γ2	Trafficking of $GABA_A$ receptors from the Golgi apparatus to the synaptic membrane	Wang *et al.*, 1999
AP2	β1-3, $\gamma2_{L-S}$ and δ	Regulation of $GABA_A$ receptor endocytosis	Kittler *et al.*, 2000a Kittler *et al.*, 2004a
GODZ	γ1-3	Targeting of $GABA_A$ receptors to the synaptic membrane	Keller *et al.*, 2004
BIG2	β1-3	Trafficking of $GABA_A$ receptors from the Golgi to the plasma membrane	Charych *et al.*, 2004
Plic1	α1-3, α6, β1-3	Regulation of $GABA_A$ receptor cell surface expression	Bedford *et al.*, 2001
HAP1	β1-3	Regulation of $GABA_A$ receptor cell surface expression	Kittler *et al.*, 2004b
GRIF-1	β2	Trafficking factor	Beck *et al.*, 2002
PKC	β1, β3	Modulation of receptor function	Brandon *et al.*, 1999
Receptor for activated C kinase-1 (RACK-1)	β1, α1	Facilitation of $GABA_A$ receptor phosphorylation by PKC	Brandon *et al.*, 1999
gC1q-R	β1-3	Modulation of receptor function	Schaerer *et al.*, 2001
A-kinase anchoring protein (AKAP) 79/150	β1, β3	Facilitation of $GABA_A$ receptor phosphorylation by PKA by targeting PKA to the receptor	Brandon *et al.*, 2003
PRIP-1, PRIP-2	β1-3	Regulation of $GABA_A$ receptor endocytosis by facilitating $GABA_A$ receptor dephosphorylation by PP1 or PP2A	Terunuma *et al.*, 2004 Kanematsu *et al.*, 2006
Dopamine D5 receptors	γ2	Cross-inhibition of $GABA_A$ receptor activity	Liu *et al.*, 2000
Glyceraldehyde-3-phosphate dehygrogenase	α1	Phosphorylation of $GABA_A$ receptors	Laschet *et al.*, 2004

Table 1.2. A summary of the known $GABA_A$ receptor associated proteins

1998). Conversely, disruption of gephyrin expression using antisense oligonucleotides resulted in a decrease in γ2 subunit-containing $GABA_A$ receptor localisation at postsynaptic sites (Essrich *et al.*, 1998). In agreement with this study, Lévi *et al.* (2004) showed that only reduced levels of γ2 subunit-containing $GABA_A$ receptors were expressed in hippocampal neurone cultures of gephyrin knock-out mice. Further, GABAergic electric activity could be recorded in these neurones. Therefore it was suggested that $GABA_A$ receptors could be clustered at postsynaptic membranes in a gephyrin-independent mechanism. Gephyrin was proposed to maintain those receptors that were already inserted in the postsynaptic membrane rather than promoting their insertion at these sites. No study has yet shown a direct interaction between gephyrin and $GABA_A$ receptors.

Dystrophin is found at GABAergic synapses, co-localised with $GABA_A$ receptors and gephyrin. Targeted disruption of dystrophin expression results in a reduction in the size and number of $GABA_A$ receptor clusters at the synapse. Therefore, dystrophin was suggested to be important for the stabilisation of $GABA_A$ receptors at the synapse although again as for gephyrin, a direct interaction between dystrophin and $GABA_A$ receptors has not been shown yet (Lüscher and Keller, 2004).

1.3.2.2. $GABA_A$ receptor trafficking to the cell surface

Several $GABA_A$ receptor-associated proteins involved in $GABA_A$ receptor trafficking processes were identified, mostly using the yeast two-hybrid system.

1.3.2.2.1. The $GABA_A$ receptor associated protein, GABARAP

GABARAP is a 17-kDa protein that was identified in a yeast two-hybrid screen using the intracellular loop (IL) of the $GABA_A$ receptor γ2 subunit (γ2-IL) as a bait. GABARAP interacts specifically with the γ2 subunit (Wang *et al.*, 1999). Association of GABARAP with the γ2 subunit is modulated by the phospholipase-C related inactive protein-1, PRIP-1, described in section 1.2.2.3 (Kanematsu *et al.*, 2002). GABARAP is a microtubule-associated protein (Wang *et al.*, 1999). It associates also with gephyrin *in vitro* and the trafficking protein, N-ethylmaleimide-sensitive factor (NSF) *in vitro* and *in vivo* (Kneussel *et al.*, 2000; Kittler *et al.*, 2001). In neurones, GABARAP is not co-localised with $GABA_A$ receptors and gephyrin at postsynaptic sites. Instead, GABARAP is found co-localised with the NSF to intracellular membranes including the Golgi apparatus in the soma. It was therefore suggested that GABARAP was involved in the transport of $GABA_A$ receptors from the Golgi to the plasma membrane

(Kittler *et al.*, 2001). Accordingly, overexpression of GABARAP in neurones led to an increase in $GABA_A$ receptor cell surface expression (Chen *et al.*, 2000; Leil *et al.*, 2004).

1.3.2.2.2. The adaptor protein 2 complex, AP2

$GABA_A$ receptors can be removed from the plasma membrane by endocytosis to be either recycled to the cell surface or degraded (Connolly *et al.*, 1999). $GABA_A$ receptor endocytosis is a clathrin-dependent mechanism requiring the multi-subunit adaptor protein 2 complex, AP2, and the GTPase, dynamin (Kittler *et al.*, 2000a). AP2 interacts specifically with the intracellular loops of $GABA_A$ receptor β1, β2, β3, $\gamma2_{L-S}$ and δ subunits in brain extracts (Kittler *et al.*, 2000a; Kittler *et al.*, 2004a; section 1.2.2.3). AP2 was proposed to facilitate the recruitment of $GABA_A$ receptors to clathrin-coated vesicles for the removal of receptors from the synaptic membrane.

1.3.2.2.3. The Golgi apparatus-specific protein with a DHHC zing finger domain, GODZ

The novel palmitoyltransferase, GODZ, was identified as a $GABA_A$ receptor γ2 subunit interacting protein using the SOS recruitment yeast two-hybrid system (see Chapter 5) (Keller *et al.*, 2004). Palmitoylation is a post-translational modification that regulates the cell surface expression and clustering of γ2 subunit-containing $GABA_A$ receptors in neurones (Rathenberg *et al.*, 2004). GODZ binds specifically to a 14-amino acid region that is conserved in all γ subunits but is absent from α and β subunits. This region contains 5 cysteine residues potentially modified by GODZ. Mutation of these residues to alanines resulted in a loss of synaptic γ2 subunit-containing $GABA_A$ receptor clusters in neurones (Rathenberg *et al.*, 2004). Therefore GODZ was proposed to be involved in the trafficking and clustering of $GABA_A$ receptors to the synapses.

1.3.2.2.4. The brefeldin A-inhibited GDP/GTP exchange factor 2, BIG2

BIG2 was identified as a $GABA_A$ receptor β3 subunit binding protein in a yeast two-hybrid screen using the $GABA_A$ receptor subunit β3-IL as a bait. BIG2 interacts also with the intracellular domain of $GABA_A$ receptor β1 and β2 subunits but not with α or γ subunits. BIG2 was proposed to promote the exit of assembled $GABA_A$ receptors from the ER and/or Golgi to the plasma membrane (Charych *et al.*, 2004).

1.3.2.2.5. The ubiquitin-like protein, Plic-1

Plic-1 was found to interact with the $GABA_A$ receptor α1-IL in a yeast two-hybrid screen (Bedford *et al.*, 2001). Plic-1 also associates with the intracellular loops of

$GABA_A$ receptor α2-α6 and β1-β3 subunits. In neurones, Plic-1 co-localises with $GABA_A$ receptors in intracellular compartments and at synaptic sites thereby suggesting a role for Plic-1 in $GABA_A$ receptor trafficking. Further, Plic-1 was shown to stabilise the $GABA_A$ receptor intracellular pools by preventing the degradation of internalised receptors by the proteasome.

1.3.2.2.6. The huntingtin-associated protein 1, HAP1

HAP1 was also isolated in a yeast two-hybrid screen using the $GABA_A$ receptor subunit β1-IL as a bait (Kittler *et al.*, 2004b). HAP1 can also interact with $GABA_A$ receptor subunits β2-IL and β3-IL *in vitro*. It co-localises with intracellular and cell surface γ2 subunit-containing $GABA_A$ receptors in dendrites and axons in neurones. When HAP1 is overexpressed in neurones, the proportion of endocytosed receptors degraded in lysosomes is decreased while the number of cell surface receptors is increased. Thus, HAP1 was proposed to play a role in $GABA_A$ receptor endocytosis by blocking degradation of internalised receptors and promoting their reinsertion in the plasma membrane. HAP1 is described in more detail in section 1.3.2.

1.3.2.3. $GABA_A$ receptor associated proteins and phosphorylation

$GABA_A$ receptor endocytosis is regulated by phosphorylation. Hence, $GABA_A$ receptor β and γ subunits harbor consensus sequences for phosphorylation by PKA, PKC and the tyrosine kinase, Src, within their intracellular domain (Kittler and Moss, 2003). Phosphorylation of a $GABA_A$ receptor subunit can interfere with its association with an associated protein and thus affect the receptor trafficking (e.g. Kittler *et al.*, 2004a). Alternatively, a $GABA_A$ receptor interacting protein can facilitate the phosphorylation/dephosphorylation of the receptor thereby modulating the receptor activity (e.g. Kanematsu *et al.*, 2006). Two examples are described hereafter (see also Table 1.2).

As explained earlier, association of AP2 with $GABA_A$ receptors is thought to facilitate clathrin-mediated endocytosis of cell surface $GABA_A$ receptors (Kittler *et al.*, 2000a). AP2 binds to residues 401-410 within the $GABA_A$ receptor β3-IL (Kittler *et al.*, 2004a). This region is highly conserved amongst β subunits and it contains 2 serine residues (Ser-408/Ser-409) phosphorylated by PKC and PKA *in vitro* and *in vivo* (Kittler and Moss, 2003). The affinity of AP2 for $GABA_A$ receptor β3 subunits was shown to be considerably reduced following phosphorylation of Ser-408/Ser-409 (Kittler *et al.*, 2004a). Further the number of cell surface receptors in neurones was increased

following following phosphorylation of the subunit. This was demonstrated by measuring $GABA_A$ receptor-mediated currents in the presence of phosphorylated or non-modified peptides mimicking the AP2-binding site on $GABA_A$ receptor β3 subunits (Kittler *et al.*, 2004a). Application of non-modified peptides resulted in an increase in $GABA_A$ receptor-mediated currents while phosphorylated peptides had no effect on these currents. This was because non-modified peptides competed with $GABA_A$ receptor β3 subunits for an interaction with AP2 thereby preventing the binding of $GABA_A$ receptors to AP2. This may have resulted in a reduction in receptor internalisation, thus in an increase in receptor cell surface number and thus in an increase in $GABA_A$ receptor-mediated currents. In contrast, phosphorylated peptide have a low affinity for AP2 and therefore they do not prevent the binding of the receptor to AP2. As a result the receptor endocytosis remained as in non-treated cells. Thus it was proposed that phosphorylation of $GABA_A$ receptor β3 subunits may regulate $GABA_A$ receptor endocytosis by modulating the interaction between the receptor and AP2.

The phospholipase-C related inactive protein-1, PRIP-1, was initially identified as a GABARAP associated proteins in a yeast two-hybrid screen using GABARAP as a bait (Kanematsu *et al.*, 2002). PRIP-1 associates with $GABA_A$ receptor β subunits and with protein phosphatases 1 and 2A, PP1 and PP2A (Terunuma *et al.*, 2004; Kanematsu *et al.*, 2006). Another PRIP isoform, PRIP-2 has been identified. Like PRIP-1, PRIP-2 interacts with GABARAP, $GABA_A$ receptor β subunits, PP1 and PP2A (Terunuma *et al.*, 2004; Kanematsu *et al.*, 2006). PRIP-1 co-localises with cell surface $GABA_A$ receptors in cortical neurones. Further PRIP-1 forms a complex with $GABA_A$ receptors and PP2A in brain as demonstrated by co-immunoprecipitation from brain extracts (Kanematsu *et al.*, 2006). PRIP-1 was shown to be necessary for the targeting of PP2A to $GABA_A$ receptors by using PRIP-1, PRIP-2 double knock-out mice. Dephosphorylation of $GABA_A$ receptors by PP2A is essential for $GABA_A$ receptor clathrin-dependent endocytosis. It was proposed that PRIP-1 and PRIP-2 were adaptor proteins linking $GABA_A$ receptors to PP2 and that PRIP proteins played a role in $GABA_A$ receptor clathrin-mediated endocytosis by modulating their phosphorylation state.

1.4. THE $GABA_A$ RECEPTOR INTERACTING FACTOR-1, GRIF-1

1.4.1. Identification and characterisation

$GABA_A$ receptor interacting factor-1, GRIF-1, was originally isolated from a rat brain cDNA library through its interaction with the intracellular loop of the $GABA_A$ receptor β2 subunit, β2-IL, in a yeast two-hybrid screen (Beck *et al.*, 2002). Initially, β2-IL was selected as a bait because $GABA_A$ receptor β2 subunits are highly expressed in brain, predominantly associated with $GABA_A$ receptor α1 and γ2 subunits (McKernan and Whiting, 1996; section 1.3). Further, $GABA_A$ receptor β2 subunits are crucial for the trafficking of α1β2γ2 $GABA_A$ receptor subtypes to the cell surface (Connolly *et al.*, 1996a). Lastly, the β2 subunit intracellular domain is exposed to cytoplasmic components during clustering and trafficking events.

GRIF-1 associates specifically with $GABA_A$ receptor β2-IL but not with $GABA_A$ receptor α1-IL, β1-IL, β3-IL, γ2-IL as demonstrated by yeast two-hybrid assays (Beck *et al.*, 2002). The interaction between GRIF-1 and β2-IL was of low affinity compared to a positive control used in the yeast two-hybrid assays. The association between GRIF-1 and $GABA_A$ receptor β2 subunits was confirmed by pull-down assays and also by immunoprecipitation experiments following transfection of HEK 293 cells with constructs encoding GRIF-1 and $GABA_A$ receptor β2 subunits. However *in vivo* evidence for this interaction is still lacking.

GRIF-1 is a 913 amino acid protein with a calculated M_r of 102 kDa and an isoelectric point of 5.14. GRIF-1 forms disulphide-bridge linked homodimers (G. Ojla, K. Brickley and F.A Stephenson, unpublished observations). GRIF-1 exists as 3 splice variants, GRIF-1a, GRIF-1b and GRIF-1c, that differ in their C-termini (Beck *et al.*, 2002; Iyer *et al.*, 2003a) (Table 1.3). GRIF-1a is the full length GRIF-1 and it is referred to as GRIF-1.

GRIF-1 isoform	Lenght (amino acids)	Missing GRIF-1a domain	Calculated M_r (kDa)	Tissue distribution	Reference
GRIF-1a	913	-	102	Forebrain, cerebellum, heart, skeletal muscle, testes	Beck *et al.*, 2002
GRIF-1b	672	673-913	88	Forebrain, heart, skeletal muscle	Beck *et al.*, 2002
GRIF1-c	848	620-688	98	Brain, heart, lung, smooth muscle tissue	Iyer *et al.*, 2003a

Table 1.3. A Table summarising the main features of GRIF-1 splice variants

As shown in Figure 1.6, GRIF-1 (GRIF-1a) is encoded by a gene containing 16 exons. GRIF-1b lacks exon 15 and part of exon 16 (Beck *et al.*, 2002). It is the shortest GRIF-1 splice variant with 672 amino acids and a predicted M_r of 80 kDa. GRIF-1c lacks exon 15 (Iyer *et al.*, 2003a). It is a 848 amino acid protein with a predicted M_r of 98 kDa. Analysis of GRIF-1 tissue distribution by immunoblotting using anti-GRIF-1_{8-633} antibodies revealed 2 immunoreactive bands with M_r ~ 115 kDa and 106 kDa in brain, heart and muscle showing that GRIF-1 is expressed exclusively in excitable tissues (Beck *et al.*, 2002). An immunoreactive band with M_r ~ 88 kDa detected in heart and muscle showed that GRIF-1b is expressed in these tissues. Only low levels of GRIF-1b were detected in brain. GRIF-1c was detected in brain, muscles, heart and lungs (Iyer *et al.*, 2003a).

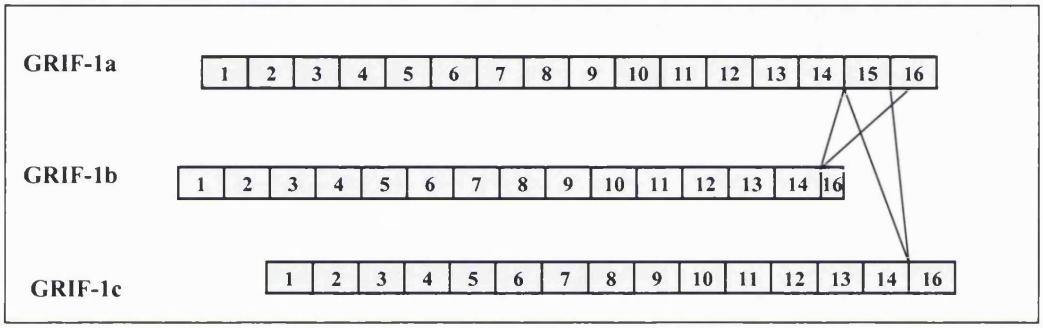

Figure 1.6. A representation of the genes encoding GRIF-1 splice variants. The gene encoding for GRIF-1 contains 16 exons. This gene encodes 3 splice variants: GRIF-1a (GRIF-1) is the full length isoform, GRIF-1b lacks exon 15 and part of exon 16, GRIF-1c lacks exon 15.

Bioinformatic analyses of the deduced amino acid sequence of GRIF-1 predicted 2 N-terminal coiled-coil domains at residues 133-188 and at residues 202-355 and a proline rich region at residues 756-793 (Beck *et al.*, 2002) (Figure 1.7). Phosphorylation consensus sequences for PKA (2 predicted sites, Ser-384 and Ser-726), PKC (16 predicted sites), tyrosine kinase (1 predicted site, Tyr-273) and casein kinase II (15 predicted sites) were also identified on GRIF-1 deduced amino acid sequence. Several predicted *O*-glycosylation sites were detected in the C-terminal domain of GRIF-1 (Iyer *et al.*, 2003a).

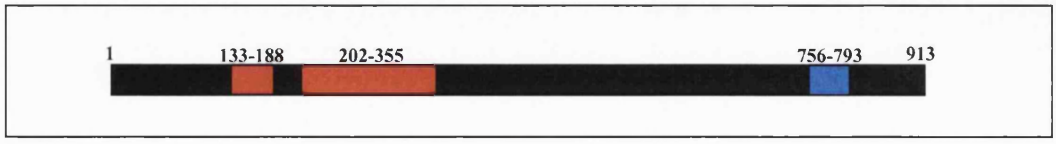

Figure 1.7. A schematic representation of GRIF-1. GRIF-1 contains 2 predicted N-terminal coiled-coil regions, an a proline rich C-terminal domain. , coiled-coil domain, , proline rich domain.

Sequence homologies searches using BLAST were carried out to identify proteins related to GRIF-1. GRIF-1 shares 88% amino acid similarity with the human protein of unknown function KIAA0549/ALS2CR3, the GRIF-1 human homologue (Hadano *et al.*, 2001). Like GRIF-1, KIAA0549/ALS2CR3 interacts with $GABA_A$ receptor β2-IL (Beck *et al.*, 2002). The gene encoding ALS2CR3 was mapped to chromosome 2q33-2q34, the juvenile amyotrophic lateral sclerosis critical region. However, there is no evidence for a role of ALS2CR3 in amyotrophic lateral sclerosis. GRIF-1 also has 60% amino acid similarity with the human protein KIAA1042 also known as β-*O*-linked *N*-acetylglucosamine transferase (OGT) interacting protein of 106 kDa (OIP106) (Iyer *et al.*, 2003a). OIP106 is the GRIF-1 human orthologue. It is described in section 1.3.2. GRIF-1 shares also 47% amino acid similarity over 848 residues with Milton, a *Drosophila* protein involved in mitochondrial transport to the synapse (Stowers *et al.*, 2002; section 1.4.2). Milton may be the GRIF-1 *Drosophila* orthologue. GRIF-1 has also 47% amino acid similarity over 306 amino acids with the rat protein, HAP1, a protein involved in intracellular trafficking processes (Li *et al.*, 1995; sections 1.1.5, 1.3.2 and 1.4.2). Based on its sequence homologies with the trafficking proteins, Milton and HAP1, and based on its association with $GABA_A$ receptor β2-IL, GRIF-1 was proposed to serve as a $GABA_A$ receptor trafficking protein (Beck *et al.*, 2002). As discussed in the next section (section 1.4.2), GRIF-1, OIP106, Milton and HAP1 are thought to be the members of a new family of coiled-coil proteins.

GRIF-1 interacting proteins other than $GABA_A$ receptor β2 subunits (Beck *et al.*, 2002) have been recently identified. Those are the molecular motor protein, kinesin-1, and the post-translational modification enzyme, OGT (Brickley *et al.*, 2005; Iyer *et al.*, 2003a; Pozo *et al.*, 2004). Because of its association with kinesin, GRIF-1 is also named trafficking protein, kinesin binding 2 (TRAK2), and because of its association with OGT, GRIF-1 is also named OIP98. GRIF-1 interacting proteins are described in section 1.3.3 and they are the focus point of this PhD thesis.

Table 1.4 summarises the nomenclature used to name GRIF-1 and its related proteins in the literature. In rat GRIF-1 is named OIP98 or GRIF-1. In human, GRIF-1 is referred to as ALS2CR3, humilt2 or TRAK2. In *Drosophila*, the name, Milton, is used to design the *Drosophila* GRIF-1 related protein. The GRIF-1 human orthologue is referred to as KIAA1042, humilt1 or TRAK1 in human and to as OIP106 in rat. In this PhD thesis, the names GRIF-1, OIP106 and Milton will be used.

Species	Nomenclature
Rattus norvegicus	GRIF-1 = OIP98
Homo sapiens	ALS2CR3 = humilt2= TRAK2
Drosophila melanogaster	Milton

Species	Nomenclature
Rattus norvegicus	OIP106
Homo sapiens	humilt1= TRAK1

Table 1.4. A summary of the GRIF-1 and OIP106 nomenclature in the litterature

1.4.2. GRIF-1 and the new family of coiled-coil proteins

Recent evidence suggests that GRIF-1, OIP106, Milton, and possibly HAP1 could belong to a new family of coiled-coil proteins involved in trafficking events (Figure 1.8) (Brickley *et al.*, 2005; Glater *et al.*, 2006). OIP106, Milton and HAP1 are described hereafter.

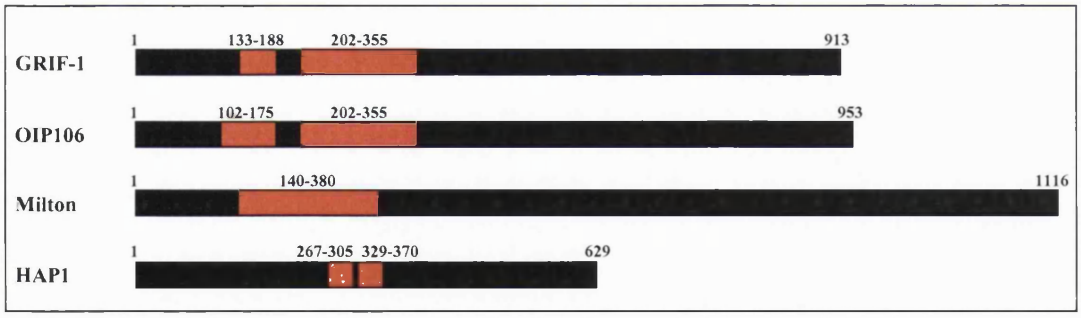

Figure 1.8. A schematic representation of GRIF-1 and the new family of coiled-coil proteins. GRIF-1, OIP106, Milton and HAP1 all have at least an N-terminal coiled-coil region. These proteins have high amino acid amino sequence similarities within their N-terminal coiled-coil regions. , coiled-coil domain.

1.4.2.1. The OGT-interacting protein of 106 kDa, OIP106

OIP106 is a 953 amino acid protein with 2 predicted N-terminal coiled-coil regions (residues 104-175 and 202-354). OIP106 and GRIF-1 share 76% amino acid similarity within their coiled-coil regions and therefore they were proposed to belong to the same family of coiled-coil proteins. OIP106 was named after its interaction with the post-translational modification enzyme, OGT (Iyer *et al.*, 2003a; section 1.4.3). OIP106 is

expressed in excitable and non-excitable tissues with a M_r ~ 115 kDa (Iyer *et al.*, 2003a; Brickley *et al.*, 2005). OIP106 is also expressed in the nucleus of Hela cells where it forms a complexe with RNA-polymerase II and OGT (Iyer *et al.*, 2003a). Therefore OIP106 was proposed to play a role in the regulation of transcription by targeting OGT to RNA-polymerase II for post-translational modification (Iyer *et al.*, 2003a). Interestingly, OIP106 is localised only in the cytoplasm in OIP106 transfected HEK 293 cells (Brickley *et al.*, 2005). Like GRIF-1, OIP106 associates with the molecular motor kinesin-1 in brain and it aggregates mitochondria in OIP106 transfected HEK 293 cells (Brickley *et al.*, 2005; section 1.4.4). OIP106 was recently reported to co-immunoprecipitate $GABA_A$ receptors from hypertonic, *hyrt*, mutant mice brainstem and spinal cord extracts by using antibodies directed against $GABA_A$ receptor α1 subunits (Gilbert *et al.*, 2006). Hypertonia is a condition characterised by limb stiffness. It may be caused by a deficit in $GABA_A$ receptor-mediated inhibition as suggested by the low levels of $GABA_A$ receptors found in brain and spinal cord of *hyrt* mice. The gene encoding OIP106 is mutated in *hyrt* mice. A 20-bp deletion in the last exon results in a premature stop codon at position 824. The mutation in OIP106 was proposed to affect $GABA_A$ receptor trafficking in *hyrt* mice brain and spinal cord (Gilbert *et al.*, 2006).

1.4.2.2. Milton

Milton was identified in a genetic mutation screen in *Drosophila* retina, searching for proteins involved in axons and synaptic terminals physiology (Stowers *et al.*, 2002). Milton is a 1116 amino acid protein with a predicted N-terminal coiled-coil domain (residues 140-380). The Milton coiled-coil region shares 55% amino acid similarity with the GRIF-1 coiled-coil regions. Milton has 4 isoforms that differ in their N-terminal domains (Glater *et al.*, 2006). Like GRIF-1 and OIP106, Milton associates with OGT (Glater *et* al., 2006). Several lines of evidence suggest that Milton is a kinesin-associated protein necessary for axonal transport of mitochondria in *Drosophila* neurones (Stowers *et al.*, 2002). First, Milton immunoprecipitates KHC from fly head extracts and it co-sediments with the mitochondrial marker cytochrome C on sucrose gradients of fly head extracts. Second, Milton co-localises with both KHC and mitochondria in peripheral nerve axons. In addition, overexpression of Milton in HEK 293 cells results in mitochondrial aggregation. Finally, in Milton mutants, mitochondria are found within the neuronal cell body. No mitochondria are seen within the axon or at the axon terminals (Stowers *et al.*, 2002; Gorska-Andrzejak *et al.*, 2003; Glater *et al.*, 2006; section 1.1.4). Binding of Milton to KHC and mitochondria is mediated via

different Milton domains (Glater *et al.*, 2006). The Milton N-terminal domain (residues 138-450) interacts with the KHC cargo binding domain (residues 810-891) while the Milton C-terminal region (residues 750-1116) is necessary for mitochondrial association. Milton is linked to mitochondria via the Rho-GTPase, dmiro (Guo *et al.*, 2005). Association of the Milton/dmiro/mitochondria complex to KHC does not require KLC as shown by immunoprecipitation and co-localisation experiments in African green monkey fibroblasts (Glater *et al.*, 2006).

1.4.2.3. The huntingtin-associated protein 1, HAP1

HAP1 was initially identified by a yeast two-hybrid screen searching for huntingtin-associated proteins (Li *et al.*, 1995; section 1.1.5). HAP1 is a 629 amino acid brain protein with 2 coiled-coil domains (residues 267-305 and 329-370). HAP1 shares 56% amino acid similarity with the GRIF-1 coiled-coil regions. In rat brain HAP1 exits as 2 splice variants, HAP1-A and HAP1-B, that differ in their C-terminal regions (Li *et al.*, 1995). In humans, a single HAP1 isoform, similar to the rat HAP1-A, is expressed.

HAP-1 interacts with the KLCs of the anterograde motor, kinesin-1 (McGuire *et al.*, 2006) and with dynactin/p150^{Glued}, a protein associated with the retrograde motor, dynein (Engelender *et al.*, 1997). HAP1 is involved in intracellular trafficking of BDNF and in $GABA_A$ receptor endocytosis (sections 1.1.5 and 1.4.2.2; Gauthier *et al.*, 2004; Kittler *et al.*, 2004b). HAP1 may play an important role in neuronal development as it promotes neurite outgrowth (McGuire *et al.*, 2006; Rong *et al.*, 2006). HAP1 may also be involved in intracellular signalling as it binds to the Rho-GTPase, Duo (Colomer *et al.*, 1997) and to the type 1 inositol (1,4,5)-triphosphate calcium release receptor in brain (Tang *et al.*, 2003).

1.4.3. GRIF-1 interacting proteins

1.4.3.1. $GABA_A$ receptor β2 subunits

As described in section 1.3.1, GRIF-1 was originally identified by virtue of its interaction with $GABA_A$ receptor subunit β2-ILs in a yeast two-hybrid screen (Beck *et al.*, 2002; section 1.3.1). The GRIF-1/β2-IL binding sites were mapped by yeast two-hybrid interaction assays (Beck *et al.*, 2002). The N-terminal GRIF-1 coiled-coil region (residues 124-283) was shown to be the minimal β2 subunit interacting site on GRIF-1. The $GABA_A$ receptor β2 subunit domain between residues 324-394 (Ymer *et al.*, 1989) was found to be the minimal GRIF-1 binding domain on β2-ILs. As mentioned in

section 1.4.1, GRIF-1/$GABA_A$ receptor β2 subunit interactions have been substantiated *in vitro* but not *in vivo*. This will be discussed in detail in Chapter 3.

1.4.3.2. OGT

OGT and *N*-acetyl-β-D-glucosaminidase are post-translational modification enzymes. They catalyse the addition and removal of *N*-acetylglucosamine (O-GlcNAc) moities to serine and threonine residues of nuclear and cytoplasmic proteins (Wells *et al.*, 2001). O-GlcNAc is a dynamic and reversible post-translational modification similar to phosphorylation. It regulates the function of a wide range of proteins such as neurofilaments, transcription factors or cell adhesion molecules (Iyer and Hart, 2003). OGT acts reciprocally to kinases by modifying the same, or adjacent, serine/threonine residues as kinases. This is the so-called "YinOYang" relationship, i.e. a residue is either phosphorylated or *O*-glycosylated. OGT has been proposed to participate in signal transduction events by modulating the phosphorylation state of proteins (Wells *et al.*, 2001).

OGT is encoded by a single gene mapped to chromosome X that is essential for cell survival (Shafi *et al.*, 2000). This gene encodes 2 OGT splice variants, nucleocytoplasmic OGT (ncOGT) and mitochondrial OGT (mOGT), that differ by their size, structure, cellular location and activity levels (Kreppel *et al.*, 1997; Lubas *et al.*, 1997; Love *et al.*, 2003; Chapter 4). In brain, ncOGT is a homodimer or homotrimer formed by 3 catalytic subunits of 110 kDa (Kreppel *et al.*, 1999). Each subunit is composed of 11.5 N-terminal tetratricopeptide repeats (TPRs) and a C-terminal catalytic domain (Haltiwanger *et al.*, 1992). mOGT is an homodimer or homotrimer of a 103-kDa subunit. Each subunit contains an N-terminal mitochondrial targeting sequence, 9 N-terminal TPRs and a C-terminal catalytic domain (Love *et al.*, 2003). As mentioned in section 1.1.3.1, TPRs mediate protein/protein interactions. They facilitate OGT di- or trimerisation state and OGT/substrate interactions (Kreppel *et al.*, 1999). It is thought that additional proteins may regulate the association of OGT with its substrates. OGT is post-translationally modified by *O*-glycosylation and tyrosine phosphorylation but the functional significance of these modifications is not known (Kreppel *et al.*, 1997). OGT activity is regulated by the local concentration of uridine diphosphate-*N*-GlcNAc, the donor sugar of GlcNAc (Kreppel *et al.*, 1999).

OGT forms stable complexes with GRIF-1 and OIP106 *in vitro* and *in vivo* (Iyer *et al.*, 2003a; Pozo *et al.*, 2004; Chapter 4). GRIF-1/OGT and OIP106/OGT interactions were discovered in a yeast two-hybrid screen searching for OGT regulatory proteins (Iyer *et*

al., 2003a). GRIF-1 and OIP106 binding site were mapped to the N-terminal TRPs of OGT (residues 11-463) (Iyer *et al.*, 2003a; Iyer *et al.*, 2003b). GRIF-1 and OIP106 can also be *O*-glycosylated by OGT (Iyer *et al.*, 2003a). It was proposed that GRIF-1 and OIP106 could target OGT to its substrate in different intracellular compartments, thereby regulating OGT function. The functional significance of GRIF-1/OGT complexes is discussed in Chapters 4 and 6.

1.4.3.3. Kinesin-1 heavy chains, KIF5s

Recently, GRIF-1 and OIP106 were shown to associate with the human kinesin-1 heavy chains, the KIF5s (Brickley *et al.*, 2005). As described in section 1.2, kinesin-1 proteins are molecular motors consisting of 2 KHCs, the KIF5s, and 2 KLCs (Figure 1.2 C). They transport cargoes such as organelles, mRNAs and neurotransmitter receptors anterogradely along microtubules (section 1.2; Table 1.1). As mentioned in section 1.2, 3 different KIF5s isoforms have been identified in mouse brain, KIF5A, KIF5B and KIF5C. KIF5A and KIF5B are pan-neuronal isoforms whereas KIF5C is expressed only in motor neurones (Kanai *et al.*, 2000). KIF5B is also present in non-neuronal tissues. The KIF5 isoforms show a high degree of amino acid sequence homologies over their N-terminal motor domain and their C-terminal cargo-binding domain (Kanai *et al.*, 2000). Knock-down studies suggested a specific role for KIF5B in mitochondrial transport (Tanaka *et al.*, 1998; section 1.1.4). Indeed, disruption of KIF5B gene expression was lethal and analyses of extra-embryonic KIF5B mutant cells showed an abnormal perinuclear mitochondrial distribution in these cells (Tanaka *et al.*, 1998). This phenotype could be rescued by overexpressing KIF5A or KIF5C, thus suggesting a redundancy in the 3 isoform functions (Kanai *et al.*, 2000). Depletion of KIF5C expression is not lethal but it results in a decrease in brain size and in the number of motor neurones (Kanai *et al.*, 2000).

The GRIF-1 *Drosophila* orthologue, Milton, was proposed to be a kinesin-1-associated protein, although no direct interaction between Milton and kinesin-1 was demonstrated (Stowers *et al.*, 2002). Thus it was tested whether GRIF-1 could interact with kinesin-1 (Brickley *et al.*, 2005). In brain, GRIF-1 immunoprecipitated KIF5A. In GRIF-1-transfected HEK 293 cells, GRIF-1 immunoprecipitated endogenous KIF5B. Finally, GRIF-1 immunoprecipitated KIF5C following exogenous expression of GRIF-1 and KIF5C in HEK 293 cells. The GRIF-1/KIF5C interaction was direct as shown by yeast two-hybrid studies and the GRIF-1 binding domain on KIF5C was mapped to GRIF-1 residues 124-283. Thus GRIF-1 could associate with the 3 KIF5 isoforms. In the same

study, OIP106 was shown to associate with KIF5A, KIF5B and KIF5C in a manner similar to GRIF-1. However, yeast two-hybrid studies revealed that the OIP106/KIF5C interaction was not direct (Brickley *et al.*, 2005).

1.5. AIMS OF THE THESIS

As described above, transport of synaptic proteins, $GABA_A$ receptors and organelles to the correct location within neurones are regulated by several mechanisms. GRIF-1 was proposed to participate in these regulatory events by acting as a trafficking factor (Beck *et al.*, 2002). The general objective of this thesis was to delineate the function of GRIF-1 in intracellular transport processes. The first aim was to characterise further the interactions between GRIF-1 and the $GABA_A$ receptor β2 subunits and between GRIF-1 and the molecular motor, kinesin-1. This was achieved using a confocal microscopy approach. The second aim was to analyse a partial cDNA encoding a putative GRIF-1 interactor. The third aim of the thesis was to investigate the potential use of the CytoTrap® yeast two-hybrid system to identify new GRIF-1 binding partners.

CHAPTER 2

MATERIAL AND METHODS

2.1. MATERIALS

2.1.1. Materials

Polyethylene glycol (PEG) mwt-8000 and 3500, dimethylsulphoxide (DMSO), dimethyl formamide (DMF), ethidium bromide, lithium acetate, DNA sodium salt from salmon testes, D(+)-galactose, D(+)-raffinose, L-isoleucine, L-valine, L-adenine hemisulphate salt, L-arginine HCl, L-histidine HCl monohydrate, L-leucine, L-lysine HCl, L-methionine, L-phenylalanine, L-threonine, L-tryptophan, L-tyrosine, L-uracil, L-glutamic acid, L-aspartic acid, L-serine, poly D-lysine hydrobromide, DL-lysine, β-mercaptoethanol, ampicillin, kanamycin, chloramphenicol, benzamidine, bacitracin, soybean trypsin inhibitor, chicken egg trypsin inhibitor, phenylmethylsulphonyl fluoride (PMSF), 4-(2-hydroxyethyl)-1-piperazineethanesulfonic acid (HEPES), ethylene glycol bis(2-aminoethyl ether)-N,N,N'N'-tetraacetic acid (EGTA), 4-hydroxycinnamic acid (p-coumaric acid), 5-amino-2, 3-dihydro-1, 4-phthalazedinedione (luminol), sodium dodecyl sulphate (SDS), Tween-20, Triton X-100, protein-A Sepharose, protein-G Sepharose, bovine serum albumin (BSA), goat serum, foetal bovine serum, Dulbecco's Modified Eagle Medium/Nutrient F-12 Ham powder (DMEM/F-12), Hank's balanced salt solution (Hbss), sodium bicarbonate solution, trypsin-ethylenediaminetetraacetic acid (EDTA), Hispeed Plasmid Maxi preparation kit were purchased from SIGMA-Aldrich Company Ltd. (Poole, UK). Penicillin/streptomycin, Luria-Bertani (LB) broth, agar, *Taq* DNA polymerase and seeblue prestained protein standards were purchased from Invitrogen (Paisley, UK). DNA molecular weight markers and restriction enzymes were purchased from MBI Fermentas (Tyne and Wear, UK). *Pfu* DNA polymerase, deoxynucleotides (dATP, dCTP, dGTP, dTTP) were purchased from Promega (Southampton, UK). Shrimp alkaline phosphatase (SAP) and nitrocellulose membranes were from Amersham Pharmacia Biotech Ltd. (Buckinghamshire, UK). Protogel, N,N,N',N'-tetramethylethylenediamine (TEMED) and ammonium persulphate were from National Diagnostics (Hessle, UK). Bio-Rad Protein Assay was purchased from Bio-Rad Laboratories Ltd. (Hertfordshire, UK). Yeast extract, 5-bromo-4-chloro-3-indolyl-β-D-galactopyranoside (X-GAL), isopropyl-β-D-thiogalactopyranoside (IPTG) and dithiothreitol (DTT) were from Melford Laboratories Ltd. (Ipswich, UK). Bacto peptone, yeast nitrogen base without amino acids and yeast dropout supplements were from BD Biosciences-Clontech (California, USA). D(+)-glucose, agarose, ammonium sulphate, magnesium chloride, magnesium sulphate, Tris(hydroxymethyl)methylamine

(Tris-base), sodium acetate, sodium chloride, sodium hydrogen phosphate, ethanol, methanol, isopropyl alcohol, microscope slides and cover glasses were from VWR International Ltd. (Poole, Dorset, UK), mounting solution CFPVOH and anti-fading agent AF100 were from CitiFluor ltd. (Leicester, UK) and clear nail vanish was from Maybelline (Boots, London, UK). The CytoTrap® vector kit and the QuikChange® site-directed mutagenesis kit were purchased from Stratagene (Amsterdam, Netherlands). The gel extraction and PCR purification kits were purchased from QIAgen (West Sussex, UK).

2.1.2. Bacteria and yeast genotypes

The yeast strains, *S.cerevisae* cdc25Hα (MATα, ura3-52, his3-200, ade2-101, lys2-801, trp1-901, leu2-3, 112cdc25-2, Gal+) (Stratagene) and AH109 (MATα, trp 1-901, leu2-3, 112, ura3-52, his3-200, gal4Δ, gal80Δ, LYS2 : : GAL1 $_{UAS}$ -GAL1$_{TATA}$-HIS3, GAL2$_{UAS}$-GAL2$_{TATA}$-ADE2, URA : : MEL1$_{UAS}$-MEL1$_{TATA}$-lacZ) (BD Biosciences-Clontech), were used to perform yeast two-hybrid assays. The bacteria strains, *E.coli* XL1-Blue (endA1, gyrA96(nal^R), thi-1, recA1, relA1, lac, glnV44, F'[::Tn10 proAB$^+$ lacI^q Δ(lacZ)M15] hsdR17(r_K^- m_K^+) (Stratagene), was used in mutagenesis experiments and *E.coli* DH5α (supE44, delta lac U169 (phi 80 lacZ delta M15), hsdR17, recA1, endA1, gyrA96, thi-1, relA1, hsdR17(r_K^- m_K^+), F$^-$), was used in all other experiments involving the use of bacteria.

2.1.3. Mammalian cell lines

Human embryonic kidney cells (HEK) 293 were from the European Cell Culture collection. Transformed African green monkey kidney fibroblasts (COS-7 cells) were a gift from Dr. Andrew Stoker (Institute of Child Health, UCL, London, UK).

2.1.4. Cloning vectors and plasmids

Cloning vectors and constructs used in this PhD thesis are described in Tables 2.1-2.4.

2.1.5. Oligonucleotide primers

Oligonucleotide primers were purchased from Sigma-Proligo (Paris, France). The sequences of the primers used for polymerase chain reaction (PCR) amplification, mutagenesis and nucleotide sequencing of defined constructs are described in Table 2.5. Oligonucleotide primers used for PCR and sequencing were of basic grade. For mutagenesis, oligonucleotide primers were always HPLC purified by the manufacturer.

Table 2.1. A summary of the yeast expression cloning vectors and yeast control plasmids used for yeast two-hybrid studies

Cloning vector	Description*	Supplier#	Size (kb)
pGAD10	ADH 1 promoter, AD, LEU2, AMP	BD Biosciences-Clontech	6.7
pGBKT7	ADH 1 promoter, DNA-BD, TRP1, KAN	BD Biosciences-Clontech	7.3
pVA3-1	ADH 1 promoter, DNA-BD, murine p53 protein,TRP1, KAN	BD Biosciences-Clontech	9.4
pTD1-1	ADH 1 promoter, AD, SV40 large T-antigen, LEU2, AMP	BD Biosciences-Clontech	10.0
pSos	ADH 1 promoter, human SOS protein ($hSOS_{1-1067}$), LEU2, Amp^r	Stratagene	11.3
pMyr	GAL 1 promoter, *src* myristylation signal, URA3, CAM	Stratagene	5.6
pSos-MAFB	ADH 1 promoter, $hSOS_{1-1067}$, full length MAFB protein, LEU2, AMP	Stratagene	12.0
pMyr-MAFB	GAL 1 promoter, *src* myristylation signal, full length MAFB protein, URA3, CAM	Stratagene	6.9
pSos-Col I	ADH 1 promoter, $hSOS_{1-1067}$, murine 72 kDa type IV $collagenase_{148-357}$, LEU2, AMP	Stratagene	11.9
pMyr-LaminC	GAL 1 promoter, *src* myristylation signal, human lamin C_{67-230}, URA3, CAM	Stratagene	6.5
pMyr-SB	GAL 1 promoter, *src* myristylation signal, Sos-binding protein, URA3, CAM	Stratagene	7.2

*ADH 1, alcohol dehydrogenase 1; AD, activation domain ; LEU2, leucine auxotrophy gene; DNA-BD, DNA binding domain; TRP1, tryptophan auxotrophy gene; URA3, leucine auxotrophy gene; AMP, ampicillin resistance; KAN, kanamycin resistance; CAM, chloramphenicol resistance.

Table 2.2. A summary of the yeast expression constructs that were generated and used for yeast two-hybrid studies

Vector	Description*	Source	Size (kb)
pGAD10-mOGT$_{40-374}$	ADH 1 promoter, AD, mOGT$_{40-374}$, LEU2, AMP	Matchmaker rat brain cDNA library	7.6
pGBKT7-GRIF-1 $_{545-913}$	ADH 1 promoter, DNA-BD, GRIF-1$_{545-913}$, TRP1, KAN	Mike Beck	8.4
pSos-GRIF-1$_{1-913}$	ADH 1 promoter, hSOS$_{1-1067}$, GRIF-1$_{1-913}$, LEU2, AMP	Karine Pozo	13.9
pMyr-GRIF-1$_{1-913}$	GAL 1 promoter, *src* myristylation signal, GRIF-1$_{1-913}$, URA3, CAM	Karine Pozo	8.7
pMyr-β2-IL$_{303-427}$	GAL 1 promoter, *src* myristylation signal, GABA$_A$ Receptor β2 subunit$_{303-427}$, URA3, CAM	Karine Pozo	6.4

*ADH 1, alcohol dehydrogenase 1; AD, activation domain; LEU2, leucine auxotrophy gene; DNA-BD, DNA binding domain; TRP1, tryptophan auxotrophy gene; URA3, leucine auxotrophy gene; AMP, ampicillin resistance; KAN, kanamycin resistance; CAM, chloramphenicol resistance.

Table 2.3. A summary of the mammalian expression cloning vectors used

Cloning vector	Description*	Supplier	Size (kb)
pCIS	CMV promoter, AMP	A gift from Genentech Inc. (CA, USA)	4.4
pCMVTag4a	CMV promoter, C-terminal FLAG-tag, KAN	Stratagene	4.3
pcDNA4HisMax	CMV promoter, N-terminal His-tag, Xpress epitope, entero-kinase recognition site, AMP	Invitrogen	5.3
pEYFP-C1	CMV promoter, EYFP, KAN	BD Biosciences-Clontech	4.7
pECFP-C1	CMV promoter, ECFP, KAN	BD Biosciences-Clontech	4.7

* CMV, cytomegalovirus; AMP, ampicillin resistance; KAN, kanamycin resistance; EYFP, enhanced yellow fluorescent protein; ECFP, enhanced cyan fluorescent protein.

Table 2.4. A summary of the mammalian expression constructs generated and used

Cloning vector	Description*	Supplier#	Size (kb)
pCIS-GRIF-1	CMV promoter, GRIF-$1_{1\text{-}913}$, AMP	K. Brickley	7.8
pCMVTag4a-GRIF-1	CMV promoter, GRIF-$1_{1\text{-}913}$, FLAG, KAN	M. Beck	7.0
pEYFP-GRIF-1	CMV promoter, EYFP, GRIF-$1_{1\text{-}913}$, KAN	A.M. Salgueiro	7.7
pECFP-GRIF-1	CMV promoter, ECFP, GRIF-$1_{1\text{-}913}$, KAN	A.M. Salgueiro	7.7
pcDNAHisMax-KIF5C	CMV promoter, His-tag, Xpress epitope, entero-kinase recognition site, $KIF5C_{1\text{-}957}$, AMP	K. Brickley	8.1
pCMVmycKIF5C-MD	CMV promoter, c-myc epitope, $KIF5C_{1\text{-}335}$, KAN	M.J. Smith	5.3
pCMVmycKIF5C-NMD	CMV promoter, c-myc epitope, $KIF5C_{336\text{-}957}$, KAN	M.J. Smith	7.1
pCMVmycKLC	CMV promoter, c-myc epitope, KLC, KAN	M.J. Smith	4.8
pN-EYFP-KIF5C	CMV promoter, EYFP, $KIF5C_{1\text{-}957}$, KAN	A.M. Salgueiro	7.6
pC-EYFP-KIF5C	CMV promoter, $KIF5C_{1\text{-}957}$, EYFP, KAN	K. Pozo	7.6
pN-ECFP-KIF5C	CMV promoter, ECFP, $KIF5C_{1\text{-}957}$, KAN^r	K. Pozo	7.6
pC-ECFP-KIF5C	CMV promoter, $KIF5C_{1\text{-}957}$, ECFP, KAN	K. Pozo	7.6
pEYFP-KIF5C-MD	CMV promoter, EYFP, $KIF5C_{1\text{-}335}$, KAN	K. Pozo	5.7
pEYFP-KIF5C-NMD	CMV promoter, $KIF5C_{336\text{-}957}$, EYFP, KAN	K. Pozo	7.3
pCIS-$GABA_AR$-$\beta2^{EYFP}$	CMV promoter, $GABA_AR$-β2 subunit, EYFP, AMP^r	K. Pozo	6.9
pCIS-$GABA_AR$-β2	CMV promoter, rat $GABA_AR$-β2 subunit, AMP	K. Brickley	6.2
pCIS-$GABA_AR$-γ2	CMV promoter, rat $GABA_AR$-γ2 subunit, AMP	K. Brickley	6.3
pcDM8-$GABA_AR$-α1	CMV promoter, bovine $GABA_AR$-α1 subunit, AMP	Not known	6.7

pcDNAHisMax-mOGT$_{40-374}$	CMV promoter, His-tag, Xpress epitope, entero-kinase recognition site, mOGT$_{40-374}$, AMP	K. Pozo	6.3
pCMVTag4a-OGT	CMV promoter, OGT$_{1-1067}$, C-terminal FLAG-tag, KAN	K. Pozo	7.4
pEYFP-OGT	CMV promoter, EYFP, OGT$_{1-1067}$, KAN	K. Pozo	7.8
pECFP-EYFP	CMV promoter, ECFP, EYFP, KAN	A gift from Dr. L. He (National Institute of Health, Bethesda, USA)	5.4
pECFP-ER	CMV promoter, ECFP, KDEL sequence, KAN	BD Biosciences-Clontech	4.8
pDsRed1-Mito	CMV promoter, DsRed1, human cytochrome C oxidase$_{1-29}$, KAN	A gift from Dr. R.J. Harvey (School of Pharmacy, London, UK)	4.8
pShuttle-OGT	CMV promoter, OGT$_{1-1067}$, KAN	A gift from Dr. G.W. Hart (John Hopkins University, Baltimore, USA)	7.2

* CMV, cytomegalovirus; AMP, ampicillin resistance; KAN, kanamycin resistance; EYFP, enhanced yellow fluorescent protein; ECFP, enhanced cyan fluorescent protein.
# All constructs were generated in house or were a gift from other laboratories. The source indicates the name of the person who generated the construct.

Table 2.5. Oligonucleotide primer sequences used for nucleotide sequencing and PCR amplification of DNA

Name	Sequence
pGAD10 forward sequencing primer	5'-CAGTTGAAGTGAACTTGCGGGG-3'
11(1) cDNA forward sequencing primer 1	5'-GGCTCATTGCCTACAGATTGTC-3'
11(1) cDNA forward sequencing primer 2	5'-GCCTCATTTCCCTGATGCATAC-3'
11(1) cDNA forward sequencing primer 3	5'-GCAACCTGGCTTGTGTGTAC-3'
11(1) cDNA forward sequencing primer 4	5'-GGCTTCCATTCACAAGGATTCAGG-3'
11(1) cDNA forward sequencing primer 5	5'-GGAGATGCAGGATGTTCAGG-3'
pCMV4A forward sequencing primer	5'-CGGTGGGAGGTCTATATAAGC-3'
pCMV4A reverse sequencing primer	5'-CGACTCACTATAGGGCGAATTG-3'
pSos forward sequencing primer	5'-CCAAGACCAGGTACCATG-3'
pMyr forward sequencing primer	5'-ACTACTAGCAGCTGTAATAC-3'

pcDNAHisMax forward sequencing primer	5'-TAGCATGACTGGTGGACAGC-3'
pEYFP-C1 sequencing primer	5'-TACCAGCAGGAGGTGGATCGTATCAA-3'
pEYFP-C1 sequencing primer 2	5'-CATGGTCCTGCTGGAGTTCGTG-3'
$GABA_AR$-$\beta2^{EYFP}$ subunit sequencing primer	5'-ACTGTCCTGACGATGACCACAATC-3'
GRIF1/*EcoRI* forward primer	5'-TATA**GAATTC**ATGAGTCTGTCCCAG-3'
GRIF1/*SalI* reverse primer	5'-TATA**GTCGAC**TCAGTCTTCCTTCAGGATAC-3'
GRIF1/*BamH1* forward primer	5'-CGC**GGATCC**CGATGAGTCTGTCCCAG-3'
GRIF1/*NotI* reverse primer	5'-ATTT**GCGGCCGC**TCAGTCTTCCTTCAGG-3'
$GABA_AR$-β2 subunit/*SalI* reverse primer	5'-ATA**GTCGAC**CCGATCAATGGCGTTCACATC-3'
$GABA_AR$-β2 subunit/*EcoRI* forward primer	5'-T**GAATTC**GTCAACTACATCTTCTTTGGGAG-3'
$GABA_AR$-β2 subunit/*BamH1* forward primer	5'-CGC**GGATCC**CGGTCAACTACATCTTCTTT-3'
$GABA_AR$-β2subunit/*NotI* reverse primer	5'-ATTT**GCGGCCGC**CCGATCAATGGCGTTCAC-3'
EYFP/*BssHII* forward primer	5'-TTT**GGCGCGCC**ATGGTGAGCAAGGGCGAGG-3'
EYFP/*BssHII* reverse primer	5'-TT**GGCGCGCC**CCTTGTACAGCTCGTCCATG-3'
KIF5c/*EcoRI* forward primer	5'-TTAT**GAATTC**TATGGCGGATCCAGCCGA-3'
KIF5c/*SalI* reverse primer	5'-TCTA**GTCGAC**CCTTTCTGGTAGTGAGTGG-3'
KIF5c/*NheI* forward primer	5'-TCTA**GCTAGC**TATGGCGGATCCAGCC-3'
KIF5c/*NheI* reverse primer	5'-TCTA**GCTAGC**CCTTTCTGGTAGTGAGTGG-3'
KIF5cNMD/*NheI* forward primer	5'-GCC**GCTAGC**CATGGAACTGACAGCAGAAG-3'
KIF5cMD/*XhoI* forward primer	5'-CCG**CTCGAG**GGATGGCGGATCCAGCCGAAT-3'
KIF5cMD/*EcoRI* reverse primer	5'-CCG**GAATTC**TTATAGGTTCACAGAGACTGT-3'
EYFP/*NotI* forward primer	5'-ATTT**GCGGCCGC**TATGGTGAGCAAGGGCG-3'
EYFP/*EcoRI* reverse primer	5'-TTT**GAATTC**TCACTTGTACAGCTCGTCC-3'
OGT/*BamHI* forward primer	5'-TATA**GGATCC**ATGGCGTCTTCCGTGGGCAA-3'
OGT/*EcoRV* reverse primer	5'-ATA**GATATC**GGCTGACTCAGTGACTTCAAC-3'
OGT/*HindIII* forward primer	5'-CCC**AAGCTT**CCATGGCGTCTTCCGTGGGCA-3'
OGT/*BamHI* reverse primer	5'-CGC**GGATCC**TCAGGCTGACTCAGTGACTTC-3'
$GABA_AR$-β2 subunit C1012G mutagenic forward primer	5'-GAGGACCCCAGCGCGAAAAGAAAGCAGCTG-3'
$GABA_AR$-β2 subunit C1012G mutagenic reverse primer	5'-CAGCTGCTTTCTTTTCGCGCTGGGGTCCTC-3'

$GABA_AR$-β2 subunit A1013C mutagenic forward primer	5'-GGACCCCAGCGCGCAAAGAAAGCAGCTG-3'
$GABA_AR$-β2 subunit A1013C mutagenic reverse primer	5'-CAGCTGCTTTCTTTGCGCGCTGGGGTCC-3'

The name of the restriction enzyme added at the 5'-end is indicated in italics and the sequence of the restriction site in bold.

2.1.6. Antibodies

Primary antibodies were either from commercial sources or were generated and affinity-purified in house by Dr. Kieran Brickley. A summary of the primary antibodies that were used for immunoblotting, immunoprecipitation and immunocytochemistry experiments is shown in Table 2.6. Secondary antibodies were from commercial sources only. Anti-mouse, anti-rabbit and anti-sheep horseradish peroxidase-conjugated immunoglobulin G (IgGs) were from Amersham Pharmacia Biotech, anti-rabbit AlexaFluor® 594 conjugated IgGs were purchased from Molecular Probes-Invitrogen.

2.2. METHODS

2.2.1. Bacteria protocols

2.2.1.1. Bacteria maintenance

Bacteria were grown either in Luria-Bertani (LB broth) or on LB agar plates (LB broth supplemented with 1.7% agar) overnight at 37°C.

2.2.1.2. Preparation of glycerol stocks

A single colony was used to inoculate 5 ml LB broth and grown overnight at 37°C. The overnight culture (1 ml) was added to 0.5 ml 50% (v/v) sterile-filtered glycerol, mixed by inversion and stored at -80°C.

2.2.1.3. Preparation of chemo-competent bacteria

Chemo-competent bacteria were prepared according to the protocol of Nishimura *et al.* (1990). LB broth (5 ml) was inoculated with a single DH5α *E. coli* colony and grown overnight at 37°C, with shaking. An aliquot of this preculture (0.5 ml) was used to inoculate 50 ml LB broth supplemented with 10 mM $MgSO_4$ and 0.2% (w/v) glucose (media A). The culture was grown at 37°C, with shaking, to a mid-logarithmic phase ($OD_{\lambda=600nm}$ = 0.7-0.9). The culture was incubated for 10 min on ice, centrifuged at 2500 g for 10 min at 4°C. The cell pellet was resuspended in 0.5 ml ice-cold media A, and then mixed with 2.5 ml ice-cold sterile storage solution (36% (v/v) glycerol, 12% (w/v) polyethylene glycol (PEG) mwt-8000, 12 mM $MgSO_4$, in LB broth). Competent cells

Table 2.6. A summary of the primary antibodies that were used in immunoblotting, immunoprecipitation and immunocytochemistry experiments

Antibody	Host species	Antigen	Origin
GRIF-$1_{8\text{-}633}$	Rabbit polyclonal	GRIF-1 8-633	In-house (Beck *et al.*, 2002)
GRIF-$1_{879\text{-}884}$	Sheep polyclonal	CNSGGSLLGGLRRNQSL	In-house (Brickley *et al.*, 2005)
FLAG	Rabbit polyclonal	CDYKADDEEK	In-house (Smith *et al.*, 2006)
$GABA_A$Receptor $\beta2_{381\text{-}395}$ subunit	Rabbit polyclonal	KAGLPRHSFGRNAL	In-house (Pollard and Stephenson., 1997)
$GABA_A$Receptor $\alpha1_{1\text{-}14}$ subunit	Rabbit polyclonal	QPSQDELKDNTTVFC	In-house (Duggan *et al.*, 1989)
$GABA_A$Receptor $\alpha1_{413\text{-}429}$ subunit	Sheep polyclonal	ATYLNREPQLKAPTPHQ	In-house (Pollard *et al.*, 1993)
$GABA_A$Receptor $\gamma2_{1\text{-}15}$ subunit	Rabbit polyclonal	QKSDDDYEDYASNKTC	In-house (Stephenson *et al.*, 1990)
GFP (ab6556)	Rabbit polyclonal	Full length GFP	Abcam (Cambridge, UK)
Kinesin 5C (ab5630)	Rabbit polyclonal	AVHAIRGGGGSSSNSTHY QK	Abcam (Cambridge, UK)
HisG	Mouse monoclonal	HHHHHHG	Invitrogen (Paisley, UK)
Myc-Tag 4A6	Mouse monoclonal	EQKLISEEDL	Upstate USA Inc. (Charlottesville, VA, USA)
Anti-58K Golgi protein (ab6284)	Mouse monoclonal	Full lenght rat microtubule-binding peripheral Golgi membrane 58 kDa protein	Abcam (Cambridge, UK)

were divided into 0.1 ml aliquots in pre-chilled microtubes and used immediately or stored at -80°C until use.

2.2.1.4. Transformation of chemo-competent bacteria by heat shock

A frozen aliquot of chemo-competent cells was thawed on ice, mixed with 2-5 ng plasmid DNA and kept on ice for 30 min. The cell-DNA mixture was incubated for exactly 1 min at 42°C, then chilled on ice for 5 min. The cells were mixed with 0.9 ml SOC media (2% (w/v) tryptone, 0.5% (w/v) yeast extract, 10 mM NaCl, pH 7.0, 2.5 mM KCl, 10 mM $MgCl_2$, 10 mM $MgSO_4$, 20 mM glucose) and incubated for 1 h at 37°C with gently shaking. The cell suspension was centrifuged at 6000 g for 2 min. The pellet was resuspended in 150 µl SOC media and spread onto LB agar plates supplemented with the appropriate antibiotic. This was either 50-100 µg/ml ampicillin, kanamycin or chloramphenicol.

2.2.1. Recombinant DNA protocols

2.2.2.1. Small scale purification of plasmid DNA

A single colony was used to inoculate 5 ml LB broth containing the appropriate antibiotic and grown for 12-16 h at 37°C with shaking at 250 rpm. Cells (1.5 ml) were pelleted by centrifugation at 15000 g at room temperature and resuspended in 200 µl resuspension buffer (50 mM Tris-HCl, pH 8.0, 10 mM ethylenediaminetetraacetic acid (EDTA), 100 µg/ml RNase A) by pipetting up and down. The lysis buffer (200 µl) (200 mM NaOH, 1% (w/v) sodium dodecyl sulphate (SDS)) was added and tubes were inverted gentle. The lysate (chromosomal DNA, denatured proteins, cellular debris) was precipitated with 200 µl neutralisation buffer (3 M potassium acetate, pH 5.5). The plasmid DNA was separated from the precipitated lysate by centrifugation at 15000 g for 10 min at room temperature (RT). The supernatant was transferred to a clean microfuge tube and plasmid DNA was precipitated by adding 1 volume isopropanol with mixing by inversion. The DNA-isopropanol solution was centrifuged for 10 min as before. The supernatant was removed and the pellet was washed with ice-cold 70% (v/v) ethanol (200 µl) and centrifuged for 2 min as before. The supernatant was removed and the DNA pellet was dried for 15 min at RT. The DNA was resuspended in 30 µl 10 mM Tris-HCl, pH 8.5 and stored at -20°C until use.

2.2.2.2. Large scale purification of plasmid DNA

Plasmid DNA was purified using the HiSpeed Plasmid Purification Kit. A single colony was used to inoculate 5 ml LB broth containing the appropriate antibiotic and grown for

8 h at 37°C with shaking. A large culture was made by inoculating 250 ml LB broth, supplemented with the appropriate concentration of antibiotic with 0.5 ml of overnight bacterial culture, and incubated for 12-16 h at 37°C with shaking. Bacterial cells were harvested by centrifugation at 5000 g for 10 min at 4°C. The pellet was resuspended in 12 ml resuspension buffer by pipetting up and down. The lysis buffer (12 ml) was added and the cell suspension was mixed by inversion and incubated for 5 min at RT. Chilled neutralisation buffer (12 ml) and binding buffer were added to the cell lysate and mixed by inversion. The mixture was immediately transferred into a filter syringe and incubated for 5 min at RT. Meanwhile a column containing a silica membrane was equilibrated by adding 12 ml column preparation solution and centrifuging for 2 min at 3000 g in a swinging bucket centrifuge. The cell lysate was added to the equilibrated column and centrifuged as before. This step was repeated once. The silica membrane was washed by adding 12 ml washing solution I and centrifuging the column as before. Washing solution II (12 ml) was added and the column was centrifuged at 3000 g for 5 min. The DNA was eluted from the membrane by adding 2 ml TE (10 mM Tris-HCl, pH 8.0, 1 mM EDTA) and centrifuging for 5 min at 2000 g. The eluate was transferred onto the column and centrifuged again for 5 min at 3000 g. This step was repeated. Purified plasmid DNA was analysed by spectrophotometry and restriction enzyme digestion, divided into 0.05 ml fractions and stored at -20°C until use. A working aliquot was kept at 4°C.

2.2.2.3. Determination of the concentration and purity of DNA by spectrophotometry

The concentration of DNA was determined by measuring the absorbance at $\lambda = 260$ nm, where 50 μg/ml double-stranded DNA has an $OD_{\lambda=260nm} = 1$. The purity of the DNA was calculated from the ratio $OD_{\lambda=260nm}/OD_{\lambda=280nm}$. This ratio is equal to ~ 1.8-2 for a pure DNA preparation, free of proteins.

2.2.2.4. DNA amplification by polymerase chain reaction (PCR)

Oligonucleotide design- The oligonucleotide primer sequences were designed according to the following rules. Oligonucleotide primer sequences must be specifically complementary to the flanking sequence of the DNA to amplify. They should be 15 to 30 bases long, with a GC content of 40 to 60% and end with a 3'-GC clamp to increase the priming efficiency. A run of more than 3 identical bases in the primer sequence and a run of three or more C or G at the 3'-end should be avoided. A melting temperature

(Tm) of 55-80°C is recommended. When adding the sequence of a restriction site at the 5'-end of a primer, 4 extra-bases must be added according to the enzyme manufacturer's recommendations, upstream of the restriction site sequence, to provide a binding site for the restriction enzyme,

e.g 5'-TATA **GAATTC** ATGAGTCTGTCCCAG-3'
Extra bases *Restriction site* *DNA sequence to amplify*

The melting temperature was estimated by the "Wallace rule" (Suggs *et al.*, 1981): Tm = 2°C x (number of A and T residues) + 4°C x (number of G and C residues) for primers 15-20 bases long. For longer primers (20-70 bases), the melting temperature was estimated by the following: Tm = 81.5 + 0.41 (% GC) - 675/*N* (Bolton and McCarthy, 1962) where *N* is the number of bases in the oligonucleotide sequence. The oligonucleotide primers that were used for PCR reactions and nucleotide sequencing of DNA constructs are summarised in Table 2.5. Oligonucleotides were stored at a concentration of 10 μM at -20°C, upon arrival.

PCR reaction- PCR reactions were performed in a Hybaid PCR Express thermocycler (VWR, Lutterworth, UK). The PCR mix was generally made of 100-250 ng template DNA, 1.5 mM $MgCl_2$, 0.2 μM forward primer, 0.2 μM reverse primer, 200 μM dNTP mix (200 μM dATP, 200 μM dCTP, 200 μM dGTP, 200 μM dTTP), reaction buffer, 1 unit DNA polymerase (*Taq* or *Pfu*) in a final volume of 100 μl. A standard PCR amplification cycle was performed by denaturing the template DNA at 95°C for 1 min. The primers were allowed to hybridise to the DNA at an annealing temperature (Ta) of 2-5°C below the lowest Tm of the primer set. The DNA was elongated at 72°C, in the presence of *Taq* or *Pfu* DNA polymerase for the appropriate time, i.e. 1 min/kb for *Taq* and 2 min/kb for *Pfu*. This amplification cycle (denaturation-hybridation-elongation) was repeated 25-30 times. The amplification of the template DNA was analysed by flat bed agarose gel electrophoresis (section 2.2.2.9). The PCR product was extracted from flat bed agarose gel or purified using the QIAgen Gel extraction kit or QIAgen PCR purification kit, respectively before further applications (sections 2.2.2.10 and 2.2.2.11).

2.2.2.5. Site-directed mutagenesis

Mutations in target DNA sequences were introduced using the QuikChange® site-directed mutagenesis kit following the manufacturer's instructions.

Design of the mutagenic oligonucleotide primers- Oligonucleotide primers were designed according to the manufacturer's recommendations. For each mutation, two primers were designed which hybridise to the same sequence on opposite strands of the plasmid. The primers were 25-45 bp long, with the mutation in the middle of the sequence. They had a melting temperature greater or equal to 78°C and a minimum GC content of 40%. The 3'-end of each primer contained one or more G or C. Mutagenic oligonucleotide primers are shown in Table 2.5.

Mutagenesis reaction- A reaction mix containing 5-50 ng of template DNA, 125 ng of each primer, 5 µl reaction buffer 10 x and 2.5 U *Pfu* turbo DNA polymerase was prepared to a final volume of 50 µl. A control reaction was also carried out using 10 ng pWhitescript control plasmid and the appropriate primers. The mutated DNA strand was generated by using the programme:

Step	Cycles	Temperature	Time
1	1	95°C	30 sec
2	12	95°C	30 sec
		55°C	1 min
		68°C	1 min/kb plasmid

The amplification step was followed by the addition of 1 µl *DpnI* for 1 h at 37°C. The amplified product was used to transform XL1-blue supercompetent *E.coli* cells by heat–shock as described in section 2.2.1.4. Transformed cells were plated on an LB agar plate containing the appropriate antibiotic and incubated overnight at 37°C. DNA was isolated from the transformants and verified by nucleotide sequencing.

2.2.2.6. Restriction enzyme digestion

DNA was digested by adding 20 units restriction enzyme per µg DNA to digest (1-5 µg DNA depending on the experiment), in the appropriate reaction buffer (e.g. the buffer EcoRI+ was used to digest DNA by *EcoRI*). The reaction mix was incubated at the appropriate temperature (e.g. 37°C for *EcoRI*) for 1-2.5 h. The digestion was verified by 1% flat bed agarose gel electrophoresis (section 2.2.2.9). After the digestion, DNA was purified as explained in section 2.2.2.11.

2.2.2.7. Dephosphorylation of the 5'- DNA end of the digested cloning vector

Shrimp alkaline phosphatase (SAP) (0.5 units) was added to 1-5 µg digested and purified vector and incubated at 37°C for 1 h. After the reaction, SAP was inactivated by heating at 65°C for 20 min.

2.2.2.8. DNA ligation reactions

Insert DNA and cloning vector with compatible ends were ligated using T4 DNA ligase. Ratios of insert:vector of 1:1 and 3:1 were mixed with 1 unit T4 DNA ligase in reaction buffer, in a final volume of 10 µl. The reaction mix was incubated for 4 h at 20°C, or overnight at 16°C, or overnight using a programme cycling between 1 min at 10 °C and 1 min at 30°C (Lund *et al.*, 1996). At 30°C the ligase activity of the enzyme is optimal and at 10°C the DNA is very stable, thus resulting in an increased ligation efficiency.

2.2.2.9. Flat bed agarose gel electrophoresis

Agarose gels (1%) were made by adding 0.5 g agarose to 50 ml TBE buffer (89 mM Tris, 89 mM boric acid, 2 mM EDTA, pH 8.5). The agarose was melted by heating the solution. Ethidium bromide (20 µg) was added to the agarose solution and mixed by swirling. The solution was cooled to RT and poured into an electrophoresis unit assembled as indicated by the manufacturer (Flowgen, VWR, Lutterworth, UK). The gel was allowed to solidify for 30 min and covered with 50 ml TBE buffer. DNA samples to be analysed were mixed with sample buffer (0.25% (w/v) bromophenol blue, 0.25% (w/v) xylene cyanol FF, 40% (w/v) sucrose in H_2O) and loaded onto the gel. A DNA size marker was applied to a parallel lane of the gel. Electrophoresis was carried out for 1 h at constant voltage, i.e. 55 V. DNA was visualised by exposing the gel to UV light.

2.2.2.10. Extraction of DNA fragments from agarose gels

DNA fragments were separated according to their size by flat bed electrophoresis (section 2.2.2.9) on a 2% agarose gel. The fragment of interest was excised from the gel and extracted using the QIAgen gel extraction kit, following the manufacturer's instructions. The gel slice was weighed and solubilised by adding 3 volumes buffer QG at 50°C for 10 min in a thermomixer. The melted gel slice was mixed with 1 volume isopropanol, transferred to a QIAquick spin column and centrifuged for 1 min at 15000 g to bind the DNA to the column. The DNA was washed by adding 0.75 ml buffer PE and centrifuging as before. The DNA was eluted from the column with 30 µl elution buffer EB and used immediately or stored at 4°C until use. The purification efficiency was assessed qualitatively by flat bed agarose gel electrophoresis.

2.2.2.11. DNA purification of digestion and PCR products

Unwanted salts or enzymes were removed from DNA using the QIAgen PCR purification kit. The DNA sample was mixed with 3 volumes binding buffer PB and

transferred to a QIAquick spin column. The DNA was allowed to bind to the resin by centrifuging at 15000 g for 1 min at RT. The DNA was washed with 0.75 ml washing buffer by centrifuging as before. The DNA was eluted from the resin in 30 µl elution buffer EB by centrifuging as before. The purified DNA was used immediately or stored at -20°C until use.

2.2.2.12. Ethanol precipitation of DNA

DNA was mixed with cold sodium acetate 3 M, pH 5.2, 4°C (0.1 DNA sample volume) and ice-cold 100% (v/v) ethanol (2 DNA sample volumes) by pipetting up and down. The DNA solution was stored at -20°C for at least 1 h or 30 min at -80°C. The DNA sample was centrifuged at 15000 g for 15 min at 4°C and the supernatant was discarded. The sample was centrifuged again for 5 min as before to remove the remaining supernatant. Ice-cold 70% (v/v) ethanol (200 µl) was added to the pellet and centrifuged for 5 min as before. The supernatant was removed and the remaining ethanol was evaporated by heating the samples at 37°C for 15 min. The pellet was resuspended in the desired volume of sterile bi-distilled water (ddH_2O) or 10 mM Tris-HCl, pH 8.0.

2.2.2.13. Bioinformatic analysis

For sequence analysis, the homology search program Blast (Altschul *et al.*, 1997), sequence alignment program ClustalW (Thompson *et al.*, 1994) and other programs available on Expasy web-sites (e.g. Expasy tools from www.expasy.ch) were used.

2.2.2.14. Nucleotide sequencing of DNA constructs

Nucleotide sequencing of defined DNA constructs was performed by MWG-Biotech (Ebersberg, Germany). Alternatively, the ABI PRISM 310 Genetic Analysis System (Applied Biosystems, Foster city, CA, USA) was used following the procedure described in appendix 4.1.

2.2.3. Yeast protocols

2.2.3.1. Yeast maintenance

GAL4 yeast strain

The yeast strain, AH109, was grown in YPAD broth (1% (w/v) yeast extract, 2% (w/v) bacto-peptone, 2% (w/v) dextrose, 40 mg adenine/l) at 30°C for 16 h with shaking or on YPAD agar (YPAD broth supplemented with 2% (w/v) bacto-agar) at 30°C.

CytoTrap® yeast strain

Cdc25Hα strain was grown either in YPAD broth at 25°C for 16 h or on YPAD agar plate at 25°C for 4 days.

2.2.3.2. Preparation of glycerol stock of yeast cells

Yeast cells were scraped from a provided glycerol stock and streaked onto a YPAD agar plate using an inoculation loop. They were incubated at 30°C (AH109) or 25°C (cdc25Hα) for 4 days. A single colony was used to inoculate 5 ml YPAD broth. The cells were grown for 18 h to a late growth phase ($OD_{\lambda=600nm}$ = 0.8-1). This culture (1 ml) was added to 0.5 ml sterile-filtered 50% (v/v) glycerol. The cell suspension was mixed by inversion and stored at -80°C.

2.2.3.3. Verification of the yeast strain phenotype

The phenotype of the cdc25Hα yeast strain was checked prior to performing a CytoTrap® assay. Cells were streaked from the glycerol stock onto a plate containing a glucose minimal media lacking tryptophan, leucine, histidine and uracil (-W, -L, -H, -U) and incubated at 25°C for 4 days. No growth was expected under these conditions. The temperature-sensitive phenotype was checked by streaking cdc25Hα cells from the glycerol stock onto a YPAD agar plate and incubated at 37°C for 4 days. The temperature-sensitive strain, cdc25Hα, cannot grow at 37°C.

2.2.3.4. Preparation of competent yeast cells and transformation

Competent cells were prepared and transformed according to the protocol of Schiestl and Gietz (1989).

Preparation of the competent cells- A starter culture was prepared by inoculating 5 ml fresh YPAD-broth with a single AH109 yeast colony and this was grown for 16 h at 30°C, with shaking at 250 rpm. The $OD_{\lambda=600nm}$ was determined. This preculture was used to make a 50 ml culture with a starting $OD_{\lambda=600nm}$ = 0.15 and incubated at 30°C until an $OD_{\lambda=600nm}$ = 0.4 was attained. The cells were harvested by centrifugation at 2500 g for 5 min at RT and the supernatant was removed. The pellet was resuspended in 25 ml sterile ddH_2O and centrifuged as before. The ddH_2O was removed and the pellet was resuspended in 10 ml LISORB (100 mM lithium acetate, 10 mM Tris, pH 8.0, 1 mM EDTA, pH 8.0, 1 M sorbitol) and centrifuged as before. The cell pellet was resuspended in 300 µl LISORB. Boiled single stranded salmon sperm DNA (80 µl of a 2 mg/ml stock) and 1 ml LIPEG (100 mM lithium acetate, 10 mM Tris, pH 8.0, 1 mM EDTA, pH 8.0, 40% (w/v) PEG [mwt 3350]) were added to the LISORB. The cell suspension was then divided into 130 µl aliquots and used immediately.

Transformation of competent cells- Yeast cells were transformed by adding 0.2 μg of each plasmid DNA, mixed by vortexing and incubated for 20 min at RT. DMSO (12 μl) was added to each aliquot and the cells were heat-shocked at 42°C for 10 min. The cells were centrifuged at 15000 g for 1 min and resuspended in 200 μl sterile ddH_2O. Transformants (100 μl) were plated on a synthetic dropout medium lacking tryptophan and leucine, SD (-W, -L), and on a dropout media lacking tryptophan, leucine, uracil, histidine, SD (-W, -L, -H, -U), for the detection of protein-protein interactions. Cells were incubated at 30°C for 4-10 days.

These protocols were adapted for the preparation of competent cdc25Hα yeast cells as follows:

-cultures were grown at 25°C;

-the 50 ml culture had a starting $OD_{\lambda=600nm}$ = 0.2-0.3 and was grown to an $OD_{\lambda=600nm}$ = 0.7.

Transformants were plated onto a synthetic glucose minimal medium (1.7 g/l yeast nitrogen base without amino acids, 5 g/l ammonium sulphate, 20 g/l galactose, 10 g/l raffinose, 1.7% (w/v) agar) lacking uracil and leucine, SD glucose (-U, -L) and incubated at 25°C for 4-6 days.

2.2.3.5. Detection of protein-protein interactions

2.2.3.5.1. GAL4 yeast two-hybrid system

Nutritional selection - Protein-protein interactions were detected on SD (-W, -L, -H, -U). For each co-transformation, colony forming units (cfu) grown on SD (-W, -L, -H, -U) were counted. The number of cfu/plate is proportional to the strength of the interaction between the 2 proteins that are expressed in the yeast.

β-Galactosidase filter lift assay - Colonies grown on SD (-W, -L, -H, -U) plates were transferred onto a filter-paper. The filter was frozen in liquid nitrogen for 1 min and thawed at RT. This filter was placed on another filter that was pre-soaked with 2 ml Z-buffer (60 mM Na_2HPO_4, 40 mM NaH_2PO_4, 10 mM KCl, 0.1 mM $MgSO_4$, pH 7.0) containing 1mg/ml 5-bromo-4-chloro-3-indolyl-β-D-galactopyranoside (X-GAL) dissolved in dimethylformamide (DMF), 0.27% (v/v) β-mercaptoethanol. The filters were incubated at 37°C up to 8 h, until the appearance of blue colonies.

2.2.3.5.2. CytoTrap® yeast two-hybrid system

Colonies (3) from each co-transformation (section 2.2.3.4) were picked and resuspended in 25 µl sterile ddH_2O. These cell suspensions (2.5 µl each) were transferred to a galactose minimal medium, i.e. SD galactose (-U, -L) plate, a glucose minimal medium, i.e. SD glucose (-U, -L) plate, and incubated at 37°C for 4-10 days. As a control, duplicates of these plates were incubated at 25°C for 4-10 days.

2.2.3.6. Extraction of recombinant proteins from the yeast cells

The expression of bait and target fusion proteins was checked by extracting proteins from the appropriate yeast lysates followed by immunobloting analysis (section 2.2.4.11). A single colony from each transformed yeast strain was used to inoculate 5 ml selective media and grown until the culture was saturated ($OD_{\lambda=600nm} > 1$). The cells were harvested by centrifugation at 1000 g for 5 min at RT. The pellet was resuspended in 200 µl cell lysis buffer (140 mM NaCl, 2.7 mM KCl, 10 mM Na_2HPO_4, 1.8 mM KH_2PO_4, pH 7.4, 1% (v/v) Triton X-100) containing protease inhibitors (1 mM PMSF, 1 µM pepstatin A, 100 µM leupeptin, 1 µg/ml chymostatin, 10 µg/ml aprotinin). The cell suspension was supplemented with an equal volume of acid-washed glass beads and was mixed by vortexing for 5 min at 4 °C. The cell lysate was collected by centrifuging at 15000 g for 5 min at 4°C. The supernatant was removed and kept on ice. Cell lysis buffer (100 µl) was added to the glass-bead pellet and was mixed by vortexing. The cell lysate was collected by centrifugation as before. The two supernatants were pooled, aliquoted and used immediately or stored at -20°C until analysis.

2.2.4. Mammalian cell culture and protein expression protocols

2.2.4.1. Maintenance of mammalian cell lines and sub-culturing

Human embryonic kidney (HEK) 293 cells- HEK 293 cells were routinely maintained in DMEM/F-12 media containing 10 % foetal bovine serum in 250 ml flasks at 37°C, 5% CO_2. One day prior to transfection, they were sub-cultured when reaching 70-80% confluency. The culture media was removed and cells were rinsed with 10 ml Hank's buffered salt solution (HBSS), trypsinised with 2 ml trypsin-EDTA for 20-60 sec and removed from the flask surface by slapping the flask. DMEM/F-12 media (10 ml) was added and cells were resuspended by pipetting up and down. This cell solution was added to 40 ml DMEM/F-12 media and mixed by inversion (suspension A). This suspension was distributed to clean, sterile 250 ml flasks (12 ml/flask). Cells were incubated at 37°C, 5% CO_2 until transfection.

For confocal microscopy studies, autoclaved coverslips were incubated in a poly D-lysine solution (0.1 mg/ml) either overnight at RT or for 1 h at RT, rinsed twice with sterile ddH_2O and dried for 20 min at RT, in a cell culture hood. Coverslips (2-4) were transferred to a sterile 35 x 10 mm Petri-dish. HEK 293 cells were sub-cultured as before. Suspension A (1 ml) was added to 5 ml DMEM/F-12 media, mixed by inversion and transferred to the Petri-dishes (2.5 ml/dish). Cells were incubated at 37°C, 5% CO_2 until transfection.

African green monkey fibroblast (COS-7 cells)- COS-7 cells were routinely maintained and sub-cultured as explained for HEK 293 cells except from the trypsination step. COS-7 cells were incubated with 2 ml trypsin-EDTA for 1 min at 37°C, 5% CO_2 and scraped from the 250 ml flask surface using a platic rod. DMEM/F-12 media (10 ml) was added to the flask and cells were resuspended by pipetting up and down. The cell suspension was mixed by inversion to 40 ml DMEM/F-12 media, yielding to suspension B that was transferred (12 ml) to a clean 250 ml flask.

For confocal microscopy studies, the same procedure as for HEK 293 cells was followed except that suspension B (1 ml) was mixed to 7 ml DMEM/F-12 media prior to transfer to the Petri-dishes.

2.2.4.2. Cell culturing from a frozen stock

An aliquot of frozen HEK 293 or COS-7 cells (1 ml) was thawed at 37°C and mixed by inversion to 50 ml pre-warmed DMEM/F-12 media. Cells were centrifuged at 1800 g for 10 min at 4°C and the supernatant was discarded. The cell pellet was resuspended in 12 ml fresh pre-warmed DMEM/F-12 media by pipetting up and down, transferred to a 250 ml flask and incubated at 37°C, 5% CO_2 for 24 h. The media was replaced by 12 ml fresh pre-warmed DMEM/F-12 media. Cells were routinely cultured as described in section 2.2.4.1.

2.2.4.3. Preparation of frozen stocks of HEK 293 and COS-7 cells

HEK 293 and COS-7 cells were cultured to 70% confluency and trypsinised as described in 2.2.4.1. Cells were resuspended in 10 ml pre-warmed DMEM/F-12 media. The contents of 2 flasks were pooled in a 50 ml tube and the cells were centrifuged at 1800 g for 10 min at 4°C. The supernatant was removed and the pellet was resuspended in 4.8 ml pre-warmed DMEM/F-12 supplemented with 10% foetal bovine serum and 10% filter sterilised DMSO. The solution was mixed thoroughly and aliquoted (1.5 ml) into cryotubes. The tubes were wrapped in tissue and stored at -80°C overnight. The tubes were transferred to a -150°C freezer on the following day and stored until use.

2.2.4.4. Transfection of HEK 293 and COS-7 cells by the calcium phosphate method

For each transfection, a 250 ml flask of HEK 293 cells was placed at 37°C, 7.5% CO_2 for 3 h. Plasmid DNA solution (450 µl) was prepared by adding the DNA (10 µg) to the appropriate volume of 1 in 10 TE buffer. A total plasmid DNA concentration of 10 µg was used for each flask. The calcium-DNA precipitate was prepared by adding 50 µl 2.5 M $CaCl_2$, pre-warmed to 37°C, to the DNA and shaking vigorously for 15 sec. This solution was pipetted dropwise (1 drop/3 sec) to 500 µl HBS buffer (50 mM 4-(2-hydroxyethyl)-1-piperazineethanesulfonic acid (HEPES), pH 8.0, 280 mM NaCl, 1.1 mM Na_2HPO_4). The resulting DNA mixture was added to the cell culture flask and mixed gently by moving the flask. The flask was incubated at 37°C, 5% CO_2 for 24-36 h, until transfected cells were harvested.

For confocal microscopy studies, Petri-dishes of HEK 293 or COS-7 cells were placed at 37°C, 7.5% CO_2 for 3 h. For each dish, a total plasmid DNA concentration of 1 µg was used. Plasmid DNA solution was prepared by adding 10 µg DNA to 1 in 10 TE buffer to a final volume of 450 µl. $CaCl_2$ (2.5 M, 50 µl) was added to the plasmid DNA solution and mixed by shaking for 15 sec. The calcium-DNA precipitate was pipetted dropwise to 500 µl HBS buffer. This final DNA mixture (100 µl, i.e. 1 µg total DNA) was added to each dish. Cells were incubated at 37°C, 5% CO_2 for 24-48 h, until imaged.

The plasmid DNAs used to transfect HEK 293 or COS-7 cells were:

-pEYFP-C1	-pCMV-FLAG-GRIF-1	-pCMVmycKLC
-pECFP-C1	-pN-EYFP-KIF5C	-pCMVmycKIF5C-MD
-pECFP-EYFP	-pN-ECFP-KIF5C	-pCMVmycKIF5C-NMD
-pECFP-ER	-pC-EYFP-KIF5C	-pCIS-$GABA_AR$-$\beta2^{EYFP}$
-pECFP-GRIF-1	-pC-ECFP-KIF5C	-pCMV- FLAG-OGT
-pDsRed1-Mito	-pcDNAHisMax-KIF5C	-pEYFP-OGT
-pEYFP-GRIF-1	-pEYFP-KIF5C-MD	-pcDNAHisMax-mOGT $_{40-374}$
-pCIS-GRIF-1	-pEYFP-KIF5C-NMD	

The different combination of plasmid DNAs used to transfect HEK 293 and/or COS-7 cells were:

-pCIS-GRIF-1 (5 μg) + pcDNAHisMax-KIF5C (5 μg)

-pCIS-GRIF-1 (5 μg) + pN-EYFP-KIF5C

-pCIS-GRIF-1 (5 μg) + pC-EYFP-KIF5C (5 μg)

-pCIS-GRIF-1 (5 μg) + pEYFP-KIF5C-MD (5 μg)

-pCIS-GRIF-1 (5 μg)+ pEYFP-KIF5C-NMD (5 μg)

-pECFP-GRIF-1 (5 μg) + pcDNAHisMax-KIF5C (5 μg)

-pECFP-GRIF-1 (5 μg)+ pN-EYFP-KIF5C (5 μg)

-pECFP-GRIF-1 (5 μg) + pC-EYFP-KIF5C (5 μg)

-pECFP-GRIF-1 (5 μg) + pEYFP-KIF5C-MD (5 μg)

-pECFP-GRIF-1 (5 μg) + pEYFP-KIF5C-NMD (5 μg)

-pECFP-GRIF-1 (2 μg) + pN-EYFP-KIF5C (2 μg) + pCMVmycKLC (4 μg)

-pEYFP-GRIF-1 (5 μg) + pECFP-ER (5 μg)

-pN-EYFP-KIF5C (5 μg) + pECFP-ER (5 μg)

-pCIS-GRIF-1 (3.3 μg) + pN-EYFP-KIF5C (3.3 μg) + pECFP-ER (3.3 μg)

-pECFP-GRIF-1 (8 μg) + pDsRed1-Mito (2 μg)

-pN-ECFP-KIF5C (8 μg) + pDsRed1-Mito (2 μg)

-pECFP-GRIF-1 (4 μg) + pN-ECFP-KIF5C (4 μg) + pDsRed1-Mito (2 μg)

-pCIS-$GABA_AR$-β2 (3.3 μg) + pCIS-$GABA_AR$-γ2 (3.3 μg) + pcDM8-$GABA_AR$-α1 (3.3 μg)

-pCIS-$GABA_AR$-β2EYFP (3.3 μg) + pCIS-$GABA_AR$-γ2 (3.3 μg) + pcDM8-$GABA_AR$-α1 (3.3 μg)

-pCIS-GRIF-1 (2 μg) + pcDNAHisMax-mOGT $_{40\text{-}374}$ (8 μg)

-pCIS-GRIF-1 (3 μg) + pCMVTag4a-OGT (7 μg)

-pCMVTag4a-GRIF-1 (3 μg) + pEYFP-OGT (7 μg)

-pECFP-GRIF-1 (5 μg) + pEYFP-OGT (5 μg)

-pECFP-KIF5C (5 μg) + pEYFP-OGT (5 μg)

2.2.4.5. Harvesting of transfected HEK 293 cells and preparation of the total cell homogenates

HEK 293 cells were removed from the incubator 24-36 h after transfection. The culture media was removed and the flask was rinsed twice with 10 ml ice-cold phosphate buffer saline, PBS (136.9 mM NaCl, 2.68 mM KCl, 10 mM Na_2HPO_4, 1.76 mM KH_2PO_4, pH 7.4). Ice-cold PBS (10 ml) was added to the flask and the cells were scraped using a plastic rod and transferred to a 15-ml tube. The cells were centrifuged at 1000 g for 5 min at 4°C. The supernatant was removed and the cell pellet was resuspended in 1 ml homogenisation buffer (10 mM HEPES, pH 7.4, 145 mM NaCl, 1 mM ethylene glycol bis(2-aminoethyl ether)-N,N,N'N'-tetraacetic acid (EGTA), 0.1 mM $MgCl_2$) containing protease inhibitors (0.1 mg/ml soybean trypsin inhibitor, 0.1 mg/ml chicken egg trypsin inhibitor, 0.1 mg/ml bacitracin, 0.1 mg/ml benzamidine, 1 mM PMSF). The cell pellet was homogenised using a glass-glass homogeniser and transferred to a 1.5 ml tube. The total cell homogenate was used immediately or frozen in liquid nitrogen prior to storage at -20°C until use.

2.2.4.6. Preparation of soluble and detergent soluble fractions of transfected HEK 293 cells

Total cell homogenates (section 2.2.4.5) of transfected HEK 293 cells were centrifuged at 100000 g for 30 min at 4°C. The supernatant, i.e soluble fraction, was removed and kept on ice. The pellet was resuspended in 1 ml homogenisation buffer containing 1% (v/v) Triton X-100 and protease inhibitors as in 2.2.4.5 and incubated 1 h at 4°C. The detergent soluble fraction was obtained by centrifuging at 100000 g for 30 min at 4°C. The supernatant was kept on ice. The pellet was either resuspended in 500 µl homogeneisation buffer for analyses or discarded. Alternatively, total cell homogenates of co-transfected HEK 293 cells (section 2.2.4.5) were prepared in 2 ml homogeneisation buffer containing 1% (v/v) Triton X-100 and protease inhibitors (same as in section 2.2.4.5), solubilised 1 h at 4°C and centrifuged as before. The supernatant, i.e. detergent soluble fraction, was used immediately for co-immunoprecipitation experiments (section 2.2.4.7).

2.2.4.7. Co-immunoprecipitation assays

Detergent solubilised extracts of co-transfected HEK 293 cells (section 2.2.4.6) were supplemented with an equal volume of homogenisation buffer containing protease inhibitors (as in section 2.2.4.5). Primary antibodies (5-10 µg) were added to the extract

and incubated for 90 min at 37°C with gentle shaking. Alternatively, antibodies were incubated overnight at 4°C with gentle shaking. Immune pellets obtained using polyclonal anti-rabbit primary antibodies were precipitated by incubation with protein-A Sepharose beads (20 µl) for 1 h at 37°C. Protein-G Sepharose beads (20 µl) were added to immune pellets containing polyclonal anti-sheep IgGs and incubated for 1 h at 37°C. Sepharose beads were sedimented by centrifugating at 200 g for 2 min at 4°C. The supernatant was removed and the pellet was transferred to a clean 1.5 ml tube and centrifuged for 15 sec at 200 g. The immune pellet was washed 3 times by adding 1 ml homogenisation buffer containing 0.5% (v/v) Triton X-100 and centrifuging as before. The pellet was resuspended in SDS-PAGE sample buffer (section 2.2.4.10) and analysed by SDS-PAGE followed by western-blotting (sections 2.2.4.10 and 2.2.4.11).

2.2.4.8. Determination of the protein concentration

Protein concentrations were determined using the Bio-Rad Protein Assay. The assay was performed according to the manufacturer's instructions. Bovine serum albumin (BSA) standard solutions were prepared by diluting a BSA stock-solution to 0.2, 0.45, 0.7, 0.9, 1.4 mg/ml. The standard solution or test sample (100 µl) was added to 5 ml of the dye reagent provided in the kit, mixed by vortexing and incubating at RT for 5-60 min. The $OD_{\lambda = 595nm}$ was determined by spectrophotometry and a standard curve was established using the $OD_{\lambda=595nm}$ of the standard solutions. The protein concentration of the samples was determined using the standard curve.

2.2.4.9. Methanol/chloroform precipitation of proteins

Total cell homogenates, soluble or detergent soluble extracts of transfected HEK 293 cells were precipitated prior to electrophoresis analysis. Protein samples (50 µl) were mixed by vortexing with methanol (150 µl). Chloroform (50 µl) was added and mixed by vortexing. Bi-distilled H_2O (150 µl) was added and mixed by vortexing. The sample-methanol-chloroform-ddH_2O mix was centrifuged at 15000 g for 4 min at RT. The upper phase was removed. Methanol (50 µl) was added to the remaining solution, mixed by vortexing and centrifuged at 15000 g for 5 min at RT. The supernatant was carefully discarded and the protein pellet was dried under vacuum for 15 min. Precipitated proteins were either dissolved in SDS-PAGE sample buffer (section 2.2.4.10) or stored at -20°C until use.

2.2.4.10. Separation of proteins by sodium dodecyl sulphate polyacrylamide gel (SDS-PAGE) electrophoresis

Polyacrylamide gels were prepared according to Laemmli (1970).

2.2.4.10.1. Preparation of resolving and stacking polyacrylamide gels

The resolving gel - For the analysis of 60-200 kDa proteins, 7.5% resolving gels were prepared by adding 2.2 ml resolving gel buffer 4 x (1.5 M Tris pH 8.8, 8 mM EDTA, 0.4% (w/v) SDS), 2.2 ml acrylogel (30% acrylamide:bisacrylamide (37:1)), 16 µl N,N,N',N'-tetramethylethylenediamine (TEMED) and 4.4 ml ddH2O. Proteins with a molecular size of 20-60 kDa were analysed using a 10% resolving gel, that was prepared by supplementing the resolving gel buffer 4 x (2.2 ml) with 3.3 ml acrylogel, 16 µl TEMED and 3.3 ml ddH2O. The solutions were degassed for 20 min under vacuum. An aluminium and a glass plate, separated by 1.5 mm plastic spacers, were assembled in a gel caster (Hoefer, Amersham Pharmacia Biotech Ltd.). The resolving gel solution was supplemented with 66 µl ammonium persulphate (APS) 10% (w/v), mixed and poured between the assembled plates. The top of the resolving solution was overlaid with 50% butanol (v/v) and allowed to polymerise at RT for 30 min. The plates were removed from the gel caster and the top of the gel was washed with distilled water. The plates were placed in the electrophoresis unit (Mighty small, Amersham Pharmacia Biotech Ltd.). The base of the gel was covered with electrode buffer (50 mM Tris pH 8.8, 400 mM glycine, 1.8 mM EDTA, 0.2% (w/v) SDS). The top of the gel was cleaned from water by capillarity using a filter paper prior to pouring the stacking gel.

The stacking gel - The stacking gel (4%) was prepared by mixing 1 ml stacking gel buffer 4 x (0.5 M Tris pH 6.8, 8 mM EDTA, 0.4% SDS), 0.6 ml acrylogel (30% acrylamide:bisacrylamide (37:1)), 5 µl TEMED and 2.6 ml ddH_2O. The solution was degassed under vacuum for 20 min. APS 10% (w/v) (80 µl) was added to the degassed solution. The stacking gel was poured to the top of the separating gel, a gel comb was inserted and the gel was allowed to polymerise at RT for 30 min. After polymerisation, electrode buffer (as before) was added to the electrophoresis until the top of the stacking gel was covered.

2.2.4.10.2. Preparation and loading of protein samples

Precipitated protein samples (2.2.4.9) were dissolved in 15 µl SDS-PAGE sample buffer (10 mM NaH_2PO_4, pH 7.0, 10% (v/v) glycerol, 0.015% (v/v) bromophenol blue and 2.5% (w/v) SDS) containing 135 mM DTT and boiled 4 min at 95°C. The gel comb

was removed from the stacking gel and the wells were rinsed with electrode buffer. Protein samples (15 µl) were loaded into the wells using a Hamilton's syringe. Molecular weight markers (M_r = 250, 98, 64, 50, 36, 30, 16 kDa) were loaded in a parallel well. Wells with no samples were filled with 15 µl SDS-PAGE sample buffer.

2.2.4.10.3. SDS-PAGE electrophoresis

Electrophoresis was carried out at constant current, i.e.10 mAmp per gel for 3 h, until the dye front reached the bottom of the gel.

2.2.4.11. Western-blotting

After separation of proteins by electrophoresis, proteins were transferred from the SDS-PAGE gel onto a nitrocellulose membrane and analysed by immunoblotting.

Electrophoretic transfer of proteins to nitrocellulose membranes - After electrophoresis, the plates were removed from the electrophoresis unit. A sponge was placed on a plastic blot holder. Blotting paper (2 pieces) and 1 piece of nitrocellulose filter, all pre-equilibrated in transfer buffer (12.5 mM Tris pH 8.5, 96 mM glycine, 40% (v/v) methanol) were placed on the sponge. The separating gel was placed on the top of the nitrocellulose membrane. The gel was covered with 2 pieces of blotting paper. Air pockets were removed by rolling a pipette on the blotting paper. The blotting paper was covered with a sponge, the blot holder was closed and placed in an electro-tranfer tank (Hoefer, Amersham Pharmacia Biotech Ltd.) filled with transfer buffer as above. The electrophoretic transfer was performed overnight at constant voltage, i.e. 14 V. The tank was cooled down by circulating water.

Detection of proteins - The nitrocellulose membrane was removed from the plastic blot holder and washed in PBS for 10 min. Non specific sites were blocked by incubation in PBS containing 5% (w/v) powdered milk and 0.1% (v/v) Tween-20 at 37°C for 1 h with shaking. The membrane was incubated with the primary antibody (Table 2.6) diluted to the appropriate concentration, in general 1 µg/ml, in PBS containing 2.5% (w/v) powdered milk for 90 min at 37°C or overnight at 4°C with shaking. The membrane was washed with PBS containing 2.5% (w/v) powdered milk and 0.1% (v/v) Tween-20 for 10 min at 37°C with shaking. This washing step was repeated 3 times. The membrane was incubated with the appropriate horseradish peroxidase-conjugated secondary antibody diluted to a concentration of 0.5 µg/ml in PBS containing 2.5% (m/v) powdered milk at 37°C for 1 h with shaking. The membrane was washed with PBS containing 0.2% (v/v) Tween-20 for 20 min with shaking. This step was repeated 3

times. Finally the membrane was washed in PBS for 10 min. The membrane was incubated with enhanced chemi-luminescence mix (800 mM luminol, 100 mM Tris, pH 8.5, 11 μg/μl p-coumaric acid, 10 μl H_2O_2) for 1 min exactly with gentle shaking. Proteins were visualised by imaging the membrane for 2-10 min with the GeneGnome (Syngene Bio Imaging, Cambridge, UK). Pictures were stored in the computer and analysed with the Syngene software provided with the GeneGnome.

2.2.4.12. Fixation of cells

Dishes of HEK 293 or COS-7 cells were removed from the incubator 24-72 h after transfection. Coverslips were washed with 2.5 ml pre-warmed HBSS for 1 min at RT and fixed in 2.5 ml pre-warmed 4% (w/v) paraformaldehyde, pH 7.6, for 10 min at 37°C, 5% CO_2. Each coverslip was washed 3 times in PBS and mounted onto a microscope slide in 10 μl mounting solution containing an anti-fading agent. Coverslips were sealed with clear nail vanish and kept at 4°C until analysed.

2.2.4.13. Immunocytochemistry

Cells were plated onto coverslips, transfected and fixed as described in sections 2.2.4.4 and 2.2.4.12. After fixation, each coverslip was washed 3 times in TBS (10 mM Tris, pH 7.4, 145 mM NaCl), for 5 min at RT and cells were permeabilised with 0.2% (v/v) Triton X-100 for 10 min at RT. Coverslips were washed as before. Non-specific sites were blocked by incubation of each coverslip with a solution containing 10% (w/v) goat serum, 4% (w/v) BSA, 0.1% (w/v) DL-lysine (100 μl/coverslip) for 1 h at RT in the dark. Primary antibodies were diluted to the appropriate concentration in solution D (5% (w/v) goat serum, 2% (w/v) BSA, 0.1% (w/v) DL-lysine), added to the coverslip (60 μl) and incubated at 4°C overnight in the dark. Coverslips were washed 3 times as before. Secondary antibodies (60 μl) were diluted to the appropriate concentration in solution D and added to the coverslips for 50 min at RT in the dark. Coverslips were washed with TBS for 7 min in the dark. This step was repeated 5 times and coverslips were mounted onto a microscope slide as in section 2.2.4.12. The coverslips were sealed and stored at 4°C until imaged.

The primary antibodies used were rabbit polyclonal anti-GRIF-$1_{8\text{-}633}$ (0.1 μg/ml) and rabbit polyclonal anti-58K Golgi protein (1 in 2000) IgGs. Secondary antibodies were anti-rabbit AlexaFluor®594-conjugated IgGs and they were always used at a concentration of 5.5 μg/ml.

2.2.5. Confocal microscopy imaging of transfected mammalian cells

Fixed transfected HEK 293 and COS-7 cells were imaged with an inverted LSM510 Meta laser-scanning confocal microscope (Zeiss, Germany) and visualised using a 63 x immerged oil objective with a numerical aperture of 1.4. For each image, the pinhole diameter was of ~ 1 Airy unit and the resolution was of 12 bits over 512 x 512 or 1024 x 1024 pixels. The lasers were either a 30 mW argon laser used at 50% of its full power and containing the lines λ = 458, 477, 488 and 514 nm or a 1 mW λ = 543 nm HeNe laser. Confocal sections, or Z-stacks, were generated with a Z-step size of 0.36 μm. The stacks were saved on the computer. Images were analysed using the LSM510 software provided with the microscope.

2.2.5.1. Imaging of a cell containing a single fluorophore

2.2.5.1.1. Single channel imaging mode

Transfected HEK 293 and COS-7 cells were imaged on a single channel, i.e. single-track mode of the microscope. Enhanced cyan fluorescent protein (ECFP) was excited with the λ = 458 nm laser line and emission fluorescence between λ = 475-525 nm was collected with a band-pass (BP) filter, BP 475-525. Enhanced yellow fluorescent protein (EYFP) was excited at λ = 514 nm and emission fluorescence above λ = 530 nm was recorded with a long-pass (LP) filter, LP 530. DsRed1 and AlexaFluor®594 were excited with the λ = 545 nm HeNe laser and emission fluorescence above λ = 560 nm was collected with a LP 560. Each excitation laser was paired with one or more of the dichroic mirrors available on the microscope: the λ = 458 nm excitation laser line was used with a λ = 458 nm dichroic mirror, the λ = 514 nm laser line with the λ = 458/514 nm dichroic mirrors and the λ = 545 nm HeNe laser with the λ = 488/543 nm. The detailed procedure for the imaging of a fluorophore in the single channel imaging mode is shown in Figure 2.1.

2.2.5.1.2. Generation of a fluorophore reference spectrum: imaging of a cell containing a single fluorophore in the lambda mode

For each fluorophore, a reference spectra was generated using the lambda mode of the microscope as described in the section 2.2.5.2.2. In this imaging mode, an image of the test sample is captured at each wavelength of a defined range, i.e. lambda stacks, on a Meta detector. By plotting the fluorescence intensity obtained for each wavelength versus the wavelength, an emission spectrum of the sample is generated.

STEP 1: Select a transfected cell in the visual mode of the microscope

STEP 2: Click on the icon "LSM" to return to the confocal mode

STEP 3: Select the single- or multi-track imaging mode by clicking on the corresponding icon. Choose excitation laser(s), dichroic mirrors and emission fluorescence collection filter (sections 2.2.5.1.1 and 2.2.5.2.1)

STEP 4: Capture an image of the sample by clicking on "Find"

STEP 5: Reduce the level of background and saturation using the "gain" and "offset" functions

STEP 6: Image a Z-stack series by selecting "Z-stack" followed by "Find"

STEP 7: Save the images on the computer

Figure 2.1. Detailed procedure for the imaging of transfected cells in the single- or multi-track mode of the LSM510 Meta confocal microscope

An HEK 293 cell expressing a single fluorescent fusion protein or a single protein labelled with a fluorescent dye conjugated antibody was imaged in the lambda mode. ECFP and EYFP were excited as in 2.2.5.1.1. Alternatively, EYFP was excited using the λ = 488 nm laser line with the λ = UV/488/543/633 dichroic mirrors. DsRed1 and AlexaFluor®594 were excited at λ = 545 nm with the HeNe laser with the λ = UV/488/543/633 dichroic mirrors. For each fluorophore, emitted fluorescence was collected on the Meta detector between λ = 456.5-650 nm, every 10.7 nm. Emission spectra were generated using the LSM510 software. All spectra were saved in the spectra database. The detailed procedure for the imaging of a fluorophore in the lambda mode is shown in Figure 2.2. An example of the emission spectrum obtained for each fluorophore is shown on Figure 2.3.

STEP 1: Select a transfected cell in the visual mode of the microscope

STEP 2: Click on the icon "LSM" to return to the confocal mode

STEP 3: Select the lambda imaging mode by clicking on the corresponding icon. Choose excitation laser(s), dichroic mirrors and the emission fluorescence collection range (sections 2.2.5.1.1 and 2.2.5.2.1)

STEP 4: Capture a lambda stack of the sample by clicking on "Find"

STEP 5: Reduce the level of background and saturation using the "gain" and "offset" functions
STEP 6: Repeat step 4

STEP 7: Get the emission spectra as follows: click on the icon "Mean", click on the icon "ROI" and overlay the cell analysed. Save the emission spectrum in the spectra database

Figure 2.2. Detailed procedure for the imaging of transfected cells in the lambda mode of the LSM510 Meta confocal microscope

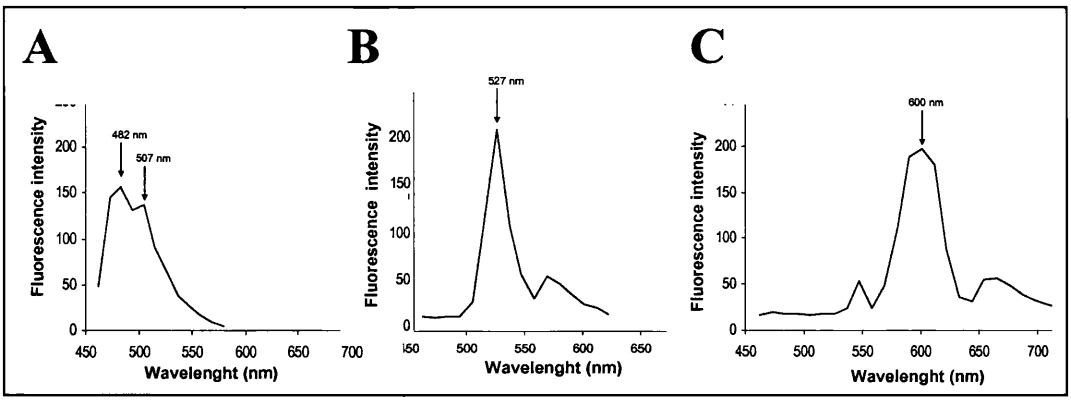

Figure 2.3. Generation of ECFP, EYFP and DsRed1-Mito emission spectra using the lambda imaging mode of the LSM510 Meta confocal microscope. An HEK 293 cell transfected with either A, pECFP-C1, B, pEYFP-C1 or C, pDsRed1-Mito was fixed 24 h post-transfection and imaged as described in section 2.2.5.1.2. A, ECFP was excited at λ = 458 nm, B, EYFP was excited at λ = 514 nm and, C, DsRed1-Mito was excited at λ = 543 nm. Fluorescence emissions were collected between λ = 456.5-617 nm, every 10.7 nm. The arrows indicate the fluorescence emission peak of A, ECFP (λ = 482 nm), B, EYFP (λ = 527 nm) and C, DsRed1-Mito (λ = 600 nm).

2.2.5.2. Imaging of a cell containing multiple fluorophores

2.2.5.2.1. Imaging a cell in the multi-track mode

Multi-colour fluorescence imaging was done by sequential imaging of fluorophores on different channels, using the multi-track mode of the microscope. The detailed procedure for the imaging of fluorophore in the multi-track mode is shown in Figure 2.1. Excitation laser lines, dichroic mirrors and emission filters were selected depending on fluorophore combinations and to minimize possible bleedthrough between fluorophores. The problem of fluorophore bleedthrough is discussed in Chapter 3. Briefly, it was not possible to avoid the bleedthrough between fluorophore in the multi-track mode using the filters available on the microscope. However it was possible to reduce the bleedthrough to a background level (Figure 2.4 A-C). For each fluorophore combination, the settings were as described in Table 2.7. For all the combinations, the λ = 458 nm laser line was used at 15-25% of its full power, the λ = 488 nm and the λ = 514 nm laser lines at 2-5% of their full power, the λ = 545 nm HeNe laser at 50-100% of its full power.

Table 2.7. A summary of the settings used for the imaging of multiple fluorophores

Fluorophore combination	Imaged fluorophore	Excitation (λ nm)	Dichroic mirrors (λ nm)	Emission filters (λ nm)
ECFP + EYFP	ECFP	458	458/514	BP 475-525
	EYFP	514		LP 530
ECFP + DsRed1	ECFP	458	488/543	BP 475-525
	DsRed1	545		LP 560
ECFP + EYFP + DsRed1	ECFP	458	UV/488/543/633	BP 475-525
	EYFP	488		BP 505-530
	DsRed1	545		LP 560
ECFP + AlexaFluor®594	ECFP	458	488/543	BP 475-525
	AlexaFluor®594	545		LP 560
ECFP + EYFP + AlexaFluor®594	ECFP	458	UV/488/543/633	BP 475-525
	EYFP	488		BP 505-530
	DsRed1	545		LP 560

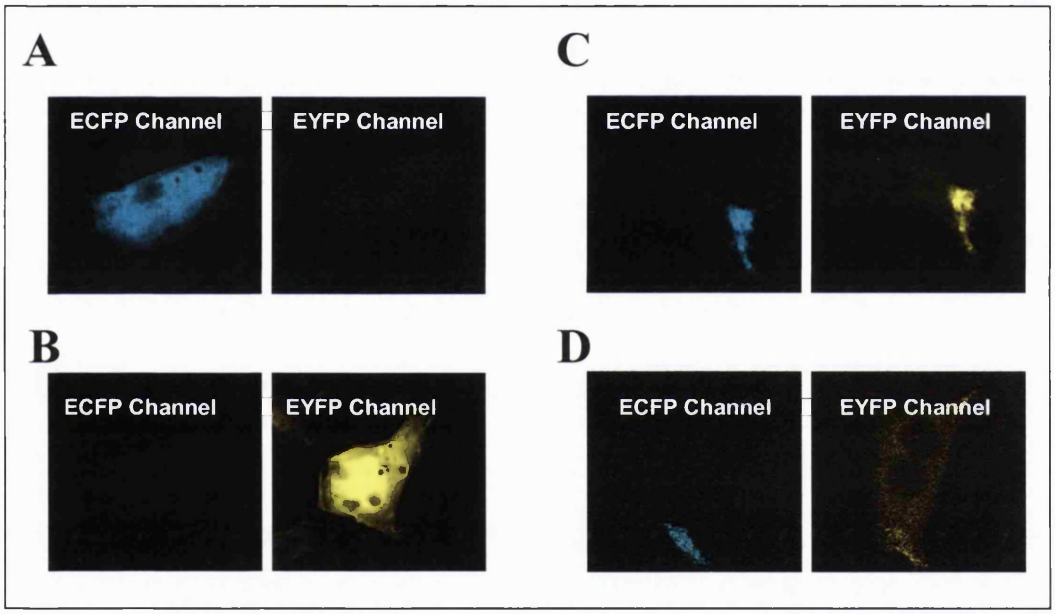

Figure 2.4. Imaging of ECFP and EYFP. HEK 293 cells were transfected with A, a pECFP-fusion construct and B, a pEYFP-fusion construct. Cells were fixed 24 h post-transfection and imaged using the λ = 458 nm and the λ = 514 nm laser lines in the multi-track imaging mode. A, background fluorescence is detected in the EYFP channel although no EYFP is expressed. B, background fluorescence is detected in the ECFP channel although no ECFP is expressed. A and B show the bleedthrough between ECFP and EYFP. C, D, HEK 293 cells were co-transfected with a pECFP-fusion construct + pEYFP-fusion construct, fixed 24 h post-transfection and imaged using the λ = 458 nm and the λ = 514 nm laser lines in C, the multi-track imaging mode and D, the lambda mode. Fluorescences were detected in both channels. The images in D show the real contribution of each fluorophore. The fluorescences in C are similar to the fluorescence in D. This shows that the fluorescences detected in C are not artefacts due to fluorophore bleedthrough but they correspond to the real contribution of ECFP and EYFP.

2.2.5.2.2. Lambda mode imaging

The lambda mode is characterised by a Meta detector used in conjunction with a Meta hardware (Dickinson *et al.*, 2001). This hardware uses a mathematical algorithm to decompose a mixed emission spectra for a sample containing 2-3 fluorophores into the emission spectrum of a single fluorophore. The decomposition or unmixing step is carried out using reference spectra that were generated with samples containing a single fluorophore (section 2.2.5.1.2). Following the unmixing step, images showing the real contribution of each fluorophore present in the test sample are generated (1 image/fluorophore) (Figure 2.4 D). An overlaid image of all fluorophores is also generated.

Lambda stacks of a transfected HEK 293 or COS-7 cell containing 2-3 fluorophores were generated by exciting the sample and collecting emitted fluorescence at the appropriate wavelengths. ECFP, EYFP and DsRed1 or AlexaFluor®594 were excited using the laser lines and dichroic mirrors described in 2.2.5.2.1 and emitted fluorescence was collected on the Meta detector between λ = 456.5-650 nm, every 10.7 nm. Mixed emission spectra were obtained using the "Mean" function and decomposed linearly using the "Unmix" function. Unmixed images were saved on the computer. The detailed procedure for the imaging of fluorophores in the lambda mode is shown in Figure 2.2.

2.2.5.3. FRET analyses

2.2.5.3.1. Definition, detection and applications of FRET

The principle of FRET

FRET is a non-radiative, dipole-induced dipole energy transfer from a fluorescent donor molecule in an electronic excited state to a fluorescent acceptor molecule that is located in very close proximity (Förster, 1948). Excitation of the donor at the appropriate wavelength results in excitation of the acceptor that in turn emits fluorescence. Consequently the donor fluorescence emission intensity is decreased whereas the acceptor fluorescence emission intensity is increased. Accordingly, the donor fluorescence lifetime, i.e. the time the fluorophore stays in an electronic excited state, is decreased whereas the acceptor fluorescence lifetime is increased. FRET is used to detect protein-protein interactions in live or fixed cells and to measure the distance separating the associated proteins (reviewed by Selvin, 1995).

FRET efficiency is dependent on: (i) the distance between donor and acceptor, r (nm) (r < 10 nm for most donor/acceptor pairs), (ii) the relative orientation of the donor and acceptor, k^2 (k^2 = 2/3 for randomly oriented donor and acceptor), with k a geometric factor, (iii) the overlap of the donor emission and acceptor absorption spectra, J (λ) (M^{-1}. cm^{-1}. nm^{-1}), (iv) the donor quantum yield (ratio of photon emitted by photon absorbed), Q, (v) the refractive index of the media, n ($M^{-1}.cm^{-1}$), (vi) the Förster radius, R_0. R_0 represents the distance at which 50% of the energy transfer occurs. R_0 varies depending on the donor/acceptor pair. It has been determined experimentally for different donor/acceptor pairs (Patterson *et al.*, 2000; Handbook of Molecular Probes). R_0 is given by the equation $R_0 = (k^2 . n^{-4} . Q . J(\lambda))^{1/6} . 9.7.10^2$ where J(λ) is defined by $J(\lambda) = \int F(\lambda).\varepsilon(\lambda).\lambda^4.d\lambda / \int F(\lambda).d\lambda$, with F(λ), the fluorescence emission intensity of the donor at the wavelength, λ and ε(λ) ($M^{-1}.cm^{-1}$), the extinction coefficient of the acceptor at the wavelength, λ.

The FRET efficiency, *E*, is given by the equation $E = R_0^6 / (R_0^6 + r^6)$. In general, *E* is determined experimentally and the latter equation is used to deduce the distance r separating the 2 fluorophores.

A diagram describing the principle of FRET is shown in Figure 2.5.

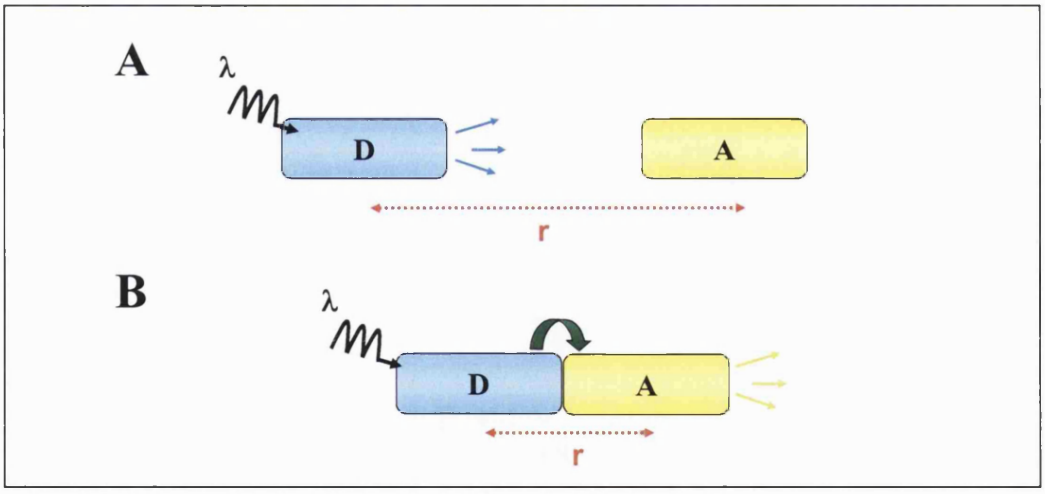

Figure 2.5. A diagram describing the principle of FRET between 2 fluorophores. FRET occurs between a donor fluorophore (D) and an acceptor fluorophore (A) that are in close proximity. When FRET occurs, excitation of the donor at the appropriate wavelength (λ) results in excitation of the acceptor. A, No FRET occurs because D and C are too far away. Excitation of D at λ results in emission of D fluorescence. B, FRET occurs because D and A are in close proximity. Excitation of D at λ results in excitation of A and emission of A fluorescence, as a result of FRET.

Donor and acceptor pairs

FRET donors and acceptors are either fluorescent dyes or fluorescent proteins. Fluorescent dyes such as fluorescein and eosin are linked chemically either to the proteins of interest or to an antibody directed against the proteins of interest (reviewed in Selvin, 1995). Fluorescent proteins are genetic variants of EGFP (section 3.1.2). The most commonly used donor/acceptor pairs are EBFP/EGFP (blue/green) and ECFP/EYFP (cyan/yellow) (see section 3.1.2) (Tsien, 1998; Miyawaki and Tsien, 2000; Shaner *et al.*, 2005). Fluorescent proteins are genetically fused to the proteins of interest thereby generating fluorescent chimeras that are expressed in cells without any extra steps such as purification or labelling of the proteins of interest being required. Acceptors can also be non-fluorescent molecules such as the ligand FlasH that was used as an acceptor for ECFP to study G protein-coupled receptor activation in living cells (Hoffmann *et al.*, 2005). Donors and acceptors within a pair are chosen so that the donor emission spectrum overlaps with the acceptor excitation spectrum as shown for ECFP and EYFP in Figure 2.6.

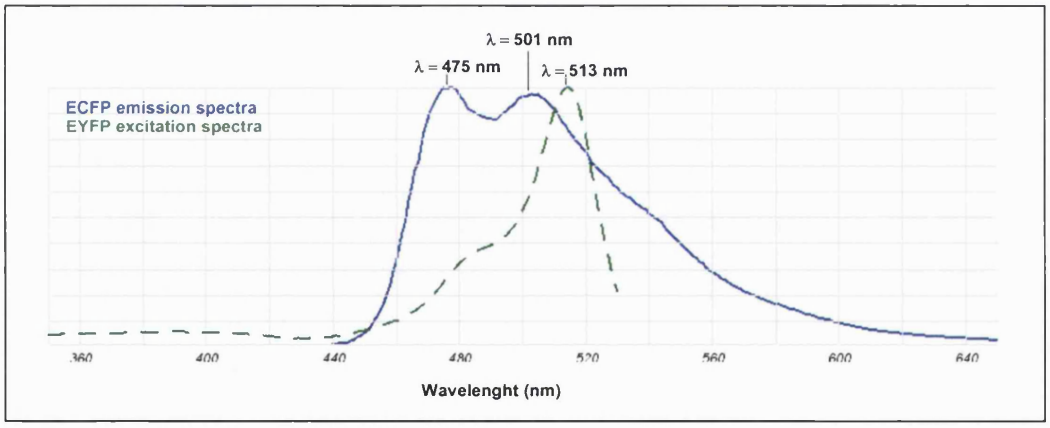

Figure 2.6. A diagram showing the overlap of ECFP emission spectrum and EYFP excitation spectrum. The ECFP emission peaks and EYFP excitation peak are indicated on the top of each spectrum. (These spectra were generated using the Fluorescence Spectra Viewer, http://probes.invitrogen.com/resources/spectraviewer/).

Detection of FRET

As explained before, FRET causes a decrease in donor fluorescence emission and lifetime and an increase in acceptor emission fluorescence and lifetime. Based on these effects, different methods were developed to detect and quantify FRET.

Sensitized emission measurements- This method measures the changes of both donor and acceptor fluorescence emissions following excitation of the donor molecule only (Hamori *et al.*, 1980). Therefore the donor is excited at a specific wavelength and the

resulting donor and acceptor fluorescence emissions are collected on 2 different channels, i.e. donor channel and FRET channel respectively, and they are compared. Acceptor emissions higher than donor emissions indicate that FRET occurred. To obtain an accurate and quantitative FRET value, it is necessary to correct mathematically the acceptor emission values for the spectral cross-talk (Mahajan *et al.*, 1998). Sensitized emission measurements are performed using either a fluorescence microscope (Hamori *et al.*, 1980, Miyawaki *et al.*, 1997; Day *et al.*, 2001), a flow-sorter (Hamori *et al.*, 1980) or a fluorometer (Lin *et al.*, 1997; Miyawaki and Tsien, 2000).

Acceptor photobleaching- This method measures changes in donor fluorescence emissions following photobleaching of the acceptor (Mekler *et al.*, 1994). The principle of acceptor photobleaching FRET measurements between ECFP and EYFP is shown in Figure 2.7. A major consequence of FRET is a reduction in donor emissions. Photobleaching the acceptor prevents FRET from occurring and results in the donor fluorescence emission recovery. The measurements are carried out by exciting the donor at a specific wavelength and recording the donor fluorescence emission before and after photobleaching the acceptor. An increase in donor fluorescence following acceptor photobleaching indicates that FRET occurred. This is a qualitative FRET measurement that is performed using either a fluorimeter, a fluorescence microscope (Day *et al.*, 2001), a flow-cytometer (He *et al.*, 2003) or a laser-scanning confocal microscope (Karpova *et al.*, 2003). Confocal microscopy is preferentially used for acceptor photobleaching FRET measurements as it enables the bleaching of small areas in a cell instead of bleaching the whole cell. This is a great advantage for the study of membrane proteins (Verveer *et al.*, 2001). In addition, confocal microscope softwares have been improved to measure fluorescence emissions free of spectral cross talk contaminations, thus enabling a more accurate FRET quantification (Dickinson *et al.*, 2001).

Donor photobleaching- This method is based on the observation that a fluorophore with a long fluorescence lifetime is photobleached faster than a fluorophore with a shorter one (Bastians and Squire, 1999). Since FRET results in a reduction in donor fluorescence lifetime, photobleaching a donor involved in a FRET process takes longer than photobleaching a free donor. By calculating the time necessary to photobleach a donor in the presence or in the absence of an acceptor, it is possible to deduce the FRET efficiency.

Fluorescence lifetime imaging microscopy, FLIM- This method measures the variation in the donor fluorescence lifetime in the presence and the absence of the acceptor following excitation of the donor (Bastians and Squire, 1999). FLIM is performed either on a conventional fluorescence microscope or on a confocal microscope. This detection method is appropriate for FRET measurements in live cells whereas photobleaching based techniques should be performed in fixed cells.

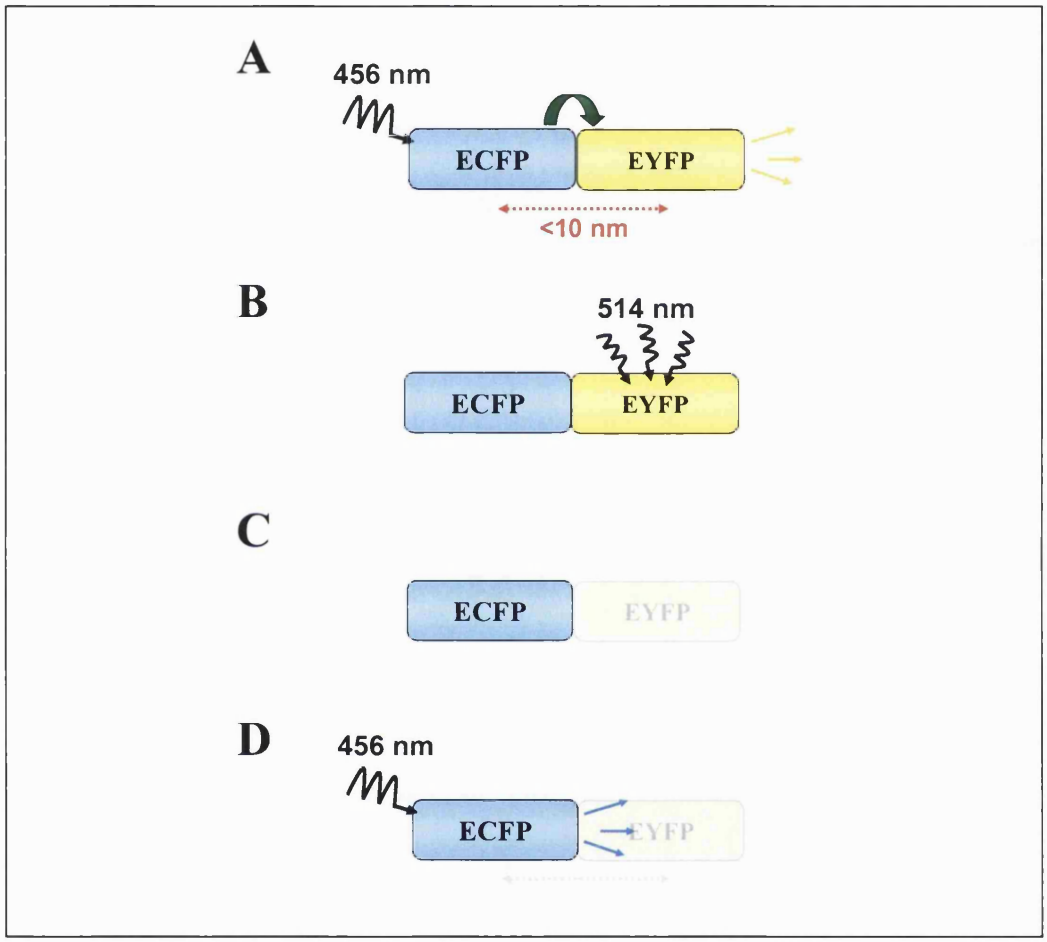

Figure 2.7. A diagram describing the principle of the detection of FRET between ECFP and EYFP by acceptor photobleaching. This diagram shows that photobleaching the acceptor, i.e. EYFP, results in a disparition of EYFP fluorescence and in an increase in donor, i.e. ECFP, fluorescence following excitation of the donor. A, FRET occurs between ECFP and EYFP located within 10 nm of each other. As a result, excitation of ECFP at λ = 456 nm results in excitation of EYFP and emission of EYFP fluorescence. B, EYFP is photobleached at an appropriate wavelenght, i.e. λ = 514 nm resulting in C, a destruction of EYFP fluorophore. D, an increase in ECFP fluorescence emissions is detected following excitation of ECFP at λ = 456 nm.

Applications

FRET imaging was successfully used to detect inter-molecular interactions *in vivo* to study protein dynamics in live cells. For example, the interaction between the neuronal

proteins, syntaxin-1 and Munc-18, was studied by tagging the proteins with either ECFP or EYFP and detecting FRET by using 2 methods: acceptor photobleaching and sensitized emission measurements (Liu *et al.*, 2004). Inter-molecular FRET was also used to study heteromeric ion channel assembly such as the α4β2 nicotinic acetylcholine receptor (Nashmi *et al.*, 2003). This was performed by tagging the α4 and β2 subunits with ECFP or EYFP in their intracellular loop and measuring FRET between both subunits by acceptor photobleaching.

Intra-molecular FRET was used to develop molecular indicators for the *in vivo* detection of intracellular calcium concentrations (Miyawasaki *et al.*, 1997), enzyme activity (Miyawasaki and Tsien, 2000) and protein phosphorylation (Nagai *et al.*, 2000), *in vivo*.

2.2.5.3.2. Determination of FRET efficiencies by acceptor photobleaching

Using the multi-track imaging mode of the LSM510 Meta

HEK 293 cells were co-transfected with constructs encoding both EYFP and ECFP fusion proteins, fixed 24-48 h after transfection and analysed for FRET in the multi-track imaging mode of the microscope. The test sample was excited with the λ = 458 nm laser line paired with a λ = 458 nm dichroic mirror. ECFP and EYFP emitted fluorescences were collected on 2 different channels. ECFP emissions were collected between λ = 475-525 nm with a band-pass (BP) filter 475-525 and EYFP emissions above λ = 530 nm were collected with a long pass (LP) filter 530. An area of co-localisation was selected and EYFP was photobleached for 20 sec in this area using the λ = 514 nm laser line at full power. The cell was imaged again with the λ = 458 nm laser line paired with a λ = 458 nm dichroic mirror and ECFP and EYFP emitted fluorescences were collected on 2 different channels as before.

(iv) FRET efficiency, *E*, was calculated with the equation $E = [(I_{after,pb} - I_{before,pb}) / (I_{after,pb})] \times 100$, with $I_{before,pb}$, ECFP fluorescence intensity pre-photobleaching and $I_{after,pb}$, ECFP fluorescence intensity post-photobleaching.

Using the lambda imaging mode of the LSM510 Meta

An HEK 293 cell expressing both EYFP and ECFP fusion proteins was imaged in the lambda mode. Lambda stacks were generated by exciting the test sample with λ = 458 nm laser line paired with a λ = 458 nm dichroic mirror and collecting emitted fluorescence on the Meta detector between λ = 456.5-617 nm, with a 10.7 nm increment. A defined area of co-localisation in the cell was selected and EYFP, in this

region, was photobleached by using the $\lambda = 514$ nm laser line at full power for 30 s. The cell was imaged post-photobleaching with the $\lambda = 458$ nm laser line as before. The mixed signals generated pre- and post-photobleaching were unmixed using ECFP and EYFP reference spectra with the LSM510 Meta hardware package.

Relative FRET efficiencies were calculated according to Liu *et al.* (2004). The relative energy transfer efficiency was measured as the increase in ECFP emission fluorescence after photobleaching EYFP. Only cells where EYFP was bleached at least 80% were used for the calculations. Fluorescence intensity values were obtained from the unmixed data. These values were corrected for background fluorescence (~10%) measured in a region containing an untransfected cell. Relative FRET efficiency was calculated as follows: $[(I_{after,pb} - I_{before,pb}) / (I_{after,pb})] \times 100$ with $I_{before,pb}$, ECFP fluorescence intensity pre-photobleaching and $I_{after,pb}$, ECFP fluorescence intensity post-photobleaching. Pre- and post-photobleaching values were taken at t = 1.6 sec and at t = 32 sec respectively. FRET efficiency values were corrected for pseudo-FRET. Pseudo-FRET was measured by applying the photobleaching protocol to cells that were transfected with pECFP only. Pseudo-FRET efficiencies were substracted from the calculated relative FRET efficiencies of the test samples. As a further control, relative FRET efficiencies were also calculated for an area of co-localisation that was not photobleached when possible. This was to ensure that the determined FRET efficiencies were not artefacts due to the photobleaching protocol. FRET values in the photobleached region were compared to:

(i) FRET values obtained in the unbleached region using a paired t-test

(ii) FRET values obtained for the negative control using an unpaired t-test

If the FRET value in the photobleached region was significantly different from the values obtained in the unbleached region and for the negative control, it was concluded that FRET occurred (Karpova *et al.*, 2003). For significancy, a p-value lower than 0.01 was chosen. The detailed procedure for the measurement of FRET efficiencies by acceptor photobleaching is shown on Figure 2.8. An example of FRET measurement by acceptor photobleaching is shown on Figure 2.9.

STEP 1: Choose a fluorescent cell co-transfected with ECFP and EYFP. Select the excitation laser line λ = 458 nm, the λ = 458 nm dichroic mirror and an emission fluorescence collection range between λ = 456.5-517 nm

STEP 2: Generate a lambda scan by clicking on "Find". Reduce the level of background and saturation using the "gain" and "offset" functions to optimise the brightness and saturation. Generate a lambda stack again

STEP 3: Obtain the mixed emission spectra by selecting "Lambda Mean"

STEP 4: Click on the "Bleaching" icon. Select a region of co-localisation to photobleach. Go to the "Time series" window and start the bleaching: photobleach EYFP with the λ = 514 nm laser line, at full power

STEP 5: Obtain the mixed emission spectra after photobleaching by selecting "Mean"

STEP 6: "Unmix" the mean mixed emission spectrum and get pre- and post-photobleaching images showing the real contribution of each fluorophore

STEP 7: Quantify FRET efficiency

Figure 2.8. Detailed procedure for the measurement of acceptor photobleaching FRET between ECFP and EYFP using the lambda mode of the LSM510 Meta confocal microscope

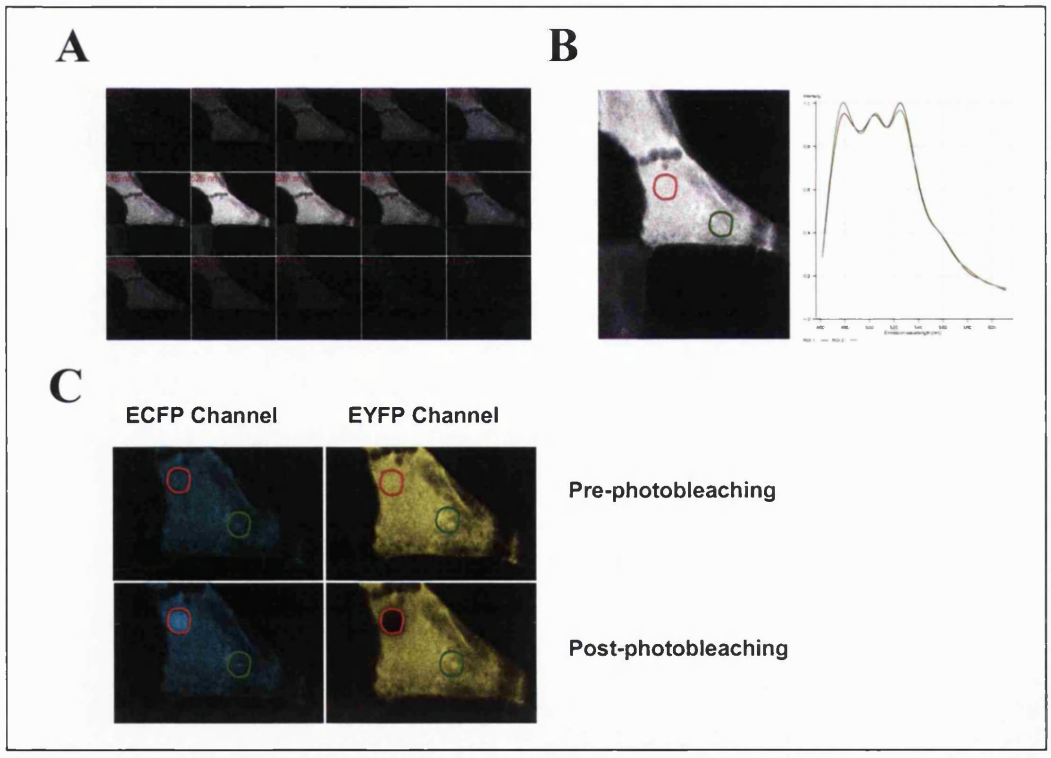

Figure 2.9. An example of FRET acceptor photobleaching measurement. A, an HEK 293 cell transfected with pECFP-EYFP is imaged using the lambda mode of the microscope. A lambda stack is generated for a range λ = 456.5-620 nm every ~ 10.7 nm following excitation of the sample with the λ = 458 nm laser line. B, the mean lambda stack is obtained by clicking on the icon "Mean". Two areas of ECFP/EYFP co-localisation (red and green boxes, left panel) are selected within the cell. For each area, a mixed emission spectrum is automatically generated (red and green, right panel). C, EYFP was photobleached in the red area resulting in a decrease in EYFP fluorescence and in an increase in ECFP emission fluorescence. The "Unmixed" pictures before and after photobleaching are shown in C. They are obtained using the function "Unmix".

CHAPTER 3

MOLECULAR CHARACTERISATION OF GRIF-1 AND KINESIN-1 HEAVY CHAINS INTERACTIONS BY CONFOCAL MICROSCOPY IMAGING STUDIES

3.1. INTRODUCTION

3.1.1. Rationale for the use of confocal microscopy imaging to investigate GRIF-1/kinesin-1 interactions

Little is known about the role of GRIF-1 in brain. As described in section 1.4, GRIF-1 is related to the human trafficking protein, HAP-1, and to the *Drosophila* kinesin-associated protein, Milton. GRIF-1 associates with $GABA_A$ receptor β2 subunits and with the molecular motor, kinesin-1 (Beck *et al.*, 2002; Brickley *et al.*, 2005). Therefore GRIF-1 was proposed to play a role in kinesin-1-dependent transport processes by linking kinesin-1 to cargoes such as $GABA_A$ receptor β2 subunits. The function of GRIF-1 was initially investigated in crude homogenates of GRIF-1-transfected cells using several biochemical methods such as immunoprecipitations (Beck *et al.*, 2002; Brickley *et al.*, 2005). A different approach involving intact cells could provide further information on GRIF-1 function.

The green fluorescent protein (GFP) and its variants are commonly used as reporters to study protein localisation in transfected cells (see section 3.1.2). Proteins of interest are genetically fused to GFP, expressed in cells and visualised by confocal or fluorescence microscopy. Several proteins within a cell can be visualised simultaneously and co-localisation studies carried out by tagging them with different GFP spectral variants such as enhanced cyan fluorescent protein (ECFP) and enhanced yellow fluorescent protein (EYFP) (see section 3.1.2). For example, the neuronal proteins, syntaxin-1 and Munc-18, were labelled with ECFP and EYFP respectively and their subcellular localisation within the same cell was analysed by confocal microscopy imaging (Liu *et al.*, 2004).

The HEK 293 and COS-7 mammalian cell lines are widely used for confocal microscopy imaging studies because they are easy to grow and to transfect. They do not express GRIF-1 endogenously and thus they are appropriate for the study of GRIF-1 cellular location following the transient expression of a fluorescently-tagged GRIF-1. Since GRIF-1 interacts with the prototypic kinesin heavy chain, KIF5C (Brickley *et al.*, 2005), analyses of GRIF-1 distribution in the presence of KIF5C could provide further understanding on the role of GRIF-1 in intracellular kinesin-1-based trafficking events.

This chapter describes the confocal microscopy imaging study of GRIF-1 and KIF5C in HEK 293 and COS-7 cells using GRIF-1 and KIF5C constructs fused to GFP variants (see section 3.1.2).

3.1.2. The green fluorescent protein, GFP: a marker to study protein localisation

GFP was initially isolated from the jellyfish, *Aequorea victoria*, as a protein co-purified with the chemiluminescent protein, aequorin. GFP was characterised and shown to emit bright green fluorescence following excitation at λ = 395 nm or λ = 475 nm without additional co-factors or substrates (Morise *et al.*, 1974). Following the cloning of the gene encoding GFP (Prasher *et al.*, 1992), the GFP amino acid sequence was deduced and its structure was solved (Ormö *et al.*, 1996; Yang *et al.*, 1996; reviewed by Tsien, 1998). GFP is a 238 amino acid protein, formed by 11 β-strands, the so-called "β-can" structure and an axial α-helix to which a three-residue chromophore (Ser-65, Tyr-66, Gly-67) is attached. To emit fluorescence, the chromophore needs to be buried in the β-can structure.

Expression of GFP in heterologous systems revealed that the protein was still able to emit bright green fluorescence as initially observed with purified GFP (Chalfie *et al.*, 1994). Since then, GFP has been used as a reporter gene to study gene expression and protein dynamics in cells, tissues and organisms (reviewed in Tsien, 1998; Zhang *et al.*, 2002).

To improve the fluorescence, the expression and the folding properties of wild-type GFP in mammalian cells, the protein was engineered leading to several GFP variants such as EGFP (reviewed by Tsien, 1998). Addition of mammalian codons and mutation of Phe-64 to Leu improved GFP expression in mammalian cells and folding of the chromophore at 37°C. Mutation in the chromophore or in adjacent residues yielded GFP variants with different spectral properties, i.e. different excitation and emission spectra. They are used in combination to study simultaneously the function of different proteins in the same cell, tissue or organism. For multi-colour imaging, GFP variants are also used in combination with fluorescent proteins isolated from other organisms such as the red fluorescent protein, DsRed, from the coral *Discosoma sp.* (Matz *et al.*, 1999). Further, GFP variants such as ECFP and EYFP are commonly used as donor and acceptor for the detection of FRET (section 3.1.3.2). ECFP contains 6 mutations, Phe-64 to Leu, Ser-65 to Thr, Tyr-66 to Trp, Asn-146 to Ile, Met-153 to Thr, Val-163 to Ala (Heim *et al.*, 1994; Heim and Tsien, 1996;

Angres and Green, 1999) and it has its maximal excitation and emission peaks at λ = 433 nm and λ = 475 nm, respectively. EYFP has 4 mutations, i.e. Ser-65 to Gly, Val-68 to Leu, Ser-72 to Ala and Thr-203 to Tyr. EYFP is excited at λ = 514 nm and emits at λ = 527 nm (Rizzuto *et al.*, 1996). A new generation of GFP variants with improved spectral properties has been recently developed for multi-colour imaging and FRET studies (reviewed in Shaner *et al.*, 2005).

3.1.3. Aim of this chapter

The aim of this chapter was to investigate the putative role of GRIF-1 as an adaptor protein involved in kinesin-1-based intracellular trafficking using a confocal microscopy imaging approach. Therefore fluorescent GRIF-1 and fluorescent KIF5C probes were generated, characterised and their distribution in mammalian cell lines was analysed.

3.2. RESULTS

To examine the function of GRIF-1 in kinesin-1-mediated transport, GRIF-1 and the prototypic kinesin-1, KIF5C, were fused to ECFP or EYFP by molecular cloning. The fluorescent GRIF-1 and fluorescent KIF5C fusion proteins were characterised according to their molecular weight and their ability to behave as the non-fluorescent GRIF-1 and non-fluorescent KIF5C proteins in immunoprecipitation assays following expression in HEK 293 cells. After characterisation, their distribution in transfected HEK 293 and COS-7 cells was examined by confocal microscopy imaging. The functional significance of GRIF-1 and KIF5C interactions was further investigated following transfection of COS-7 cells with fluorescent-tagged GRIF-1, fluorescent-tagged KIF5C and fluorescent-tagged organelle markers.

The results presented in this section were published in part in Smith *et al.* (2006) and in Pozo and Stephenson (2006).

3.2.1. Preparation of ECFP-GRIF-1, EYFP-GRIF-1, ECFP-KIF5C, EYFP-KIF5C and truncated EYFP-KIF5C chimeras

GRIF-1 was N-terminally tagged with either ECFP or EYFP since previous tagging of GRIF-1 with short tags at this end of the protein did not alter GRIF-1 binding properties (Beck *et al.*, 2002). As described in chapter 1.1, KIF5C contains functional domains at both ends, i.e an N-terminal microtubule binding site and a C-terminal cargo binding site. It was not known whether addition of a fluorescent protein would interfere with these. Therefore ECFP or EYFP were fused to either the KIF5C N-terminal end or to the KIF5C C-terminal end. Fluorescent truncated KIF5C chimeras were also generated to determine the GRIF-1 binding sites on KIF5C. Hence the motor domain of KIF5C, KIF5C-NMD, was N-terminally fused to EYFP while the non-motor domain of KIF5C, KIF5C-NMD, was C-terminally tagged with EYFP. The sub-cloning strategy for all constructs is shown in Table 3.1.

GRIF-1 constructs- GRIF-1 was amplified by PCR from pCIS-GRIF-1 and ligated in frame into the *EcoRI/SalI* restriction sites of pECFP-C1 and pEYFP-C1 cloning vectors to yield pECFP-GRIF-1 and pEYFP-GRIF-1 respectively (Appendices 3.1-3.7).

Fusion protein	Construct	Vector*	Insert	Oligonucleotide primers used for PCR amplification	Restriction sites
EYFP-GRIF-1	pEYFP-GRIF-1	Y	GRIF-$1_{1\text{-}913}$	GRIF1/*EcorI* forward primer GRIF1/*SalI* reverse primer	*EcoRI/SalI*
ECFP-GRIF-1	pECFP-GRIF-1	C	GRIF-$1_{1\text{-}913}$	GRIF1/*EcorI* forward primer GRIF1/*SalI* reverse primer	*EcoRI/SalI*
N-EYFP-KIF5C	pN-EYFP-KIF5C	Y	KIF5$C_{1\text{-}957}$	KIF5c/*EcoRI* forward primer KIF5c/*SalI* reverse primer	*EcoRI/SalI*
N-ECFP-KIF5C	pN-ECFP-KIF5C-	C	KIF5$C_{1\text{-}957}$	KIF5c/*EcoRI* forward primer KIF5c/*SalI* reverse primer	*EcoRI/SalI*
C-EYFP-KIF5C	pC-EYFP-KIF5C	Y	KIF5$C_{1\text{-}957}$	KIF5c/*NheI* forward primer KIF5c/*NheI* reverse primer	*NheI*
C-ECFP-KIF5C	pECFP-GRIF-1	C	KIF5$C_{1\text{-}957}$	KIF5c/*NheI* forward primer KIF5c/*NheI* reverse primer	*NheI*
EYFP-KIF5C-MD	pEYFP-KIF5C-MD	Y	KIF5$C_{1\text{-}336}$	KIF5cMD/*XhoI* forward primer KIF5cMD/*EcoRI* reverse primer	*XhoI/EcoRI*
EYFP-KIF5C-NMD	pEYFP-KIF5C-NMD	Y	KIF5$C_{336\text{-}957}$	KIF5cNMD/*NheI* forward primer KIF5c/*NheI* reverse primer	*NheI*

Table 3.1. A summary of the cloning strategies used for the generation of fluorescently-tagged GRIF-1 and fluorescently-tagged KIF5C fusion proteins.
*The cloning vectors used were either pEYFP-C1 (Y) or pECFP-C1 (C). The name of the oligonucleotide primers refers to the sequences in Table 2.5.

KIF5C constructs- KIF5C was amplified by PCR from pcDNAHisMax-KIF5C and sub-cloned in frame into the *EcoRI/SalI* restriction sites of pECFP-C1 and pEYFP-C1, yielding pN-ECFP-KIF5C and pN-EYFP-KIF5C respectively. The KIF5C PCR product was sub-cloned in frame into the *NheI* restriction site of pECFP-C1 and pEYFP-C1 to generate pC-ECFP-KIF5C and pC-EYFP-KIF5C respectively (Appendix 3.8)

Truncated KIF5C constructs- The motor domain (MD) of KIF5C (residues 1-335) was amplified from pcDNAHisMax-KIF5C and sub-cloned in frame into the *XhoI/EcoRI* restriction sites of pEYFP-C1 to yield pEYFP-KIF5C-MD. The non-motor domain (NMD) of KIF5C (residues 336-957) was amplified from pcDNAHisMax-KIF5C and ligated in frame into the *NheI* restriction site of pEYFP-C1 to yield pEYFP-KIF5C-NMD (Appendix 3.9).

3.2.2. Molecular size of ECFP-GRIF-1, EYFP-GRIF-1, ECFP-KIF5C, EYFP-KIF5C and truncated EYFP-KIF5C chimeras

To test whether the molecular size of the fluorescent GRIF-1 and fluorescent KIF5C chimeras was consistent with the addition of ECFP or EYFP, the M_r of each fluorescent fusion protein was compared to the M_r of the non-fluorescent protein, i.e. GRIF-1, KIF5C, KIF5C-MD and KIF5C-NMD, by immunoblotting following expression of each construct in HEK 293 cells. Since fluorescent GRIF-1 and fluorescent KIF5C fusion proteins were to be used for confocal microscopy imaging studies, it was also necessary to ensure that ECFP or EYFP were not cleaved from GRIF-1 or KIF5C and thus the fluorescence observed by confocal microscopy was obtained from fluorescent GRIF-1 or KIF5C fusion proteins. Therefore immunoblotting analyses were carried out using both anti-GFP antibodies and either anti-GRIF-$1_{8\text{-}633}$, anti-KIF5C or anti-c-Myc antibodies. Homogenates of untransfected cells were used as a control for the specificity of the immunoreactive bands detected by each antibody.

GRIF-1 constructs- Anti-GRIF-$1_{8\text{-}633}$ antibodies recognised 3 major bands with M_r = 115 kDa, M_r = 93 kDa and M_r = 85 kDa in homogenates of cells transfected with pCIS-GRIF-1 (Figure 3.1, lane 2). Additional bands of lower molecular size were also detected. The immunoreactive band with M_r = 115 kDa corresponded to that predicted for GRIF-1. The bands with M_r = 93 kDa, M_r = 85 kDa and with lower molecular size may be either

proteolytic or not fully post-translationally modified variants of GRIF-1. In homogenates of cells transfected with pECFP-GRIF-1 or pEYFP-GRIF-1, anti-GRIF-1_{8-633} antibodies recognised a major immunoreactive band with M_r = 143 kDa and 3 minor bands with M_r = 115 kDa, M_r = 93 kDa and M_r = 85 kDa (Figure 3.1, lanes 3, 4). The band with M_r =143 kDa corresponded to that predicted for ECFP-GRIF-1 and EYFP-GRIF-1. The 115-kDa band had a molecular size consistent with the size of non-fluorescent GRIF-1 suggesting that ECFP-GRIF-1 could be proteolytically cleaved giving 2 moieties, ECFP and GRIF-1. However this 115-kDa immunoreactive band is also recognised by anti-GFP antibodies (Figure 3.1, lanes 7, 8) thus showing that ECFP-GRIF-1 is not cleaved. The bands with M_r = 93 kDa and M_r = 85 kDa are also detected by the anti-GFP in homogenates of cells transfected with pECFP-GRIF-1 or pEYFP-GRIF-1 (Figure 3.1, lanes 7, 8). These bands may be proteolytic variants of ECFP-GRIF-1 or EYFP-GRIF-1. Anti-GFP antibodies detected major immunoreactive bands with M_r = 143 kDa consistent with the size expected for ECFP-GRIF-1 or EYFP-GRIF-1. No bands were detected when probing homogenates of cells transfected with pCIS-GRIF-1 with anti-GFP antibodies.

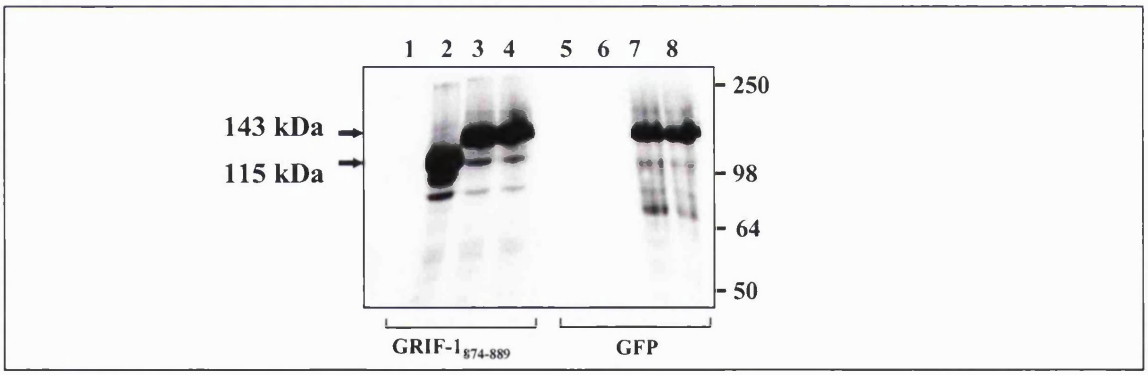

Figure 3.1. Molecular size characterisation of ECFP-GRIF-1 and EYFP-GRIF-1. Homogenates of HEK 293 cells transfected with either pCIS-GRIF-1, pECFP-GRIF-1 or pEYFP-GRIF-1 were analysed by immunoblotting using antibodies as indicated on the abcissa. Lanes 1, 5, homogenates of untransfected cells; lanes 2, 6, homogenates of cells transfected with pCIS-GRIF-1; lanes 3, 7, homogenates of cells transfected with pECFP-GRIF-1; lanes 4, 8, homogenates of cells transfected with pEYFP-GRIF-1. The molecular weight standards (kDa) are shown on the right. Immunoreactive bands of interest are indicated by an arrow, M_r (GRIF-1) = 115 kDa, M_r (ECFP-GRIF-1) = 143 kDa, M_r (EYFP-GRIF-1) = 143 kDa. This immunoblot is representative of n = 3 experiments from n = 3 independent transfections.

KIF5C constructs- Anti-KIF5C antibodies recognised a single immunoreactive band with M_r = 115 kDa in homogenates of cells transfected with pcDNAHisMax-KIF5C consistent with that predicted for His-tagged KIF5C (Figure 3.2 A, lane 2; Figure 3.2 B, lane 2). A single band with M_r = 143 kDa was detected in homogenates of cells transfected with either

pN-ECFP-KIF5C (Figure 3.2 A, lanes 3), pC-ECFP-KIF5C (Figure 3.2 A, lanes 4), pN-EYFP-KIF5C (Figure 3.2 B, lanes 3) or pC-EYFP-KIF5C (Figure 3.2 B, lanes 4). This immunoreactive band corresponded to that predicted for N-ECFP-KIF5C, C-ECFP-KIF5C, N-EYFP-KIF5C or C-EYFP-KIF5C. This M_r = 143 kDa immunoreactive band was also detected by anti-GFP antibodies (Figure 3.2 A, lanes 7, 8; Figures 3.2 B, lanes 7, 8).

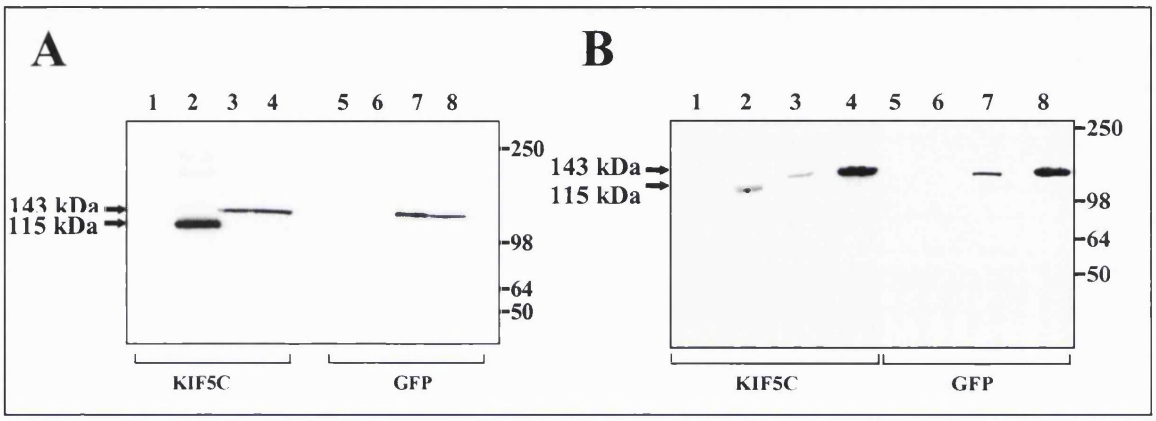

Figure 3.2. Molecular size characterisation of EYFP-KIF5C and ECFP-KIF5C. Homogenates of HEK 293 cells transfected with either pcDNAHisMax-KIF5C, pN-EYFP-KIF5C, pC-EYFP-KIF5C, pN-ECFP-KIF5C or pC-ECFP-KIF5C were analysed by immunoblotting using antibodies as indicated on the abscissae. A, expression of EYFP-KIF5C, B, expression of ECFP-KIF5C. The layout is the same in A and B. Lanes 1, 5, homogenates of untransfected cells; lanes 2, 6, homogenates of cells transfected with pcDNAHisMax-KIF5C; lanes 3, 7, homogenates of cells transfected with pN-EYFP-KIF5C or pN-ECFP-KIF5C; lanes 4, 8, homogenates of cells transfected with pC-EYFP-KIF5C or pC-ECFP-KIF5C. The molecular weight standards (kDa) are shown on the right. Immunoreactive bands of interest are indicated by an arrow, M_r (His-tagged KIF5C) = 115 kDa, M_r (N-EYFP-KIF5C) = 143 kDa, M_r (C-EYFP-KIF5C) = 143 kDa, M_r (N-ECFP-KIF5C) = 143 kDa, M_r (C-ECFP-KIF5C) = 143 kDa. These immunoblots are representative of n = 3 experiments from n = 3 independent transfections.

KIF5C truncated mutants- Anti-c-Myc antibodies revealed an immunoreactive band with M_r = 39 kDa in homogenates of cells transfected with pCMVKIF5C-MD (Figure 3.3 A, lane 2). This was consistent with the M_r predicted for c-Myc-tagged KIF5C-MD. Anti-GFP antibodies recognised a M_r = 64 kDa immunoreactive band in homogenates of cells transfected with pEYFP-KIF5C-MD, consistent with the M_r predicted for EYFP-KIF5C-MD (Figure 3.3 A, lane 6).

Anti-KIF5C antibodies recognised a M_r = 98 kDa band in homogenates of cells transfected with pCMVKIF5C-NMD consistent with the size predicted for non-fluorescent KIF5C-NMD (Figure 3.3 B, lane 2). In homogenates of cells transfected with pEYFP-KIF5C-NMD, anti-KIF5C antibodies detected 2 bands with M_r = 98 kDa and M_r = 139 kDa (Figure 3.3 B, lane 3). The 139-kDa band had a size consistent with that of EYFP-KIF5C-

NMD, within the 10% range expected in SDS-PAGE electrophoresis. The 98-kDa band is consistent with the size expected for KIF5C-NMD and it is not detected by anti-GFP antibodies in pEYFP-KIF5C-NMD transfected cell homogenates (Figure 3.3 B, lane 6). This indicates that EYFP-KIF5C-NMD can be proteolytically degraded in 2 moieties, EYFP and KIF5C-NMD, upon expression in HEK 293 cells. Anti-GFP antibodies recognised 2 immunoreactive bands with M_r = 139 kDa and M_r = 136 kDa in homogenates of cells transfected with pEYFP-KIF5C-NMD (Figure 3.3 B, lane 6). The band with M_r = 139 kDa band corresponded to that expected for EYFP-KIF5C-NMD and the band with M_r = 136 kDa may be a not fully post-translationally modified form of EYFP-KIF5C-NMD. Indeed KIF5C-NMD has been shown to be highly phosphorylated in its NMD (Hollenbeck, 1993).

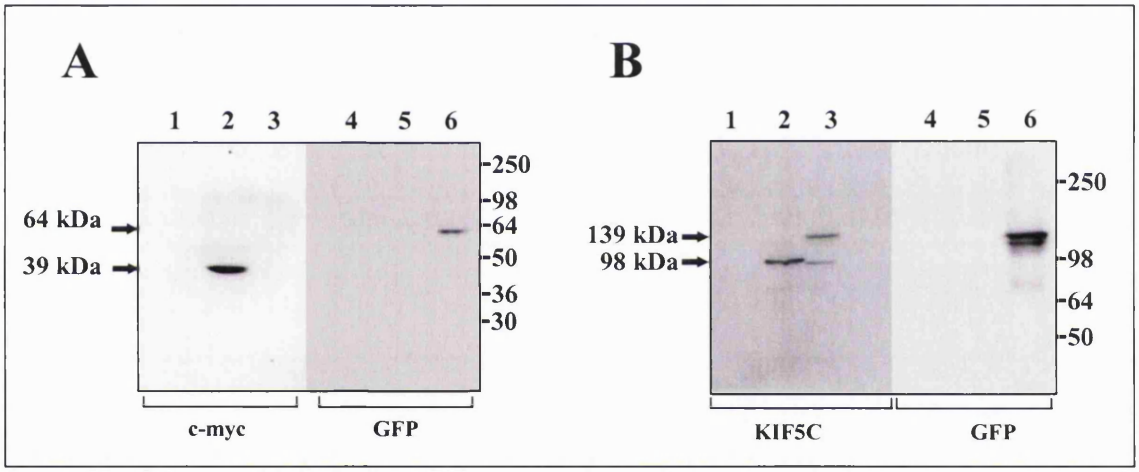

Figure 3.3. Molecular size characterisation of EYFP-KIF5C truncated constructs. A, homogenates of HEK 293 cells transfected either with pCMVKIF5C-MD or pEYFP-KIF5C-MD and B, homogenates of HEK 293 cells transfected with either pCMVKIF5C-NMD or pEYFP-KIF5C-NMD were analysed by immunoblotting using antibodies as indicated on the Figure. A, lanes 1, 4, homogenates of untransfected cells; lanes 2, 5, homogenates of cells transfected with pCMVKIF5C-MD; lanes 3, 6, homogenates of cells transfected with pEYFP-KIF5C-MD. B, lanes 1, 4, homogenate of untransfected cells; lanes 2, 5, homogenates of cells transfected with pCMVKIF5C-NMD; lanes 3, 6, homogenates of cells transfected with pEYFP-KIF5C-NMD. The molecular weight standards (kDa) are shown on the right. Immunoreactive bands of interest are indicated with an arrow, M_r (c-Myc-tagged KIF5C-MD) = 39 kDa, M_r (EYFP-KIF5C-MD) = 64 kDa, M_r (c-Myc-tagged KIF5C-NMD) = 98 kDa, M_r (EYFP-KIF5C-NMD) = 139 kDa. These immunoblots are representative of n = 3 experiments from n = 3 transfections.

To summarise, in all cases, the fluorescent-tagged proteins showed an increase of ~ 30 kDa consistent with the addition of ECFP or EYFP (Figure 3.4). Further, this increase in M_r was seen with both specific antibodies as appropriate, showing no tendency for protein

degradation except for a small proportion of EYFP-KIF5C-NMD as detected by anti-KIF5C antibodies.

A

GRIF-1 fluorescent constructs

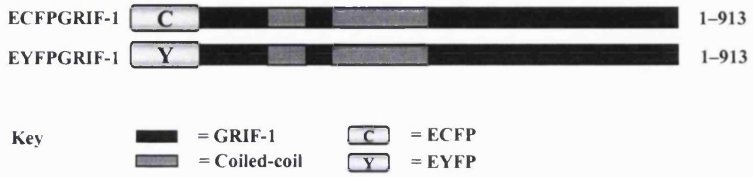

B

KIF5C fluorescent constructs

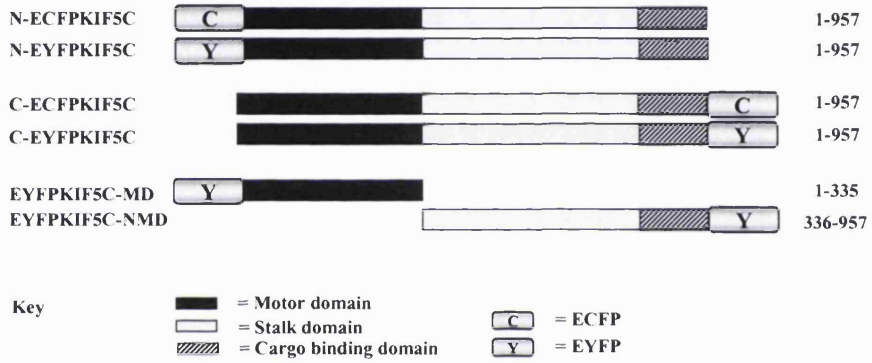

C

Fusion protein	Calculated M_r (kDa)	Experimental M_r (kDa)
EYFP-GRIF-1	129	143
ECFP-GRIF-1	129	143
N-EYFP-KIF5C	139	143
N-ECFP-KIF5C	139	143
C-EYFP-KIF5C	139	143
C-ECFP-KIF5C	139	143
EYFP-KIF5C-MD	65	64
EYFP-KIF5C-NMD	108	139

Figure 3.4. A Figure summarising the structure and molecular weight (M_r) of GRIF-1 and KIF5C fluorescent fusion proteins. A, GRIF-1 fluorescent constructs; B, KIF5C fluorescent constructs and C, a Table summarising the calculated and experimental M_r.

3.2.3. Characterisation of ECFP-GRIF-1, EYFP-GRIF-1, ECFP-KIF5C, EYFP-KIF5C and truncated EYFP-KIF5C chimeras according to their protein-protein interaction properties

It was necessary to show that the addition of ECFP or EYFP did not interfere with the intrinsic properties of GRIF-1, KIF5C, KIF5C-MD and KIF5C-NMD. Non-fluorescent GRIF-1 has been shown to associate with His-tagged KIF5C and c-Myc-tagged KIF5C-NMD but not with c-Myc-tagged KIF5C-MD in immunoprecipitation studies (Brickley *et al.*, 2005; Smith *et al.*, 2006). To investigate whether fluorescent GRIF-1, fluorescent KIF5C, fluorescent KIF5C-MD and fluorescent KIF5C-NMD behaved as the non-fluorescent GRIF-1, non-fluorescent His-tagged KIF5C, non-fluorescent c-Myc-tagged KIF5C-MD and non-fluorescent c-Myc-tagged KIF5C-NMD, respectively, immunoprecipitation experiments were carried out. Detergent soluble extracts of HEK 293 cells co-transfected with different combinations of fluorescent or non-fluorescent GRIF-1 and KIF5C constructs were prepared and immunoprecipitations were performed using either sheep polyclonal anti-GRIF-$1_{874-889}$ antibodies or non-immune sheep IgGs as a control. The immune pellets were analysed by immunoblotting using first anti-GRIF-1 antibodies to show that GRIF-1 was specifically immunoprecipitated and thus that the immunoprecipitation was successful. Then, either anti-HisG, anti-KIF5C or anti-GFP antibodies were used to detect the protein that was co-immunoprecipitated with the GRIF-1 construct.

Association properties of ECFP-GRIF-1- Immune pellets from cells co-transfected with pECFP-GRIF-1 + pcDNAHisMax-KIF5C were probed with either anti-GRIF-1_{8-633} antibodies or anti-HisG antibodies. Anti-GRIF-1_{8-633} antibodies recognised an immunoreactive band with M_r = 143 kDa in the detergent soluble fraction and in the immune pellet, but not in the non-immune control pellet, indicating that ECFP-GRIF-1 was expressed and specifically immunoprecipitated (Figure 3.5 A, lanes 1-3). Anti-HisG antibodies detected an M_r = 115 kDa band in the immune pellet but not in the control pellet thus showing that His-tagged KIF5C was co-immunoprecipitated with ECFP-GRIF-1 (Figure 3.5 A, lanes 4-6). Immune pellets of cells co-transfected with pECFP-GRIF-1 + pN-EYFP-KIF5C were analysed with either anti-GRIF-$1_{874-889}$ antibodies or anti-KIF5C antibodies. Anti-GRIF-$1_{874-889}$ antibodies recognised an immunoreactive band with M_r =

143 kDa in the detergent soluble fraction and in the immune pellet, but not in the non-immune control pellet, indicating that ECFP-GRIF-1 was expressed and specifically immunoprecipitated (Figure 3.5 B, lanes 1-3). When probing with anti-KIF5C antibodies, a band with M_r = 143 kDa was detected (Figure 3.5 B, lanes 4, 5). This band was not visible in the control pellet (Figure 3.5 B, lane 6). Immune pellets of cells co-transfected with pECFP-GRIF-1 + pC-EYFP-KIF5C were analysed with anti-GRIF-$1_{874-889}$ antibodies or anti-KIF5C antibodies. As before, anti-GRIF-$1_{874-889}$ antibodies recognised an immunoreactive band with M_r = 143 kDa in the detergent soluble fraction and in the immune pellet, but not in the non-immune control pellet, indicating that ECFP-GRIF-1 was expressed and specifically immunoprecipitated (Figure 3.5 C, lanes 1-3). Anti-KIF5C antibodies detected a band with M_r = 143 kDa (Figure 3.5 C, lanes 4, 5). This band was not visible in the control pellet (Figure 3.5 C, lane 6). This indicated that N-EYFP-KIF5C and C-EYFP-KIF5C were specifically co-immunoprecipitated with ECFP-GRIF-1.

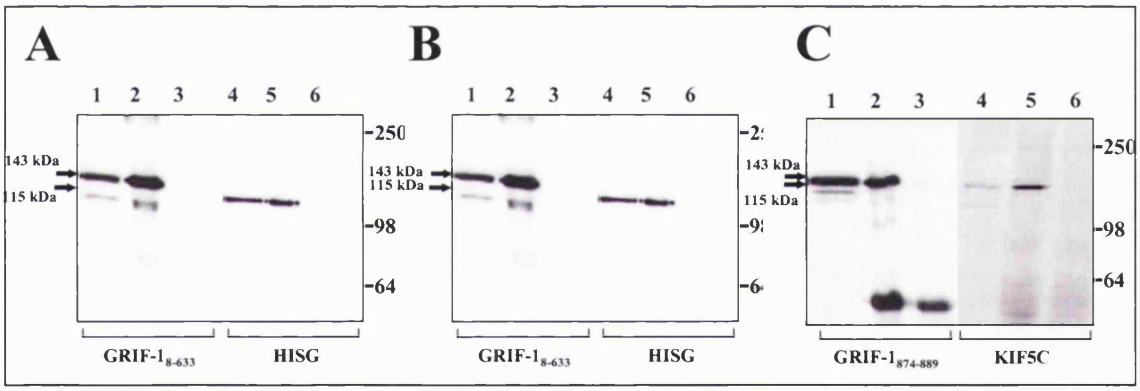

Figure 3.5. Demonstration by immunoprecipitation that ECFP-GRIF-1 associates with His-tagged KIF5C, N-EYFP-KIF5C and C-EYFP-KIF5C. Detergent soluble extracts of HEK 293 cells co-transfected with either A, pECFP-GRIF-1 + pcDNAHisMax-KIF5C, B, pECFP-GRIF-1 + pN-EYFP-KIF5C or C, pECFP-GRIF-1 + pC-EYFP-KIF5C were prepared 24 h after transfection. Immunoprecipitation experiments were carried out using either sheep anti-GRIF-$1_{874-889}$ antibodies or sheep non-immune IgGs. Immune pellets were analysed by immunoblotting using antibodies as indicated on the abcissae. The gel layout is identical in A, B and C, where lanes 1, 4, detergent soluble extract; lanes 2, 5, immune pellet; lanes 3, 6, non-immune pellet. The molecular weight standards (kDa) are shown on the right. Immunoreactive bands of interest are indicated by an arrow, M_r (His-tagged KIF5C) = 115 kDa, M_r (ECFP-GRIF-1) = M_r (N-EYFP-KIF5C) = M_r (C-EYFP-KIF5C) = 143 kDa. These immunoblots are representative of n = 3 immunoprecipitations from n = 3 transfections.

Association properties of EYFP-KIF5C- Immune pellets of cells co-transfected with pCIS-GRIF-1 + pN-EYFP-KIF5C were probed with either anti-GRIF-1_{8-633} antibodies or anti-KIF5C antibodies (Figure 3.6 A). Anti-GRIF-1_{8-633} antibodies recognised an immunoreactive band with M_r = 115 kDa in the detergent soluble fraction and in the

immune pellet, but not in the non-immune control pellet, indicating that GRIF-1 was expressed and specifically immunoprecipitated (Figure 3.6 A, lanes 1-3). Anti-KIF5C antibodies detected a band with M_r = 143 kDa band in the immune pellets but not in the control pellets thereby indicating that N-EYFP-KIF5C was associated with non-fluorescent GRIF-1 (Figure 3.6 A, lanes 4-6). Immune pellets of cells co-transfected with pCIS-GRIF-1 + pC-EYFP-KIF5C were probed with either anti-GRIF-$1_{874-889}$ antibodies or anti-KIF5C antibodies. (Figure 3.6 B). As before, anti-GRIF-$1_{874-889}$ antibodies recognised an immunoreactive band with M_r = 115 kDa in the detergent soluble fraction and in the immune pellet, but not in the non-immune control pellet, indicating that GRIF-1 was expressed and specifically immunoprecipitated (Figure 3.6 B, lanes 1-3). When probing with anti-KIF5C antibodies, an M_r = 143 kDa band was recognised in the immune pellets but not in the control pellets thereby indicating that C-EYFP-KIF5C was associated with non-fluorescent GRIF-1 (Figure 3.6 B, lanes 4-6). Further, as shown earlier (Figure 3.6 B, C), both N-EYFP-KIF5C and C-EYFP-KIF5C were associated with ECFP-GRIF-1.

Association properties of truncated EYFP-KIF5C constructs- Immune pellets of cells co-transfected with pCIS-GRIF-1 + pEYFP-KIF5C-MD were probed with either anti-GRIF-1_{8-633} antibodies or anti-GFP antibodies (Figure 3.7 A). As mentioned before, anti-GRIF-1_{8-633} antibodies recognised an immunoreactive band with M_r = 115 kDa in the detergent soluble fraction and in the immune pellet, but not in the non-immune control pellet, showing that GRIF-1 was expressed and specifically immunoprecipitated (Figure 3.7 A, lanes 4-6). When probing with anti-GFP antibodies, no immunoreactivity was detected in either immune nor control pellets (Figure 3.7 A, lanes 1-3). This showed that EYFP-KIF5C-MD was not associated with GRIF-1 as predicted by Smith *et al.* (2006). Immune pellets of cells co-transfected with pECFP-GRIF-1 + pEYFP-KIF5C-MD were also probed with either anti-GRIF-1_{8-633} antibodies or anti-GFP antibodies. Anti-GRIF-1_{8-633} antibodies recognised an immunoreactive band with M_r = 143 kDa in the detergent soluble fraction and in the immune pellet, but not in the non-immune control pellet, showing that ECFP-GRIF-1 was expressed and specifically immunoprecipitated (Figure 3.7 B, lanes 4-6). Again, no immunoreactivity was detected by anti-GFP antibodies in either immune nor control pellets (Figure 3.7 B, lanes 1-3). This showed that EYFP-KIF5C-MD was not associated with ECFP-GRIF-1 in agreement with Smith *et al.* (2006).

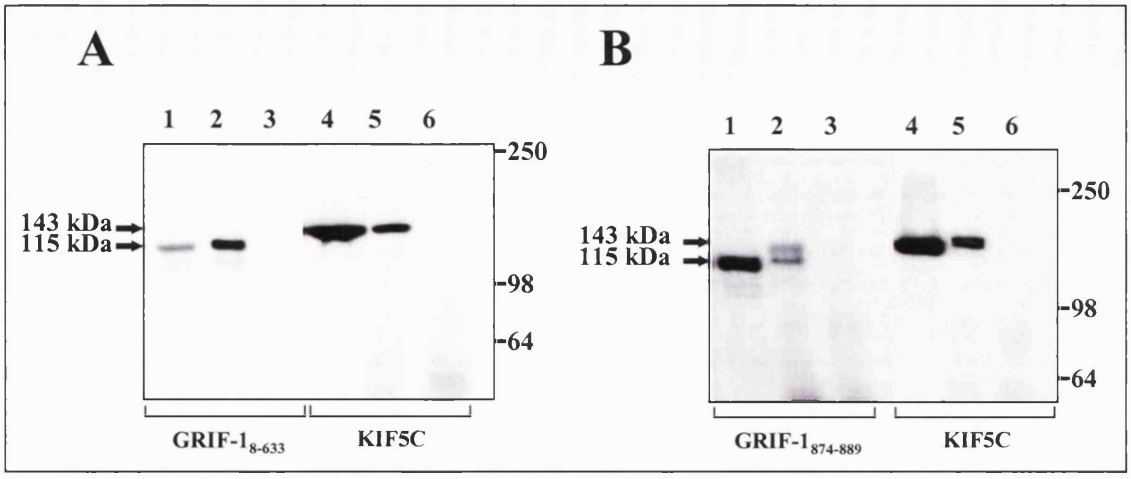

Figure 3.6. Demonstration by immunoprecipitation that EYFP-KIF5C associates with GRIF-1. Detergent soluble extracts of HEK 293 cells co-transfected with either A, pCIS-GRIF-1 + pN-EYFP-KIF5C or B, pCIS-GRIF-1 + pC-EYFP-KIF5C were prepared 24 h post-transfection. Immunoprecipitation experiments were carried out using either sheep anti-GRIF-$1_{874-889}$ antibodies or non-immune IgGs. Immune pellets were analysed by immunoblotting using antibodies as indicated on the abcissae. The gel layout is identical in A and B where lanes 1, 4, detergent soluble extract; lanes 2, 5, immune pellet; lanes 3, 6, non-immune pellet. The molecular weight standards (kDa) are shown on the right. Immunoreactive bands of interest are indicated by an arrow, M_r (GRIF-1) = 115 kDa, M_r (N-EYFP-KIF5C) = M_r (C-EYFP-KIF5C) = 143 kDa. These immunoblots are representative of n = 3 immunoprecipitations from n = 3 transfections.

Immune pellets of cells co-transfected with pCIS-GRIF-1 + pEYFP-KIF5C-NMD were analysed with either GRIF-1_{8-633} antibodies or anti-KIF5C antibodies (Figure 3.8 A). Anti-GRIF-1_{8-633} antibodies recognised an immunoreactive band with M_r = 115 kDa in the detergent soluble fraction and in the immune pellet, but not in the non-immune control pellet, showing that GRIF-1 was expressed and specifically immunoprecipitated (Figure 3.8 A, lanes 4-6). When using anti-KIF5C antibodies, a band with M_r = 139 kDa was detected in the immune pellets, but not in the control pellets showing that EYFP-KIF5C-NMD was associated with non-fluorescent GRIF-1 (Figure 3.8 A, lanes 1-3). Immune pellets of cells co-transfected with pECFP-GRIF-1 + pEYFP-KIF5C-NMD were also analysed with either GRIF-1_{8-633} antibodies or anti-KIF5C antibodies (Figure 3.8 B). Anti-GRIF-1_{8-633} antibodies recognised an immunoreactive band with M_r = 115 kDa in the detergent soluble fraction and in the immune pellet, but not in the non-immune control pellet, showing that GRIF-1 was expressed and specifically immunoprecipitated (Figure 3.8 B, lanes 4-6). Anti-KIF5C antibodies detected a band with M_r = 139 kDa in the immune pellets, but not in the control pellets showing that EYFP-KIF5C-NMD was also associated with ECFP-GRIF-1 (Figure 3.8 B, lanes 1-3)

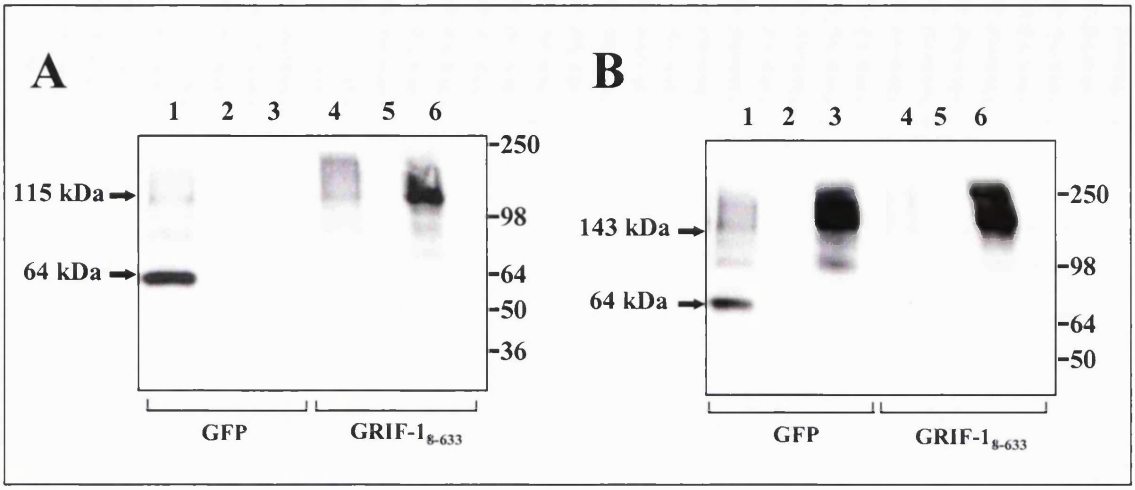

Figure 3.7. Demonstration by immunoprecipitation that EYFP-KIF5C-MD does not associate with GRIF-1 and ECFP-GRIF-1. Detergent soluble extracts of HEK 293 cells co-transfected with either A, pCIS-GRIF-1 + pEYFP-KIF5C-MD or B, pECFP-GRIF-1 + pEYFP-KIF5C-MD were prepared 24 h post-transfection. Immunoprecipitation experiments were carried out using either sheep anti-GRIF-$1_{874-889}$ antibodies or non-immune IgGs as a control. Immune pellets were analysed by immunoblotting using antibodies as indicated on the abcissae. The gel layout is identical in A and B where lanes 1, 4, detergent soluble extract; lanes 2, 5, non-immune pellet; lanes 3, 6, immune pellet. The molecular weight standards (kDa) are shown on the right. Arrows indicate the immunoreactive bands of interest, M_r (EYFP-KIF5C-MD) = 64 kDa, M_r (GRIF-1) = 115 kDa, M_r (ECFP-GRIF-1) = 143 kDa. These immunoblots are representative of n = 3 immunoprecipitations from n = 3 independent transfections.

To summarise, ECFP-GRIF-1 associated with either non-fluorescent His-tagged KIF5C or fluorescent KIF5C; EYFP-KIF5C and EYFP-KIF5C-NMD associated with either non-fluorescent GRIF-1 or fluorescent GRIF-1; EYFP-KIF5C-MD did not associate with either non-fluorescent GRIF-1 or fluorescent GRIF-1. Thus immunoprecipitation experiments showed that the association properties of GRIF-1, KIF5C, KIF5C-MD and KIF5C-NMD were not modified by the addition of either ECFP or EYFP.

Experiments with EYFP-GRIF-1, N-ECFP-KIF5C and C-ECFP-KIF5C constructs were not performed. However, it could be predicted that the same results would be obtained whether ECFP or EYFP are used since these 2 proteins differ by only 9 amino-acids within the chromophore region (section 3.1.2).

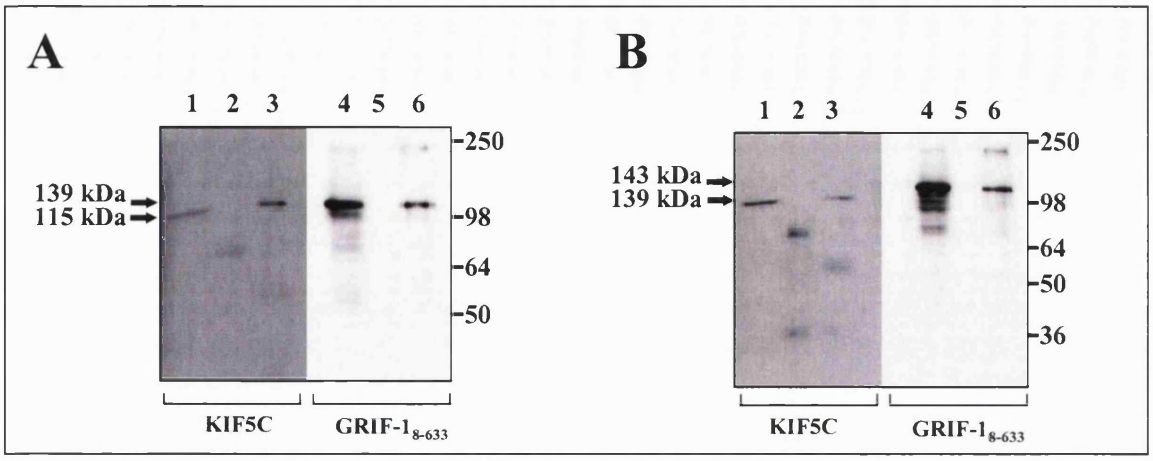

Figure 3.8. Demonstration by immunoprecipitation that EYFP-KIF5C-NMD associates with GRIF-1 and ECFP-GRIF-1. Detergent soluble extracts of HEK 293 cells co-transfected either with A, pCIS-GRIF-1 + pEYFP-KIF5C-NMD or B, pECFP-GRIF-1 + pEYFP-KIF5C-NMD were prepared 24 h post-transfection. Immunoprecipitation experiments were carried out using either sheep anti-GRIF-$1_{874-889}$ antibodies or non-immune IgGs as a control. Immune pellets were analysed by immunoblotting using antibodies as indicated on the abcissae. The gel layout is identical in A and B where lanes 1, 4, detergent soluble extract; lanes 2, 5, non-immune pellet; lanes 3, 6, immune pellet. The molecular weight standards (kDa) are shown on the right. Immunoreactive bands of interest are indicated by an arrow, M_r (EYFP-KIF5C-NMD) = 139 kDa, M_r (GRIF-1) = 115 kDa, M_r (ECFP-GRIF-1) = 143 kDa. These immunoblots are representative of n = 3experiements.

3.2.4. Confocal microscopy imaging of ECFP-GRIF-1, EYFP-GRIF-1, ECFP-KIF5C, EYFP-KIF5C and truncated EYFP-KIF5C chimeras in transfected HEK 293 and COS-7 cells

Fluorescent GRIF-1 and KIF5C fusion constructs were shown to behave as non-fluorescent GRIF-1 and non-fluorescent KIF5C, respectively, and therefore they were used to study the subcellular distribution of GRIF-1 and KIF5C in transfected mammalian cell lines by confocal microscopy imaging. Initial studies were carried out in HEK 293 cells. However, a better resolution was obtained by using COS-7 cells. This cell line is more generally used for subcellular localisation studies because cells have a large cytoplasm allowing a clearer distinction of subcellular compartments. Thus subcellular localisation studies were also carried out in COS-7 cells.

Because identical localisation patterns were observed for ECFP-GRIF-1 and EYFP-GRIF-1, results obtained for ECFP-GRIF-1 only are shown here. Similarly, identical distribution profiles were seen for ECFP-KIF5C and EYFP-KIF5C and only an example, i.e. EYFP-KIF5C, is shown in the results.

3.2.4.1. Single construct expression analysis

HEK 293 and COS-7 cells were transfected with either ECFP-GRIF-1, EYFP-KIF5C or truncated EYFP-KIF5C chimeras, fixed 24-48 h post-transfection and imaged as in section 2.2.5.2.1. The cellular distribution of each fluorescent contruct is reported hereafter.

ECFP-GRIF-1- In HEK 293 cells transfected with pECFP-GRIF-1, fluorescence was localised within the cell cytoplasm with an enrichment in the cytoplasmic regions adjacent to the nucleus and at the edge of the cell (Figures 3.9 A, B). Also, the fluorescence had a tubular, vesicular aspect. This pattern is consistent with immunocytochemistry experiments where HEK 293 cells were transfected with pCIS-GRIF-1 and labelled with anti-GRIF-1_{8-633} antibodies (Beck *et al.*, 2002). In transfected COS-7 cells, the fluorescence was also detected within the cell cytoplasm with a tubular, vesicular shape, enriched at the periphery of the cell nucleus (Figures 3.9 C, D). No ECFP-GRIF-1 fluorescence was detected in COS-7 cell processes. The same perinuclear distribution was observed when pCIS-GRIF-1-transfected COS-7 cells were immunostained with anti-GRIF-1_{8-633} antibodies (Figure 3.10). In these cells, the fluorescence was still seen as tubular, vesicular. The perinuclear distribution observed in both cell types suggests that GRIF-1 might be localised to perinuclear organelles such as the Golgi apparatus, the endoplasmic reticulum (ER) or the endosomes. Further, in both cell types, ECFP-GRIF-1 fluorescence also showed a filamentous pattern that was reminiscent of the cytoskeleton. This indicates that GRIF-1 might be associated with cytoskeleton elements consistent with GRIF-1 association with the microtubule motor, kinesin (Brickley *et al.*, 2005).

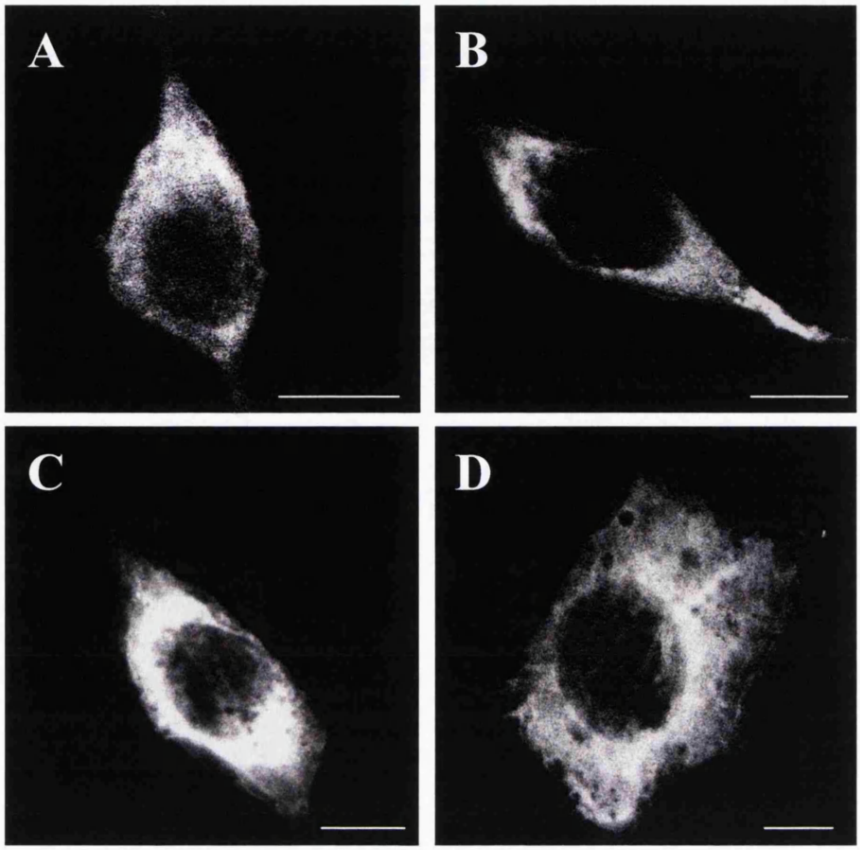

Figure 3.9. Expression of ECFP-GRIF-1 in transfected HEK 293 and COS-7 cells. Confocal sections of HEK 293 and COS-7 cells transfected with pECFP-GRIF-1. Cells were fixed 24-48 h post-transfection and imaged. A, B, HEK 293 cells; C, D, COS-7 cells. The same distribution was observed in pEYFP-GRIF-1 transfected cells. The images are representative of at least n = 20 cells observed for n = 3 independent transfections. Scale bars, 10 μm

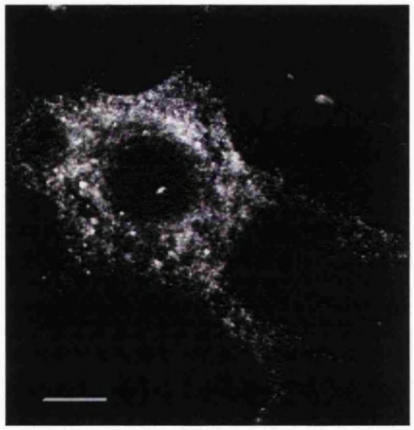

Figure 3.10. Expression of GRIF-1 in transfected COS-7 cells. Confocal section of a COS-7 cell transfected with pCIS-GRIF-1. The cell was fixed 36 h post-transfection, permeabilised and GRIF-1 was detected using anti-GRIF-$1_{8\text{-}633}$ primary antibodies and AlexaFluor®594-labelled secondary antibodies. This cell is representative of n = 10 cells observed for n = 2 independent transfections. Scale bar, 10 μm

EYFP-KIF5C- In HEK 293 (Figure 3.11 A, B) and COS-7 cells (Figure 3.11 C, D) transfected with pN-EYFP-KIF5C, the fluorescence was diffused throughout the cell cytoplasm. Also EYFP-KIF5C fluorescence displayed a filamentous pattern (Figures 3.11 B, D). This might result from an association of EYFP-KIF5C with microtubules as previously shown by Verhey *et al.* (1998) who overexpressed c-Myc-tagged rat kinesin heavy chain in microtubule-stained COS-7 cells. Further, in COS-7 cells, fluorescence was accumulated at the tips of cellular processes when they were present. As mentioned earlier, the same distribution was observed in HEK 293 and COS-7 cells transfected with pC-EYFP-KIF5C thus suggesting that the addition of EYFP at the N- or at the C-terminal of KIF5C did not interfere with KIF5C cellular location.

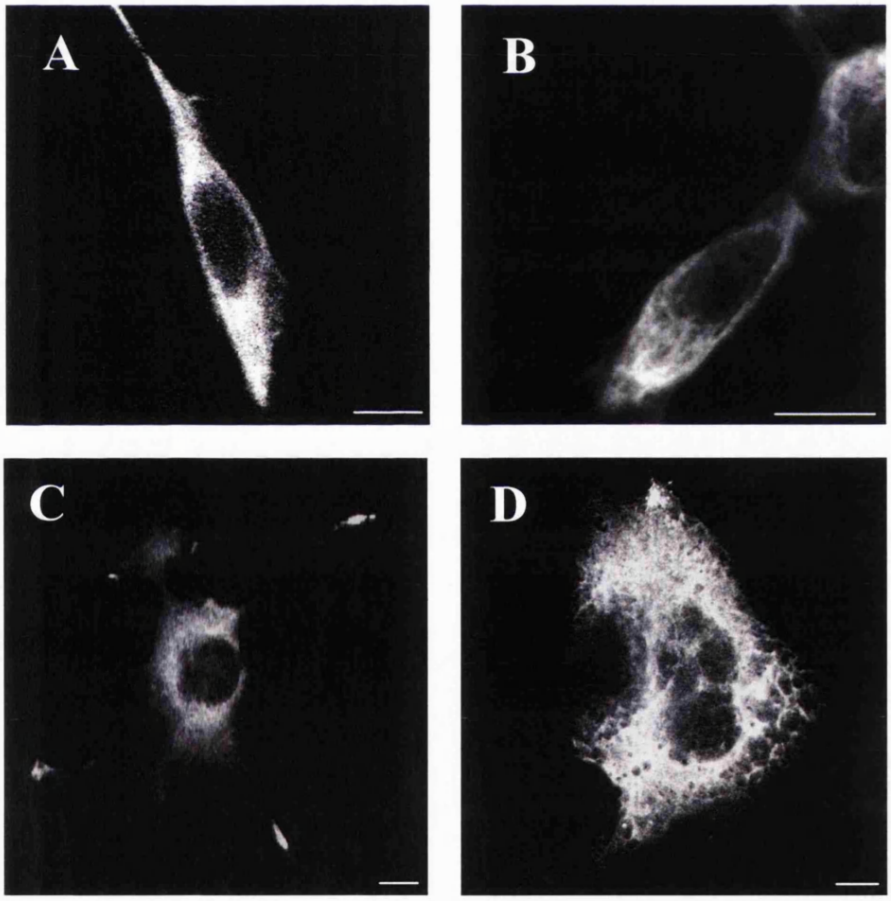

Figure 3.11. Expression of EYFP-KIF5C in transfected HEK 293 and COS-7 cells. Confocal sections of HEK 293 and COS-7 cells transfected with pN-EYFP-KIF5C Cells were fixed 24-48 h post-transfection and imaged. A, B, HEK 293 cells; C, D, COS-7 cells. The same distribution patterns were observed in cells transfected with either pC-EYFP-KIF5C, pC-ECFP-KIF5C or pN-EYFP-KIF5C. The images are representative of at least n = 20 cells observed for n = 3 independent transfections. Scale bars, 10 μm.

EYFP-KIF5C-MD- More than 50% of HEK 293 cells transfected with pEYFP-KIF5C-MD showed multiple cytoplasmic vacuolae (Figure 3.12 A). EYFP-KIF5C-MD fluorescence was localised in the cell cytoplasm as filamentous structures (Figures 3.12 A), consistent with the existence of a microtubule binding site within the KIF5C-MD (Kuznetsov *et al.*, 1989; Navone *et al.*, 1992). In other cells (~ 50%), fluorescence was also seen in the cell nucleus (Figures 3.12 B). The same observations were performed in COS-7 cells transfected with pEYFP-KIF5C-MD. Similarly, the cells appeared vacuolated (Figure 3.12 C, D). Also, the fluorescence was distributed diffusely in the cytoplasm including the nucleus (55% of analysed cells) (Figures 3.12 C, D). As described for HEK 293 cells, in 25% of analysed COS-7 cells, the fluorescence was detected as filamentous structures consistent with an association of EYFP-KIF5C-MD with microtubules (Figure 3.12 C).

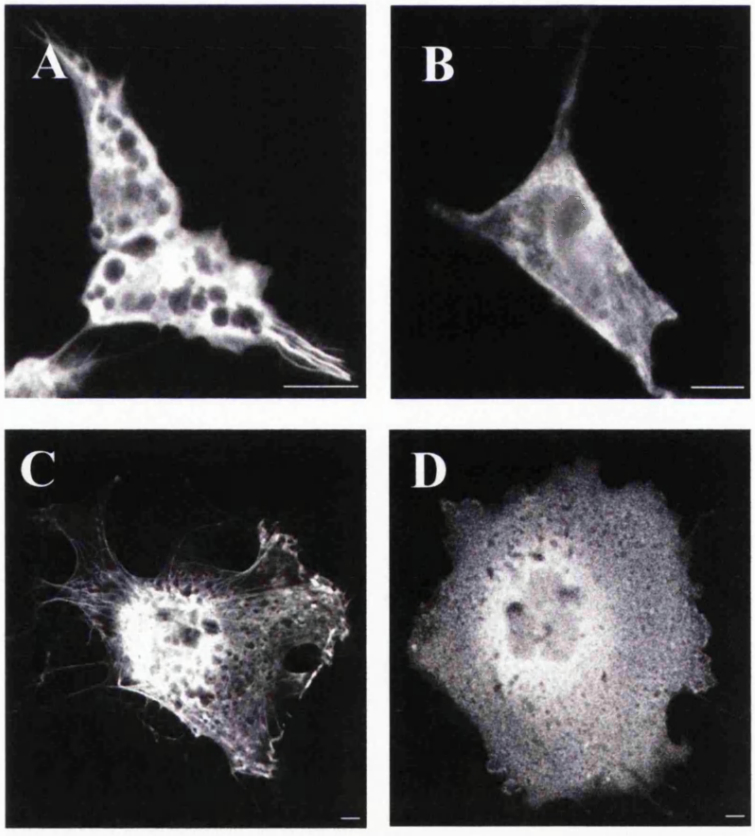

Figure 3.12. Expression of EYFP-KIF5C-MD in transfected HEK 293 and COS-7 cells. HEK 293 and COS-7 cells were transfected with pEYFP-KIF5C-MD, fixed 24-48 h post-transfection and imaged. A, confocal section of a transfected HEK 293 cell; B, Z-stack (n = 20 sections) of a transfected HEK 293 cell; C, D, confical sections of transfected COS-7 cells. These images are representative of n = 20 cells observed for n = 3 transfections. Scale bars, 10 μm.

EYFP-KIF5C-NMD- In HEK 293 cells transfected with pEYFP-KIF5C-NMD, fluorescence was localised within the cytoplasm as filamentous structures also suggesting an association with the cytoskeleton (Figure 3.13 A). The same fluorescence distribution was observed in COS-7 cells transfected with pEYFP-KIF5C-NMD (Figures 3.13 B, C). Navone *et al.* (1992) observed also a filamentous profile when they expressed the NMD of human KHC in CV-1 cells. They showed that these filaments were microtubules and that a second microtubule-binding site was present on the NMD of human KHC.

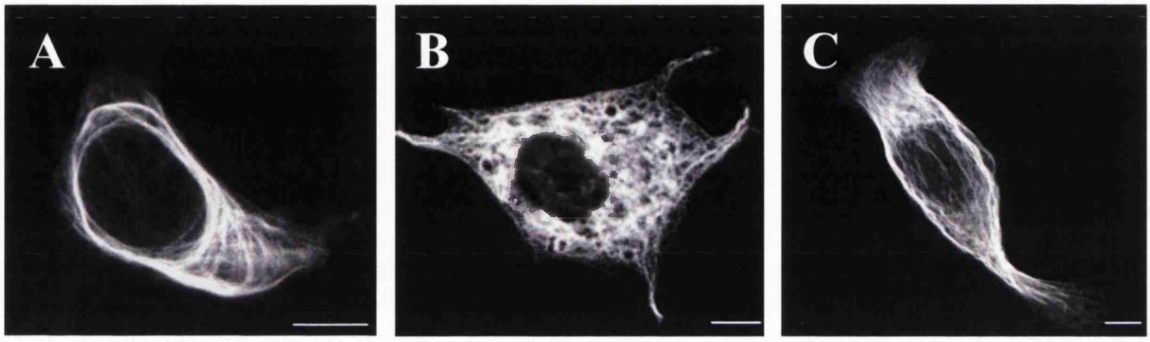

Figure 3.13. Expression of EYFP-KIF5C-NMD in transfected HEK 293 and COS-7 cells. Confocal sections of HEK 293 and COS-7 cells transfected with pEYFP-KIF5C-NMD. Cells were fixed 24-48 h after transfection and imaged. A, HEK 293 cells; C, B, COS-7 cells. These images are representative of at least n = 20 cells observed for n = 3 independent transfections. Scale bars, 10 μm.

3.2.4.2. Co-expression studies

HEK 293 and COS-7 cells were co-transfected with ECFP-GRIF-1 and an EYFP-KIF5C construct, fixed 24-48 h post-transfection and imaged using the settings described in section 2.2.5.2. The cellular distribution of ECFP-GRIF-1 and an EYFP-KIF5C construct in transfected COS-7 cells is described hereafter.

ECFP-GRIF-1 + EYFP-KIF5C- In HEK 293 cells co-transfected with pECFP-GRIF-1 + pN-EYFP-KIF5C, ECFP-GRIF-1 fluorescence was localised exclusively at the end of the cell, adjacent to the cell membrane instead of being mainly cytoplasmic as seen in single construct expression experiments (Figure 3.14 B). Tubular, vesicular structures similar to those observed in single transfections were still distinguishable. EYFP-KIF5C fluorescence was also visualised concentrated at the cell periphery toward the end of the cell (Figure 3.14 A). In some cells, EYFP-KIF5C fluorescence was still diffused in the cell cytoplasm as seen in single transfections. ECFP-GRIF-1 and EYFP-KIF5C fluorescence were co-localised in the region adjacent to the cell membrane displaying a tubular pattern as shown

on the overlaid image (Figures 3.14 C). In co-transfected COS-7 cells, ECFP-GRIF-1 fluorescence localisation was changed comparing to single transfections. Instead of showing a cytoplasmic perinuclear localisation, ECFP-GRIF-1 fluorescence was concentrated in a region adjacent to the cell membrane although minor fluorescence remained in the cytoplasm (Figure 3.14 H). ECFP-GRIF-1 fluorescence was

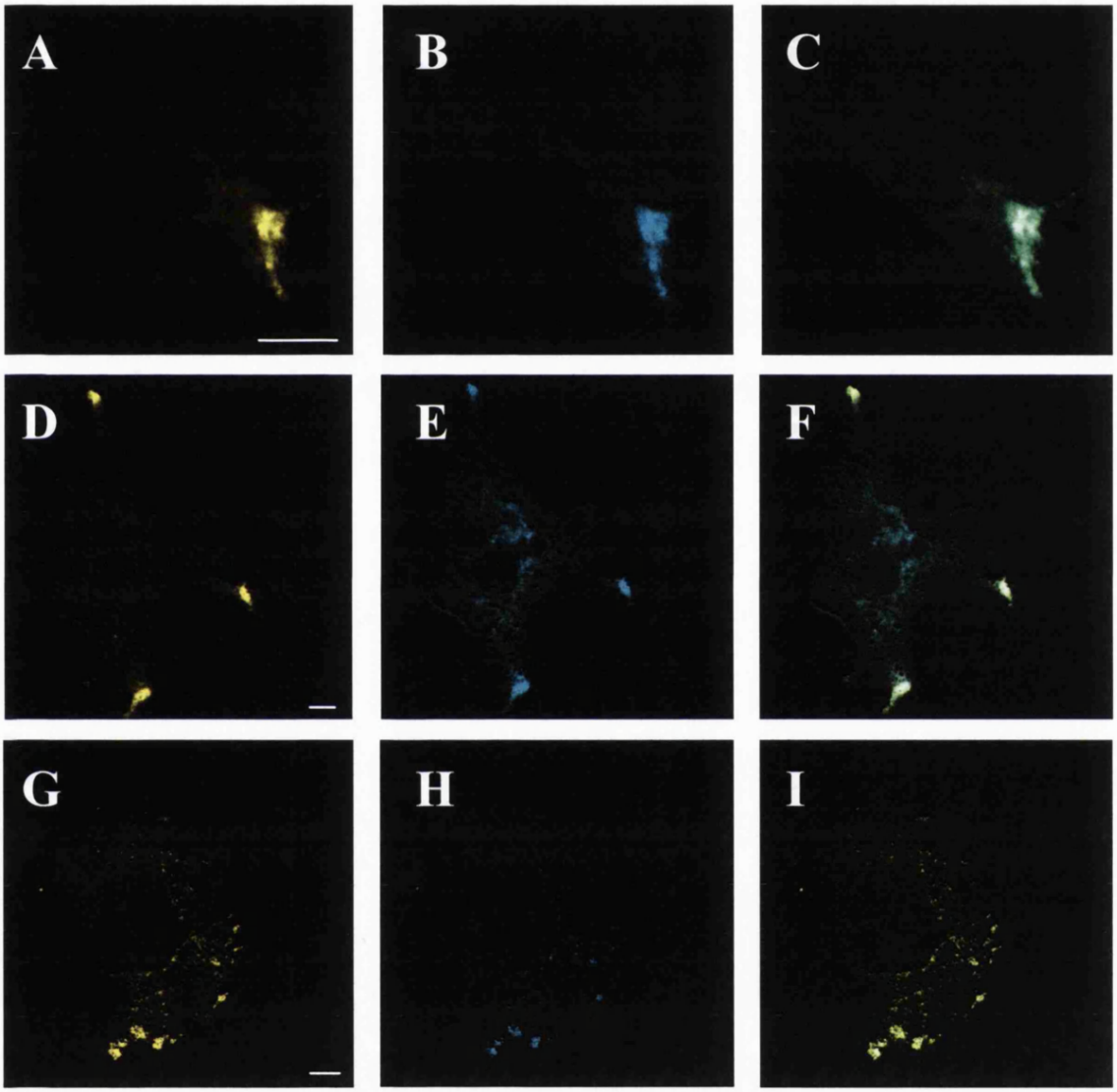

Figure 3.14. ECFP-GRIF-1 and EYFP-KIF5C co-localise at the cell periphery in transfected HEK 293 and COS-7 cells. Confocal sections of HEK 293 and COS-7 cells co-transfected with pECFP-GRIF-1 and pN-EYFP-KIF5C. Cells were fixed 24–48 h after transfection and imaged. A-C, HEK 293 cells; D-I, COS-7 cells. A, D, G, N-EYFP-KIF5C; B, E, H, ECFP-GRIF-1; C, F, I, overlaid pictures of (A + B), (D + E), (G + H) respectively. The same distribution was observed in cells transfected with pECFP-GRIF-1 + pC-EYFP-KIF5C, pEYFP-GRIF-1 + pN-ECFP-KIF5C, pEYFP-GRIF-1 + pC-pECFP-KIF5C. These images are representative of at least n = 20 cells observed for n = 3 independent transfections. Scale bars, 10 μm.

particularly accumulated in cellular extensions when they were formed and tubular structures were still visible (Figures 3.14 E). EYFP-KIF5C fluorescence was also modified comparing to single construct expression experiments. EYFP-KIF5C fluorescence was accumulated exclusively in the vicinity of the cell membrane and in cellular extensions when they were formed. In some cells, EYFP-KIF5C fluorescence was also localised diffusely within the cell cytoplasm as previously reported in single construct expression experiments (Figures 3.14 D, G). ECFP-GRIF-1 and EYFP-KIF5C fluorescences were co-distributed in the area adjacent to the cell membrane and in cellular processes as indicated on the overlaid image (Figures 3.14 F, I). In some cells, ECFP-GRIF-1 and EYFP-KIF5C fluorescences were also co-distributed as small clusters within the cell cytoplasm in the vicinity of the cell membrane (Figures 3.14 G, H, I). The same observations were made in HEK 293 and COS-7 cells co-transfected with pECFP-GRIF-1 and pC-EYFP-KIF5C. Overall these observations suggest that co-expression of EYFP-KIF5C with ECFP-GRIF-1 caused a re-distribution of ECFP-GRIF-1 fluorescence to EYFP-KIF5C-containing regions adjacent to the cell membrane or to cellular processes in co-transfected HEK 293 and COS-7 cells. This is consistent with an interaction between the 2 proteins. Further, the ECFP-GRIF-1 tubular pattern suggests that GRIF-1 is still localised to the same organelle as in single transfections.

To show that the fluorescence accumulation at the cell periphery was not an experimental artefact due to dimerisation of ECFP and EYFP, ECFP-GRIF-1 and ECFP-KIF5C were also co-expressed each with a different EYFP-tagged chimera in HEK 293 cells. EYFP-OGT was used as a control as this construct was available in the laboratory. As explained in Chapter 1, OGT is a $M_r \sim 120$ kDa cytoplasmic protein forming trimers. OGT is a GRIF-1 associated protein therefore it is expected to co-localise with GRIF-1 in co-transfected HEK 293 cells. OGT has never been reported to be associated with KIF5C. The cellular localisation of EYFP-OGT expressed on its own or with ECFP-GRIF-1 in HEK 293 cells is described in detail in Chapter 4. Briefly in EYFP-OGT transfected HEK 293 cells, the fluorescence was diffused throughout the cell cytoplasm with some enrichment visible along the membrane. These transfected cells contained several vacuolae. Cells co-expressing ECFP-GRIF-1 + EYFP-OGT displayed also a vacuolated pattern. In these cells, EYFP-OGT fluorescence was co-localised with ECFP-GRIF-1 fluorescence in the

cytoplasm and along the cell membrane. No fluorescence accumulation in any region of the cell was observed (Chapter 4, Figure 4.17). Again, HEK 293 cells co-expressing ECFP-KIF5C + EYFP-OGT were vacuolated and EYFP-OGT fluorescence was as described above (Figure 3.15 A, B, C). ECFP-KIF5C fluorescence was diffused throughout the cell cytoplasm as observed in single construct transfections (Figure 3.15 B). No fluorescence accumulation was detected in these cells. This was in contrast with the observations in pECFP-GRIF-1 + pEYFP-KIF5C transfected cells. Thus co-expression of ECFP-GRIF-1 + EYFP-OGT and ECFP-KIF5C + EYFP-OGT did not cause fluorescence to accumulate in a single area of the cell cytoplasm. Therefore the fluorescence accumulation observed in cells co-expressing ECFP-GRIF-1 + EYFP-KIF5C is due to the physiological functions of GRIF-1 and KIF5C and it is not an experimental artefact due to the ability of ECFP and EYFP to dimerise.

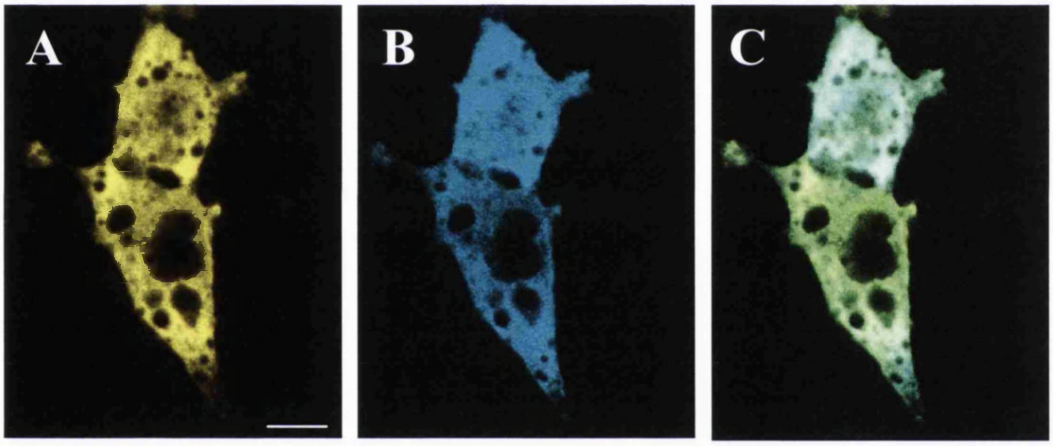

Figure 3.15. Demonstration that the distribution pattern observed in cells co-expressing ECFP-GRIF-1 and EYFP-KIF5C is not an artefact. Confocal section of HEK 293 cells transfected with pECFP-KIF5C and pEYFP-OGT. Cells were fixed 36 h post-transfection and imaged. A, EYFP-OGT; B, ECFP-KIF5C; D, overlaid picture of (A + B). This cell is representative of n = 5 cells imaged for n = 1 transfection. Scale bar, 10 μm.

ECFP-GRIF-1 + EYFP-KIF5C-MD- In HEK 293 cells co-transfected with pECFP-GRIF-1 + pEYFP-KIF5C-MD, ECFP-GRIF-1 fluorescence was localised in the cell cytoplasm as described in single construct expression experiments. EYFP-KIF5C-MD fluorescence was also cytoplasmic as seen when it was expressed on its own. Co-transfected cells also contained several cytoplasmic vacuolae as described before (Figure 3.16 A, B, C). The same observations were performed in COS-7 cells co-transfected with pECFP-GRIF-1 + pEYFP-KIF5C-MD (Figure 3.16 D, E, F). Thus, co-expression of EYFP-KIF5C-MD had

no effect on the localisation of ECFP-GRIF-1 fluorescence in co-transfected HEK 293 and COS-7 cells consistent with their failure to interact.

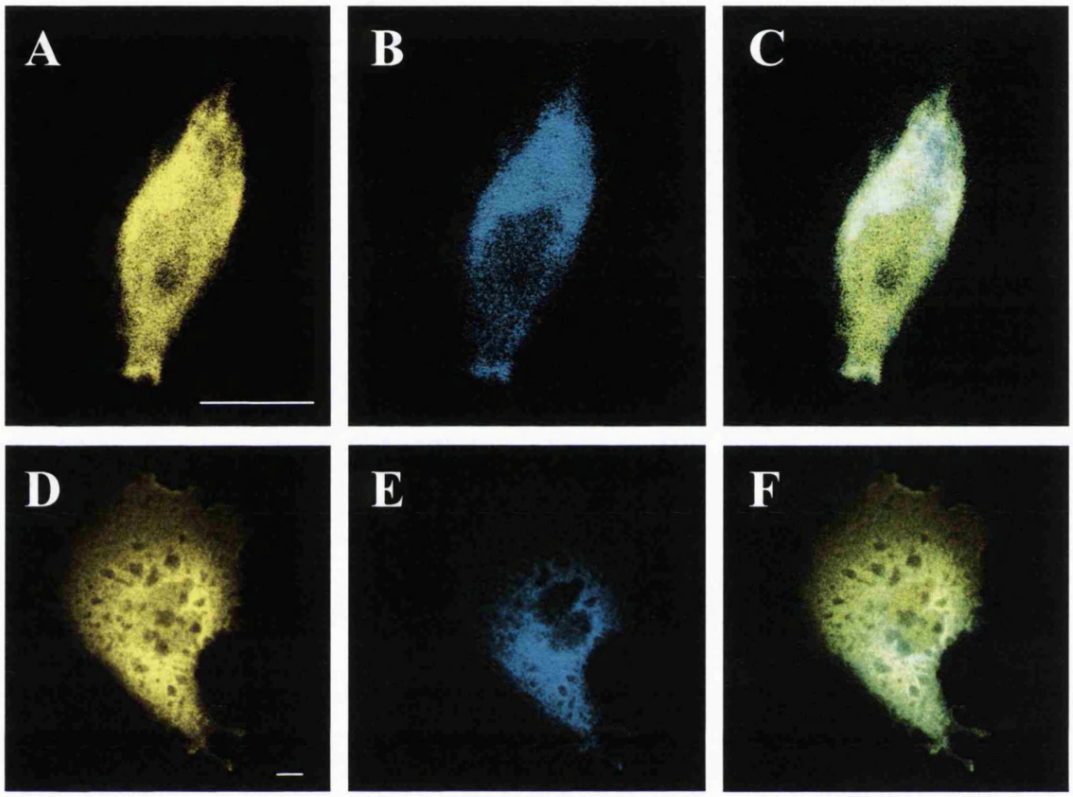

Figure 3.16. Expression of EYFP-KIF5C-MD does not change ECFP-GRIF-1 localisation in transfected HEK 293 and COS-7 cells. Confocal sections of HEK 293 and COS-7 cells were co-transfected with pECFP-GRIF-1 + pEYFP-KIF5C-MD, fixed 24-48 h post-transfection and imaged. A, B, C, HEK 293 cells; D, E, F, COS-7 cells. A, D, EYFP-KIF5C-MD; B, C, ECFP-GRIF-1; C, D, overlaid pictures of (A + B), (C + D) respectively. These images are representative of at least n = 20 cells observed for n = 3 independent transfections. Scale bars, 10 μm.

ECFP-GRIF-1 + EYFP-KIF5C-NMD- In HEK 293 cells co-transfected with pECFP-GRIF-1 + pEYFP-KIF5C-NMD, ECFP-GRIF-1 fluorescence was visualised within the cell cytoplasm as described in single construct transfections (Figure 3.17 B). However, the distribution of EYFP-KIF5C-NMD fluorescence was modified (Figure 3.17 A). Instead of showing a filamentous cytoplasmic pattern, EYFP-KIF5C-NMD fluorescence was localised in ECFP-GRIF-1-enriched cytoplasmic regions (Figure 3.17 C). This suggests that GRIF-1 might compete with the microtubule binding site on the KIF5C-NMD. The same fluorescence localisation patterns were observed in COS-7 cells co-transfected with pECFP-GRIF-1 + pEYFP-KIF5C-MD (Figure 3.17 A, B, C). Thus co-expression of ECFP-

GRIF-1 caused a re-distribution of EYFP-KIF5C-NMD fluorescence to ECFP-GRIF-1 enriched regions in the cytoplasm of co-transfected HEK 293 and COS-7 cells.

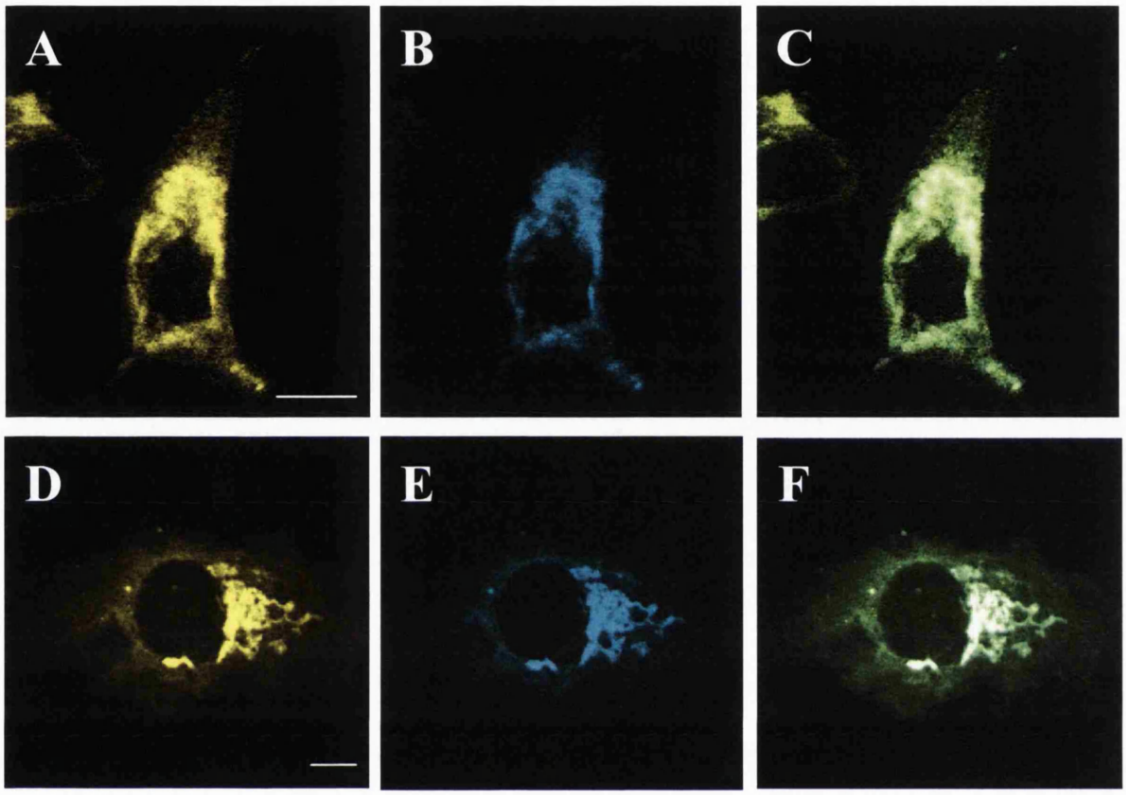

Figure 3.17. EYFP-KIF5C-NMD is concentrated in ECFP-GRIF-1 enriched regions in co-transfected HEK 293 and COS-7 cells. Confocal sections of HEK 293 and COS-7 cells co-transfected with pEYFP-KIF5C-NMD. Cells were fixed 24-48 h post-transfection and imaged. A-C , HEK 293 cells; D-F, COS-7 cells. A, D, EYFP-KIF5C-NMD; B, E, ECFP-GRIF-1; C, F, overlaid pictures of (A + B), (D + E) respectively. The images are representative of at least n = 20 cells observed for n = 3 independent transfections. Scale bars, 10 μm.

In summary, these observations suggest that GRIF-1 could associate with the NMD of KIF5C but not with the MD of KIF5C as shown in the immunoprecipitation assays (section 3.2.1.3). These results substantiate yeast-two hybrid studies that mapped the GRIF-1 binding domain on KIF5C to the KIF5C non-motor domain (Smith *et al.*, 2006).

3.2.5. Further characterisation of the subcellular localisation of GRIF-1 and KIF5C by confocal microscopy imaging studies using organelle markers

GRIF-1 association with the non-motor cargo binding domain of kinesin-1 heavy chain, KIF5C, (Smith *et al.*, 2006) suggests that GRIF-1 could serve as an adaptor protein linking kinesin-1 to a cargo. Further, recent studies have reported that overexpression of GRIF-1 in HEK 293 cells resulted in mitochondrial aggregation to GRIF-1 enriched regions (Brickley *et al.*, 2005).

To gain further insights into GRIF-1 function, transfected COS-7 cells were labelled with fluorescent organelle markers and the subcellular distribution of GRIF-1, KIF5C, GRIF-1 and KIF5C in these cells was analysed by confocal microscopy imaging. The mitochondria were visualised using a DsRed1-tagged mitochondrial targeting sequence, i.e. DsRed1-Mito, the endoplasmic reticulum (ER) was identified using an ECFP-tagged KDEL ER targeting sequence, i.e. ECFP-ER, and the Golgi apparatus was detected with antibodies recognising the 58 K Golgi protein. COS-7 cells were transfected as described in the text below and fixed 24-72 h post-transfection. Where necessary, transfected cells were permeabilised, stained for either GRIF-1 or the Golgi marker p58K and imaged as explained in section 2.2.5.2.1.

Mitochondria- In COS-7 cells transfected with pDsRed1-Mito, labelled mitochondria were distributed evenly throughout the cell cytoplasm (Figure 3.18). They were visualised as distinct cytoplasmic vesicular organelles.

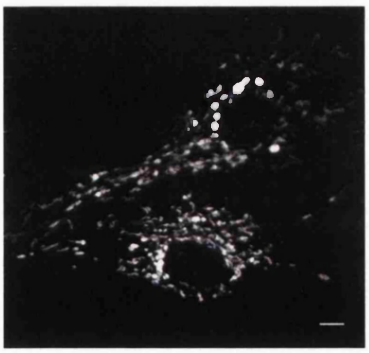

Figure 3.18. Mitochondria are distributed evenly in COS-7 cell cytoplasm. Confocal section of COS-7 cells transfected with pDsRed1-Mito. Cells were fixed 36-72 h post-transfection and imaged. These cells are representative of n = 12 cells observed for n = 3 independent transfections. Scale bar, 10 μm.

In COS-7 cells co-transfected with pDsRed1-Mito + pECFP-GRIF-1, ECFP-GRIF-1 fluorescence was localised in the cell cytoplasm with some enrichment in the perinuclear region and again tubular, vesicular structures were visible as reported for pECFP-GRIF-1 transfections. All the DsRed1-Mito fluorescence, i.e. mitochondria, was concentrated in ECFP-GRIF-1 enriched regions in the vicinity of the nucleus (Figure 3.19). This observation is in agreement with a previous study showing that mitochondria were aggregated in GRIF-1 enriched regions in pCIS-GRIF-1 transfected HEK 293 cells (Brickley *et al.*, 2005). Further this suggests that the vesicular structures described in ECFP-GRIF-1 transfected cells are mitochondria and thus that GRIF-1 might be localised or associated to mitochondria.

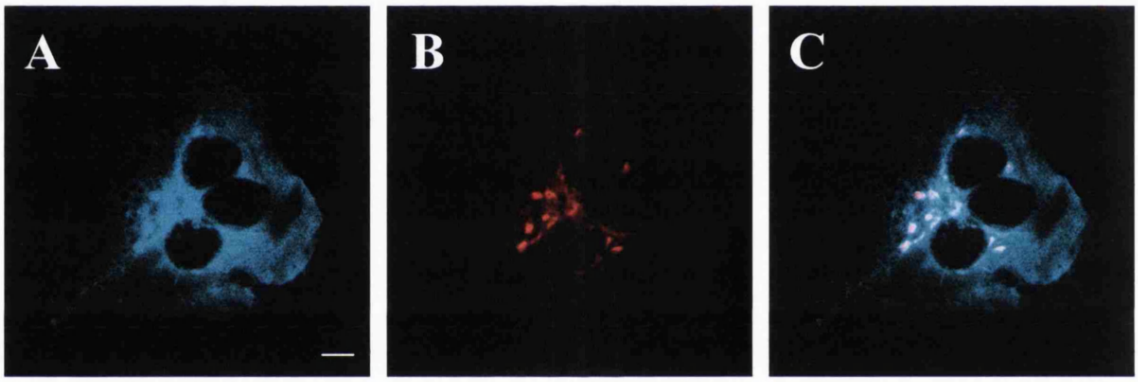

Figure 3.19. ECFP-GRIF-1 aggregates mitochondria in transfected COS-7 cells. Confocal section of a COS-7 cell transfected with pECFP-GRIF-1 + pDsRed1-Mito. The cell was fixed 36-72 h post-transfection and imaged. A, ECFP-GRIF-1; B, DsRed1-Mito; C, merged picture of (A + B). This cell is representative of n = 18 cells observed for n = 3 independent transfections. Scale bar, 10 μm.

In COS-7 cells co-transfected with pN-ECFP-KIF5C + pDsRed1-Mito, ECFP-KIF5C fluorescence was found in the cell cytoplasm as reported for pN-EYFP-KIF5C transfections. DsRed1-Mito fluorescence was seen evenly distributed in the cell cytoplasm as seen for pDsRed1-Mito transfections (Figure 3.20). This suggests that ECFP-KIF5C overexpression does not affect the cellular localisation of mitochondria.

In COS-7 cells co-transfected with pN-EYFP-KIF5C + pECFP-GRIF-1 + pDsRed1-Mito, ECFP-GRIF-1 and EYFP-KIF5C fluorescences were co-localised at the cell periphery as seen in pN-EYFP-KIF5C + pECFP-GRIF-1 co-transfections. DsRed1-Mito fluorescence, i.e. mitochondria, was accumulated and co-localised with ECFP-GRIF-1 and EYFP-KIF5C fluorescences in this region, although some DsRed1-Mito fluorescence, i.e. mitochondria, remained in the cell cytoplasm (Figure 3.21 A-F). In co-transfected COS-7 cells forming

cellular extensions, ECFP-GRIF-1 and EYFP-KIF5C fluorescences were concentrated and co-localised at the end of the extensions as in pECFP-GRIF-1 + pN-EYFP-KIF5C co-transfections (Figure 3.21 G-L). DsRed1-Mito fluorescence was also found accumulated and co-localised with ECFP-GRIF-1 and EYFP-KIF5C fluorescences in the cellular extensions although some remaining DsRed1-Mito fluorescence was still visible in the cell cytoplasm.

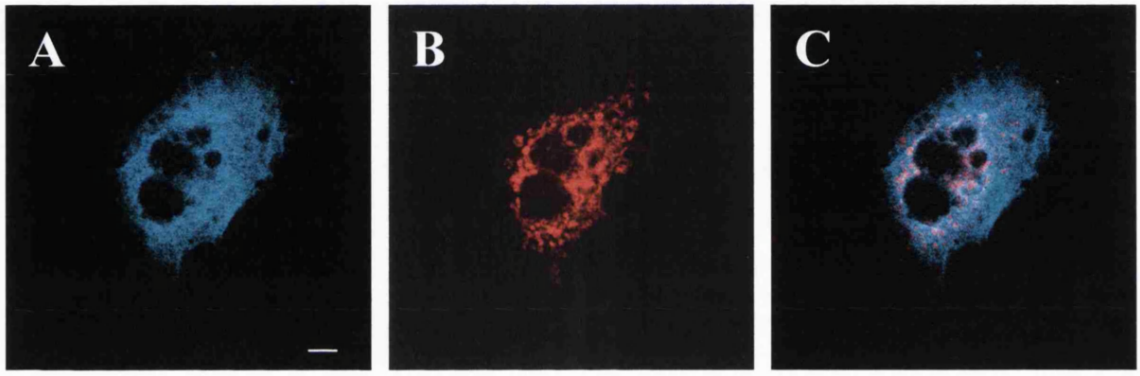

Figure 3.20. ECFP-KIF5C has no effect on mitochondrial distribution in transfected COS-7 cells. Confocal section of a COS-7 cell transfected with pN-ECFP-KIF5C and pDsRed1-Mito. The cell was fixed 36-72 h post-transfection and imaged. A, N-ECFP-KIF5C; B, DsRed1-Mito; C, merged picture of (A + B). The same results were observed for pC-ECFP-KIF5C. This cell is representative of n = 11 cells observed for n = 3 independent transfections. Scale bar, 10 μm.

These distribution patterns showed that in the presence of GRIF-1 the mitochondrial distribution was changed: (i) mitochondria were aggregated to GRIF-1 enriched regions, (ii) no changes were seen in the presence of KIF5C, (iii) mitochondria were co-localised with GRIF-1 and KIF5C. This suggests a role for GRIF-1 in recruiting mitochondria to kinesin-1 heavy chains, KIF5C.

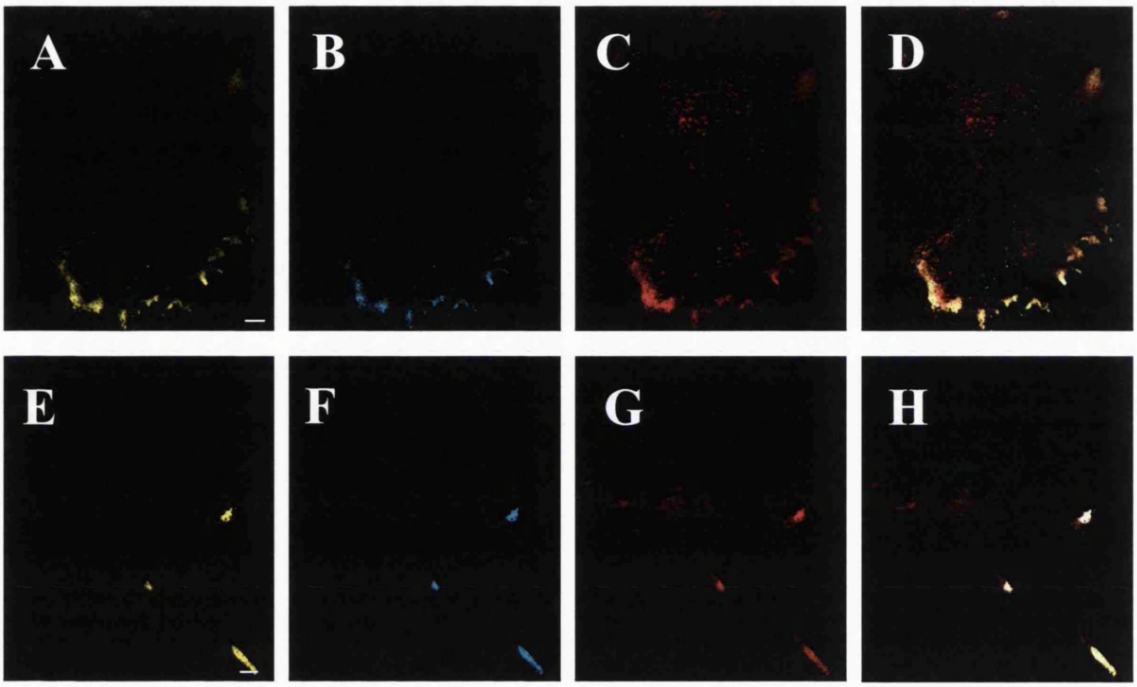

Figure 3.21. Mitochondria co-distribute with ECFP-GRIF-1 and EYFP-KIF5C at the cell periphery and in cellular processes in transfected COS-7 cells. The Figure shows two examples of COS-7 cells co-transfected with pECFP-GRIF-1 + pN-EYFP-KIF5C + pDsRed1-Mito, i.e. confocal sections of A-F, a cell with little or short cellular processes and G-L, a cell with long cellular extensions. Cells were fixed 36-72 h post-transfection and imaged. A, E, EYFP-KIF5C; B, F, ECFP-GRIF-1; C, G, DsRed1-Mito; D, H, merged pictures of (A + B + C), (E + F + G) respectively. These cells are representative of n = 25 cells observed for n = 3 independent transfections. Scale bars, 10 μm.

Golgi apparatus- In untransfected COS-7 cells stained for the Golgi apparatus using antibodies directed against the 58 K Golgi protein, immunoreactivity was detected in the perinuclear region of the cell (Figure 3.22).

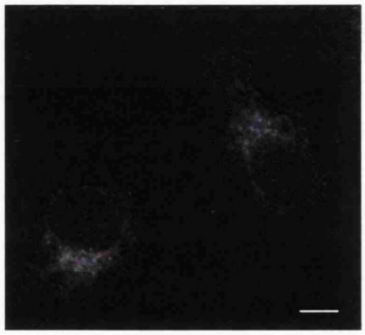

Figure 3.22. The Golgi apparatus is located in the cytoplasmic perinuclear region in COS-7 cells. Confocal section of untransfected COS-7 cells. Cells were fixed, permeabilised, stained with anti-58K golgi protein antibodies followed by AlexaFluor®594 conjugated secondary antibodies and imaged. This image is representative of n = 5 cells observed for n = 3 independent transfections. Scale bar, 10 μm. This experiment was performed by Dr K. Brickley.

In COS-7 cells transfected with pECFP-GRIF-1 and stained for the Golgi apparatus, ECFP-GRIF-1 fluorescence was co-distributed with the Golgi apparatus immunoreactivity in the vicinity of the nucleus (Figure 3.23). This might result either from: (i) an artefact of the overexpression procedure, i.e. large amounts of ECFP-GRIF-1 are synthesized and processed through the Golgi apparatus following transfection of pECFP-GRIF-1, ii) from an association of GRIF-1 with the Golgi apparatus, iii) from an association of GRIF-1 with endosomes that are organelles localised in the Golgi region (Soldati and Schliwa, 2006) or iv) from an association of GRIF-1 with the microtubule minus-ends at the centrosome, i.e. the microtubule organisation centre, a structure shown to be localised in the Golgi region (Kellogg *et al.*, 1994).

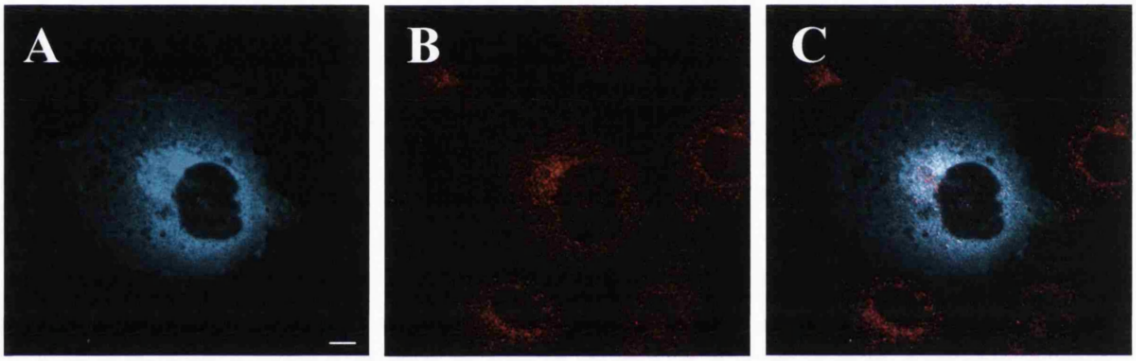

Figure 3.23. ECFP-GRIF-1 co-localises with the Golgi apparatus in transfected COS-7 cells. Confocal section of a COS-7 cell transfected with pECFP-GRIF-1. The cell was fixed 36 h post transfection, stained with anti-58K Golgi protein antibodies followed by AlexaFluor®594 secondary antibodies and imaged. A, ECFP-GRIF-1; B, 58K Golgi protein; C, overlaid picture of (A + B) This cell is representative of n = 8 cells observed for n = 3 independent transfections. Scale bar, 10 μm. This experiment was performed by Dr K. Brickley.

In COS-7 cells that were transfected with pN-ECFP-KIF5C and stained for the Golgi, ECFP-KIF5C fluorescence was in the cytoplasm as mentioned before and it was not co-distributed with the Golgi apparatus immunoreactivity (Figure 3.24).

In COS-7 cells co-transfected with pECFP-GRIF-1 + pN-EYFP-KIF5C and stained for the Golgi apparatus, ECFP-GRIF-1 and EYFP-KIF5C fluorescences were concentrated at the cell periphery or in cellular extensions as described earlier and they were not co-localised with the Golgi apparatus (Figure 3.25). The morphology of the Golgi apparatus was not altered following the redistribution of GRIF-1 to the cell periphery thereby showing that GRIF-1 is not located within the Golgi and that GRIF-1 is not involved in the maintenance of the Golgi structure.

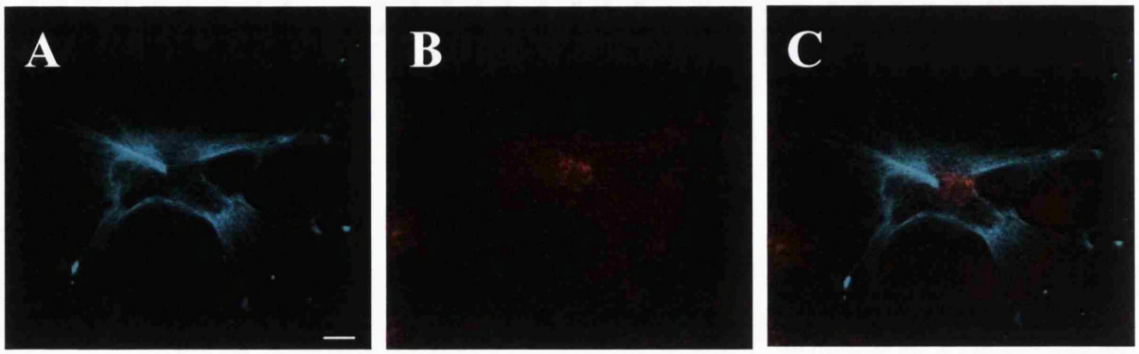

Figure 3.24. ECFP-KIF5C does not co-localise with the Golgi apparatus in transfected COS-7 cells. Confocal section of a COS-7 cell transfected with pECFP-KIF5C. The cell was fixed 36 h post-transfection, stained with anti-58K Golgi protein antibodies followed by AlexaFluor®594 secondary antibodies and imaged. A, ECFP-KIF5C; B, 58K Golgi protein; C, overlaid picture of (A + B). This cell is representative of n = 6 cells observed for n = 3 independent transfections. Scale bar, 10 μm. This experiment was performed by Dr K. Brickley.

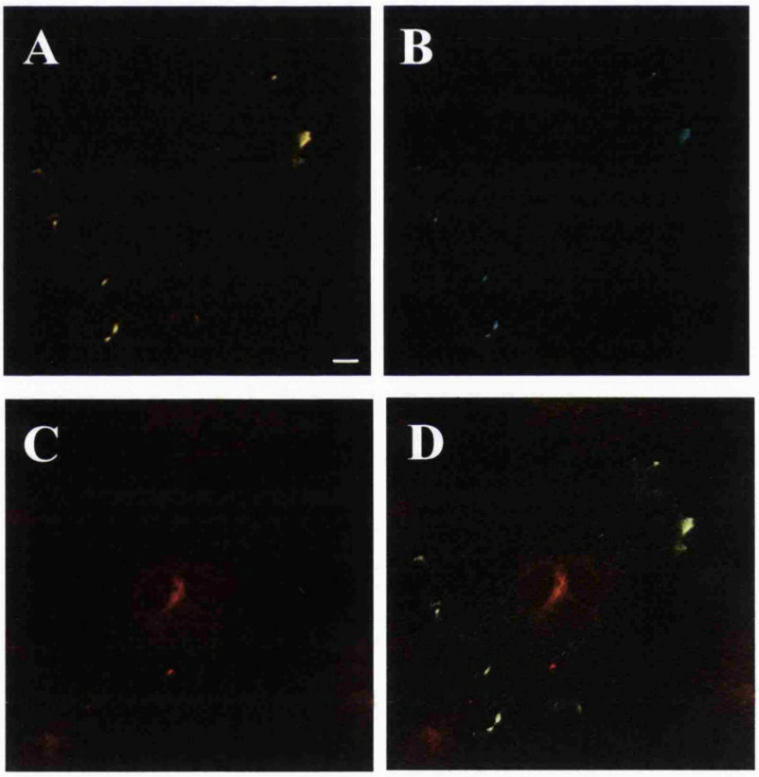

Figure 3.25. ECFP-GRIF-1 and EYFP-KIF5C do not co-localise with the Golgi apparatus in transfected COS-7 cells. Confocal section of a COS-7 cell transfected with pECFP-GRIF-1 and pN-EYFP-KIF5C. The cell was fixed 36 h post-transfection, stained with anti-58K Golgi protein antibodies followed by AlexaFluor®594 secondary antibodies and imaged. A, EYFP-KIF5C; B, ECFP-GRIF-1; C, 58K Golgi protein; D, overlaid picture of (A + B + C). This cell is representative of n = 8 cells observed for n = 3 independent transfections. Scale bar, 10 μm. This experiment was performed by Dr K. Brickley.

Endoplasmic reticulum- In COS-7 cells transfected with pECFP-ER, the fluorescence was localised around the nucleus and in the cytoplasmic region adjacent to the nucleus forming a tubular network (Figure 3.26). This distribution pattern was not changed in the presence of either EYFP-GRIF-1 or EYFP-KIF5C as described hereafter.

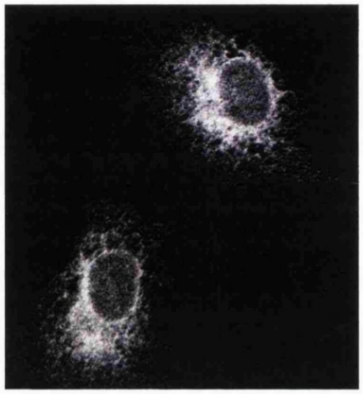

Figure 3.26. The endoplasmic reticulum is located in a cytoplasmic perinuclear region of COS-7 cells. Confocal section of COS-7 cells transfected with pECFP-ER. Cells were fixed 40 h after transfection and imaged. This image is representative of n = 24 cells observed for n = 3 independent transfections. Scale bar, 10 μm.

In COS-7 cells co-transfected with pECFP-ER + pEYFP-GRIF-1, EYFP-GRIF-1 fluorescence was localised within the cell cytoplasm in the perinuclear region of the cell forming tubular structures (Figure 3.27). EYFP-GRIF-1 and ECFP-ER were only partially co-distributed in the area close to the nucleus as shown on the overlaid image (Figure 3.27 C). This implies that GRIF-1 is not associated with the ER.

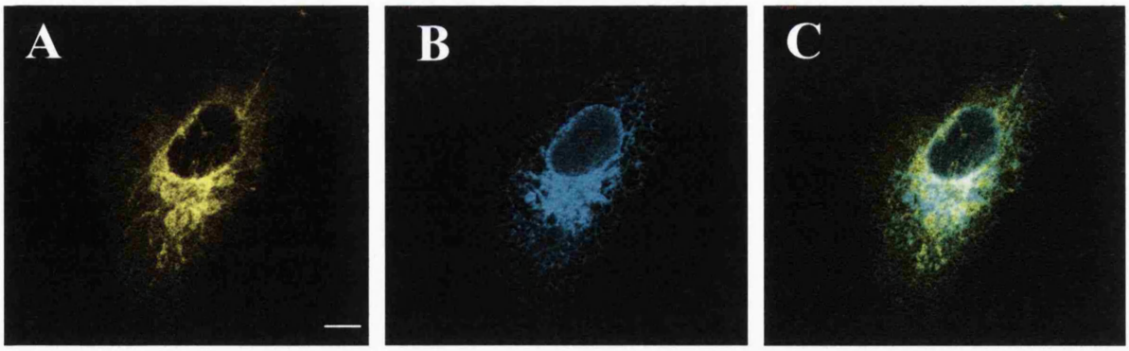

Figure 3.27. EYFP-GRIF-1 co-localises partially with the endoplasmic reticulum in transfected COS-7 cells. Confocal section of a COS-7 cell co-transfected with pEYFP-GRIF-1 + pECFP-ER. A, EYFP-GRIF-1; B, ECFP-ER; C, overlaid picture of (A + B); This image is representative of n = 10 cells observed for n = 2 independent transfections. Scale bar, 10 μm.

In COS-7 cells co-transfected with pECFP-ER + pN-EYFP-KIF5C, EYFP-KIF5C fluorescence was distributed within the cell cytoplasm. Some areas of co-localisation with

ECFP-ER fluorescence were visible throughout the cell cytoplasm consistent with a role of KIF5C in ER transport (Figure 3.28 D) (Bannai *et al.*, 2003).

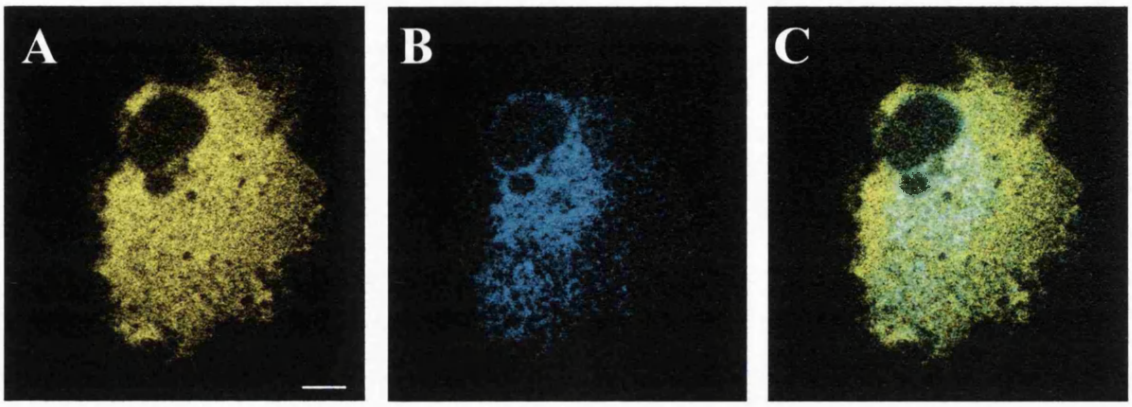

Figure 3.28. EYFP-KIF5C co-localises partially with the endoplasmic reticulum in transfected COS-7 cells. Confocal section of a COS-7 cell co-transfected with pN-EYFP-KIF5C and pECFP-ER. A, N-EYFP-KIF5C; B, ECFP-ER; C, overlaid picture of (A + B). This image is representative of n = 11 cells observed for n = 2 independent transfections. Scale bar, 10 μm.

In COS-7 cells co-transfected with pCIS-GRIF-1 + pN-EYFP-KIF5C + pECFP-ER were stained for GRIF-1 using anti-GRIF-$1_{8\text{-}633}$ antibodies (Figure 3.29). GRIF-1 immunoreactivity was concentrated in cellular extensions and it was co-localised with EYFP-KIF5C fluorescence as observed in pECFP-GRIF-1 + pN-EYFP-KIF5C transfections. The ER fluorescence was localised within the cell cytoplasm. Some ER fluorescence was also co-distributed with GRIF-1 and EYFP-KIF5C in cellular extensions (Figure 3.29 C, D), consistent with the findings that kinesin-1 is involved in ER transport (Bannai *et al.*, 2003). It is not clear from these data whether GRIF-1 plays a role in kinesin-1-mediated ER transport.

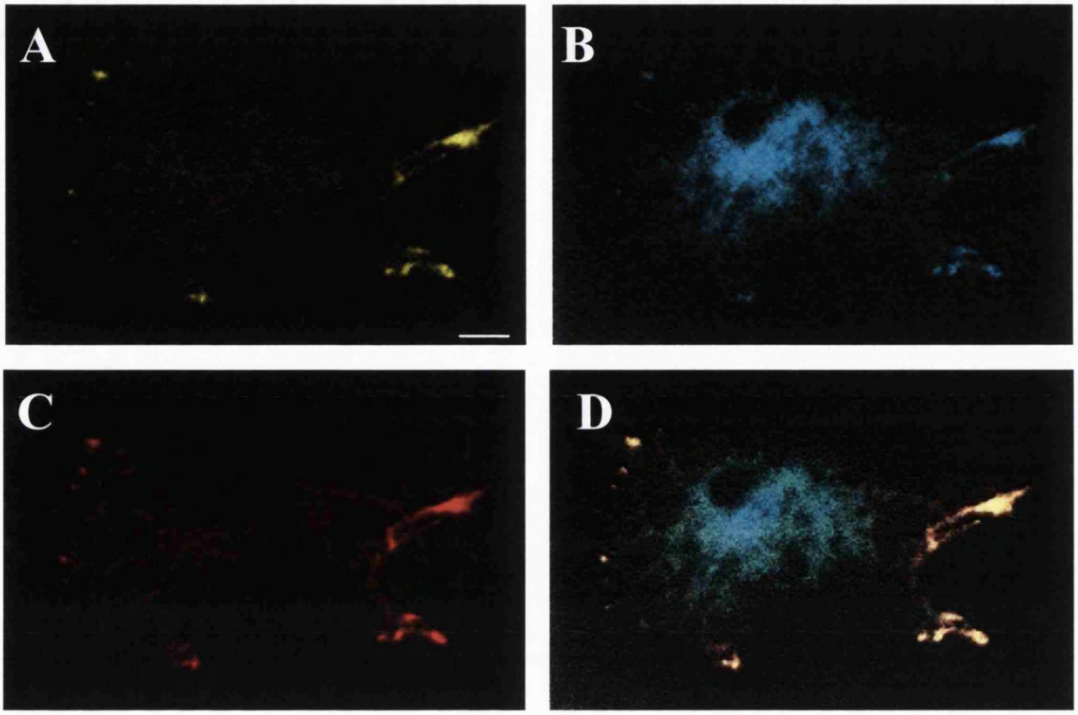

Figure 3.29. GRIF-1 and EYFP-KIF5C co-localise partially with the endoplasmic reticulum in transfected COS-7 cells. Confocal section of a COS-7 cell transfected with pCIS-GRIF-1 + pN-EYFP-KIF5C + pECFP-ER. The cell was fixed 36 h post-transfection, permeabilised and incubated with anti-GRIF-$1_{8\text{-}633}$ antibodies followed by Alexa Fluor®594 secondary antibodies and imaged. A, EYFP-KIF5C; B, ECFP-ER; C, GRIF-1; D, overlaid pictures of (A + B + C). This image is representative of n = 5 cells observed for n = 1 transfection. Scale bar, 10 μm

3.3. DISCUSSION

This chapter describes the generation and characterisation of fluorescently-tagged GRIF and fluorescently-tagged KIF5C constructs and their use in confocal microscopy imaging studies. It was shown that fusion of ECFP or EYFP to the N-terminal end of GRIF-1 did not modify GRIF-1 interacting properties for KIF5C or truncated KIF5C mutants. Similarly, addition of ECFP or EYFP to either the N- or C-terminal ends of KIF5C did not affect KIF5C interacting properties for GRIF-1.

When overexpressed on its own in mammalian cell lines, ECFP-GRIF-1 was found in the proximity of the nucleus in the Golgi region and it formed tubular, vesicular structures. Co-expression of ECFP-GRIF-1 with EYFP-KIF5C in mammalian cell lines resulted in a re-distribution of GRIF-1 to KIF5C-enriched region at the cell periphery in agreement with an interaction between GRIF-1 and KIF5C (Brickley *et al.*, 2005). Further, co-distribution analyses where ECFP-GRIF-1 was co-expressed with the MD or NMD of EYFP-KIF5C suggested that GRIF-1 may be associated with the NMD in agreement with yeast two-hybrid and immunoprecipitation analyses carried out in parallel to the work presented here (Smith *et al.*, 2006).

Studies using organelle markers indicated that GRIF-1 was localised or associated to mitochondria consistent with previous findings (Brickley *et al.*, 2005) but not to the Golgi or the ER. More importantly these studies showed that GRIF-1 was necessary for the targeting of mitochondria to KIF5C. These analyses also indicated that GRIF-1 was not involved in the maintenance of either Golgi or ER cellular location since overexpressing GRIF-1 did not affect the structure of the ER or Golgi apparatus. However, the partial localisation of GRIF-1 with the Golgi and the ER in the absence of KIF5C suggests that GRIF-1 might be involved in KIF5C-independent ER-to-Golgi or Golgi-to-ER transport processes. A recent study showed that GRIF-1 was localised to early endosomes in rat pheochromocytoma cells (PC) -12 cells (Kirk *et al.*, 2006). The tubular structures observed in ECFP-GRIF-1 transfected cells may represent early endosomes since these organelles are found in the Golgi region. Thus GRIF-1 may localise to both mitochondria and early endosomes.

Taken together these results support a role for GRIF-1 in intracellular trafficking processes. Particularly they suggest a role for GRIF-1 as a scaffolding protein linking physically

kinesin-1 to mitochondria in kinesin-1-based mitochondrial transport. In a recent report by Glater *et al.* (2006), the *Drosophila* orthologue of GRIF-1, Milton, was also shown to be localised to kinesin-1-containing regions at the cell periphery following overexpression of Milton and KIF5B in COS-7 cells. Further, Milton was also necessary for the recruitment of mitochondria to KIF5B. Overall this suggests that GRIF-1 may have a similar function to Milton in kinesin-1-directed mitochondrial tranport mechanisms.

Here, the role of GRIF-1 in transport mechanisms was addressed by comparing the distribution patterns of ECFP-GRIF-1 or EYFP-GRIF-1 to that of fluorescently-tagged KIF5C or fluorescently-tagged organelles. Co-localisation analyses were carried out qualitatively by observation of overlapping pixels in confocal microscopy images, i.e. optical sections or Z-stacks. Optical sections are performed throughout the whole cell perpendicularly to the Z-axis. Each section is a focal plane that provides fine details on the location of the fluorescent protein or fluorescent organelle inside the imaged cell in the given section. A Z-stack corresponds to the superimposition of optical sections. A line scan drawn through a Z-stack informs about the total fluorescence intensity of the layered optical sections. Thus pixels may overlap on the Z-stack although they are not even localised within the same section. Therefore co-localisation analyses should not be performed on Z-stack projections but on an optical section of the object imaged.
To improve the analyses carried out in this chapter, co-localisation could have been assessed in a quantitative manner. Some of the methods developed for this purpose are discussed hereafter (reviewed in Media Cybernetics, Application note #1; Bolte and Cordelieres, 2006). The pixel intensity from one channel can be plotted versus the pixel intensity from the other channel thereby generating a scatter plot. Co-localising pixels are distributed along the diagonal line rising from the 0 while non-co-localised pixels are close to the x and y-axis. Different correlation coefficients can be calculated to quantify the co-localisation for the whole scatter plot. These are the Pearson's coefficient, the overlap coefficients, R, and its sub-coefficients k1, k2 and the co-localisation coefficients, m1, m2. Pearson's coefficient is a ratio used to represent the correlation between 2 images. Its values range between +1 and -1 with +1 indicating perfect co-localisation, 0, an absence of correlation (random co-localisation) and -1, a complete contra-localisation. Because

intermediate negative values are difficult to interpret, a second coefficient, i.e. the overlap coefficient, R, is often measured simultaneously. This gives values ranging from 0 to 1, with 0 corresponding to contra-localisation and 1 to full co-localisation. Pearson's coefficient and the overlap coefficient, R, are relatively insensitive to variation in pixel intensity between channels caused by phenomena such as photobleaching or variation in fluorophore concentrations. However they are sensitive to the pixel ratio between each channel, the overall pixel density and to noise (Bolte and Cordelieres, 2006). To reduce the dependency of R on the pixel ratio of the channels, the overlap sub-coefficients, k1 and k2, are calculated. These represent the differences in intensities between the 2 channels. The co-localisation coefficients, m1 and m2, describe the contribution of each channel relative to the overall co-localisation in the image. The coefficients, k1, k2, m1 and m2, are still highly dependent on the noise level. Alternatively co-localisations can be evaluated for a specific intensity range (threshold) defined on the scatter plot by calculating the Manders coefficients, M1 and M2. These inform about the contribution of each channel in the co-localised area relative to the overall thresholded image. Manders coefficients can be used to estimate the co-localisation of 2 samples with different signal intensities however they are sensitive to background noise (Bolte and Cordelieres, 2006). The calculation of M1 and M2 was improved by Costes and co-workers (2004) who designed an algorithm for the automatic thresholding of the co-localisation area. This avoided the potential biais introduced by the user while setting the threshold.

The correlation coefficients discussed in this section can be calculated by imaging software such as ImageJ (http://rsb.info.nih.gov/ij/).

CHAPTER 4

FLUORESCENCE RESONANCE ENERGY TRANSFER (FRET) STUDY OF GRIF-1/KINESIN-1 AND GRIF-1/$GABA_A$RECEPTOR INTERACTIONS: ESTABLISHMENT OF A PROTOCOL FOR THE DETERMINATION OF FRET EFFICIENCIES BY ACCEPTOR PHOTOBLEACHING

4.1. INTRODUCTION

4.1.1. Rationale for the use of fluorescence resonance energy transfer, FRET, to study GRIF-1/kinesin-1 and GRIF-1/$GABA_A$ receptor interactions

As described in Chapter 1, GRIF-1 was originally identified as a $GABA_A$ receptor β2 subunit interacting protein in a yeast two-hybrid cDNA library screen. This interaction was substantiated by *in vitro* protein interaction assays and immunoprecipitation experiments following co-expression of GRIF-1 and $GABA_A$ receptor β2 subunits in HEK 293 cells (Beck *et al.*, 2002). However, it was not possible to show an interaction between GRIF-1 and $GABA_A$ receptor β2 subunits by immunoprecipitation from native rat brain. A possible explanation was that the interaction was of low affinity or transient as suggested by both quantitative yeast two-hybrid interaction studies and co-localisation experiments (Beck *et al.*, 2002). Therefore, it was necessary to develop an alternative system to study GRIF-1/$GABA_A$ receptor β2 subunit interactions in primary neuronal cells.

FRET is a technique used to detect protein-protein interactions in live or fixed cells (see for review section 2.2.5.3). It is a biophysical process by which energy is transferred from a donor fluorophore to an acceptor fluorophore located in close proximity (<10 nm), following excitation of the donor fluorophore. This energy transfer results in a modification of the fluorescence emission properties of both fluorophores thereby enabling the measurement of FRET (section 2.2.5.3). The GFP variants, ECFP and EYFP, are often used as donor and acceptor fluorophores, respectively (sections 2.2.5.3, 3.1.2). Interactions are detected by expressing 2 proteins of interest, i.e. an ECFP-tagged protein and an EYFP-tagged protein, in the same cell and measuring the variations in ECFP and EYFP emissions following excitation of ECFP only. The methods developed for the assessment of FRET efficiencies are described in section 2.2.5.3. FRET measurements are often performed in live or fixed cells using a fluorescence or confocal microscope. This enables the visualisation of the 2 interacting proteins within the cell thus providing further information on the cellular location of the interaction. For example, FRET was used to study the interaction between ECFP-syntaxin-1 and EYFP-Munc18 in fixed cells (Liu *et al.*, 2004). It was shown that ECFP-syntaxin-1 and EYFP-Munc18 interacted in the Golgi apparatus and this interaction was maintained during the transport of these proteins to the cell membrane. FRET was also

used to investigate α4β2 nicotinic acetylcholine receptor assembly by sub-cloning ECFP or EYFP in the intracellular loop of each subunit and detecting FRET between the subunits (Nashmi *et al.*, 2003). Thus FRET imaging technology was chosen to examine GRIF-1/$GABA_A$ receptor β2 subunit interactions in neurones. It was expected this would enable the tracking of low affinity or transient interactions between an ECFP-tagged GRIF-1 and an EYFP-tagged $GABA_A$ receptor β2 subunit in their physiological cellular environment.

To determine the optimal conditions for FRET imaging, it was necessary to use 2 proteins known to interact. GRIF-1 and the kinesin-1 protein, KIF5C, were shown to interact directly in yeast two-hybrid studies (Brickley *et al.*, 2005) (Chapter 1). Since FRET occurs over distances of less than 10 nm, fluorophores used to label defined domains of GRIF-1 and KIF5C are predicted to be close enough, when GRIF-1 and KIF5C interact, for FRET to be detected. Hence the GRIF-1/KIF5C pair was used as a control to establish a FRET procedure. This was performed using fluorescently-tagged GRIF-1 and fluorescently-tagged KIF5C constructs generated in Chapter 3 and a confocal microscope. Further, optimal conditions for FRET imaging were established in fixed mammalian cell lines as they are easier to maintain and to transfect than neurones.

4.1.2. Aims of this chapter

The first aim of this chapter was to establish the technique of FRET in the laboratory using 2 known interacting proteins with the ultimate aim then to study GRIF-1/$GABA_A$ receptor β2 subunit interactions. Therefore an EYFP-tagged $GABA_A$ receptor β2 subunit construct was generated to be used as a FRET acceptor for ECFP-GRIF-1. A second aim was to gather further information on the cellular distribution of GRIF-1/$GABA_A$ receptor β2 subunit association by confocal microscopy imaging of mammalian cell lines co-expressing ECFP-GRIF-1 and EYFP-tagged $GABA_A$ receptor β2 subunits. Finally FRET was used to study in more detail GRIF-1/KIF5C interactions.

4.2. RESULTS

4.2.1. Establishment of the optimal conditions for the measurement of FRET by acceptor photobleaching

FRET efficiencies between donor and acceptor were measured by photobleaching the acceptor and measuring the following increase in donor fluorescence (section 2.2.5.3). In all experiments, the FRET donor was ECFP and the FRET acceptor was EYFP. As mentioned before, the GRIF-1/kinesin-1 heavy chain, KIF5C, pair was used to perform the initial FRET measurements. The ECFP-GRIF-1, EYFP-GRIF-1, ECFP-KIF5C and EYFP-KIF5C fusion proteins generated in Chapter 3 served as FRET donors or FRET acceptors.

Both N- and C-terminal fluorescent-tagged KIF5C constructs were utilised because the GRIF-1 binding domain on KIF5C was not known at the initiation of these studies. The position of the fluorophore was of major importance for FRET studies. Since KIF5C is 80 nm in length (Hirokawa and Takemura, 2005), GRIF-1 could associate with the KIF5C N-terminal domain, the KIF5C median stalk region or the KIF5C C-terminal domain. An N-terminally tagged GRIF-1 was used because the KIF5C binding domain of GRIF-1 was previously mapped to GRIF-1 N-terminal domain, GRIF-$1_{124\text{-}283}$ (Brickley *et al.*, 2005).

FRET measurements were performed only in HEK 293 cells since it was found that they have a higher transformation efficiency and they express higher concentration of proteins compared to COS-7 cells. In addition, the low expression levels of the fluorescent proteins in COS-7 cells often resulted in sample photobleaching during the FRET imaging procedure.

The results presented in this section were published in Smith *et al.* (2006).

4.2.1.1. Determination of FRET efficiencies using the multi-track imaging mode

Initially, optimal conditions for the measurement of FRET by acceptor photobleaching were established using the multi-track imaging mode of the LSM510 Meta laser-scanning confocal microscope. Measurements were performed using different donor/acceptor pairs including either GRIF-1 as a donor, i.e. ECFP-GRIF-1, or GRIF-1 as an acceptor, i.e. EYFP-GRIF-1, in combination with the appropriate KIF5C construct, i.e. either EYFP-KIF5C or ECFP-KIF5C respectively. This was because the expression levels of co-expressed proteins could vary within a cell thereby altering the donor/acceptor stoichiometry, an important parameter for the detection of FRET as

discussed in section 4.5 (Hoppe *et al.*, 2002). The donor/acceptor pairs were ECFP-GRIF-1/N-EYFP-KIF5C, ECFP-GRIF-1/C-EYFP-KIF5C, EYFP-GRIF-1/N-ECFP-KIF5C, EYFP-GRIF-1/C-ECFP-KIF5C.

Thus HEK 293 cells were co-transfected with donor and acceptor constructs mentioned above, fixed 24-48 h after transfection and analysed for FRET. The experimental procedure was carried out as describes in section 2.2.5.3.2. The mean FRET efficiencies obtained for each donor/acceptor combination are summarised in Figure 4.1. It is shown as a percentage ± standard error of the mean (SEM).

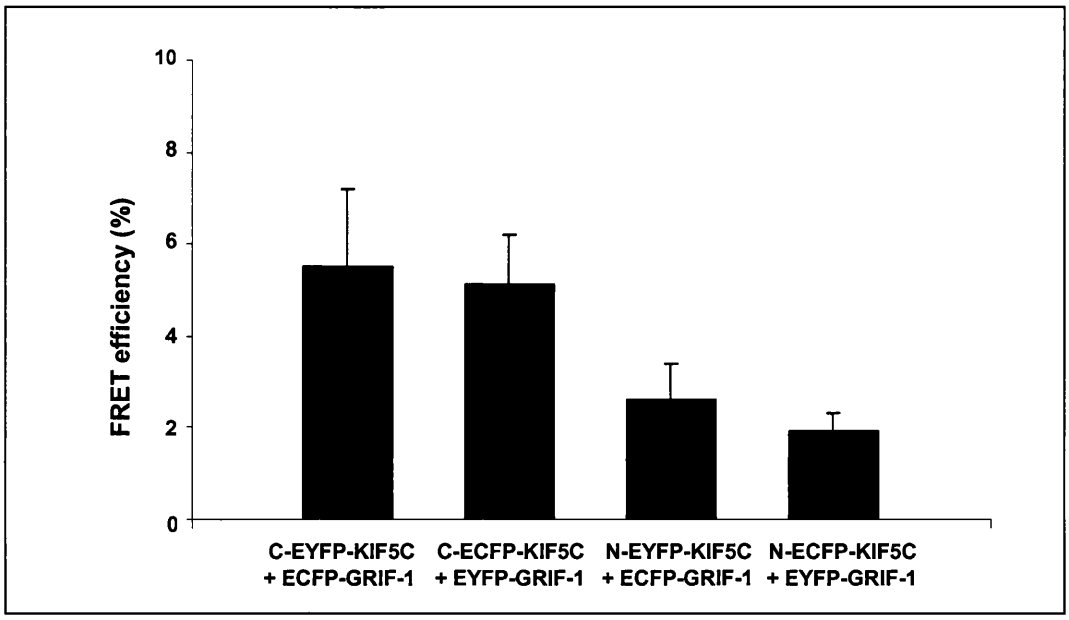

Figure 4.1. Determination of FRET efficiencies by acceptor photobleaching using the multi-track imaging mode. HEK 293 cells were transfected with either pECFP-GRIF-1 + pC-EYFP-KIF5C, pEYFP-GRIF-1 + pC-ECFP-KIF5C, pECFP-GRIF-1 + pN-EYFP-KIF5C or pEYFP-GRIF-1 + pN-ECFP-KIF5C. Cells were fixed 24 h after transfection and FRET efficiencies were measured with the acceptor photobleaching method exactly as described in section 2.2.5.3.2.1. These results are representative of at least n = 5 cells analysed from n = 2 transfections.

Similar mean FRET efficiencies were found for the pairs ECFP-GRIF-1/C-EYFP-KIF5C (5.5% ± 1.7, n = 10 cells) and EYFP-GRIF-1/C-ECFP-KIF5C (5.1% ± 1.1, n = 12 cells). Similar mean FRET values were also found for the pairs ECFP-GRIF-1/N-EYFP-KIF5C (2.6% ± 0.8, n = 5 cells) and EYFP-GRIF-1/N-ECFP-KIF5C (1.9% ± 0.4, n = 6 cells). This indicated that GRIF-1 and KIF5C could be used either as donor or acceptor for FRET without affecting the FRET efficiency. The constructs ECFP-GRIF-1 and EYFP-KIF5C were used to carry out subsequent experiments. The FRET values reported here were not corrected for background FRET signal, i.e. the pseudo-FRET (see section 2.2.5.3.2.2). These values are lower than those (corrected for pseudo-

FRET) already reported in the literature, e.g. ~ 8% FRET efficiency for a positive control using the same multi-track imaging mode (Karpova *et al.*, 2003). A positive control giving a higher FRET efficiency should be used to establish the optimal conditions to measure FRET. The accuracy of the measured values was therefore questioned. As explained in section 2.2.5.3.2.1, for FRET measurements ECFP is excited at λ = 458 nm and ECFP emissions are collected between λ = 475-525 nm using the filter available on the microscope, i.e. a BP 475-525, before and after photobleaching of EYFP. Figure 4.2 shows the excitation and emission spectra of ECFP and EYFP.

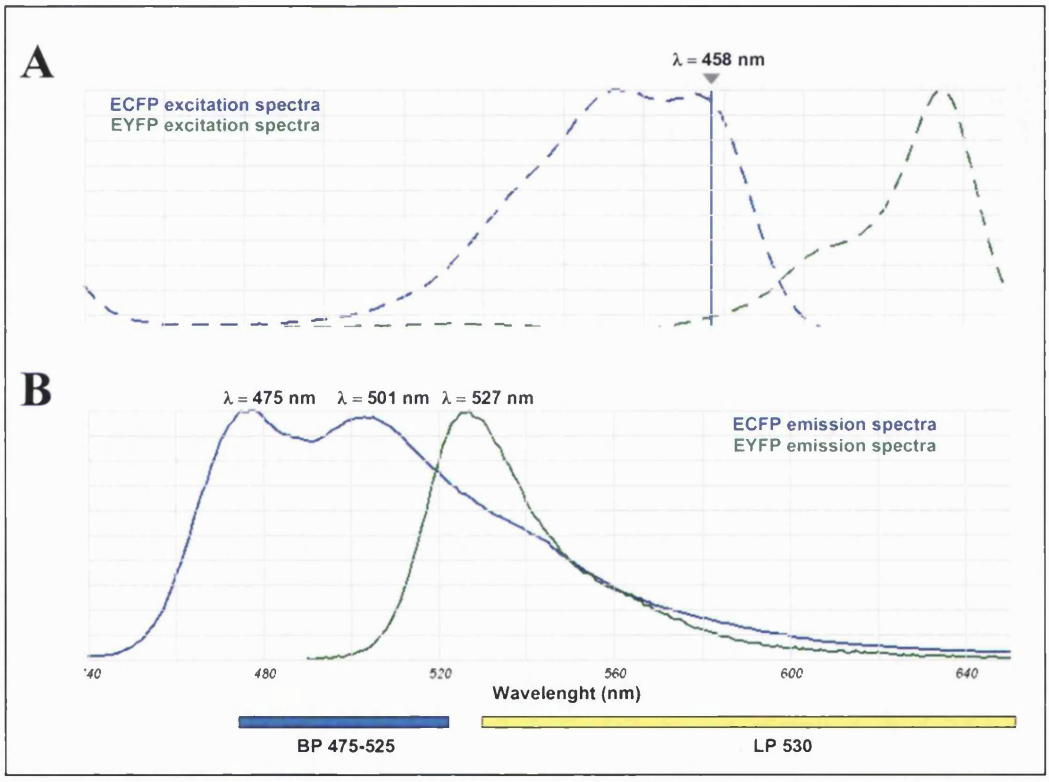

Figure 4.2. Spectral properties of ECFP and EYFP and associated problems for acceptor photobleaching FRET measurements using the multi-track mode of the confocal microscope. A, excitation spectra of ECFP and EYFP. This Figure shows that EYFP can be excited by the λ = 458 nm laser line (top of the spectra) used to excite EYFP. B, emission spectra of ECFP and EYFP. The emission peaks of ECFP and EYFP are shown on the top of the spectra. The filters used to collect ECFP emissions, i.e. BP 475-525, and EYFP emissions, i.e. LP 530 are indicated at the bottom of the spectra. The Figure shows that some EYFP fluorescence is also collected with the BP 475-525, this is the bleedthrough of EYFP in the ECFP channel.

It can be seen that EYFP can be excited at λ = 458 nm, the laser line used to excite ECFP. It can also be seen that EYFP fluorescence emissions are also partly collected with the BP 475-525 on the ECFP channel since EYFP emissions are maximal at λ = 527 nm. ECFP fluorescence emissions collected before EYFP photobleaching are not

accurate due to the bleedthrough of EYFP in the ECFP channel. Thus the calculated FRET efficiency values are not representative of the changes in ECFP fluorescence emissions pre- and post-photobleaching.

To optimise the collection of ECFP emission fluorescence and to prevent EYFP bleedthrough on ECFP channel, a different filter should be used to collect ECFP emissions such as a BP 470-505 collecting λ = 470-505 nm (Karpova *et al.*, 2003). Unfortunately such a filter was not available. Thus it was not possible to optimise a procedure for the measurement of FRET by acceptor photobleaching using the multi-track imaging mode of the microscope. An alternative system with a positive control giving higher FRET values was required.

4.2.1.2. Determination of FRET efficiencies using the lambda imaging mode

Acceptor photobleaching FRET efficiencies were measured using the lambda mode of the confocal microscope since it enables an accurate measurement of ECFP fluorescence emissions and it overcomes bleedthrough issues (see section 2.2.5.2.2). Moreover this imaging mode has already been used successfully for FRET studies (Liu *et al.*, 2004; Nashmi *et al.*, 2003). To establish the acceptor photobleaching FRET methodology, a construct encoding ECFP-EYFP dimers linked by 2 amino acids (Ser, Gly), i.e. pECFP-EYFP (a gift from Dr. L. He, NIH, Bethesda, MD, USA) was used as a positive control (He *et al.*, 2003). This construct has already been shown to give high FRET values, i.e. 24% (He *et al.*, 2003). The negative control was the co-transfection of cells with ECFP and EYFP on separate plasmids, i.e. pECFP-C1 and pEYFP-C1. As for before (section 4.2.1.1), FRET efficiencies were calculated by assessing the increase in ECFP fluorescence following EYFP photobleaching. Thus, HEK 293 cells were transfected with the positive and negative controls, pECFP-EYFP and pECFP-C1 + pEYFP-C1 respectively, fixed 24-48 h after transfection and an area of ECFP/EYFP co-localisation was photobleached and analysed for FRET. The optimised procedure is described in the method section (section 2.2.5.3.2.2). As an additional control, FRET efficiencies were also determined for a region of the cell that was not photobleached if possible. The mean FRET efficiencies obtained for each donor/acceptor combination were corrected for pseudo-FRET, i.e. a background FRET signal measured by applying the FRET procedure to cells transfected with pECFP-C1 only. To conclude that FRET occurred within a sample, 2 conditions had to be fulfilled according to Karpova et al. (2003):

- the corrected mean FRET efficiency in the photobleached region had to be significantly higher than the corrected mean FRET efficiency obtained in the unbleached region, i.e. $p < 0.01$ in a paired Student t-test.
- the corrected mean FRET efficiency had to be significantly higher than the corrected mean FRET efficiency obtained for the negative control, i.e. $p < 0.01$ in an unpaired Student t-test.

The corrected mean FRET efficiencies obtained for each combination are shown as a percentage ± SEM in Figure 4.3.

Pseudo-FRET- The pseudo-FRET was measured by applying the photobleaching protocol to HEK 293 cells transfected with pECFP-C1 only. The mean pseudo-FRET value was 2.9% ± 0.2 (n = 8 cells from n = 3 independent transfections).

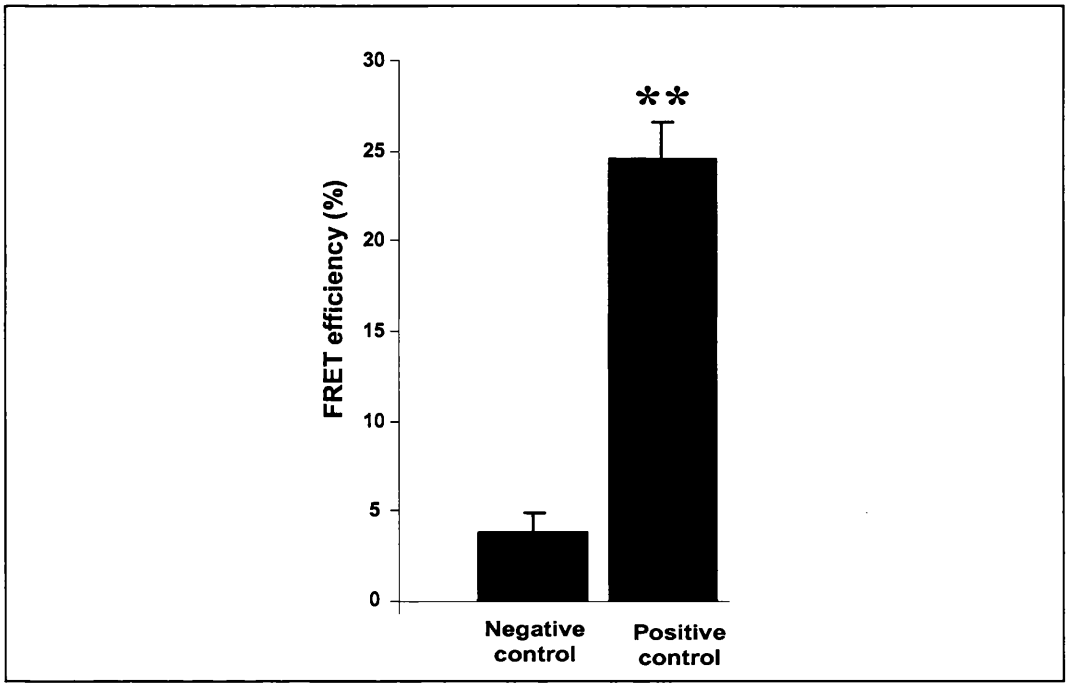

Figure 4.3. Establishment of the optimal conditions for the measurement of FRET efficiencies by acceptor photobleaching. HEK 293 cells were transfected with either the positive control, i.e. pECFP-EYFP, or the negative control, i.e. pECFP-C1 + pEYFP-C1. Cells were fixed 24 h after transfection and FRET efficiencies were measured with the acceptor photobleaching method exactly as described in section 2.2.5.3. FRET efficiencies obtained for the positive and negative controls were corrected for pseudo-FRET and background fluorescence and compared using an unpaired Student t-test.**, $p < 0.0005$. FRET efficiencies were measured for at least n = 15 cells from n = 3 independent transfections.

Positive control- FRET efficiencies for the positive control were determined using HEK 293 cells transfected with pECFP-EYFP. In the photobleached region, a corrected mean FRET efficiency of 24.6% ± 2.0 was found (n = 22 cells from n = 3 independent transfections). This value was significantly different to that obtained in the unbleached region, i.e. 1.4% ± 0.4 ($p < 0.0001$).

Negative control- FRET efficiencies for the negative control were obtained from HEK 293 cells co-transfected with pECFP-C1 and pEYFP-C1. In the photobleached region, a corrected mean FRET efficiency of 3.8% ± 0.5 was found (n = 18 cells from n = 3 independent transfections). This value was not significantly different from that obtained in the unbleached region, i.e. 3.3% ± 0.2 ($p < 0.1$).

C***omparison of the FRET values obtained for positive and negative controls-*** In the photobleached regions, the positive control had a corrected mean FRET efficiency that was significantly different from that obtained for the negative control ($p < 0.001$).

Conclusion- The corrected mean FRET value obtained for the positive control fulfilled the 2 conditions necessary to conclude that FRET had occurred. These values were in agreement with He *et al.* (2003) who found a FRET value of 24% using the same positive control. This validates the experimental procedure used to measure FRET by acceptor photobleaching.

4.2.2. Determination of FRET efficiencies between ECFP-GRIF-1 and EYFP-tagged KIF5C chimeras

In Chapter 3, co-localisation studies suggested that ECFP-GRIF-1 was associated with EYFP-KIF5C, EYFP-KIF5C-NMD but not with EYFP-KIF5C-MD. However, it was not possible to determine accurately from these studies whether ECFP-GRIF-1 interacted with the N-terminal or C-terminal domains of KIF5C-NMD. To study in more detail the interaction between GRIF-1 and KIF5C, FRET experiments were carried out.

The optimised procedure established above (section 3.2.1.2) was used to measure FRET efficiencies between ECFP-GRIF-1 and each EYFP-tagged KIF5C construct, i.e. C-EYFP-KIF5C, N-EYFP-KIF5C, EYFP-KIF5C-NMD, EYFP-KIF5C-MD.

HEK 293 cells were co-transfected with each ECFP-GRIF-1/EYFP-KIF5C combinations, fixed and analysed for FRET as described in sections 2.2.5.3.2.2. Mean FRET values obtained for each combination were corrected for pseudo-FRET and compared to the value obtained for the negative control, i.e. 3.8% ± 0.5 (section 3.2.1.2). This was possible since all the measurements were performed on the same day. The corrected mean FRET efficiencies obtained for each combination are shown as a percentage ± SEM in Figure 4.4.

ECFP-GRIF-1 + N-EYFP-KIF5C- In the photobleached region, a corrected mean FRET efficiency of 5.6% ± 0.5 (n = 15 cells from n = 3 independent transfections) was

found. This value was not significantly different from that obtained in the unbleached region, i.e. 4.5% ± 0.3 ($p < 0.025$). This value was also not different from that obtained for the negative control ($p < 0.4$). Thus, no FRET was detected.

ECFP-GRIF-1 + C-EYFP-KIF5C- In the photobleached region, a corrected mean FRET efficiency of 10.3% ± 0.7 was found (n = 20 cells from n = 3 independent transfections). This value was significantly different from that obtained in the unbleached region, i.e. 2.5% ± 0.4 ($p < 0.0005$). This value was also significantly different from that obtained for the negative control ($p < 0.001$). Thus FRET was detected.

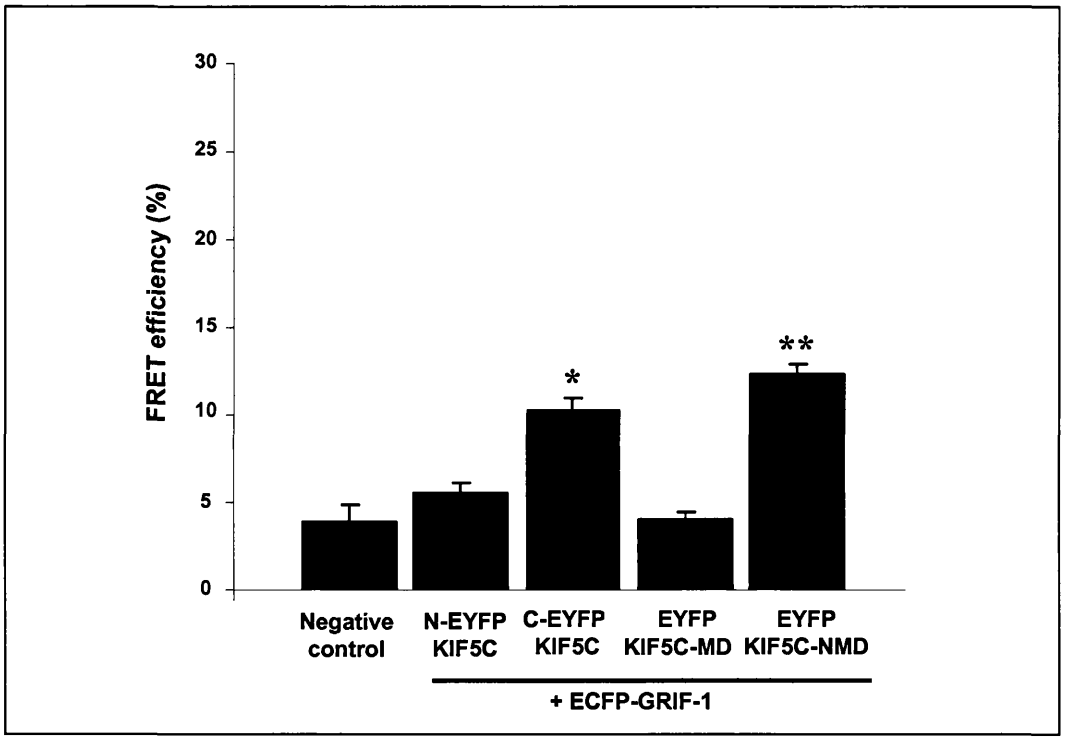

Figure 4.4. Determination of FRET efficiencies between ECFP-GRIF-1 and each EYFP-tagged KIF5C construct by acceptor photobleaching FRET imaging. HEK 293 cells were transfected with either pECFP-C1 + pEYFP-C1, pECFP-GRIF-1 + pN-EYFP-KIF5C, pECFP-GRIF-1 + pC-EYFP-KIF5C, pECFP-GRIF-1 + pEYFP-KIF5C-MD or pECFP-GRIF-1 + pEYFP-KIF5C-NMD. Cells were fixed 24 h after transfection and FRET efficiencies were measured with the acceptor photobleaching method exactly as described in section 2.2.5.3.2.2. FRET efficiencies obtained for each GRIF-1/KIF5C combination were corrected for pseudo-FRET and background fluorescence and compared to the negative control using an unpaired Student t-test.**, $p < 0.0005$. FRET efficiencies were measured for at least n = 11 cells from n = 3 independent transfections.

ECFP-GRIF-1 + EYFP-KIF5C-MD- In the photobleached region, a corrected mean FRET efficiency of 4.3% ± 0.4 was found (n = 11 cells from n = 3 independent transfections). This value was not significantly different from that obtained in the unbleached region, i.e. 1.4% ± 0.1 ($p < 0.025$). This value was also not significantly

different from that obtained for the negative control ($p < 0.9$). Thus, no FRET was detected.

ECFP-GRIF-1 + EYFP-KIF5C-NMD- In the photobleached region, a corrected mean FRET efficiency of 12.4% ± 0.5 was found (n = 16 cells from n = 3 independent transfections). This value was significantly different from that obtained in the unbleached region, i.e. 4.4% ± 0.2 ($p < 0.0005$). This value was also significantly different from that obtained for the negative control ($p < 0.001$). Thus FRET was detected.

Conclusion- Significant FRET efficiency values were obtained for the pairs ECFP-GRIF-1/C-EYFP-KIF5C and ECFP-GRIF-1/EYFP-KIF5C-NMD pairs. Since FRET occurs between ECFP and EYFP molecules at less than 10 nm distance, these results prove that indeed ECFP-GRIF-1 was directly associated with the C-terminal non-motor domain of EYFP-KIF5C.

4.2.3. Generation of an EYFP-tagged $GABA_A$ receptor β2 subunit for the confocal microscopy imaging of GRIF-1/$GABA_A$ receptor interactions

As described in section 4.1.1, evidence for GRIF-1/$GABA_A$ receptor interactions in a mammalian system is lacking. GRIF-1 was shown to immunoprecipitate $GABA_A$ receptor β2 subunits following their co-expression in HEK 293 cells. However an interaction between GRIF-1 and assembled β2 subunit-containing $GABA_A$ receptors has never been shown. Acceptor photobleaching FRET is an imaging technique to detect and visualise protein-protein interactions in fixed cells (section 2.2.5.3). It is a non-invasive technique since the physiological conditions where the interaction occurs are preserved, i.e. the interactions are assessed in intact fixed cells and not in cell homogenates. A procedure was established to measure FRET efficiencies between ECFP and EYFP by acceptor photobleaching in fixed HEK 293 cells (section 4.2.1.2). It was successfully used to identify GRIF-1/KIF5C interacting domains (section 4.2.1.3). This optimised FRET protocol together with co-localisation analyses were proposed as an alternative method to investigate GRIF-1/$GABA_A$ receptor β2 subunits and GRIF-1/$GABA_A$ receptors interactions in mammalian cell lines.

This section describes the preparation of an EYFP-tagged $GABA_A$ receptor β2 subunit construct and its expression in HEK 293 and COS-7 cells.

4.2.3.1. Sub-cloning of EYFP into the intracellular loop of the $GABA_A$ receptor β2 subunit

As described in section 1.3.1, $GABA_A$ receptor subunits are composed of an ~ 220 amino acid N-terminal extracellular domain, 4 TM domains with a ~ 100 amino acid intracellular loop between TM3 and TM4 and a short C-terminal extracellular domain. EGFP has already been used to study the assembly and cell membrane targeting of $GABA_A$ receptors in mammalian cell lines, *Xenopus* oocytes and neurones (section 3.1.1; Chapell *et al.*, 1998; Connor *et al.*, 1998, Kittler *et al.*, 2000). In these reports, EGFP was fused either at the N- or at the C-terminal domain of the $GABA_A$ receptor subunit. This was to avoid interfering with the folding and assembly properties of the subunit. The current study aims to investigate the interaction between the cytoplasmic protein, GRIF-1, and the $GABA_A$ receptor β2 subunit by FRET measurements and co-localisation analyses during $GABA_A$ receptor trafficking events. $GABA_A$ receptors are assembled in the ER, modified in the Golgi apparatus and transported to the cell surface (Connolly *et al.*, 1996b; Kittler and Moss, 2003). $GABA_A$ receptors are transported between the ER and the Golgi and between the Golgi and the cell surface enclosed in vesicles. $GABA_A$ receptor N- and C-terminal domains are located in the vesicle lumen whereas the intracellular loop is located within the cytoplasm and it is exposed to cytoplasmic proteins such as GRIF-1. Therefore it was necessary to insert EYFP in the intracellular loop of the $GABA_A$ receptor β2 subunit.

The cloning site was chosen so that it did not interfere with the GRIF-1 binding site, i.e. residues 324-394 (Beck *et al.*, 2002), nor with putative β2 subunit phosphorylation sites (Kittler and Moss, 2003). A bioinformatics analysis of the $GABA_A$ receptor β2 subunit (Ymer *et al.*, 1989) was carried out using the NetPhos 2.0 Server (www.expasy.org) (Blom *et al.*, 1999). Predicted phosphorylation sites were found between residues 342-422 (Figure 4.5). Therefore, EYFP was inserted in the region between residues 303-324. A unique restriction enzyme recognition site that was not found in either the GRIF-1 nucleotide sequence or in the $GABA_A$ receptor β2 subunit nucleotide sequence was created by site-directed mutagenesis in this cloning region. The *BssHII* restriction site, GCGCGC, was created by mutating the nucleotides C_{1012} to G and A_{1013} to C in the plasmid pCIS-$GABA_A$R-β2, yielding pCIS-$GABA_A$R-$β2_{BssHII}$ and EYFP was inserted between residues 310-312 of the $GABA_A$ receptor β2 subunit.

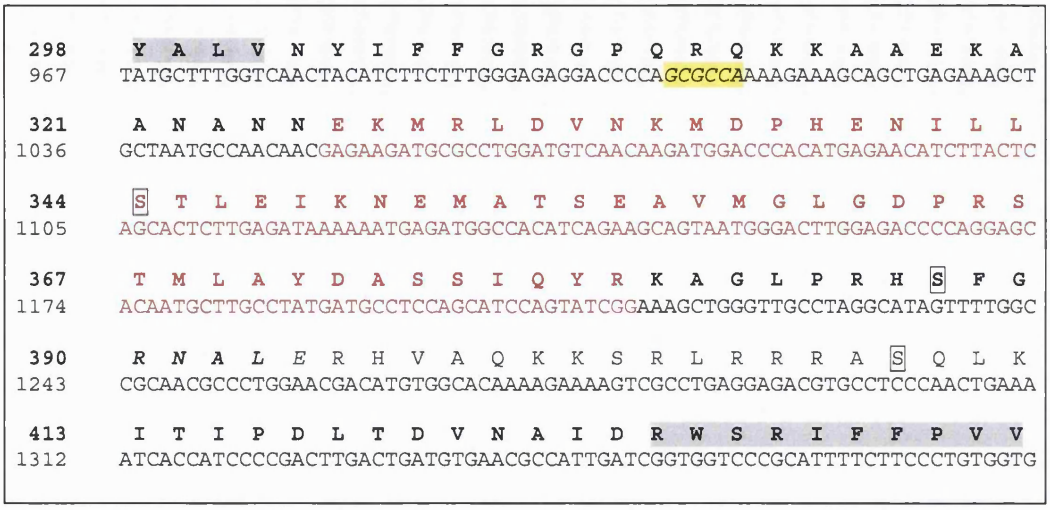

Figure 4.5. Determination of an insertion site for the sub-cloning of EYFP in the intracellular loop of the rat $GABA_A$ receptor β2 subunit. This Figure shows the oligonucleotide and deduced amino acid sequences of the intracellular loop of the rat $GABA_A$ receptor β2 subunit. The transmembrane domains, TM3 and TM4, are also represented, highlighted in grey. The GRIF-1 binding site is represented in red characters. The NetPhos 2.0 Server (Blom *et al.*, 1999) was used to determine putative phosphorylation sites. High probability predicted phosphorylation sites are boxed. EYFP was sub-cloned in the intracellular loop of the $GABA_A$ receptor β2 subunit so that it did not interfere with the GRIF-1 binding site and phosphorylation sites. The EYFP sub-cloning site is highlighted in yellow.

EYFP was amplified from pEYFP-C1 with forward and reverse oligonucleotide primers that contained the *BssHII* restriction site at their 5'-ends (Chapter 2, Table 2.5). The PCR product, $EYFP_{BssHI}$, and pCIS-$GABA_AR$-$β2_{BssHII}$ were digested with *BssHII*, pCIS-$GABA_AR$-$β2_{BssHII}$ was dephosphorylated and $EYFP_{BssHII}$ was ligated into pCIS-$GABA_AR$-$β2_{BssHII}$. The ligation product was used to transform chemically competent DH5α bacteria cells. Transformants were analysed by restriction enzyme digestion and their DNA sequence was verified by nucleotide sequencing. The sequencing results showed that EYFP was inserted in frame in pCIS-$GABA_AR$-$β2_{BssHII}$, yielding pCIS-$GABA_AR$-$β2^{EYFP}$. A plasmid map of pCIS-$GABA_AR$-$β2^{EYFP}$ is shown on Appendix 4.1.

4.2.3.2. Molecular size of EYFP-tagged $GABA_A$ receptor β2 subunits

To ensure that EYFP-tagged $GABA_A$ receptor β2 subunits had a M_r consistent with the addition of EYFP (M_r = 28 kDa), immunoblotting analyses were carried out. Homogenates of HEK 293 cells transfected with either EYFP-tagged $GABA_A$ receptor β2 subunits or wild-type $GABA_A$ receptor β2 subunits were prepared 24 h post-transfection and analysed by immunoblotting using antibodies recognising the $GABA_A$ receptor β2 $subunit_{381-395}$, i.e. anti-$GABA_A$ receptor $β2_{381-395}$. The M_r of EYFP-tagged $GABA_A$ receptor β2 subunits was compared to that of wild-type $GABA_A$ receptor β2 subunits. The result is shown in Figure 4.6.

No immunoreactive bands were detected in homogenates of untransfected HEK 293 cells (Figure 4.6, lane 1). In homogenates of cells transfected with pCIS-$GABA_AR$-β2, a band with M_r = 54 kDa was detected (Figure 4.6, lane 2). This band had the size expected for $GABA_A$ receptor β2 subunits. Additional bands with M_r ~ 50 kDa and M_r ~ 56 kDa were also visible. The lower M_r band may represent a non-*N*-glycosylated variant of $GABA_A$ receptor β2 subunits while the higher M_r band may represent a $GABA_A$ receptor β2 subunit variant glycosylated on several sites as already reported by Connolly *et al.* (1996b). In homogenates of cells transfected with pCIS-$GABA_AR$-$\beta2^{EYFP}$, a single immunoreactive band with M_r = 85 kDa was detected (Figure 4.6, lane 3). This band corresponded to that predicted for the EYFP-tagged $GABA_A$ receptor β2 subunit (Figure 4.6). No bands of lower or higher molecular weight corresponding to putative *N*-glycosylated variants were observed as in homogenates of cells transfected with the non-fluorescent subunits (compare Figure 4.6, lanes 2-3). This suggests that the insertion of EYFP in the intracellular loop might alter the conformation of the $GABA_A$ receptor β2 subunit thereby interfering with its *N*-glycosylated state. This also suggests that EYFP-tagged $GABA_A$ receptor β2 subunits might either be fully *N*-glycosylated or fully non-*N*-glycosylated and this might affect the functionality of the subunit.

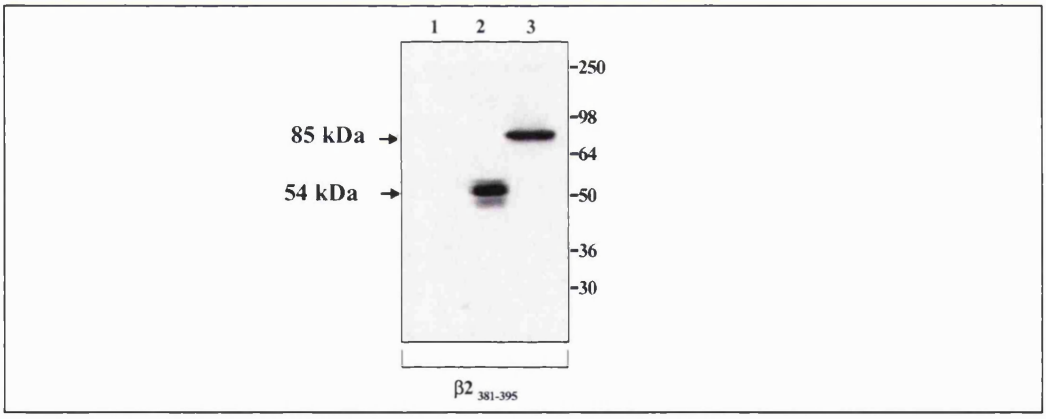

Figure 4.6. Molecular size of EYFP-tagged $GABA_A$ receptor β2 subunits . HEK 293 cells were transfected with a construct encoding either pCIS-$GABA_AR$-β2 or pCIS-$GABA_AR$-$\beta2^{EYFP}$. Homogenates were prepared 24 h after transfection and analysed by immunoblotting using anti-$\beta2_{381-395}$ antibodies. Lane 1, homogenates of untransfected cells; homogenates of cells transfected with: lane 2, pCIS-$GABA_AR$-β2 and lane 3, pCIS-$GABA_AR$-$\beta2^{EYFP}$. The molecular weight standards (kDa) are shown on the right. Immunoreactive bands of interest are indicated by an arrow, M_r ($GABA_AR$-β2) = 54 kDa, M_r ($GABA_AR$-$\beta2^{EYFP}$) = 85 kDa. This immunoblot is representative of n = 3 experiments from n = 3 independent transfections.

To summarise, EYFP-tagged $GABA_A$ receptor β2 subunits were expressed in HEK 293 cells with an increase in M_r consistent with the addition of EYFP (Figure 4.7).

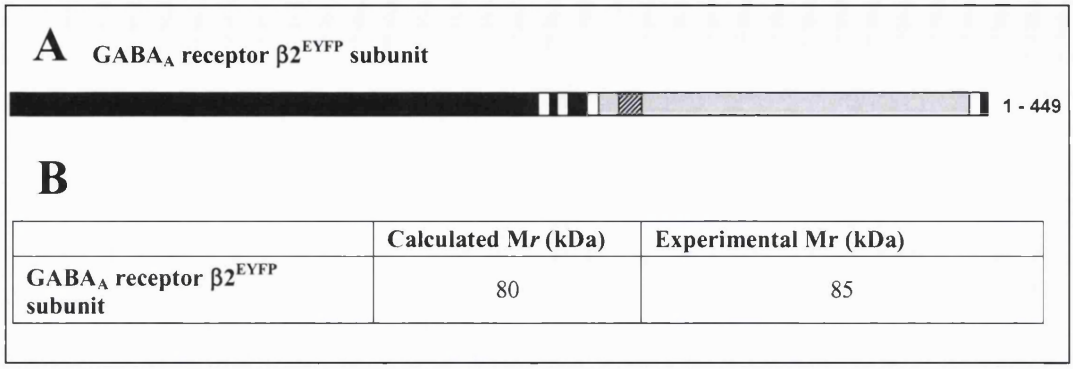

B

	Calculated Mr (kDa)	Experimental Mr (kDa)
GABA$_A$ receptor β2^{EYFP} subunit	80	85

Figure 4.7. A Figure summarising the structure and molecular weight (M_r) of EYFP-tagged GABA$_A$ receptor β2 subunits. A, a schematic diagram depicting the structure of EYFP-tagged GABA$_A$ β2 subunits with ■ , extracellular domain, □ , transmembrane domain, ▨ , EYFP, ▭ , intracellular domain. B, a Table indicating the calculated and experimental M_r.

4.2.3.3. EYFP-tagged GABA$_A$ receptor β2 subunits co-associate with α1 and γ2 GABA$_A$ receptor subunits

It was necessary to check that the addition of EYFP in the intracellular loop of GABA$_A$ receptor β2 subunits did not affect the folding and the properties of the subunits. When folded properly, these subunits associate with α1 and γ2 GABA$_A$ receptor subunits to form functional α1β2γ2 GABA$_A$ receptors in the ER that are then trafficked to the cell surface (Connolly *et al.*, 1996b). Thus, detergent soluble extracts of HEK 293 cells co-transfected with cDNA encoding α1, β2 and γ2 GABA$_A$ receptor subunits were prepared and immunoprecipitation experiments were carried out using sheep antibodies directed against the C-terminal domain of GABA$_A$ receptor α1 subunits, i.e. anti-GABA$_A$ receptor α1$_{413-429}$, or non-immune sheep IgGs as a control. Immune pellets were analysed using rabbit antibodies recognising either α1, γ2 or β2 GABA$_A$ receptor subunits, i.e. anti-GABA$_A$ receptor α1$_{1-14}$, anti-GABA$_A$ receptor γ2$_{1-15}$ or anti-GABA$_A$ receptor β2$_{381-395}$ respectively. The results are shown in Figures 4.8 A, B.

Wild-type α1β2γ2 GABA$_A$ receptor- Immune pellets of cells co-transfected with the plasmids pCIS-GABA$_A$R-β2 + pCIS-GABA$_A$R-γ2 + pcDM8-GABA$_A$R-α1 were first probed with anti-GABA$_A$ receptor α1$_{1-14}$ antibodies. A single band with M_r = 55 kDa was detected in the immune pellet (Figure 4.8 A, lane 3) but not in the control non-immune pellet (Figure 4.8 A, lane 2), thus showing that GABA$_A$ receptor α1 subunits were specifically immunoprecipitated. Interestingly 3 bands with M_r = 55 kDa, M_r = 48 kDa and M_r = 45 kDa were recognised in the detergent soluble extract used to perform the immunoprecipitation. The bands with M_r = 55 kDa corresponds to that expected for

$GABA_A$ receptor $\alpha 1$ subunit while the lower M_r bands might correspond to partially glycosylated and non-glycosolated $GABA_A$ receptor $\alpha 1$ subunit isoforms as previously reported by Connolly *et al.* (1996b). Thus anti-$GABA_A$ receptor $\alpha 1_{1\text{-}14}$ antibodies detected the fully glycosylated $GABA_A$ receptor $\alpha 1$ subunit isoform in the immune pellet (Figure 4.8, lane 3). The partially and non-glycosylated isoforms may also be present in the immune pellet but at relatively low concentrations. Therefore these isoforms cannot be detected by immunoblotting. Immune pellets were then analysed with anti-$GABA_A$ receptor $\gamma 2_{1\text{-}15}$ antibodies where 3 major bands with M_r = 90 kDa, M_r = 53 kDa and M_r = 46 kDa were detected in the immune pellet (Figure 4.8 A, lane 5). The band with M_r = 53 kDa corresponded to that expected for $GABA_A$ receptor $\gamma 2$ subunits. The bands with M_r = 90 kDa and M_r = 46 kDa were non-specific bands as reported in the initial study characterising this antibody (Stephenson *et al.*, 1990). The 3 bands were also detected in the non-immune pellet thus showing some non-specific binding (Figure 4.8 A, lane 6). Finally, immune pellets were analysed with anti-$GABA_A$ receptor $\beta 2_{381\text{-}395}$ antibodies and 2 immunoreactive bands with M_r = 54 kDa and with M_r = 40 kDa were detected (Figure 4.8 A, lane 9). The band with M_r = 54 kDa corresponded to that predicted for $GABA_A$ receptor $\beta 2$ subunits whereas the band with M_r = 40 kDa might be a proteolytic product. The band with M_r = 40 kDa was not detected in the non-immune pellet. A faint immunoreactive band with M_r = 54 kDa was detected in the non-immune pellet thus indicating some non-specific binding (Figure 4.8 A, lane 8). These results showed that $GABA_A$ receptor $\alpha 1$ subunits are associated with $\beta 2$ and $\gamma 2$ $GABA_A$ receptor subunits although some non-specific binding was detected.

EYFP-tagged $\alpha 1\beta 2^{EYFP}\gamma 2$ $GABA_A$ receptor- Immune pellets of cells co-transfected with the constructs pCIS-$GABA_AR$-$\beta 2^{EYFP}$ + pCIS-$GABA_AR$-$\gamma 2$ + pcDM8-$GABA_AR$-$\alpha 1$ were analysed with anti-$GABA_A$ receptor $\alpha 1_{1\text{-}14}$ antibodies. As described before, a single band with M_r = 55 kDa was detected in the immune pellet (Figure 4.8 B, lane 3) but not in the control non-immune pellet (Figure 4.8 B, lane 2), thus showing that $GABA_A$ receptor $\alpha 1$ subunits were specifically immunoprecipitated. As explained before this band may correspond to the fully glycosylated $GABA_A$ receptor $\alpha 1$ subunit isoform. Again the partially and non-glycosylated isoforms detected in the detergent soluble extract (Figure 4.8 B, lane 1) may also be immunoprecipitated but they are not detected by immunoblotting due to low concentrations. Immune pellets were also probed with anti-$GABA_A$ receptor $\gamma 2_{1\text{-}15}$ and 3 major bands with M_r = 90 kDa, M_r = 53

kDa and M_r = 46 kDa were detected (Figure 4.8 B, lane 5). As explained before, the band with M_r = 53 kDa corresponded to the size expected for $GABA_A$ receptor γ2 subunits and bands M_r = 90 kDa, M_r = 46 kDa were non-specific bands. No immunoreactivity was detected in the non-immune pellet showing that γ2 subunit was specifically co-immunoprecipitated with α1 subunits (Figure 4.8 B, lane 6). The immune pellet was also analysed with anti-$GABA_A$ receptor $\beta2_{381-395}$ antibodies and 2 immunoreactive bands with M_r = 85 kDa and with M_r = 55 kDa were detected (Figure 4.8 B, lane 8). The band with M_r = 85 kDa corresponded to that predicted for $GABA_A$ receptor $\beta2^{EYFP}$ subunits. The band with M_r = 55 kDa has a molecular size consistent with that of β2 subunits and therefore it might be a degradation product lacking EYFP. No degradation products were detected in initial expression analyses (section 3.2.2.2, Figure 4.6) thereby suggesting that the degradation occurred during the immunoprecipitation procedure. These bands were not recognised in the non-immune pellet (Figure 4.8 B, lane 9) thereby showing that $\beta2^{EYFP}$ subunits were specifically co-immunoprecipitated with α1 subunits. Thus these results suggest that $GABA_A$ receptor α1 subunits can associate specifically with $\beta2^{EYFP}$ and γ2 $GABA_A$ receptor subunits. However it cannot be excluded that co-association of α1, $\beta2^{EYFP}$ and γ2 $GABA_A$ receptor subunits was not an artefact due to the experimental procedure. Indeed immunoprecipitations were carried out using detergent soluble fractions of transfected HEK 293 cells overexpressing α1, $\beta2^{EYFP}$ and γ2 $GABA_A$ receptor subunits. These are all processed through the ER. Therefore the association may be non-specific and it may result from a crowding effect in the ER. Thus further experiments are needed to clarify whether $GABA_A$ receptor $\beta2^{EYFP}$ subunits can assemble with α1 and γ2 $GABA_A$ receptor subunits to form $\alpha1\beta2^{EYFP}\gamma2$ $GABA_A$ receptors that can be assembled and targeted to the cell surface.

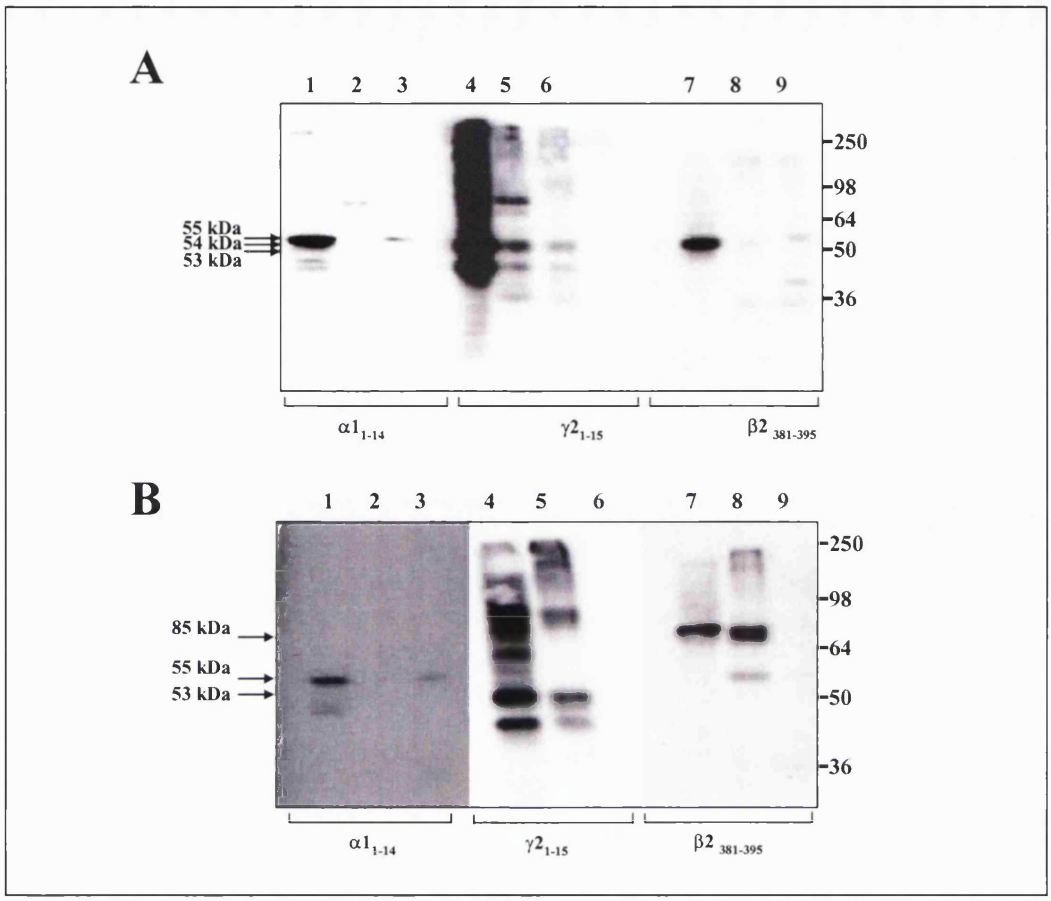

Figure 4.8. Demonstration by immunoprecipitation that $GABA_A$ receptor $\beta2^{EYFP}$ subunits associate with α1 and γ2 $GABA_A$ receptor subunits. Detergent soluble extracts of HEK 293 cells co-transfected with either A, pCIS-$GABA_A$R-β2 + pCIS-$GABA_A$R-γ2 + pcDM8-$GABA_A$R-α1 or B, pCIS-$GABA_A$R-$\beta2^{EYFP}$ + pCIS-$GABA_A$R-γ2 + pcDM8-$GABA_A$R-α1 were prepared 24 h post-transfection. Immunoprecipitation experiments were carried out using either sheep $\alpha1_{413-429}$ antibodies or sheep non-immune IgGs as a control. Immune pellets were analysed by immunoblotting using antibodies as indicated on the abcissae. A, lanes 1, 4, 7, detergent soluble extract; lanes 3, 5, 9, immune pellet; lanes 2, 6, 8, non-immune pellet. B, lanes 1, 4, 7, detergent soluble extract; lane 3, 5, 8, immune pellet; lanes 2, 6, 9, non-immune pellet The molecular weight standards (kDa) are shown on the right. Arrows indicate the immunoreactive bands of interest, M_r ($GABA_A$R-α1) = 55 kDa, M_r ($GABA_A$R-γ2) = 53 kDa, M_r ($GABA_A$R-β2) = 54 kDa, M_r ($GABA_A$R-$\beta2^{EYFP}$) = 85 kDa. These immunoblots are representative of n = 2 immunoprecipitations from n = 2 independent transfections.

4.2.3.4. Preliminary analysis of the subcellular localisation of EYFP-tagged $GABA_A$ receptor β2 subunits by confocal microscopy imaging

EYFP-tagged $GABA_A$ receptor β2 subunits, $GABA_A$ receptor $\beta2^{EYFP}$, were generated, expressed in HEK 293 cells and shown to immunoprecipitate with $GABA_A$ receptor α1 and γ2 subunits. The subcellular distribution of $GABA_A$ receptor $\beta2^{EYFP}$ subunits and of $\alpha1\beta2^{EYFP}\gamma2$ $GABA_A$ receptors and their putative association with GRIF-1 was examined by confocal microscopy imaging. Studies were carried out in transfected

COS-7 cells that were fixed 24-48 h post-transfection and imaged. The results are shown in Figures 4.9-4.13.

$GABA_A$ receptor $\beta2^{EYFP}$ subunits- In COS-7 cells transfected with pCIS-$GABA_AR$-$\beta2^{EYFP}$, the fluorescence was localised around the nucleus either as large aggregates (~ 2-5 μm long) (Figure 4.9 A) or as small tubular structures (Figure 4.9 B). Since $GABA_A$ receptor β2 subunits are retained in the ER when expressed on their own in heterologous systems (Connolly *et al.*, 1996b), these tubular structures may represent the ER.

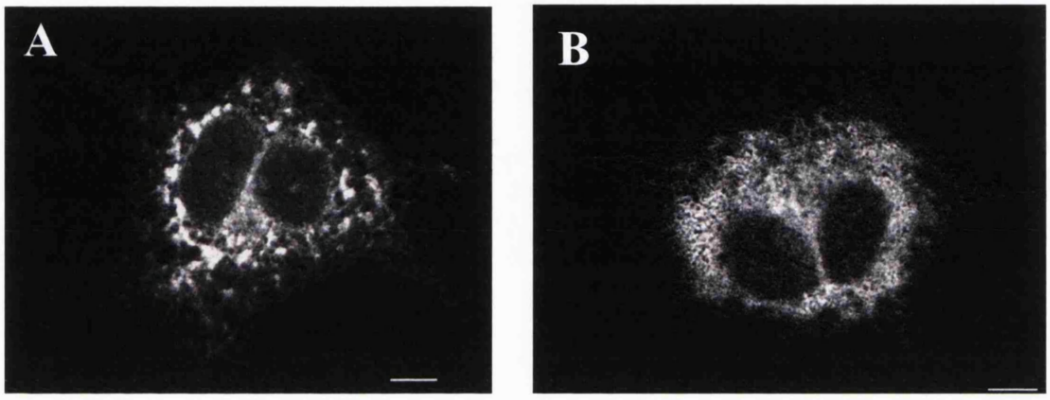

Figure 4.9. Expression of EYFP-tagged $GABA_A$ receptor β2 subunits in transfected COS-7 cells. A, B, Confocal sections of COS-7 cells transfected with pCIS-$GABA_AR$-$\beta2^{EYFP}$. Cells were fixed 24-48 h post-transfection and imaged. A, These cells are representative of n = 9 cells observed for n = 1 transfection. Scale bars, 10 μm.

$GABA_A$ receptor $\beta2^{EYFP}$ subunits and ECFP-GRIF-1- In COS-7 cells co-transfected with pECFP-GRIF-1 + pCIS-$GABA_AR$-$\beta2^{EYFP}$, EYFP-tagged $GABA_A$ receptor β2 subunit fluorescence was distributed around the nucleus forming the same tubular structures as reported for single transfections suggesting the subunit was still retained in the ER (Figure 4.10, A, D). ECFP-GRIF-1 fluorescence was concentrated in the perinuclear region as in single transfections (Chapter 3) (Figure 4.10, B, E). In some cells, ECFP-GRIF-1 was visible as tubular structures as described in Chapter 3 (Figure 4.10 E). ECFP-GRIF-1 fluorescence was only partially co-localised with EYFP-tagged β2 subunit fluorescence (Figure 4.10 C, F). ECFP-GRIF-1 fluorescence was mostly distributed in areas adjacent to EYFP-tagged β2 subunit fluorescence (Figure 4.10 C, F).

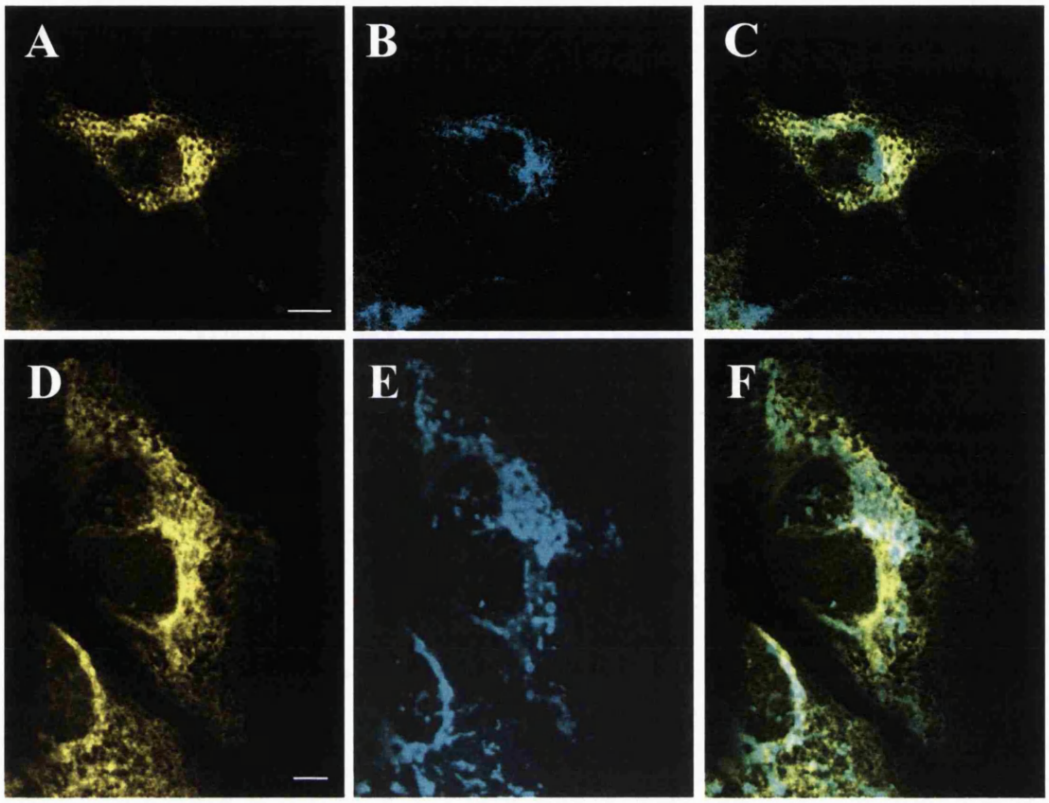

Figure 4.10. ECFP-GRIF-1 co-localises partially with EYFP-tagged $GABA_A$ receptor β2 subunits in transfected COS-7 cells. Confocal sections of COS-7 cells were co-transfected with pCIS-$GABA_A$R-$\beta2^{EYFP}$, pECFP-GRIF-1. Cells were fixed 36 h post-transfection and imaged. A, D, $GABA_A$-R $\beta2^{EYFP}$; B, E, ECFP-GRIF-1; C, F, are the merged images of (A + B) and (D + E) respectively. These cells are representative of n = 4 cells observed for n = 1 transfection. Scale bars, 10 μm.

Thus co-expression of ECFP-GRIF-1 with $GABA_A$ receptor $\beta2^{EYFP}$ subunits does not modify the cellular distribution of the subunit. Conversely the distribution of GRIF-1 is not modified by co-expression with EYFP-tagged $GABA_A$ receptor β2 subunits. ECFP-GRIF-1 has no effect over the assumed ER retention of EYFP-tagged $GABA_A$ receptor β2 subunits. Since GRIF-1 was shown to co-localise with mitochondria (Chapter 3) and $GABA_A$ receptor $\beta2^{EYFP}$ subunit might be retained in the ER, this distribution pattern might rather illustrate the known association between mitochondria and ER (Rizzuto *et al.*, 2000).

α1β2^{EYFP}γ2 $GABA_A$ receptor- In COS-7 cells co-transfected with pCIS-$GABA_A$R-$\beta2^{EYFP}$ + pCIS-$GABA_A$R-γ2 + pcDM8-$GABA_A$R-α1, the EYFP fluorescence was localised in the cell cytoplasm. In some cells, the $GABA_A$ receptor $\beta2^{EYFP}$ subunit fluorescence was distributed throughout the cell cytoplasm. In these cells, small circular aggregates (~ 2 μm diameter) were visible in a region adjacent to the cell periphery (Figure 4.11 A). This suggests that $GABA_A$ receptor $\beta2^{EYFP}$ subunits might be

trafficked to the cell surface when co-expressed with α1 and γ2 $GABA_A$ receptor subunits. In other cells, the fluorescence was accumulated in an area located between the nucleus and the membrane in agreement with an ER retention (Figure 4.11, B). Further studies are necessary to determine whether EYFP-tagged $GABA_A$ receptor β2 subunits are trafficked to the cell surface when co-expressed with α1 and γ2 $GABA_A$ receptor subunits.

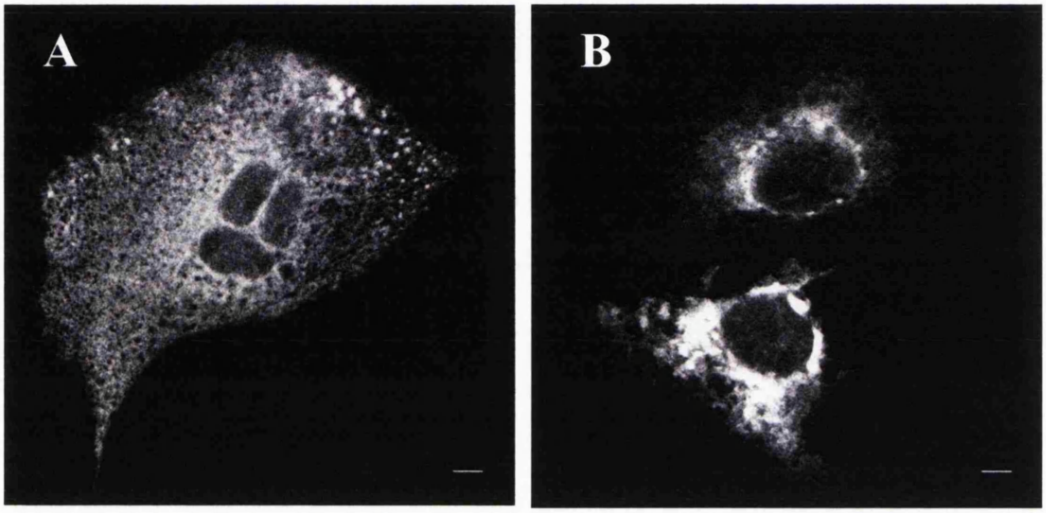

Figure 4.11. Co-expression of EYFP-tagged $GABA_A$ receptor β2 subunits, $GABA_A$ receptor α1 subunits and $GABA_A$ receptor γ2 subunits in transfected COS-7 cells. A, B, Confocal sections of COS-7 cells co-transfected with pCIS-$GABA_A$R-$\beta2^{EYFP}$, pcDM8-$GABA_A$R-α1, pCIS-$GABA_A$R-γ2. Cells were fixed 36 h post-transfection and imaged. $GABA_A$ receptor α1 subunits and $GABA_A$ receptor γ2 subunits were not labelled. The arrows in A and B indicate small aggregates. These cells are representative of n = 8 cells observed for n = 1 transfection. Scale bars, 10 μm.

α1β2^{EYFP} γ2 GABA$_A$ receptor and ECFP-GRIF-1- In COS-7 cells co-transfected with pCIS-$GABA_A$R-$\beta2^{EYFP}$ + pCIS-$GABA_A$R-γ2 + pcDM8-$GABA_A$R-α1 + pECFP-GRIF-1, $GABA_A$ receptor $\beta2^{EYFP}$ subunit fluorescence was found in the cell cytoplasm forming small aggregates (~ 1.5-4 μm long) that were distributed between the nucleus and the cell membrane (Figure 4.12 A, D, G, J). In these cells, ECFP-GRIF-1 fluorescence was found in the cytoplasmic perinuclear region, forming tubular structures (Figure 4.12, B, E, H, K). Some areas of co-localisation between ECFP-GRIF-1 and EYFP fluorescence were visible in the proximity of the nucleus (Figure 4.12, C, F, I, L). As mentioned before, this shows that ECFP-GRIF-1 does not modify the cellular distribution of α1$\beta2^{EYFP}$ γ2 $GABA_A$ receptors. This suggests that GRIF-1 does not associate with the receptor.

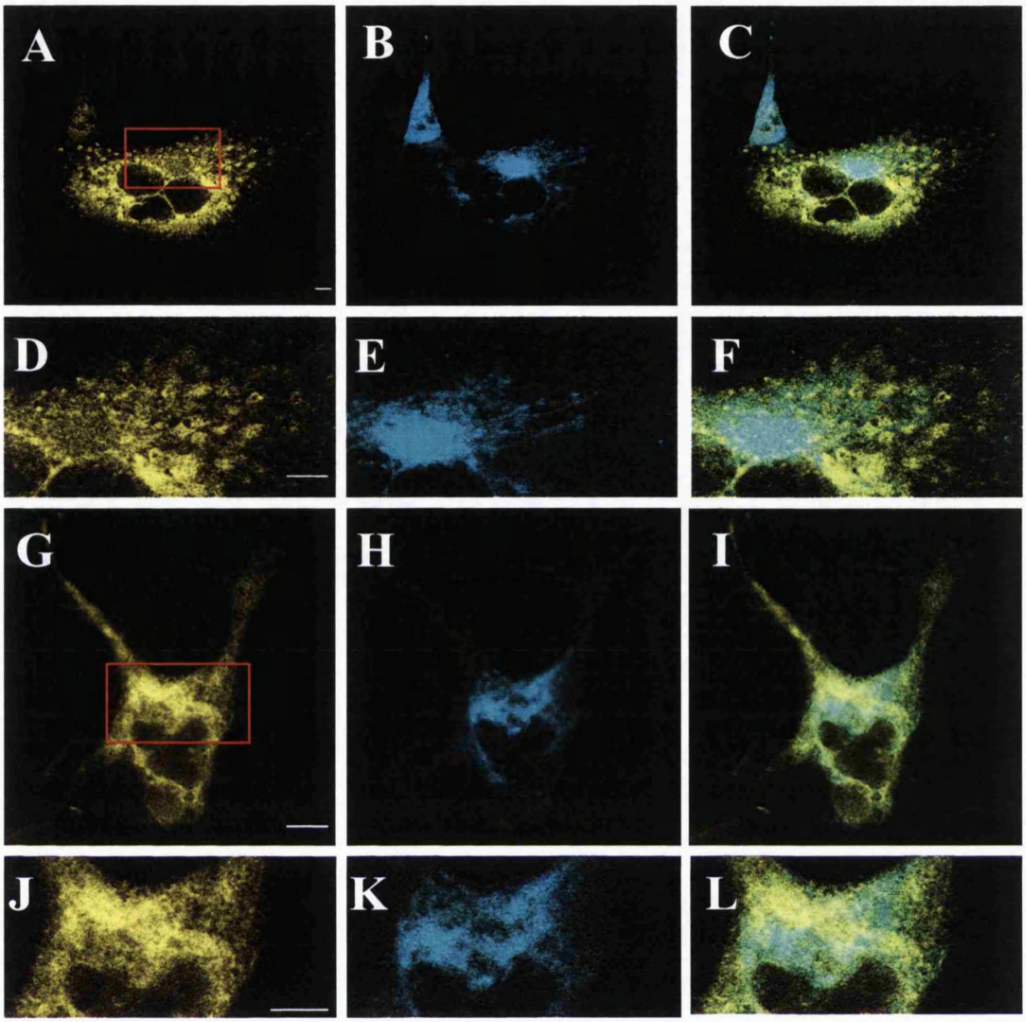

Figure 4.12. ECFP-GRIF-1 co-localises partially with $\alpha1\beta2^{EYFP}\gamma2$ $GABA_A$ receptors in transfected COS-7 cells. Confocal sections of COS-7 cells co-transfected with pECFP-GRIF-1 and constructs encoding for $\beta2^{EYFP}$ and $\gamma2$ $GABA_A$ receptor subunits, i.e. pcDM8-$GABA_A$R-$\alpha1$, pCIS-$GABA_A$R-$\beta2^{EYFP}$ and pCIS-$GABA_A$R-$\gamma2$ respectively. Cells were fixed 36 h post-transfection and imaged. A, D, G, J, $GABA_A$R-$\beta2^{EYFP}$; B, E, H, K, ECFP-GRIF-1, C, F, I, L, are merged pictures of (A + B), (D + E), (G + H) and (J + K) respectively. $\alpha1$ and $\gamma2$ $GABA_A$ receptor subunits were not labelled. F-J and P-T are enlargement of the red area in A and D respectively. These cells are representative of n = 8 cells observed for n = 1 transfection. Scale bars, 10 μm.

All together the imaging results suggest that ECFP-GRIF-1 does not associate with either $GABA_A$ receptor $\beta2^{EYFP}$ or $\alpha1\beta2^{EYFP}\gamma2$ $GABA_A$ receptors. Further, the results presented in sections 4.2.2.3 and 4.2.2.4 are not conclusive regarding the functionality and surface targeting of $GABA_A$ receptor $\beta2^{EYFP}$ subunits. The $GABA_A$ receptor $\beta2^{EYFP}$ subunit construct needs to be further characterise prior to performing FRET analyses.

As a requirement for this PhD thesis, non-permeabilised COS-7 cells transfected with constructs encoding either $GABA_A$ receptor β2 subunits, $GABA_A$ receptor $\beta2^{EYFP}$ subunits, α1β2γ2 $GABA_A$ receptors or α1$\beta2^{EYFP}$γ2 $GABA_A$ receptors were immunostained with $GABA_A$ receptor anti-α1 antibodies to determine whether α1$\beta2^{EYFP}$γ2 $GABA_A$ receptors could be trafficked to the cell surface. The results are shown on Figure 4.13.

$GABA_A$ receptor β2 subunits and $GABA_A$ receptor $\beta2^{EYFP}$ subunits- In non-permeabilised COS-7 cells overexpressing $GABA_A$ receptor β2 subunits and stained for the N-terminal extracellular domain of $GABA_A$ receptor α1 subunits, the fluorescence was weak and localised in the centre of the cell (Figure 4.13 A). This was expected since these cells do not express $GABA_A$ receptor α1 subunits. The same fluorescence pattern was observed in COS-7 cells overexpressing $GABA_A$ receptor $\beta2^{EYFP}$ subunits (Figure 4.13 B). These Figures show the background fluorescence obtained when using anti-$GABA_A$ receptor α1 antibodies.

α1β2γ2 $GABA_A$ receptors and α1$\beta2^{EYFP}$γ2 $GABA_A$ receptors- In non-permeabilised COS-7 cells overexpressing α1β2γ2 $GABA_A$ receptors and stained for the N-terminal extracellular domain of $GABA_A$ receptor α1 subunits, the fluorescence was distributed at the cell periphery consistent with a cell surface targeting of assembled α1β2γ2 $GABA_A$ receptors (Figure 4.13 C). Background fluorescence was also visible in the center of the cell as described before. The same fluorescence pattern was observed in non-permeabilised COS-7 cells overexpressing α1$\beta2^{EYFP}$γ2 $GABA_A$ receptors and stained as before (Figure 4.13 D). This showed that $\beta2^{EYFP}$ subunit-containing $GABA_A$ receptors can be assembled and trafficked to the cell surface.

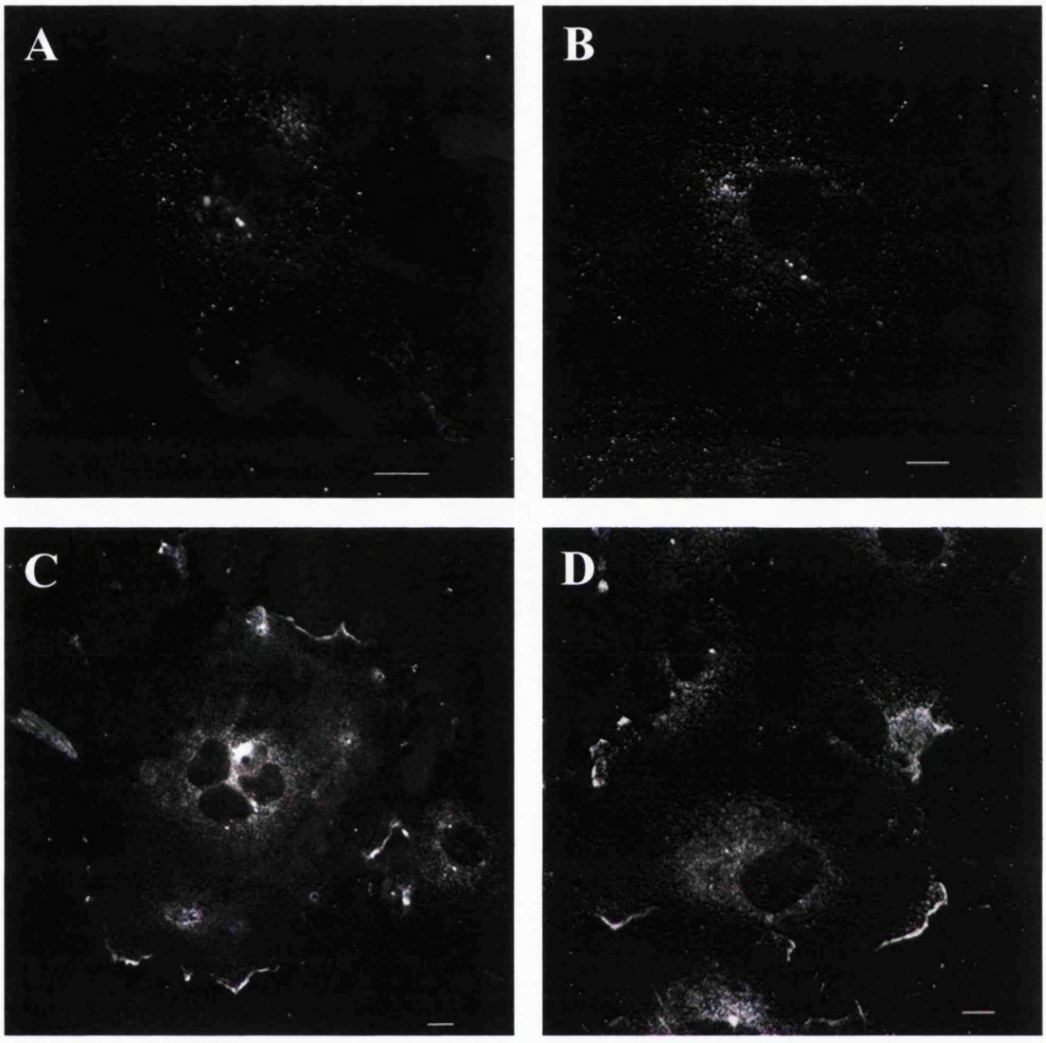

Figure 4.13. $\alpha 1\beta 2^{EYFP}\gamma 2$ $GABA_A$ receptors are targeted to the cell surface in transfected COS-7 cells. Confocal sections of COS-7 cells co-transfected with constructs encoding for either $\alpha 1\beta 2\gamma 2$ $GABA_A$ receptor subunits or $\alpha 1\beta 2^{EYFP}\gamma 2$ $GABA_A$ receptor subunits. Cells were fixed 36 h post-transfection. Non-permeabilised cells were stained for the extracellular N-terminal domain of $GABA_A$ receptor $\alpha 1$ subunits and imaged. A, $GABA_A$ receptor $\beta 2$ subunits, B, $GABA_A$ receptor $\beta 2^{EYFP}$ subunits, C, $\alpha 1\beta 2\gamma 2$ $GABA_A$ receptors, D, $\alpha 1\beta 2^{EYFP}\gamma 2$ $GABA_A$ receptors. These cells are representative of n = 4 cells observed for n = 2 transfections. Scale bars, 10 μm. This experiment was performed by Dr. K. Brickley.

4.3. DISCUSSION

The overall aim of this chapter was to develop a methodology for the study of GRIF-1/$GABA_A$ receptor β2 subunits and GRIF-1/β2 subunit-containing $GABA_A$ receptors interactions in mammalian cells. The technique of acceptor photobleaching FRET imaging was successfully established in the laboratory using the lambda mode of a laser scanning confocal microscope. The FRET procedure was validated using positive and negative controls that showed FRET efficiencies similar to that found in the literature (Liu *et al.*, 2004; He *et al.*, 2003).

FRET measurements were carried out to map the GRIF-1 binding domain on KIF5C. It was found that GRIF-1 interacted with the C-terminal non-motor domain of KIF5C in agreement with the findings in Chapter 3. Smith *et al.* (2006) refined the mapping of GRIF-1 binding site on KIF5C by yeast two-hybrid assays showing that GRIF-1 interacted with the cargo binding domain of KIF5C, a region found within the KIF5C C-terminal non-motor domain. In addition, the *Drosophila* orthologue of GRIF-1, Milton, was recently shown to interact with the C-terminal cargo binding domain of KIF5B (Glater *et al.*, 2006). Taken together, these results further support a role for GRIF-1 as an adaptor protein essential for kinesin-based transport of cargoes along microtubules similar to that shown for Milton.

FRET values obtained for the GRIF-1/KIF5C test samples were lower than the positive control. The stoichiometry of donor and acceptor expressed in an analysed cell has been reported to potentially affect FRET efficiency (Hoppe *et al.*, 2002; Karpova *et al.*, 2003). Optimal FRET values are obtained for a donor/acceptor stoichiometry of 1/1 where each donor/acceptor pair is involved in a FRET event. Here, the positive control encodes an ECFP-EYFP fusion protein where ECFP and EYFP are part of the same protein. Equal amounts of ECFP and EYFP are expressed in a given cell thereby giving a high FRET efficiency. In contrast, ECFP-GRIF-1 and EYFP-KIF5C constructs are encoded by 2 different plasmids. The same promoter, i.e. a CMV promoter, is found on both plasmids. Therefore similar amounts of ECFP-GRIF-1 and EYFP-KIF5C should be expressed in a given cell. However it has already been reported that expression levels of 2 proteins can vary within a cell despite the expression being controlled by the same promoter (Hoppe *et al.*, 2002). Therefore the lower FRET values observed in the test samples might result from a donor/acceptor stoichiometry different from 1/1. Equal amounts of expressed ECFP-GRIF-1 and EYFP-KIF5C could be ensured by generating

an ECFP-GRIF-1/EYFP-KIF5C concatamer. In this construct, ECFP-GRIF-1 and EYFP-KIF5C should be linked by a spacer long enough to allow ECFP-GRIF-1 and EYFP-KIF5C to move "freely" in the cell and not to force the interaction between GRIF-1 and KIF5C.

In this chapter, an EYFP-tagged $GABA_A$ receptor β2 subunit, $\beta2^{EYFP}$, was generated for FRET studies with ECFP-GRIF-1. Imaging studies showed that $GABA_A$ receptor $\beta2^{EYFP}$ subunits were trafficked to the cell surface following co-expression with $GABA_A$ receptor subunits α1 and γ2 in COS-7 cells. This was expected since addition of ECFP in the intracellular loop of the nicotinic receptor α4 subunits that have a structure similar to that of $GABA_A$ receptor β2 subunits, did not affect either the assembly of α4 and β2 subunits or their trafficking to the cell surface (Nashmi *et al.*, 2003). However it is not known whether $\beta2^{EYFP}$ subunit-containing $GABA_A$ receptors are functional and can be activated by GABA. Because ECFP-GRIF-1 and $GABA_A$ receptor $\beta2^{EYFP}$ subunits were only partially co-localised when co-expressed in COS-7 cells, it seems unlikely that an interaction would be detected by acceptor photobleaching FRET imaging. Indeed in previous studies, a FRET signal was detected only when the fluorescent proteins co-distributed exactly following their expression in cells (Liu *et al.*, 2004; Nashmi *et al.*, 2003, section 4.2.1.1).

In summary, this chapter reports a methodology to carry out acceptor photobleaching FRET analyses between ECFP and EYFP tagged proteins. This can be applied to the study of any interactions provided the addition of ECFP or EYFP to the proteins of interest do not affect their functions. The finding that GRIF-1 interacts with the C-terminal cargo binding domain of KIF5C substantiates a role for GRIF-1 as a scaffold protein linking kinesin-1, KIF5C, to its cargo. A different method should be sought for the study of transient GRIF-1/$GABA_A$ receptors interactions

CHAPTER 5

MOLECULAR STUDIES OF THE INTERACTION BETWEEN GRIF-1 AND THE POST-TRANSLATIONAL MODIFICATION ENZYME, OGT

5.1. INTRODUCTION

5.1.1. Rationale

Initially, the function of GRIF-1 was not known and little information about GRIF-1 related proteins was available. Therefore, a yeast two-hybrid screen of a rat brain cDNA library was carried out to identify other GRIF-1 interacting proteins to gain further insights into the function of GRIF-1 (M. Beck and F.A. Stephenson, unpublished observations). Initially, GRIF-$1_{1\text{-}913}$ was used as a bait to screen a Matchmaker II rat brain cDNA library using the GAL4 yeast two-hybrid system. However, GRIF-$1_{1\text{-}913}$ was found to yield auto-activation of transcription factor activity. Therefore GRIF-$1_{1\text{-}913}$ deletion constructs were generated and each tested for the ability to activate reporter gene activity. GRIF-$1_{545\text{-}913}$ was the largest construct that did not yield reporter gene activation thus it was used as the bait for the rat brain cDNA library screen. Four different cDNAs encoding 4 putative GRIF-1 interacting proteins were identified (M. Beck and F.A. Stephenson, unpublished observations). The characterisation of one of them is reported here.

5.1.2. The yeast two-hybrid system

The yeast two-hybrid system is a genetic technique used to identify protein-protein interactions (Fields and Song, 1989). It is based on the principle that transcription factors are formed by 2 domains, a DNA binding domain (DNA-BD) and an activation domain (AD) that can be physically separated. The DNA-BD recognises specific DNA sequences upstream of the transcription start site, i.e. the upstream activation site. The AD cannot bind the DNA but it is necessary for transcription to occur. Thus, transcription activation requires both domains.

In the conventional yeast two-hybrid system, 2 proteins of interest are fused to either the DNA-BD or the AD of the GAL4 transcription factor. Interaction of the fusion proteins brings together GAL4 DNA-BD and GAL4 AD, thus resulting in activation of the reporter gene activity (Figure 5.1). The DNA-BD and AD fusion proteins are generated by sub-cloning the gene encoding the proteins of interest into the pGBKT7 and pGAD10 plasmid vectors respectively (Table 2.3). The pGBKT7 vector contains the gene encoding the GAL4 DNA-BD under the control of an ADH1 promoter and a tryptophan (W) nutritional selection marker (Appendix 5.1 A). The pGAD10 vector contains the gene encoding the GAL4 AD, under the control of an ADH1 promoter, and a leucine (L) nutritional selection marker (Appendix 5.1 B). Yeast cells that were co-

transformed with pGBKT7 and pGAD10 plasmids are selected on a media lacking both tryptophan and leucine, i.e. (-W, -L).

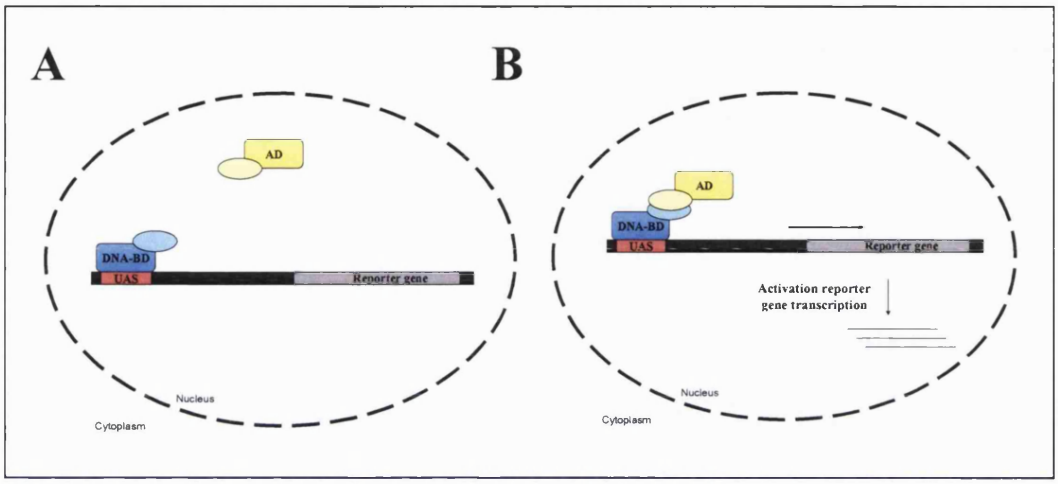

Figure 5.1. A schematic diagram depicting the principle of the GAL4 yeast two-hybrid system. Two putative interacting proteins were fused to the GAL4 DNA-BD or to the GAL4 AD and co-transformed into the yeast strain AH109. A, No interaction. The DNA-BD fusion protein binds to the upstream activation sequence but it cannot activate the reporter gene transcription. B, Interaction. The full transcription factor is reconstituted via interaction of the fusion proteins. It can now bind to the DNA and activate the reporter gene transcription.

The reporter genes used in this system are *HIS3*, *ADE2*, *MEL1* and *lacZ*. *HIS3* and *ADE2* encode enzymes involved in histidine (H) and adenine (A) biosynthesis respectively so that interactors can be detected on a media lacking both amino acids, i.e. (-H, -A). *MEL 1* and *lacZ* encode the α- and β-galactosidase enzymes, respectively. These enzyme activities are detected by performing colorimetric assays using the enzyme substrates, 5-bromo-4-chloro-3-indolyl-α-D-galactopyranoside or 5-bromo-4-chloro-3-indolyl-β-D-galactopyranoside (X-GAL). For example, β-galactosidase degrades X-GAL into dichloro-dibromo-indigo (indolyl blue) and galactose. Thus β-galactosidase activity can be detected by the formation of a blue colour.

The yeast strain, AH109, was used to perform interaction assays. It has been genetically modified so that it does not express either endogenous GAL4 nor endogenous GAL80, a GAL4 repressor (section 2.1.2). Additionally, this yeast strain has been engineered so that reporter gene expression is under the control of the GAL4 promoter.

5.1.3. Aims of the chapter

The aim of this chapter was to characterise the putative GRIF-1 interacting clone, C1, that was identified in the yeast two-hybrid screen using GRIF-$1_{545-913}$ as bait. C1 encodes a mitochondrial isoform of the post-translational modification enzyme, OGT (Chapter 1). Characterisation of GRIF-1/OGT interactions was carried out using a second OGT isoform also known to associate with GRIF-1.

5.2. RESULTS

5.2.1. Identification of mitochondrial OGT, $mOGT_{40-374}$, as a GRIF-1 interacting protein

The full nucleotide sequence of clone, C1, was obtained by nucleotide sequencing using specific oligonucleotide primers. Subsequently both the nucleotide and the deduced amino acid sequences were analysed using free online bioinformatic softwares to identify the protein encoded by clone C1. The C1/GRIF-1 interaction was substantiated in yeast two-hybrid interaction assays. Finally, C1 was sub-cloned into a mammalian expression vector and the specificity of interaction between GRIF-1 and C1 was verified by immunoprecipitation experiments.

5.2.1.1. Determination of the nucleotide sequence of the clone, C1

The clone, C1, was isolated from a commercial rat brain cDNA GAL4 yeast two-hybrid system library. This library was constructed by ligating rat brain cDNAs into the *EcoRI* restriction site of the pGAD10 cloning vector dowstream from the GAL4 promoter. Thus C1 consisted of a cDNA encoding a putative GRIF-1 interacting protein that was inserted into the *EcoRI* restriction site of pGAD10. Digestion of pGAD10-C1 by *EcoRI* showed that C1 contained a ~1000 bp insert. The nucleotide sequence of the insert was determined by nucleotide sequencing using the ABI PRISM 310 Genetic Analyser System as explained in Appendix 5.2.

A pGAD10 vector specific oligonucleotide primer that hybridised upstream of the multiple cloning site was used for initial sequencing of C1 clone inserted DNA (Figure 5.2 A). A new primer that hybridised within the sequence of the C1 clone was used to determine further sequence of the insert. New primers were designed and sequencing was carried out until the sequence of the full inserted cDNA, i.e. DNA sequence including the *EcoRI* cloning site and some pGAD10 downstream sequence, was obtained. Hence, 3 contigs were generated. The entire C1 cDNA sequence was determined by assembling the different contigs. It had an exact size of 1005 bp (Figure 5.2 B). A nucleotide BLAST search against GenBank™ rat databases showed that the inserted sequence had 97% nucleotide identity with the rat OGT cDNA sequence (Accession: NM017107).

The corresponding amino acid sequence was deduced by using Expasy tools (www.expasy.ch). No stop codon was found in +1 frame, thus showing that a single open reading frame (ORF) was present throughout the whole inserted cDNA sequence.

This ORF was in frame with the sequence of the pGAD10 vector (Figure 5.2 A). It encoded a 335 amino acid protein, with a predicted M_r = 37.4 kDa and isoelectric point pI = 5.9.

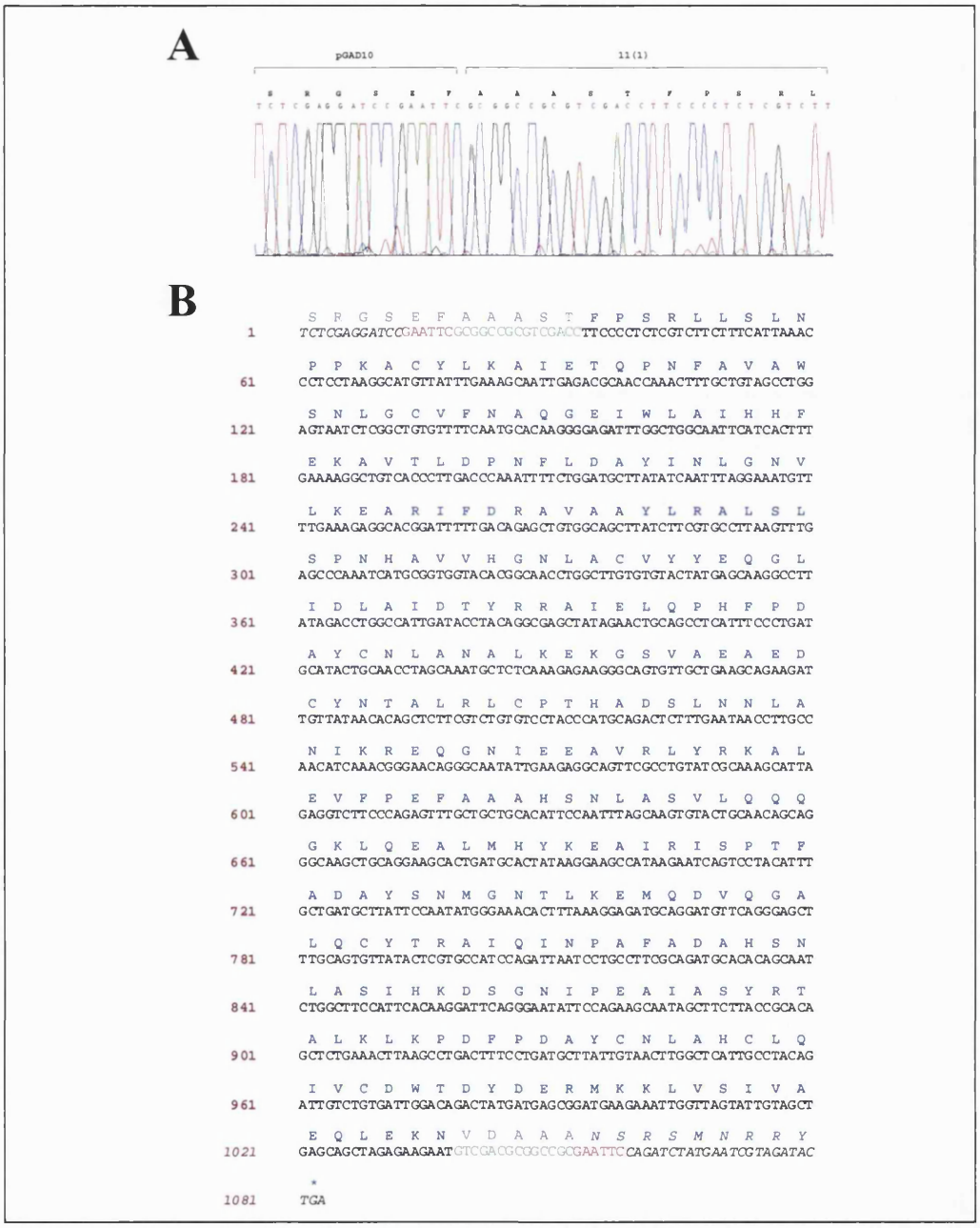

Figure 5.2. Nucleotide and deduced amino acid sequences of the C1 clone. A, oligonucleotide sequencing of C1 using an oligonucleotide primer hybridising on the vector pGAD10 upstream of the MCS shows that the inserted cDNA is in frame with the sequence of the pGAD10 vector. B, the entire nucleotide and deduced amino acid sequences of the clone C1 show that a single ORF is present throughout the inserted cDNA. GAATTC, *EcoRI* restriction site where the cDNA was inserted; GTCGAC, adaptor sequence used to generate the rat brain cDNA library; GAGCAG, nucleotide sequence of the inserted cDNA; EQLE, deduced amino acid sequence of the inserted cDNA; *VDAA*, pGAD10 deduced amino acid sequence flanking the inserted cDNA.

5.2.1.2. Bioinformatic analyses of the deduced amino acid sequence encoded by clone, C1

To characterise the 335 amino acid protein encoded by clone C1, BLAST searches against GenBank™ rat and human databases were performed. It was found that C1 had: - 97% amino acid similarity with the residues 163-490 of the rat nucleocytoplasmic (nc) isoform of OGT (Accession: NP058803), i.e. $ncOGT_{163-490}$; - 100% amino acid similarity with the residues 40-374 of the human mitochondrial (m) isoform of OGT (Accession: AAB63466), i.e. $mOGT_{40-374}$.

As described in Chapter 1, OGT is a post-translation modification enzyme, formed by 11.5 N-terminal tetratricopeptide repeats (TPRs) known to be involved in protein-protein interactions, and a C-terminal catalytic subunit. A single rat OGT isoform, i.e. the nucleocytoplasmic isoform, is reported in the GenBank™ rat databases. An additional mitochondrial OGT variant is reported in the GenBank™ human databases (Love *et al.*, 2003). The 2 isoforms differ in their N-terminal domains. In this region, a mitochondrial targeting sequence followed by a 26-amino acid hydrophobic domain is found in mOGT instead of TPRs 1-2.5 in ncOGT. Further mOGT and ncOGT differ in their subcellular localisation as suggested by their names (see Chapter 1). BLAST results were confirmed by performing a multiple alignment (ClustalW) of C1, rat ncOGT and human mOGT amino acid sequences (Figure 5.3). It can be seen that: - C1 has 100% similarity with human $mOGT_{40-374}$ as found in the BLAST analyses; - $C1_{1-11}$ has no identity with rat ncOGT; $C1_{1-11}$ is similar to the N-terminal hydrophobic domain of human mOGT; - $C1_{12-335}$ has 100% similarity with rat $ncOGT_{163-490}$. To summarise, the amino acid sequence of C1 is 100% similar to the hydrophobic sequence and to the TPRs of human mOGT, i.e. the domain 40-374 of mOGT (Figure 5.4). Therefore C1 was called $mOGT_{40-374}$.

5.2.1.3. Demonstration of the specificity of interaction between $mOGT_{40-374}$ and GRIF-1

To confirm the specificity of interaction between $mOGT_{40-374}$ and GRIF-1, it was necessary to use 2 different paradigms, i.e. yeast two-hybrid interaction assays and immunoprecipitations following expression of $mOGT_{40-374}$ and GRIF-1 in HEK 293 cells.

5.2.1.3.1. Yeast two-hybrid interaction assays

The yeast strain, *S. cerevisae* AH109, was co-transformed with different combinations of DNA-BD and GAL4 AD fusion constructs prepared in the vectors, pGBKT7 and

pGAD10, respectively (see section 5.1.2). Protein-protein interactions were detected by assessing the reporter gene activities by nutritional selection on (-L, -W, -H, -A) SD media and β-galactosidase activity assay as described in section 2.2.3.5.1. A positive control combination provided with the yeast two-hybrid interaction kit, pVA3-1/pTD1-1, was co-transformed to ensure that known protein-protein interactions could be detected. The plasmid, pVA3-1, encodes the murine oncogene, p53. The plasmid, pTD1-1, encodes the SV40 large T-antigen, a protein known to interact with p53. The negative control combinations, pGBKT7 + pGAD10-mOGT$_{40\text{-}374}$ and pGBKT7-GRIF-1$_{545\text{-}913}$ + pGAD10, were also used to check that mOGT$_{40\text{-}374}$ and GRIF-1$_{545\text{-}913}$ were not able to auto-activate the reporter genes in the absence of the binding partner.

```
OGT_rat     61 LDRSAHFSTLAIKQNPLLAEAYSNLGNVYKERGQLQEAIEHYRHALRLKPDFIDGYINLA
OGT_human    1 ------------------------------------------------------MLQG
C1_rat         ------------------------------------------------------------

OGT_rat    121 AALVAAGDMEGAVQAYVSALQYNPDLYCVRSDLGNLLKALGRLEEAKACYLKAIETQPNF
OGT_human    5 HFWLVREGIMISPSSPPPPNLFFFPLQIFPFPFTSFPSHLLSLTPPKACYLKAIETQPNF
C1_rat       1 ----------------------------------FPSRLLSLNPPKACYLKAIETQPNF
                                                  ::. *  *  .***************

OGT_rat    181 AVAWSNLGCVFNAQGEIWLAIHHFEKAVTLDPNFLDAYINLGNVLKEARIFDRAVAAYLR
OGT_human   65 AVAWSNLGCVFNAQGEIWLAIHHFEKAVTLDPNFLDAYINLGNVLKEARIFDRAVAAYLR
C1_rat      26 AVAWSNLGCVFNAQGEIWLAIHHFEKAVTLDPNFLDAYINLGNVLKEARIFDRAVAAYLR
               ************************************************************

OGT_rat    241 ALSLSPNHAVVHGNLACVYYEQGLIDLAIDTYRRAIELQPHFPDAYCNLANALKEKGSVA
OGT_human  125 ALSLSPNHAVVHGNLACVYYEQGLIDLAIDTYRRAIELQPHFPDAYCNLANALKEKGSVA
C1_rat      86 ALSLSPNHAVVHGNLACVYYEQGLIDLAIDTYRRAIELQPHFPDAYCNLANALKEKGSVA
               ************************************************************

OGT_rat    301 EAEDCYNTALRLCPTHADSLNNLANIKREQGNIEEAVRLYRKALEVFPEFAAAHSNLASV
OGT_human  185 EAEDCYNTALRLCPTHADSLNNLANIKREQGNIEEAVRLYRKALEVFPEFAAAHSNLASV
C1_rat     146 EAEDCYNTALRLCPTHADSLNNLANIKREQGNIEEAVRLYRKALEVFPEFAAAHSNLASV
               ************************************************************

OGT_rat    361 LQQQGKLQEALMHYKEAIRISPTFADAYSNMGNTLKEMQDVQGALQCYTRAIQINPAFAD
OGT_human  245 LQQQGKLQEALMHYKEAIRISPTFADAYSNMGNTLKEMQDVQGALQCYTRAIQINPAFAD
C1_rat     206 LQQQGKLQEALMHYKEAIRISPTFADAYSNMGNTLKEMQDVQGALQCYTRAIQINPAFAD
               ************************************************************

OGT_rat    421 AHSNLASIHKDSGNIPEAIASYRTALKLKPDFPDAYCNLAHCLQIVCDWTDYDERMKKLV
OGT_human  305 AHSNLASIHKDSGNIPEAIASYRTALKLKPDFPDAYCNLAHCLQIVCDWTDYDERMKKLV
C1_rat     266 AHSNLASIHKDSGNIPEAIASYRTALKLKPDFPDAYCNLAHCLQIVCDWTDYDERMKKLV
               ************************************************************

OGT_rat    481 SIVAEQLEKNRLPSVHPHHSMLYPLSHGFRKAIAERHGNLCLDKINVLHKPPYEHPKDLK
OGT_human  365 SIVADQLEKNRLPSVHPHHSMLYPLSHGFRKAIAERHGNLCLDKINVLHKPPYEHPKDLK
C1_rat     326 SIVAEQLEKN----------------------------------------------------
               ****:*****
```

Figure 5.3. Multiple alignment of C1, rat ncOGT and human mOGT. The deduced amino acid sequence of the C1 inserted cDNA was aligned with the amino acid sequences of the rat ncOGT (NP058803) and human mOGT (AAB63466) using ClustalW. The N-terminal amino acid sequences of rat ncOGT and human mOGT are represented here. This alignment shows that the C1 amino acid sequence is 100% similar to the human mOGT amino acid sequence, mOGT$_{40\text{-}374}$. C1 differs from the rat ncOGT by its first 11 amino acids. C1, like mOGT, contains tetratricopeptide repeats (TPRs) 2.5-11.5. The amino acid sequence encoding the TPRs is identical in C1, human mOGT and rat ncOGT. **MLQG**, mitochondria targeting sequence; **PPNL**, hydrophobic domain; , TPRs; *, sequence similarity between the 3 aligned amino acid sequences; ":" and ".", sequence identity between the 3 aligned amino acid sequences

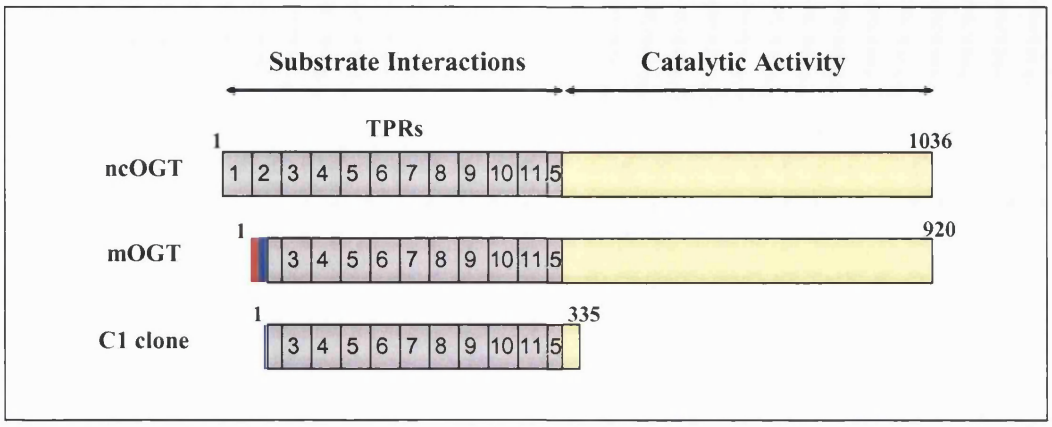

Figure 5.4. A schematic representation of the multiple alignment of C1, rat ncOGT and human mOGT. The Figure shows that ncOGT and mOGT are composed of a N-terminal domain for substrate interactions and a catalytic C-terminal domain. mOGT and ncOGT differ in their N-terminal regions. ncOGT contains 11.5 TPRs (TPRs 1-11.5) whereas mOGT has only 9 TPRs (TPRs 2.5-11.5). Instead of TPRs 1-2.5, mOGT contains a mitochondrial targeting sequence followed by a hydrophobic domain. The C1 clone is similar to a part of the mOGT hydrophobic sequence and to the following 9 TPRs, i.e. $mOGT_{40-374}$. ▯, TPR; ▮ mitochondrial targeting sequence; ▮, hydrophobic sequence.

Thus, the AH109 yeast strain was co-transformed with the test combination, pGBKT7-GRIF-$1_{545-913}$ + pGAD10-$mOGT_{40-374}$, the positive control, pVA3-1 + pTD1-1, the negative control, pGBKT7 + pGAD10, the negative control for $mOGT_{40-374}$ auto-activation, pGBKT7 + pGAD10-$mOGT_{40-374}$, the negative control for GRIF-$1_{545-913}$ auto-activation, pGBKT7-GRIF-$1_{545-913}$ + pGAD10. The results are summarised in Table 5.1. All transformants were grown on (-L, -W) SD media thereby indicating that the yeast cells were successfully co-transformed with all plasmids. Positive control plasmids grew on (-L, -W, -H, -A) SD media and β-galactosidase activity was detected, thus showing that a known interaction could be detected. Each negative control showed no growth on (-L, -W, -H, -A) SD media and no β-galactosidase activity, thereby proving that $mOGT_{40-374}$ and GRIF-$1_{545-913}$ fusion constructs were not able to cause autonomous activation. The positive and negative controls behaved as expected thus showing the authenticity of the system used. For the test combination, i.e. pGBKT7-GRIF-$1_{545-913}$ + pGAD10-$mOGT_{40-374}$, growth was observed on (-L, -W, -H, -A) SD media and β-galactosidase activity was detected. This proved that $mOGT_{40-374}$ was associated with GRIF-$1_{545-913}$ in the yeast two-hybrid interaction assay.

5.2.1.3.2. Immunoprecipitation

Generation of a His-tagged $mOGT_{40-374}$ construct- The cDNA encoding $mOGT_{40-374}$ was sub-cloned in frame into the *EcoRI* restriction sites of the vector pcDNA4HisMax to yield an N-terminal His-tagged $mOGT_{40-374}$ fusion protein, i.e. His-$mOGT_{40-374}$, with

a predicted M_r = 48 kDa (Appendix 5.3). The authenticity of the construct was verified by nucleotide sequencing.

Expression of the His-tagged mOGT$_{40-374}$ construct- To check that His-mOGT$_{40-374}$ was expressed, HEK 293 cells were transfected with pcDNA4HisMax-mOGT$_{40-374}$, cell homogenates were prepared 24 h post-transfection and analysed by immunoblotting using anti-HisG antibodies. The result is shown in Figure 5.5. A band with M_r = 48 kDa was detected in the homogenate of cells transfected with pcDNA4HisMax-mOGT$_{40-374}$ but not in the homogenate of untransfected cells. This band had a M_r corresponding to that expected for His-mOGT$_{40-374}$. Immunoreactive bands with higher M_r, i.e. M_r = 70 kDa, M_r = 95 kDa and M_r = 130 kDa, were also detected in homogenates of both untransfected and transfected HEK 293 cells, thus indicating that these higher M_r bands were non-specific bands. These results showed that His-mOGT$_{40-374}$ was expressed in transfected HEK 293 cells and that it was detected successfully by anti-HisG antibodies.

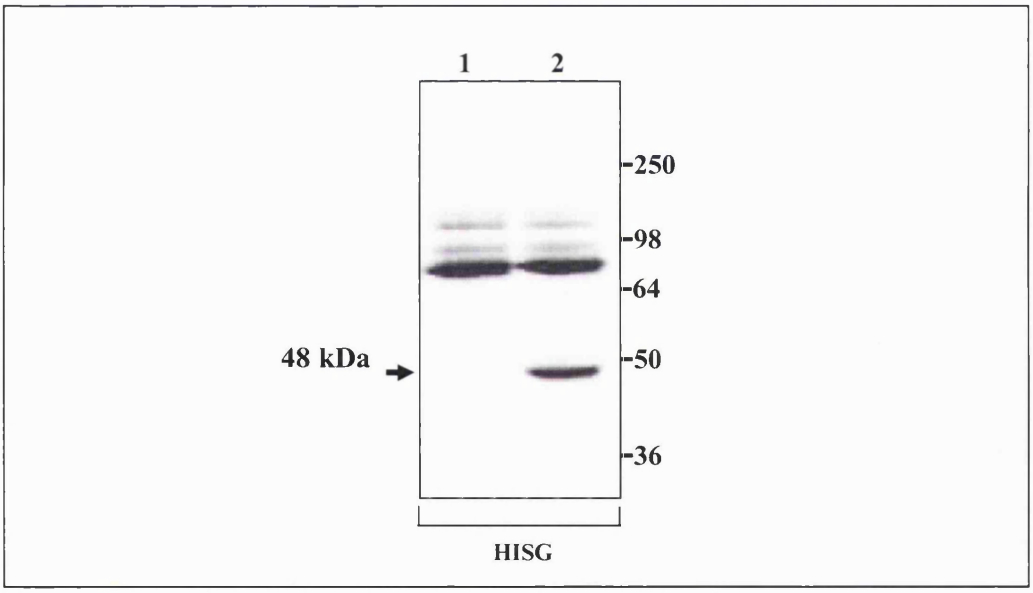

Figure 5.5. Molecular size of His-mOGT$_{40-374}$. HEK 293 cells were transfected with pcDNAHisMax-mOGT$_{40-374}$, cell homogenates were prepared 24 h post-transfection and analysed by immunoblotting using anti-HISG antibodies. Lane 1, homogenate of untransfected cells; lane 2, homogenate of cells transfected with pcDNAHisMax-mOGT$_{40-374}$. The molecular weight standards (kDa) are shown on the right. The immunoreactive band of interest is indicated by an arrow, M_r (His-mOGT$_{40-374}$) = 48 kDa. This immunoblot is representative of n = 3 experiments from n = 3 independent transfections.

Immunoprecipitation- To investigate whether mOGT$_{40-374}$ was associated with GRIF-1, HEK 293 cells were co-transfected with pCIS-GRIF-1 + pcDNA4HisMax-mOGT$_{40-374}$, detergent extracts prepared 48 h post-transfection and immunoprecipitations were carried out using anti-HisG monoclonal antibodies. Anti-dynein monoclonal antibodies were used as a negative control. The immune pellets were analysed by immunoblotting

AD vector	DNA-BD vector	Growth on (-L, -W) dropout media	Growth on (-L, -W, -H, -A) dropout media	β-Galactosidase activity
pGBKT7-GRIF-$1_{545-913}$	pGAD10-$mOGT_{40-374}$	+++	++	**
pGBKT7-	pGAD10-$mOGT_{40-374}$	+++	-	-
pGBKT7-GRIF-$1_{545-913}$	pGAD10-	+++	-	-
pGBKT7-	pGAD10-	++	-	-
pVA3-1	pTD1-1	++	++	***

Table 5.1. Demonstration by yeast two-hybrid interaction assays that $mOGT_{40-374}$ interacts with GRIF-$1_{545-913}$. The yeast strain, *S. cerevisae* AH109, was co-transformed with test and control combinations of DNA-BD and GAL4 AD fusion constructs prepared in the vectors pGBKT7 and pGAD10 respectively. Test combination: pGBKT7-GRIF-$1_{545-913}$ + pGAD10-$mOGT_{40-374}$, negative controls: pGBKT7 + pGAD10-$mOGT_{40-374}$, pGBKT7-GRIF-$1_{545-913}$ + pGAD10, pGBKT7 + pGAD10, positive control, pVA3-1 + pTD1-1. The transformants were grown on (-L, -W) SD media. Protein-protein interactions were detected by assessing the reporter gene activities by nutritional selection on (-L, -W, -H, -A) SD media and β-galactosidase activity assay. For colony growth, - = no growth, + = 1-10 colonies, ++ = 10-200 colonies, +++ = 201-500 colonies; for β-galactosidase filter lift assays where * = enzymatic activity and - = no activity. The results are representative of at least n = 3 independent co-transformations.

with anti-HisG and anti-GRIF-1_{8-633} antibodies. The results are shown in Figure 4.9. Analysis of the immune pellet using anti-HisG antibodies revealed 4 major immunoreactive bands with M_r = 30 kDa, M_r = 36 kDa, M_r = 62 kDa and M_r = 96 kDa (Figure 5.6 A). The bands with M_r = 36 kDa, M_r = 62 kDa were also found in the control pellet and thus they are non-specific bands. The band with M_r = 96 kDa was a non-specific band as seen in the previous experiment (Figure 5.6 A).

The band with M_r = 30 kDa was not seen in the non-immune pellet thus showing that it was recognised specifically by anti-HisG antibodies. This suggested that this M_r = 30 kDa band corresponded to His-mOGT$_{40-374}$ although its size was smaller than that expected, i.e. M_r = 48 kDa. This suggested that His-mOGT$_{40-374}$ was subject to proteolysis during the experiment but that the 30 kDa-proteolytic fragment was successfully immunoprecipitated by anti-HisG antibodies.

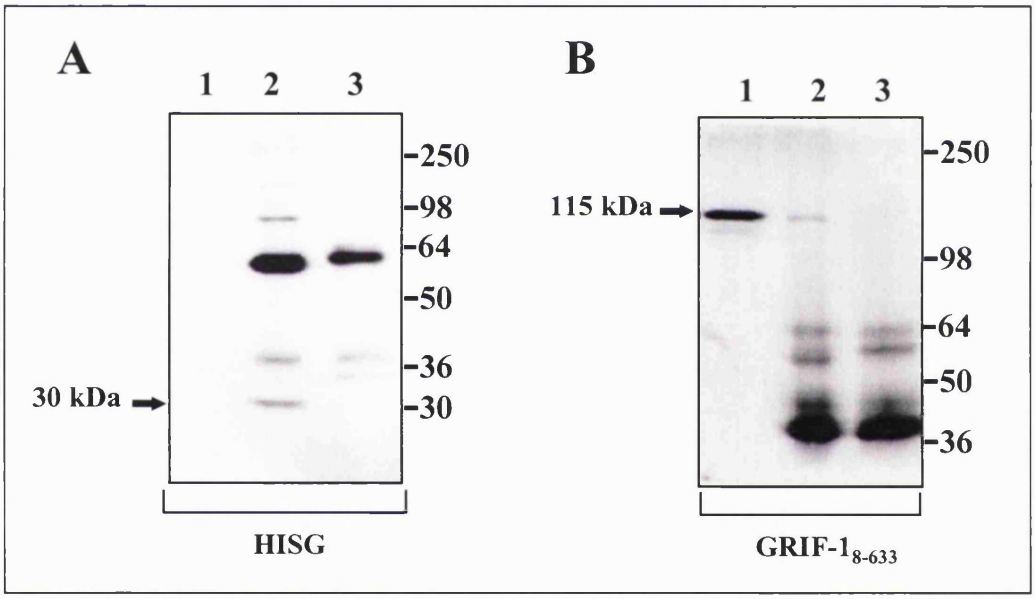

Figure 5.6. Demonstration by immunoprecipitation that His-mOGT$_{40-374}$ interacts with GRIF-1. Detergent soluble extracts of HEK 293 cells co-transfected with pCIS-GRIF-1 + pcDNAHisMax-mOGT$_{40-374}$ were prepared 24 h after transfection. Immunoprecipitations were carried out using either anti-HISG antibodies or anti-bd17 antibodies as a control. Immune pellets were analysed by immunoblotting using antibodies as indicated on the abcissae. The gel layout is the same in A and B with lane 1, detergent soluble extract; lanes 2, immune pellet; lanes 3, non-immune pellet. The molecular weight standards (kDa) are shown on the right. Immunoreactive bands of interest are indicated by an arrow, M_r (His-mOGT$_{40-374}$) = 30 kDa, M_r (GRIF-1) = 115 kDa. These immunoblots are representative of n = 2 immunoprecipitations from n = 2 transfections.

Analysis of the immune pellet using anti-GRIF-1_{8-633} antibodies revealed an immunoreactive band with M_r = 115 kDa consistent with that expected for GRIF-1 (Figure 5.6 B). Four immunoreactive bands with lower M_r were also detected in both the immune and non-immune pellets and thus were non-specific bands. These results showed that GRIF-1 was specifically immunoprecipitated by His-mOGT_{40-374}. Further, they indicate that GRIF-1 was associated with the 30 kDa His-mOGT_{40-374} proteolytic fragment.

All together, yeast two-hybrid and immunoprecipitation studies demonstrated that mOGT_{40-374} was associated specifically with the C-terminal domain of GRIF-1, i.e. GRIF-$1_{545-913}$.

5.2.2. Further characterisation of GRIF-1/OGT interactions

A rat mitochondrial OGT isoform was identified from a rat brain cDNA library and it was shown to be a new GRIF-1 interacting protein. Another study carried out in parallel with the work described here and discussed earlier in Chapter 1 identified GRIF-1 as a protein associated with rat ncOGT in a yeast two-hybrid screen using ncOGT as a bait (section 1.3.3.2; Iyer *et al.*, 2003a). Further characterisation of GRIF-1/OGT interactions was carried out using the rat ncOGT clone. As described in Table 2.2, the full length ncOGT construct, pShuttle-OGT, was a gift from the Hart laboratory. It was the ncOGT cDNA originally cloned (Kreppel *et al.*, 1997). FLAG-tagged OGT and EYFP-tagged OGT fusion constructs were generated and characterised according to their molecular size and their ability to interact with GRIF-1. The distribution of EYFP-OGT was analysed by confocal microscopy imaging in the presence or in the absence of GRIF-1.

5.2.2.1. Generation and characterisation of a FLAG-tagged nucleocytoplasmic OGT construct

A FLAG-tagged ncOGT construct was generated to carry out immunoprecipitation analysis between GRIF-1 and OGT in transfected HEK 293 cells.

Preparation of a FLAG-tagged ncOGT construct- The construct encoding full length rat ncOGT, pShuttle-OGT, was used as a template to amplify ncOGT cDNA by PCR. The PCR product, ncOGT, was sub-cloned in frame into the *BamHI/EcoRV* restriction sites of the mammalian expression vector pCMVTag4a to yield pCMVTag4a-OGT, a construct encoding a C-terminal FLAG-tagged ncOGT, i.e. FLAG-OGT (Appendix 5.4). The sequence of the construct was verified by nucleotide sequencing.

Expression of the C-terminal FLAG-tagged ncOGT construct in HEK 293 cells- To check that FLAG-OGT was expressed, HEK 293 cells were transfected with pCMVTag4a-OGT, cell homogenates were prepared 24 h after transfection and analysed by immunoblotting using rabbit anti-FLAG polyclonal antibodies. The result is shown in Figure 5.7. When probing the homogenate of transfected cells with anti-FLAG antibodies, a specific band with M_r = 111 kDa was detected. This band had a size corresponding to that expected for FLAG-OGT. Non-specific bands with M_r = 50 kDa, M_r = 72 kDa, M_r = 85 kDa, and M_r = 121 kDa, also found in homogenates of untransfected cells, were also detected. This showed that FLAG-OGT was expressed.

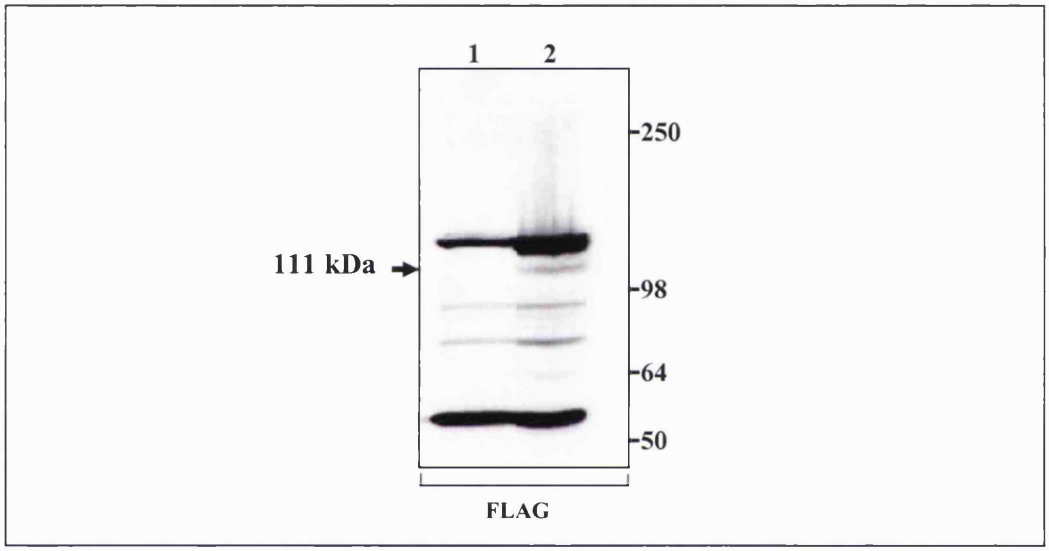

Figure 5.7. Molecular size of FLAG-OGT. Homogenates of HEK 293 cells transfected with pCMVTag4a-OGT were analysed by immunoblotting using anti-FLAG antibodies. Lane 1, homogenate of untransfected cells; lane 2, homogenate of cells transfected with pCMVTag4a-OGT. The molecular weight standards (kDa) are shown on the right. The immunoreactive band of interest is indicated by an arrow, M_r (FLAG-OGT) = 111 kDa. This immunoblot is representative of n = 3 experiments from n = 3 independent transfections.

Protein-protein interaction properties of the C-terminal FLAG-tagged ncOGT construct- Because FLAG-OGT will be used with GRIF-1 or ECFP-GRIF-1 in further studies, it was necessary to show that FLAG-OGT could associate with GRIF-1 and with ECFP-GRIF-1. Therefore HEK 293 cells were transfected, detergent soluble extracts were prepared 24-36 h post-transfection and immunoprecipitation experiments were carried out using rabbit anti-FLAG antibodies or rabbit non-immune IgGs as a control. Immune pellets were analysed by immunoblotting with anti-GRIF-$1_{8\text{-}633}$ and anti-FLAG antibodies. HEK 293 cells were co-transfected with either pCMVTag4a-

OGT + pCIS-GRIF-1 or pCMVTag4a-OGT + pECFP-GRIF-1. The results are shown in Figure 5.8.

FLAG-OGT + GRIF-1- In the immune pellet of cells co-transfected with pCMVTag4a-OGT + pCIS-GRIF-1, a band with M_r = 111 kDa was detected by anti-FLAG antibodies in the immune pellet but not in the non-immune pellet of transfected cells. This band had a size corresponding to that predicted for FLAG-OGT (Figure 5.8 A, lanes 4-6). This showed that FLAG-OGT was successfully immunoprecipitated by the anti-FLAG antibodies. A band with M_r = 115 kDa was recognised by anti-GRIF-1_{8-633} antibodies. This band had a size consistent with that predicted for GRIF-1. It was not detected in the non-immune pellet thus showing that GRIF-1 was immunoprecipitated with FLAG-OGT (Figure 5.8 A, lanes 1-3).

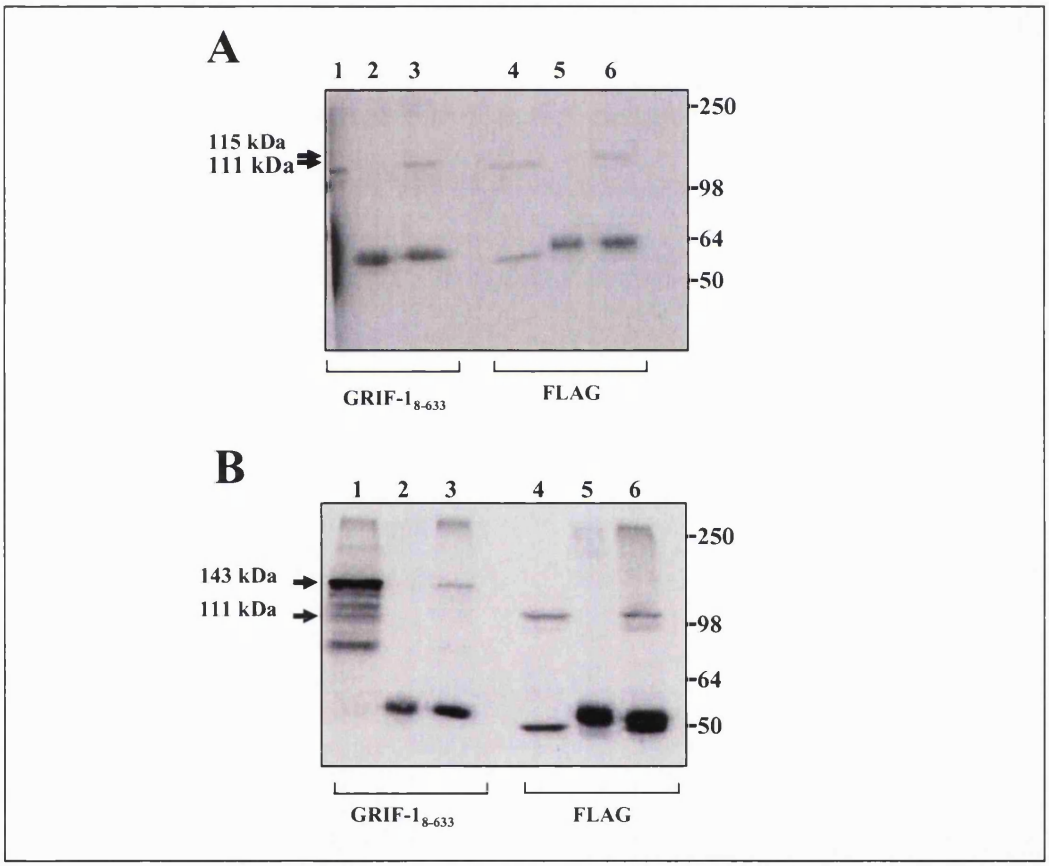

Figure 5.8. Demonstration by immunoprecipitation that FLAG-OGT interacts with GRIF-1 and ECFP-GRIF-1. Detergent soluble extracts of HEK 293 cells co-transfected with either A, pCMVTag4a-OGT + pCIS-GRIF-1 or B, pCMVTag4a-OGT + pECFP-GRIF-1 were prepared 24 h post-transfection. Immunoprecipitations were carried out using either rabbit anti-FLAG antibodies or rabbit non-immune IgGs as a control. Immune pellets were analysed by immunoblotting using antibodies as indicated on the abcissae. The gel layout is identical in A and B, where: lanes 1, 4, detergent soluble extract; lanes 2, 5, non-immune pellet; lanes 3, 6, immune pellet. The molecular weight standards (kDa) are shown on the right. Immunoreactive bands of interest are indicated by an arrow, M_r (FLAG-OGT) = 111 kDa, M_r (GRIF-1) = 115 kDa, M_r (ECFP-GRIF-1) = 143 kDa. These immunoblots are representative of n = 3 immunoprecipitations from n = 3 transfections.

FLAG-OGT + ECFP-GRIF-1- In the immune pellet of cells co-transfected with pCMVTag4a-OGT + pECFP-GRIF-1, a band with M_r = 111 kDa was detected by anti-FLAG antibodies in the immune pellet but not in the non-immune pellet of transfected cells. As for before, this band had a size corresponding to that predicted for FLAG-OGT. This showed that FLAG-OGT was successfully immunoprecipitated by the anti-FLAG antibodies (Figure 5.8 B, lanes 4-6). A band with M_r = 143 kDa was recognised by anti-GRIF-1_{8-633} antibodies. This band was not detected in the non-immune pellet and it had the size expected for ECFP-GRIF-1 thus showing that ECFP-GRIF-1 was immunoprecipitated with FLAG-OGT (Figure 5.8 B, lanes 1-3).

These experiments showed that FLAG-OGT could associate with either GRIF-1 or ECFP-GRIF-1.

5.2.2.2. Generation and characterisation of an EYFP-tagged nucleocytoplasmic OGT construct

Since a protocol to carry out FRET measurements was developed (Chapter 4), it would be interesting to use FRET to study GRIF-1/OGT interactions in mammalian cells. In the FRET studies described in Chapter 3, ECFP-GRIF-1 was successfully used as a donor. Therefore an EYFP-tagged OGT that could be used as a FRET acceptor was generated and characterised.

Preparation of an EYFP-tagged ncOGT construct- OGT was amplified by PCR from the plasmid, pShuttle-OGT, and sub-cloned in frame into the *BamHI/EcoRI* restriction sites of pEYFP-C1 yielding an N-terminal EYFP-tagged ncOGT, pEYFP-OGT (Appendix 5.5). The construct was verified by nucleotide sequencing.

Expression of EYFP-OGT in HEK 293 cells- To check that EYFP-OGT was expressed, HEK 293 cells were transfected with pEYFP-OGT, cell homogenates were prepared 24 h after transfection and analysed by immunoblotting using anti-GFP antibodies. The result is shown in Figure 5.9. A single band with M_r = 140 kDa was detected in the homogenate of transfected cells. This band corresponded to that expected for EYFP-OGT. It was not seen in homogenates of untransfected cells. This showed that EYFP-OGT was expressed in HEK 293 cells.

Protein-protein interaction properties of EYFP-OGT- To determine whether EYFP-OGT behaved as the wild-type non-fluorescent OGT according to its GRIF-1 interaction properties, immunoprecipitations were carried out. A construct encoding an N-terminal FLAG-tagged GRIF-1, i.e. pCMVTag4a-GRIF-1, was used instead of pCIS-

GRIF-1. Thus, HEK 293 cells were transfected, detergent soluble extracts prepared 24-36 h post-transfection and immunoprecipitations were performed using either rabbit anti-FLAG antibodies and rabbit non-immune IgGs as a control, or sheep anti-GRIF-$1_{879-884}$ antibodies and sheep non-immune IgGs as a control. Immune pellets were analysed by immunoblotting using anti-GFP and anti-GRIF-1_{8-633} antibodies. HEK 293 cells were transfected with either pEYFP-OGT + pCMVTag4a-GRIF-1 or pEYFP-OGT + pECFP-GRIF-1. The results are shown in Figure 5.10.

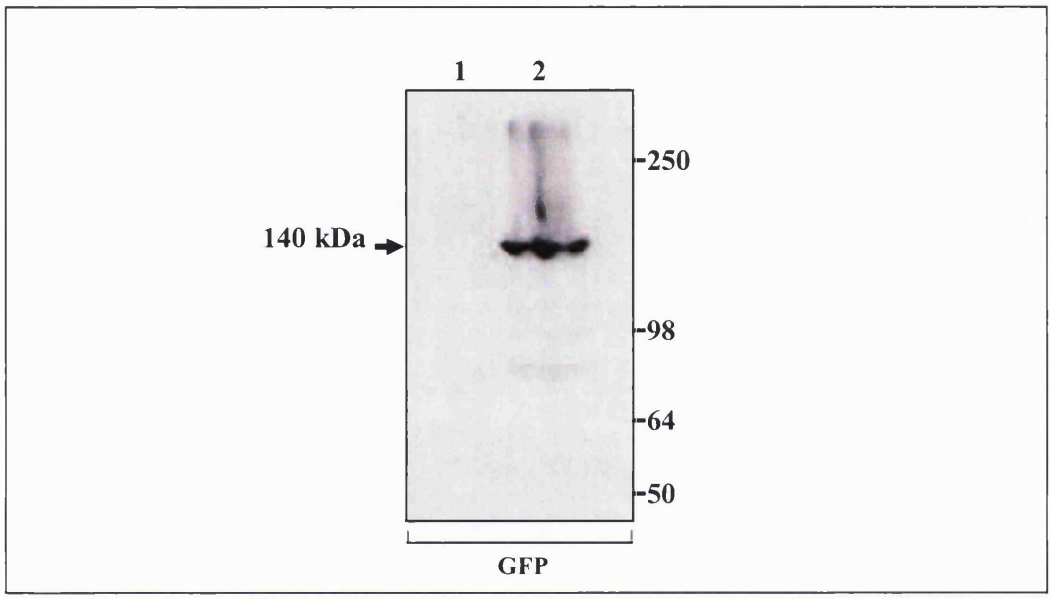

Figure 5.9. Molecular size of EYFP-OGT. Cell homogenates of HEK 293 cells transfected with pEYFP-OGT were analysed by immunoblotting using anti-GFP antibodies. Lane 1, homogenate of untransfected cells; lane 2, homogenate of cells transfected with pEYFP-OGT. The molecular weight standards (kDa) are shown on the right. The immunoreactive band of interest is indicated by an arrow, M_r (EYFP-OGT) = 140 kDa This immunoblot is representative of n = 1 experiment from n = 1 transfection.

EYFP-OGT + FLAG-GRIF-1- Immunoprecipitations were carried out using rabbit anti-FLAG antibodies or rabbit non-immune IgGs as a control (Figure 5.10 A). The immune pellet was probed with anti-GRIF-1_{8-633} antibodies and a band with M_r = 115 kDa was detected. This band corresponded to that expected for FLAG-GRIF-1 and it was not seen in the control pellet, thereby showing that FLAG-GRIF-1 was successfully immunoprecipitated by anti-FLAG antibodies (Figure 5.10 A, lanes 1-3). When the immune pellets were probed with anti-GFP antibodies, a band with M_r = 140 kDa was detected. This band had the size expected for EYFP-OGT. It was not found in the non-immune pellet. This showed that EYFP-OGT was associated with FLAG-GRIF-1 (Figure 5.10, lanes 4-6). A non-specific band with M_r = 50 kDa also visible in the non-immune pellet was also detected.

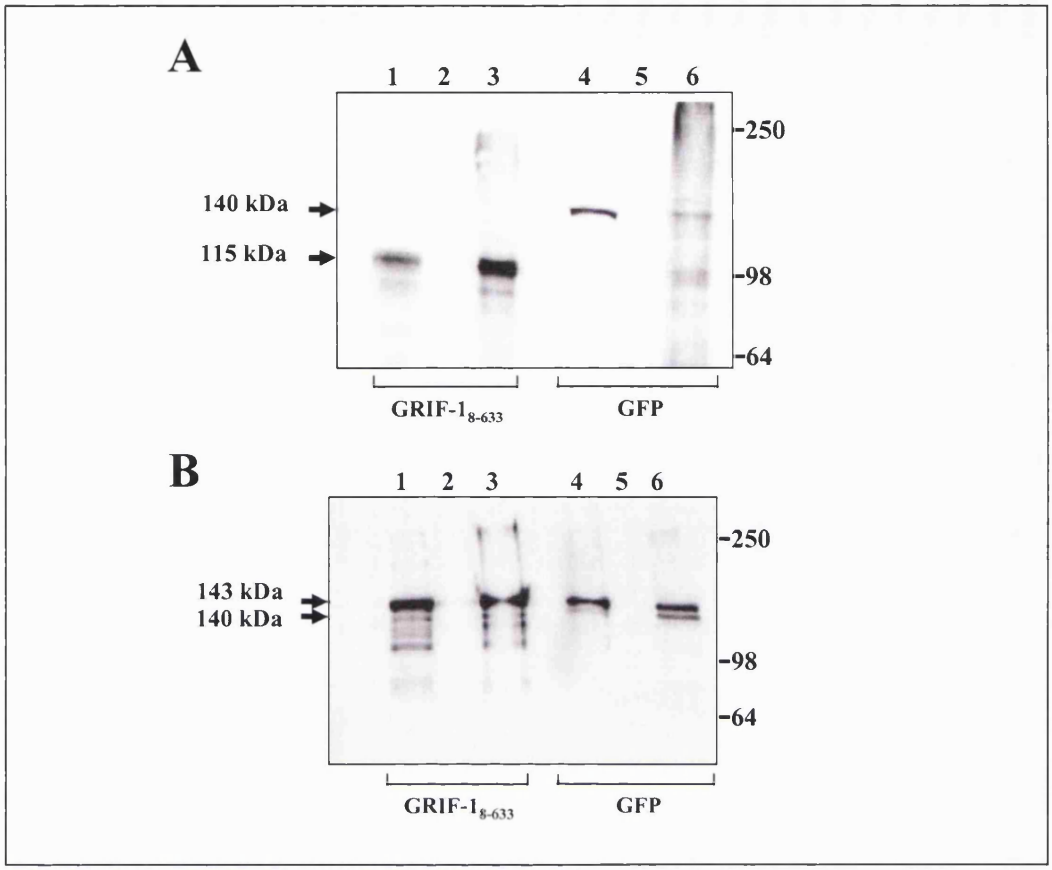

Figure 5.10. Demonstration by immunoprecipitation that EYFP-OGT interacts with FLAG-GRIF-1 and ECFP-GRIF-1. Detergent soluble extracts of HEK 293 cells co-transfected with either A, pEYFP-OGT + pCMVTag4a-GRIF-1 or B, pEYFP-OGT + pECFP-GRIF-1 were prepared 24 h post-transfection. Immunoprecipitations were carried out using A, either rabbit anti-FLAG antibodies or rabbit non-immune IgGs as a control and B, anti-GRIF-$1_{879-884}$ antibodies or non-immune sheep IgGs as a control. Immune pellets were analysed by immunoblotting using antibodies as indicated on the abcissae. The gel layout is identical in A and B, where: lanes 1, 4, detergent soluble extract; lanes 2, 5, non-immune pellet; lanes 3, 6, immune pellet. The molecular weight standards (kDa) are shown on the right. Immunoreactive bands of interest are indicated by an arrow, M_r (FLAG-GRIF-1) = 117 kDa, M_r (EYFP-OGT) = 140 kDa, M_r (ECFP-GRIF-1) = 143 kDa, M_r (EYFP-OGT) = 140 kDa. These immunoblots are representative of n = 3 immunoprecipitations from n = 3 transfections.

EYFP-OGT + ECFP-GRIF-1- Immunoprecipitations were carried out using sheep anti-GRIF-$1_{879-884}$ antibodies or sheep non-immune IgGs as a control (Figure 5.10 B). The immune pellets were analysed with anti-GRIF-1_{8-633} antibodies. A band with M_r = 143 kDa was detected. This band corresponded to that expected for ECFP-GRIF-1 and it was not seen in the control pellet, thereby showing that ECFP-GRIF-1 was successfully immunoprecipitated by anti-GRIF-$1_{879-884}$ antibodies (Figure 5.10 B, lane 1-3). When the immune pellet was probed with anti-GFP antibodies, 2 immunoreactive bands with M_r = 143 kDa and with M_r = 140 kDa were detected. Since both EYFP-OGT

and ECFP-GRIF-1 are recognised by anti-GFP and since they have similar M_r, these 2 immunoreactive bands may correspond to ECFP-GRIF-1 and EYFP-OGT respectively. These bands were not found in the non-immune pellet. This suggests that EYFP-OGT was associated with ECFP-GRIF-1 (Figure 5.10, lanes 4-6). Nevertheless, this result should be confirmed by using anti-OGT antibodies to probe the immune pellet.

5.2.2.3. Further characterisation of GRIF-1/OGT interactions by confocal microscopy imaging

To characterise further GRIF-1/OGT interactions, EYFP-OGT was expressed in HEK 293 and COS-7 cells in the presence or in the absence of ECFP-GRIF-1 and its subcellular localisation was analysed by confocal microscopy imaging. HEK 293 and COS-7 cells were transfected, fixed 24-36 h post-transfection and imaged. Cells were transfected with either pEYFP-OGT or pEYFP-OGT + pECFP-GRIF-1. The results are shown in Figures 5.11-5.12.

EYFP-OGT- In HEK 293 and COS-7 cells transfected with pEYFP-OGT, the fluorescence was localised in the cell cytoplasm with some enrichment around the nucleus (Figure 5.11). In most of the cells observed but not all, the fluorescence was also enriched at the cell periphery (Figure 5.11 B, C). Some cells appeared vacuolated (Figure 5.11 B, C). No fluorescence was detected in the cell nucleus.

EYFP-OGT + ECFP-GRIF-1- In HEK 293 and COS-7 cells co-transfected with pEYFP-OGT + pECFP-GRIF-1, EYFP-OGT fluorescence was exactly as in single construct transfections (Figure 5.12 A, D, G, J). ECFP-GRIF-1 fluorescence was cytoplasmic and enriched in the perinuclear region of the cell as seen in pECFP-GRIF-1 single construct transfections (Chapter 3). Besides, in most of the cells observed (~ 65%) ECFP-GRIF-1 fluorescence was also enriched at the cell periphery (Figure 5.12 C, F, I, L). ECFP-GRIF-1 fluorescence was co-localised with EYFP-OGT fluorescence in the area around the nucleus and at the cell periphery This is consistent with an association between GRIF-1 and OGT.

Unfortunately, time limitations restrained the use of EYFP-OGT and ECFP-GRIF-1 constructs for FRET studies.

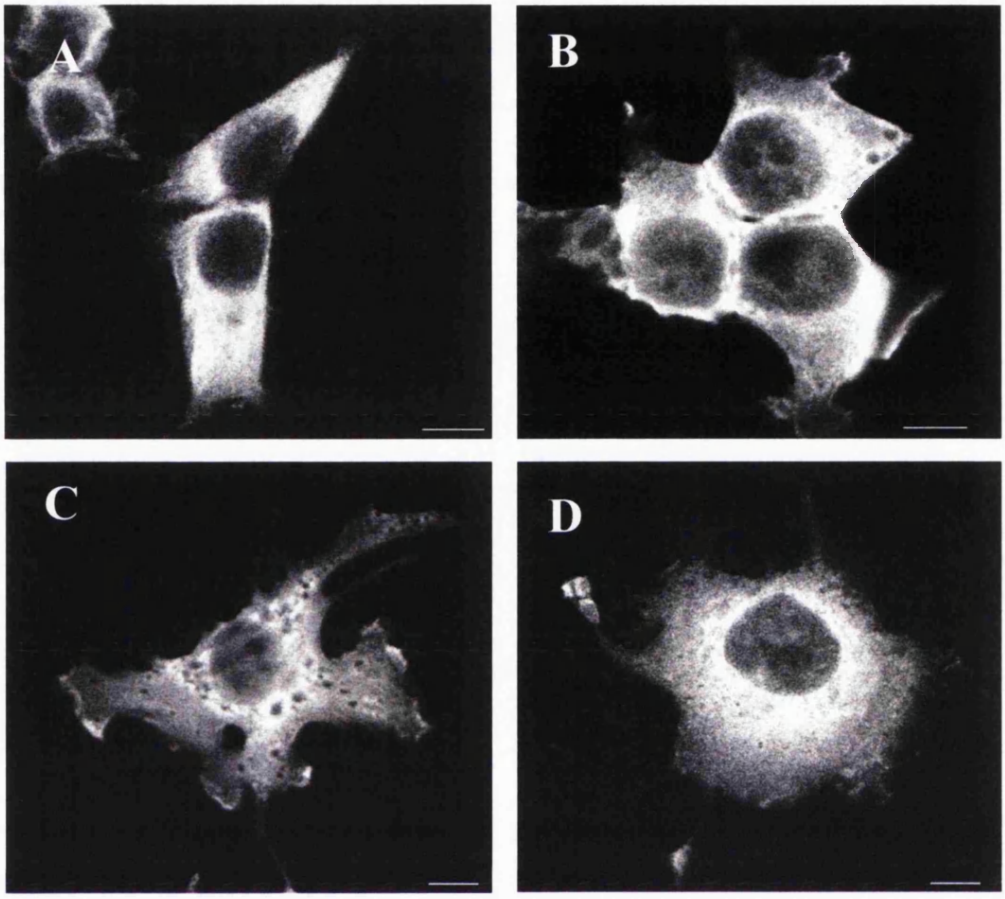

Figure 5.11. Expression of EYFP-OGT in transfected HEK 293 and COS-7 cells. Confocal sections of HEK 293 and COS-7 cells transfected with pEYFP-OGT. Cells were fixed 24-48 h post-transfection and imaged. A, B, HEK 293 cells; C, D, COS-7 cells. The images are representative of n = 27 cells observed from n = 3 independent transfections. Scale bars, 10 μm.

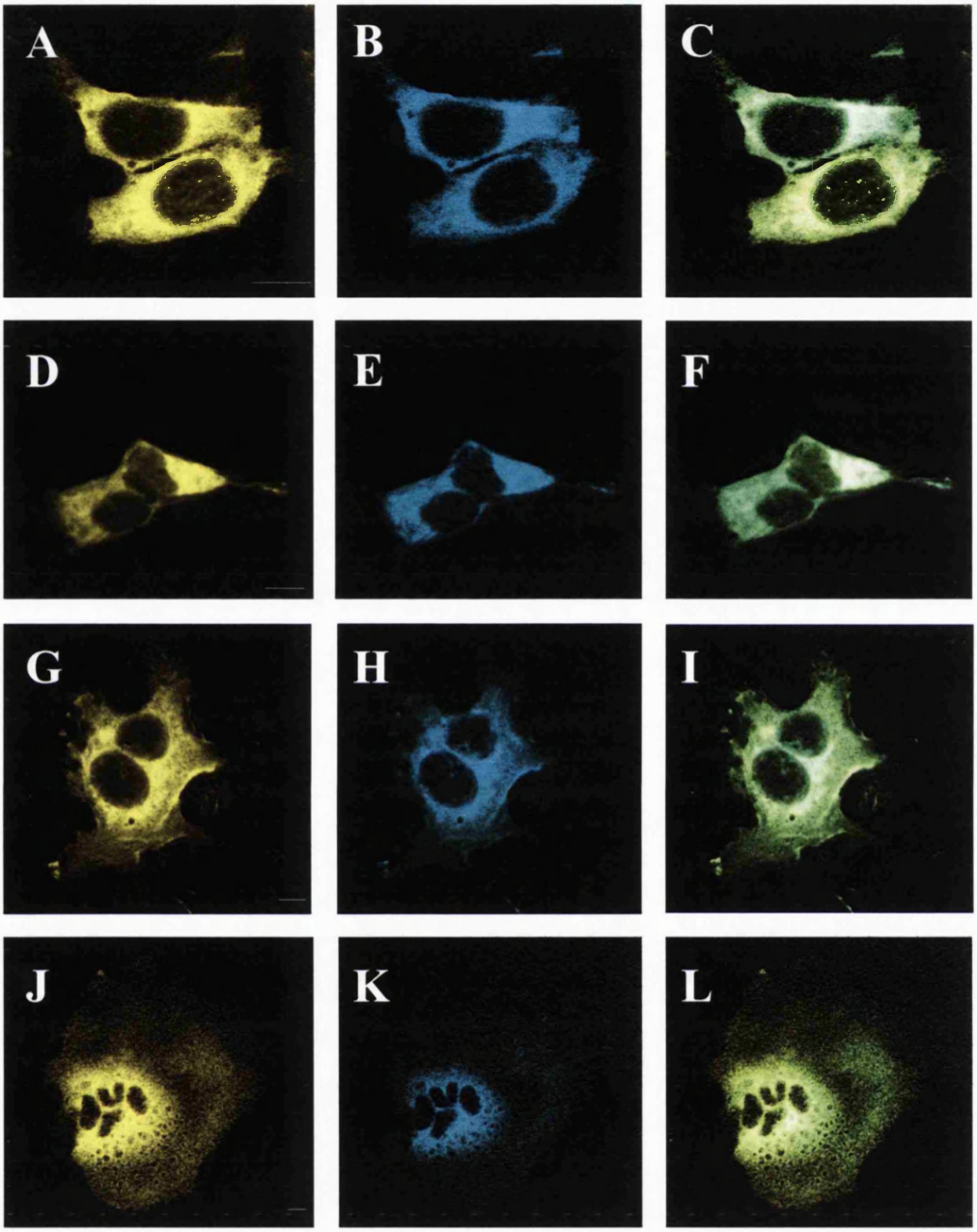

Figure 5.12. EYFP-OGT and ECFP-GRIF-1 co-localise in transfected HEK 293 and COS-7 cells. Confocal sections of HEK 293 and COS-7 cells co-transfected with pEYFP-OGT + pECFP-GRIF-1 Cells were fixed 24-48 h post-transfection and imaged. A-F, HEK 293 cells; G-L, COS-7 cells. A, D, G, J, EYFP-OGT; B, E, H, K, ECFP-GRIF-1; C, F, I, L, merged pictures of (A + B), (D + E), (G + H), (J + K). The images are representative of n = 28 cells observed from n = 3 independent transfections. Scale bars, 10 μm.

5.3. DISCUSSION

This chapter describes the association of GRIF-1 with the mitochondrial and nucleocytoplasmic OGT splice variants. OGT is a post-translational modification enzyme involved in the regulation of protein function. As described in Chapter 1, OGT modifies numerous cytoplasmic and nucleic proteins in mammalian cells by adding a N-acetylglucosamine to serine and threonine residues. OGT acts reciprocally to protein kinases in the regulation of signalling pathways (section 1.4.3.2).

5.3.1. Identification of an interaction between GRIF-1 and mOGT

Here, the characterisation of a cDNA isolated from a rat brain cDNA library in a yeast two-hybrid screen searching for GRIF-$1_{545\text{-}913}$ interactors is reported. This 1005 bp cDNA encodes residues 40-374 of the mitochondrial isoform of OGT, mOGT, and it was named $mOGT_{40\text{-}374}$. The specificity of interaction between $mOGT_{40\text{-}374}$ and GRIF-1 was confirmed by immunoprecipitation studies following co-expression of $mOGT_{40\text{-}374}$ and GRIF-1 in HEK 293 cells.

As mentioned earlier (section 1.3.3), the enzyme OGT exists as a mitochondrial and a nucleocytoplasmic splice variants, mOGT and ncOGT respectively. ncOGT is generally referred to as OGT and it is the best characterised variant (section 1.3.3). The amino acid sequences of mOGT and ncOGT are highly similar (98%). ncOGT and mOGT differ by their cellular locations, activity levels and structures (Kreppel *et al.*, 1997; Lubas *et al.*, 1997; Love *et al.*, 2003). mOGT is a 920 amino acid protein associated with the mitochondrial inner membrane (Love *et al.*, 2003). Although mOGT is catalytically active, only low amounts of mOGT-modified substrates are present within mitochondria. In contrast, ncOGT (1036 amino acids) is distributed in the nucleus and cytoplasm where high levels of ncOGT-modified moities are found (Kreppel *et al.*, 1997; Love *et al.*, 2003). mOGT and ncOGT were proposed to participate in the modulation of different cellular events with mOGT regulating mitochondrial metabolism (Love *et al.*, 2003). As described earlier (section 1.3.3.2), the enzyme is composed of an N-terminal domain for the interaction with the substrate and a C-terminal catalytic domain. ncOGT and mOGT differ in their N-terminal domains (Figure 4.6). ncOGT contains 11.5 N-terminal TPRs (TPRs 1-11.5) whereas mOGT contains only 9 TPRs (TPRs 2.5-11.5). In mOGT, TPRs 1-2.5 are replaced by a 20-amino acid mitochondrial targeting sequence necessary for mitochondrial location (Love *et al.*, 2003) and a 26-amino acid hydrophobic sequence (Figure 4.6).

The cDNA isolated in the yeast two-hybrid screen is similar to a part of the 26-amino acid hydrophobic sequence and to the following TPRs (Figure 4.6). Since this hydrophobic stretch is unique to mOGT and absent from ncOGT, it was concluded that the isolated cDNA was a partial nucleotide sequence encoding mOGT. No rat mOGT has been reported in Genbank databases yet, thus this is the first description of this variant in rat.

5.3.2. Characterisation of the interaction between GRIF-1 and ncOGT in mammalian cell lines

As described in sections 1.3.3 and 4.2.2, a yeast two-hybrid screen using OGT (ncOGT) as a bait was carried out in parallel to the study reported here (Iyer *et al.*, 2003a) and GRIF-1 was identified as an OGT-interacting protein. Here, the interaction between GRIF-1 and ncOGT was substantiated by immunoprecipitation following transfection of pCIS-GRIF-1 and pCMVTag4a-OGT in HEK 293 cells. The GRIF-1/ncOGT interaction was further investigated by confocal microscopy imaging using ECFP-GRIF and EYFP-OGT in transfected HEK 293 and COS-7 cells.

EYFP-OGT was located in a cytoplasmic region close to the nucleus and it was also enriched at the cell periphery of pEYFP-OGT transfected HEK 293 and COS-7 cells. However, EYFP-OGT was not found in the nucleus of these transfected cells. As described in section 5.2.2.2, pEYFP-OGT was generated using the OGT cDNA that was originally cloned (Kreppel *et al.*, 1997). Characterisation of the protein encoded by this cDNA, i.e. ncOGT, showed that ncOGT was distributed in the cytoplasm in transfected HEK 293 cells (Kreppel *et al.*, 1997). This was in contrast with the findings that endogenous ncOGT was located in both the nucleus and cytoplasm of CHO cells (Kreppel *et al.*, 1997). Thus, the distribution of EYFP-OGT in transfected HEK 293 and COS-7 cells is consistent with the observation of Kreppel *et al.* (1997) in transfected HEK 293 cells.

In ~ 65% of pECFP-GRIF-1 + pEYFP-OGT transfected HEK 293 and COS-7 cells observed, the distribution of ECFP-GRIF-1 was different from that observed in single transfections (Chapter 3). ECFP-GRIF-1 was localised in the cytoplasmic perinuclear region of the cell and at the cell periphery, in EYFP-OGT enriched regions, instead of beeing exclusively perinuclear as in single transfections (Chapter 3). EYFP-OGT distribution was as observed in single transfections. The variation in ECFP-GRIF-1 distribution in pECFP-GRIF-1 + pEYFP-OGT transfected HEK 293 and COS-7 cells is

consistent with an association between GRIF-1 and ncOGT. The GRIF-1/ncOGT interaction could be further characterised using the acceptor photobleaching FRET protocol established in Chapter 3. It would give more insights into the cellular location of GRIF-1/ncOGT interaction, i.e. it would define whether the proteins interact within the cytoplasm and/or at the cell periphery.

5.3.3. Determination of the GRIF-1/OGT binding sites

As reported in this chapter, GRIF-1 can associate with either mOGT or ncOGT. The initial yeast two-hybrid screen showed that the C-terminal domain of GRIF-1, i.e. GRIF-$1_{545\text{-}913}$, interacts with the N-terminal domain of mOGT, i.e. $mOGT_{40\text{-}374}$, a region including an hydrophobic sequence and 9 TPRs. Another study mapping the binding domain of OIP106, a GRIF-1 human orthologue, with OGT showed that the C-terminal domain of OIP106, i.e. $OIP106_{639\text{-}859}$, interacts with the N-terminal domain of ncOGT, i.e. $ncOGT_{167\text{-}283}$, a domain containing the TPRs 2.5-6 (Iyer *et al.*, 2003a; Iyer *et al.*, 2003b). This domain, i.e. $ncOGT_{167\text{-}283}$, shares 100% amino acid similarity with $mOGT_{51\text{-}167}$, a region including mOGT-TPRs 2.5-6 (Figures 5.3, 5.4). Thus this suggests that $mOGT_{51\text{-}167}$ (TPRs 2.5-6) is sufficient for the association of mOGT with GRIF-1. By amino acid alignment, it can be seen that $OIP106_{639\text{-}859}$ corresponds to GRIF-$1_{622\text{-}846}$ and that OIP106 and GRIF-1 share 60% amino acid identity in this region (Figure 5.13). Together with Iyer *et al.* (2003a,b), the yeast two-hybrid screen result indicates that the C-terminal domain of GRIF-1 is important for the interaction with the N-terminal region of OGT splice variants. This could be verified by carrying out acceptor photobleaching FRET measurements between ECFP-GRIF-1 and EYFP-OGT. In this case, significant FRET efficiencies between C-terminal ECFP-tagged GRIF-1 and N-terminal ECFP-tagged OGT constructs are expected.

GRIF-1 and OIP106 have been shown to be glycosylated by ncOGT (Iyer *et al.*, 2003a). Interestingly, TPRs 1-2.5 are required for efficient glycosylation of OIP106 by ncOGT (Iyer *et al.*, 2003b). As mentioned in section 5.3.1, mOGT lacks TPRs 1-2.5. Thus OIP106 and GRIF-1 might not be some substrates for mOGT. This supports the original hypothesis that mOGT and ncOGT have different functions (Love *et al.*, 2003). Accordingly, GRIF-1/mOGT and GRIF-1/ncOGT interactions may have different functional significance. The GRIF-1/ncOGT interaction was reported to be very stable (Iyer *et al.*, 2003a), thus suggesting that GRIF-1 is always associated to ncOGT. In agreement with this hypothesis, ncOGT is always co-immunoprecipitated with GRIF-1

from rat brain extracts (K. Brickley and F.A. Stephenson, unpublished observations). Since ncOGT is involved in the modulation of protein function, ncOGT might regulate GRIF-1 interactions or more generally the function of GRIF-1 or GRIF-1 associated proteins. Little is known about the GRIF-1/mOGT association. Since GRIF-1 has been shown to co-localise and to be associated with mitochondria (Chapter 3; Fransson *et al.*, 2006), GRIF-1 might play a role in targeting newly synthetised mOGT to mitochondria. Co-localisation using fluorescent-tagged mOGT, fluorescent-tagged GRIF-1 and a fluorescent mitochondrial marker could provide further insights into GRIF-1/mOGT interactions.

```
GRIF-1   602  VYHISDLEEDEEVGITFQVQQPLQLEQKPAPPPPVTGIFLPPMTSAGGPVSVATSNPGKC  661
              VY ++D EED+        +  P       P   P                    +  +PGKC
OIP106   622  VYCLNDFEEDDTGD---HISLPRLATSTPVQHP----------------ETSAHHPGKC  661

GRIF-1   662  LSFTNSTFTFTTCRILHPSD-ITQVTPS-SGFPSLSCGSSAGSASNTAVNSPAASYRLSI  719
              +S TNSTFTFTTCRILHPSD +T+VTPS +   P+ +CGS++     +T V +P     RLS+
OIP106   662  MSQTNSTFTFTTCRILHPSDELTRVTPSLNSAPTPACGSTS-HLKSTPVATPCTPRRLSL  720

GRIF-1   720  GESITNRRDSTITFSSTRSLAKLLQERGISAKVYHSPASENP-----LLQLRPKALATPS  774
               ES TN R+ST T S++  L  LL+ERGISA VY   + +        L    PK    PS
OIP106   721  AESFTNTRESTTTMSTSLGLVWLLKERGISAAVYDPQSWDRAGRGSLLHSYTPKMAVIPS  780

GRIF-1   775  TPPNSPSQSPCSSPVPFEPRVHVS--ENFLASRPAETFLQEM--YGLRPSRAPPDVGQLK  830
              TPPNSP Q+P SSP  FE +       +NFLAS+PA + L+E+    +R S +  DV
OIP106   781  TPPNSPMQTPTSSPPSFEFKCTSPPYDNFLASKPASSILREVREKNVRSSESQTDVSVSN  840

GRIF-1   831  MNLVDRLKRLGIARVV---KTPVPRENGKSREAEMGLQKPDSAVYLN-------------  874
              +NLVD+++R G+A+VV   +  VP    +      G   P  A+
OIP106   841  LNLVDKVRRFGVAKVVNSGRAHVPTLTEEQGPLLCGPPGPAPALVPRGLVPEGLPLRCPT  900
```

Figure 5.13. Alignment of the amino acid sequences of OIP106$_{639-859}$ and GRIF-1$_{622-846}$. The amino acid sequences of OIP106 and GRIF-1 were aligned using BLAST (www.ncbi.nih.gov). The OIP106 domain defined by amino acids 639-859 and the GRIF-1 domain defined by amino acids 622-846 are represented in red.

In summary, this chapter showed that GRIF-1 can associate with either mOGT or ncOGT. The interaction between GRIF-1 and mOGT was identified in a yeast two-hybrid screen. It was further substantiated by immunoprecipitation using HEK 293 cells co-transfected with GRIF-1 and mOGT. The C-terminal domain of GRIF-1 was shown to mediate the association with the N-terminal TPRs of mOGT. The interaction between GRIF-1 and ncOGT was substantiated by immunoprecipitation and studied by confocal microscopy imaging of ECFP-GRIF-1 and EYFP-OGT in transfected HEK 293 and COS-7 cells. Further analyses are necessary to understand the functional significance of GRIF-1/mOGT and GRIF-1/ncOGT interactions.

CHAPTER 6

GENERAL DISCUSSION AND FUTURE WORK

6.1. GENERAL DISCUSSION

Synaptic inhibition in brain is mainly mediated via activation of $GABA_A$ receptors by the neurotransmitter, GABA. Understanding how these receptors are transported to and maintained at the cell surface is therefore important to gain insights into the regulation of synaptic inhibition. $GABA_A$ receptor subunits contain a large cytoplasmic loop thought to be the main target for the regulation of the receptor transport and maintenance at the cell surface. In recent years, the yeast two-hybrid system was used to identify proteins associated with $GABA_A$ receptor subunits that may participate in the regulation of $GABA_A$ receptor trafficking and clustering at the synapses. One of these proteins, GRIF-1, was a protein of unknown function found specifically associated with $GABA_A$ receptor β2 subunit intracellular loops (Beck *et al.*, 2002). The aim of this PhD thesis was to investigate the function of GRIF-1 in intracellular trafficking mechanisms. This was performed using fluorescent-tagged GRIF-1 constructs and confocal microscopy imaging of GRIF-1 transfected mammalian cell lines.

Together with Smith *et al.* (2006), it was demonstrated using FRET imaging that GRIF-1 was directly associated with the C-terminal domain of the microtubule motor, kinesin-1, thereby substantiating a role for GRIF-1 as a trafficking factor. Looking for the cargo transported by the GRIF-1/kinesin-1 complex, it was shown that GRIF-1 provided a physical link between the heavy chains of kinesin-1 and mitochondria in addition to a putative role in $GABA_A$ receptor trafficking. Kinesin-1 transports anterogradely different type of cargoes across various intracellular pathways, e.g. from the Golgi to the plasma membrane and from endosome to lysosomes (Soldati and Schliwa, 2006). Further in polarised cells such as neurones, kinesin-1 targets its cargoes to given compartments such as somatic, dendritic, axonal or presynaptic compartments (Hirokawa and Takemura, 2005). It was initially thought that a unique kinesin receptor, kinectin, was expressed at the surface of all kinesin cargoes and recognised by kinesin for transport along microtubules (Vallee and Sheetz, 1996). As described in Chapter 1, it was later discovered that various adaptor proteins exist and that a specific adaptor was required for the attachment of a given cargo to kinesin (Hirokawa and Takemura, 2005). Unexpectedly, recent findings suggested that adaptors were polyvalent molecules that could connect different types of cargoes to kinesin-1. For example, the identification of GRIF-1 as a $GABA_A$ receptor associated protein suggested that GRIF-1 was specifically involved in trafficking these receptors to the plasma membrane. However

GRIF-1 was later suggested to participate in mitochondrial transportation within cells (Chapter 3, Smith *et al.*, 2006). Two recent studies further implied that GRIF-1 may also be implicated in K^+ channel Kir2.1 (Grishin *et al.*, 2006) and endosome-to-lysosome (Kirk *et al.*, 2006) trafficking events. The role of GRIF-1 as an adaptor protein linking kinesin-1 to its cargoes is discussed hereafter, focussing specially on $GABA_A$ receptors and mitochondria.

6.1.1. GRIF-1 and $GABA_A$ receptor trafficking

The most common $GABA_A$ receptor subtypes are pentamers composed of 2α, 2β, 1γ subunits (Chapter 1). The β subunits are essential for cell surface targeting of the receptors (Connolly *et al.*, 1996a). The γ subunits, i.e. γ2, are required for postsynaptic clustering of the receptors (Essrich *et al.*, 1998). Several proteins associated with the different subunits have been identified (Chapter 1, Table 1.2).

GRIF-1 interacts specifically and solely with $GABA_A$ receptors β2 subunits. In contrast, other $GABA_A$ receptor associated proteins such as AP2, BIG2, Plic1, HAP1 and PRIP-1, 2 have been shown to bind to all $GABA_A$ receptors β subunits, i.e. β1, β2 and β3 subunits. In addition, AP2 interacted with $GABA_A$ receptor γ2 and δ subunits and Plic1 with $GABA_A$ receptor α subunits. In neurones, β subunit-interacting proteins are distributed to different cellular domains suggesting they might regulate different steps of $GABA_A$ receptor trafficking to and from the plasma membrane. For example, Plic1 and BIG2 are localised to the Golgi and trans-Golgi network (TGN) respectively. They were proposed to transport newly synthetized $GABA_A$ receptors from the Golgi to the plasma membrane (Bedford *et al.*, 2001) or, for BIG2, from the TGN to the plasma membrane or from the TGN to the endosomes (Charych *et al.*, 2004). AP2 and PRIP-1, 2 are found close to the plasma membrane where they regulate the clathrin-mediated endocytosis of cell surface $GABA_A$ receptors (Kittler *et al.*, 2000a; Kanematsu *et al.*, 2006). Finally, Plic1 is also located in intracellular structures close to the plasma membrane (Bedford *et al.*, 2001) and HAP1 in intracellular clusters in dendritic shafts, axons and soma (Gutekunst *et al.*, 1998; Kittler *et al.*, 2004b). Plic1 and HAP1 were shown to regulate the fate of internalised $GABA_A$ receptors by promoting their recycling to the plasma membrane (Bedford *et al.*, 2001; Kittler *et al.*, 2004b). Plic1 prevents poly-ubiquitination and proteasomal degradation of internalised $GABA_A$ receptors and HAP1 inhibits their lysosomal degradation.

Here, GRIF-1 was shown to localise at the perinuclear Golgi region in GRIF-1-transfected COS-7 cells. Consistent with this observation, Kirk *et al.* (2006) revealed that GRIF-1 was associated with early endosomes at the perinuclear region of the cell via an interaction with the early endosomal protein, hepatocyte-growth-factor-regulated tyrosine kinase substrate (Hrs). Hrs plays a key role in the targeting of internalised mono-ubiquitinated transmembrane proteins to the lysosomes for degradation (Hurley and Emr, 2006). Hrs binds to mono-ubiquitinated proteins located to clathrin-coated sites of the early endosomes. It recruits a protein complex that initiates the formation of multi-vesicular bodies (MVB) at these sites. MVBs deliver their content, i.e. mono-ubiquitinated transmembrane proteins, to the lysosomes for degradation. GRIF-1 was shown to inhibit the degradation of internalised epithelial growth factor receptors (EGFR) when overexpressed in PC12 cells (Kirk *et al.*, 2006). GRIF-1 had no effect on EGFRs endocytosis. Thus GRIF-1 was proposed to contribute to Hrs-mediated endosome-to-lysosome protein sorting by blocking the trafficking of vesicles between endosomes and lysosomes. Concurrently, GRIF-1 was also shown to increase cell surface expression of another transmembrane protein, K^+ channel Kir2.1 (Grishin *et al.*, 2006) implying that GRIF-1 may also inhibit the degradation or internalisation of these channels and promote their recycling to the plasma membrane. These 2 studies suggest that GRIF-1 could also regulate the endosomal sorting and cell surface recycling of internalised $GABA_A$ receptors in neurones. This hypothesis is further supported by the findings that the GRIF-1 orthologues, HAP1 and OIP106, have been implicated in the regulation of $GABA_A$ receptor cell surface expression in neurones. HAP1 interacts with Hrs on early endosomes and, like GRIF-1, it was shown to regulate Hrs-mediated endosome-to-lysosome sorting (Li *et al.*, 2002). Further HAP1 was shown to prevent lysosomal degradation of internalised $GABA_A$ receptors thereby contributing to an increase in receptor recycling to the cell surface (Kittler *et al.*, 2004). A mutation of OIP106, a GRIF-1 human orthologue, leads to a reduction in $GABA_A$ receptor expression levels in hypertonic mice (Gilbert *et al.*, 2006).

As mentioned earlier, GRIF-1 binds only to $GABA_A$ receptor β2 subunits whereas HAP1 also interacts with $GABA_A$ receptor β1 and β3 subunits. The β subunit isoforms were shown to determine the destination of $GABA_A$ receptors to distinct cellular domains in Madin-Darby canine kidney (MDCK) cells (Connolly *et al.*, 1996a). These are polarised cells with an apical and a basolateral membrane that are analoguous to

axonal and somatodendritic neuronal membranes, respectively, in terms of polarity and endocytosis (Connolly *et al.*, 1996a). The β2 subunits target assembled $GABA_A$ receptors to the basolateral membrane and the β3 subunits to the apical membrane. Depending on their associated $GABA_A$ receptor β subunits, GRIF-1 and HAP1 may localise to different neuronal compartments, i.e. somatodendritic or axonal, and control the endosomal sorting of receptors internalised in each region of the same cell rather than competing for an interaction with the same GABA receptor subtype at the same cellular location. Alternatively, GRIF-1 and HAP1 may not be expressed in the same region of the brain. HAP1 is highly enriched in the hypothalamus (Li *et al.*, 2003) but the distribution of GRIF-1 in the brain is not known. It may also be possible that HAP1 is constitutively active whereas GRIF-1 might be activated in given conditions only (see later in this section). Several $GABA_A$ receptor β subunit-interacting proteins may co-exist in neurones. Based on their cellular location, each of them seems to fulfil distinct functions related either to exocytosis, endocytosis, recycling or degradation of $GABA_A$ receptors. Additional proteins associated with $GABA_A$ receptor α or γ subunits act in concert with $GABA_A$ receptor β subunit-interacting proteins to ensure the trafficking and clustering of the receptors at the synapses.

As shown in Chapter 5, GRIF-1 interacts directly and strongly with OGT, a post-translational modification enzyme that adds *N*-acetylglucosamine to serine/threonine residues of various proteins (Chapters 1, 5). OGT acts dynamically in concert with kinases in a 'Yin-O-Yang' relationship so that modified residues are either *O*-glycosylated or phosphorylated. Consistent with this notion, OGT copurifies with protein phosphatase, PP1, in rat brain extracts suggesting that PP1 dephosphorylates serine/threonine residues for subsequent *O*-glycosylation by OGT (Wells *et al.*, 2004). GRIF-1 may serve as a trafficking and scaffolding molecule that targets and links physically the OGT/PP1 complex to cell surface or internalised β2 subunit-containing $GABA_A$ receptors thereby controlling the phosphorylation state of the receptors. GRIF-1 interacts with residues 324-394 within the β2 subunit intracellular loop, a domain adjacent to serine (S) 429 (S410 in Kittler *et al.*, 2004a). S429 is conserved in all β subunits and it is important for the regulation of $GABA_A$ receptor function as it can be phosphorylated *in vitro* by PKC (Kittler and Moss, 2003). Phosphorylation of this conserved serine residue in $GABA_A$ receptor β3 subunits prevents AP2-mediated $GABA_A$ receptor endocytosis (Kittler *et al.*, 2004a). Thus GRIF-1 may play an

important role in the dynamic control of β2 subunit-containing $GABA_A$ receptor intracellular trafficking via the OGT/PP1 complex in response to extracellular stimuli. For example, insulin has been shown to increase cell surface expression of β2 subunit-containing $GABA_A$ receptors in neurones (Wan *et al.*, 1997) consistent with a decrease in receptor degradation and an increase in receptor recycling to the cell surface. The levels of OGT expression are also increased following insulin application in rat liver (Majumbar *et al.*, 2004). The expression of OGT in insulin-treated neurones has not yet been studied. In response to rising insulin concentrations, GRIF-1 might specifically target in the OGT/PP1 complex to internalised $GABA_A$ receptors. Following modification of the receptor phosphorylation state by OGT/PP1, the receptors are recycled to the cell surface instead of being degraded in the lysosomes. Insulin is a neuromodulator that participates in the regulation of food intake, a behaviour partly controlled via activation of $GABA_A$ receptors (Wan *et al.*, 1997). Thus GRIF-1 might contribute to the regulation of food intake by acting on $GABA_A$ receptor cell surface expression.

6.1.2. GRIF-1 and mitochondrial transport

In Chapter 3, GRIF-1 was shown to modify the distribution of mitochondria when overexpressed in COS-7 cells and to recruit mitochondria to kinesin-1. This suggested GRIF-1 may serve as an adaptor protein in mitochondrial trafficking along microtubules. GRIF-1 is a cytoplasmic protein devoided of a transmembrane domain. GRIF-1 binding to mitochondria was shown to be indirect and mediated by the mitochondrial Rho-GTPase, miro (Fransson *et al.*, 2006). It is a transmembrane protein composed of an N- and a C-terminal GTPase domain and 2 putative calcium binding motives (EF hands) (Fransson *et al.*, 2003). A C-terminal transmembrane domain is necessary for miro localisation to the mitochondrial outer-membrane (Fransson *et al.*, 2006). Miro co-localises with GRIF-1 and GRIF-1-aggregated mitochondria in the proximity of the nucleus following expression of GRIF-1 and miro in COS-7 cells (Fransson *et al.*, 2006). This substantiates an interaction between GRIF-1, miro and mitochondria. Similarly, Milton, the *Drosophila* orthologue of GRIF-1, was shown to interact with mitochondria via 2 different domains. The N-terminal domain of Milton interacts with the *Drosophila* mitochondrial Rho-GTPase, dmiro, and the C-terminal domain of Milton binds to an unidentified mitochondrial protein (Glater *et al.*, 2006; Guo *et al.*, 2005). dMiro has the same structure as the mammalian miro isoform. Since

miro (dmiro) arbors 2 putative calcium binding sites and since mitochondrial motility is stopped following increase in calcium concentrations (Li *et al.*, 2004), miro could contribute to the regulation of mitochondrial trafficking by binding calcium. Further GRIF-1 and Milton association with mitochondria could be regulated via miro GTPase domains.

In rat brain, 2 different adaptors can link mitochondria to kinesin. These are syntabulin and GRIF-1. As mentioned earlier, neurones are highly polarised and compartmentalised cells. Multiple metabolically demanding events occur probably simultaneously in various neuronal locations. Hence mitochondria need to be transported to different compartments at the same time. For example, neurotransmitter release at the axon terminals and insertion of neurotransmitter receptors in the dendritic membrane are 2 energy-demanding mechanisms that could occur simultaneously within a neurone. The simultaneous transport of mitochondria to different cellular locations may require different adaptors. For example, GRIF-1 could direct mitochondria to dendrites and syntabulin to axon terminals. Adaptor proteins might also help to determine the cellular destination of the cargoes transported by kinesins.

With syntabulin, the principle of dual cargo attachment and co-transport is also emerging. Syntabulin was shown to be involved in the kinesin-1-based transport of both mitochondria and syntaxin-1-containing vesicles to axon terminals in 2 different studies (Su *et al.*, 2004; Cai *et al.*, 2005). Three distinct syntabulin regions enable syntabulin/kinesin-1, syntabulin/mitochondria and syntabulin/syntaxin-1 interactions. Hence syntabulin may associate simultaneously with the 2 cargoes and with kinesin-1 for co-transport to the axon terminals. Co-transport would be less costly for the cell in terms of energy expenditure as a single kinesin could target 2 cargoes to the same destination at the same time. Similarly to syntabulin, GRIF-1 can associate with mitochondria and, albeit with low affinity, with $GABA_A$ receptors. As proposed for syntabulin, GRIF-1 could mediate the kinesin-1-based co-transport of mitochondria and $GABA_A$ receptors to the dendrites.

6.1.3. Concluding remarks

The overall aim of this PhD thesis was to understand the function of GRIF-1. When this project was initiated, GRIF-1 was known to associate with $GABA_A$ receptor β2 subunits (Beck *et al.*, 2002). It was later discovered that GRIF-1 was also associated with OGT (Chapter 5; Pozo *et al.*, 2004; Iyer *et al.*, 2003), kinesin-1 heavy chains, KIF5s

(Brickley *et al.*, 2005), and with mitochondria (Chapter 3; Smith *et al.*, 2006) via the small GTPase, miro (Fransson *et al.*, 2006). Recently, GRIF-1 was also shown to bind K^+ channels (Grishin *et al.*, 2006) and the early endosomal protein, Hrs (Kirk *et al.*, 2006). Further GRIF-1 was shown to be crucial for mitochondrial association to kinesin-1 (Chapter 3; Smith *et al.*, 2006) and to control endosomal trafficking of internalised EGFRs and probably K^+ channels to lysosomes and to the cell surface (Kirk *et al.*, 2006; Grishin *et al.*, 2006). Taking all these studies together, it can be concluded that GRIF-1 plays a function in kinesin-1 based trafficking in cells by linking kinesin-1 to a cargo. GRIF-1 seems to scaffold transmembrane receptors and organelles to kinesin-1 for anterograde transport to a given destination. Of particular interest is the interaction of GRIF-1 with OGT that can be regarded as a cargo (see section 3.1.2) or as a GRIF-1 regulatory subunit that would dynamically control the association of GRIF-1 with kinesin or with other cargoes. The GRIF-1 C-terminal domain is rich in P-X-X-P motifs that are known to interact with SH3 domains (Iyer *et al.*, 2003a; Kay *et al.*, 2000). SH3 domains are found in signalling molecules such as ras GTPase activators and in proteins associated with the cytoskeleton such as myosin or actin-binding proteins. GRIF-1 might recruit several signalling molecules and function as an anchor point for the effectors of a signal transduction pathway regulating the kinesin-1 transport of $GABA_A$ receptors and/or mitochondria in neurones. This has already been observed for the adaptor protein, JIP-1, that links APP to kinesin-1 and also functions as an anchor point for the MAP kinases activating the JNK-signalling pathway (Chapter 1).

Since the function of GRIF-1 was investigated here in non-polarised COS-7 cells, it is difficult to determine what the destination of GRIF-1-scaffolded cargoes would be in neurones. Besides, the mechanisms controlling the direction of kinesin-mediated trafficking in neurones are unknown (Chapter 1). Work from Connolly *et al.* (1996a) suggests that $GABA_A$ receptor β2 subunits are targeted to somatodendritic membranes in neurones. This indicates that GRIF-1 might target recycled β2 subunit-containing $GABA_A$ receptors to these regions. GRIF-1-related proteins also interact with kinesin-1 and for HAP1, with dynein too. HAP1 was shown to contribute to both axonal and dendritic transport of cargoes (Rong *et al.*, 2006). Milton targets mitochondria to axon terminals (Stowers *et al.*, 2003). It is not known where OIP106 cargoes are targeted.

GRIF-1, OIP106, Milton and possibly HAP-1 were proposed to form a new family of coiled-coil proteins due to the high amino acid sequence similarities between their N-terminal coiled-coil regions (Chapter 1). In line with this, the findings presented here contribute to this hypothesis by showing that GRIF-1, like Milton, was necessary for the recruitment of mitochondria to kinesin-1 heavy chains and by substantiating the interaction between GRIF-1 and OGT. A recent study showed that OIP106 was also crucial for the targeting of mitochondria to kinesin-1 heavy chains (K. Brickley, K. Pozo, M. Merlini and F.A. Stephenson, unpublished observations). Further, OIP106 binds to OGT like Milton and GRIF-1 (Chapter 1). In contrast, work from Fransson *et al.* (2006) implied that HAP1 is not related to mitochondrial trafficking. It is not known whether HAP1 is an OGT interacting protein. This suggests that GRIF-1, OIP106 and Milton are part of a same family of coiled-coil adaptor proteins involved in mitochondrial transport. HAP1 may be a more distantly related member. GRIF-1 associates directly, albeit with low affinity, with $GABA_A$ receptor β2 subunits. HAP1 interacts with $GABA_A$ receptor β subunits (Chapter 1). Recently, OIP106 was also shown to co-immunoprecipitate with α1 subunit-containing $GABA_A$ receptors in brain (Chapter 1). This suggests that the GRIF-1/OIP106 family of proteins may also be involved in $GABA_A$ receptor trafficking. It would be interesting to investigate whether Milton also interacts with $GABA_A$ receptors.

6.2. FUTURE WORK

The work presented here provides further insights into the function of GRIF-1 as a trafficking factor in mammalian cell lines (Figure 6.1). A role for GRIF-1 in kinesin-dependent mitochondrial transport was established. However little progress was made regarding the function of GRIF-1 in $GABA_A$ receptor trafficking. The recent findings of Kirk *et al.* (2006) suggest that GRIF-1 may control the endosomal sorting of internalised $GABA_A$ receptors by inhibiting their lysosomal degradation and promoting their reinsertion at the plasma membrane. The effect of GRIF-1 on $GABA_A$ receptor cell surface levels could be investigated following expression of GRIF-1 and α1β2γ2 $GABA_A$ receptors in HEK 293 or neuronal cells. The specificity of GRIF-1 for other $GABA_A$ receptor subtypes could also be tested by co-expressing different $GABA_A$ receptor subunit isoforms together with GRIF-1 in HEK 293 or neuronal cells. A more detailed study could be carried out to investigate the effect of GRIF-1 on $GABA_A$ receptor internalisation and lysosomal degradation in transfected HEK 293 or neuronal

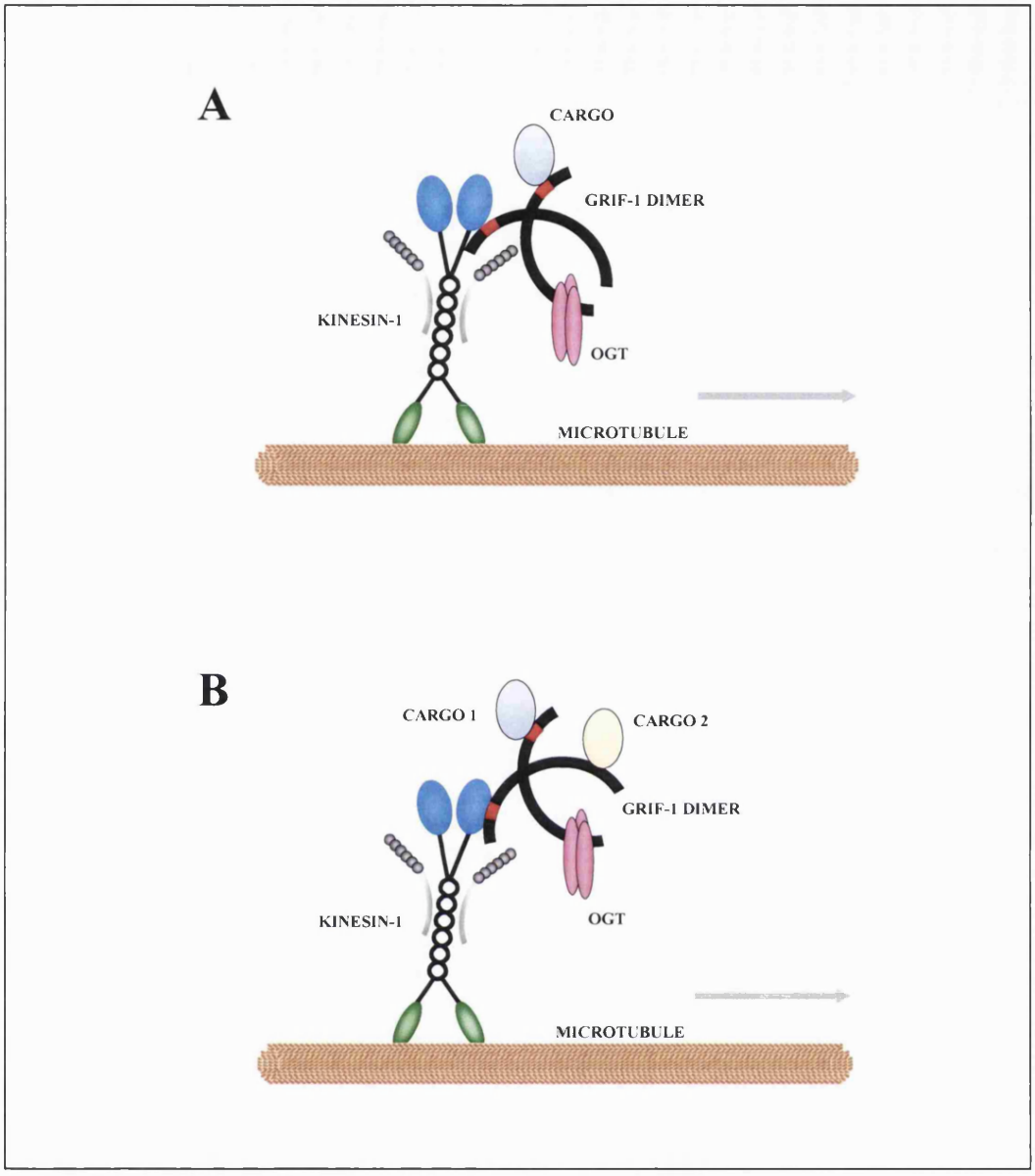

Figure 6.1. A schematic representation of GRIF-1 as an adaptor protein involved in kinesin-1-based anterograde transport. GRIF-1 is represented as a dimer. It interacts with kinesin-1 through its N-terminal coiled-coil region and with OGT through its C-terminal domain. The Figure shows that GRIF-1 could link kinesin-1 to either A, a single cargo or B, 2 cargoes for anterograde transport to a defined cellular location. Adapted from Smith *et al.*, 2006.

cells. This could be performed using a biotinylation assay in presence or absence of the lysosome inhibitor, leupeptin, as described by Kittler *et al.* (2004b).

Further work also needs to be performed to characterise GRIF-1 *in vivo*. The distribution of GRIF-1 in brain could be determined by immunostaining rat brain slices. Further GRIF-1 cellular and subcellular distribution could be analysed in primary neuronal cell using antibodies raised against GRIF-1 and against cellular organelles. A better resolution could be obtained by electron microscopy. These analyses could

confirm the nature of GRIF-1-associated organelles and reveal the destination of cargoes transported via GRIF-1-dependent mechanisms.

To further investigate the function of GRIF-1 in intracellular trafficking, a GRIF-1 knock-out mouse line could be generated and the distribution of mitochondria and $GABA_A$ receptors in these mice brains could be examined by immunostaining. Alternatively, the expression of GRIF-1 in wild-type neuronal cultures could be disrupted using small interfering RNAs and the effects on mitochondrial and $GABA_A$ receptor distributions analysed. Conversely, a fluorescently-tagged GRIF-1 could be overexpressed in wild-type neurone cultures and its co-localisation with kinesin-1, mitochondria and $GABA_A$ receptors examined. The effect of GRIF-1 downexpression or overexpression on mitochondrial transport could also be studied in GRIF-1 mutant or wild-type neuronal cultures by time-lapse confocal microscopy imaging. Since GRIF-1 human homologue, OIP106, has been linked to hypertonia, a condition found in lower motor neurone diseases, the expression of GRIF-1 in mouse model for these diseases could be investigated. The putative role of OGT as a regulator of GRIF-1 function could also be investigated in mammalian cell lines and in brain.

APPENDICES

Appendix 3.1. Vector map of pECFP-C1 cloning vector

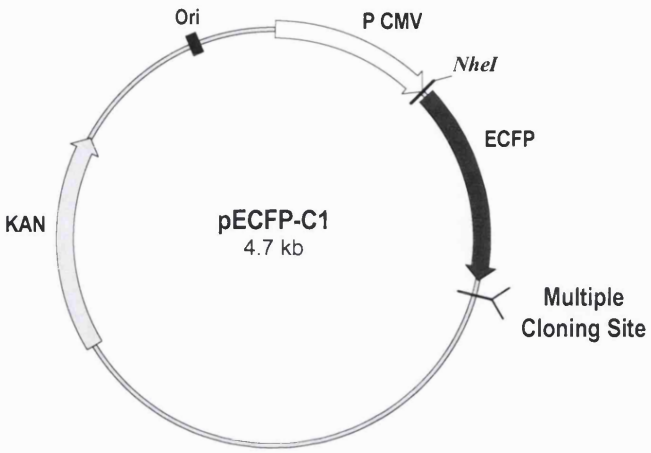

The cloning vector, pECFP-C1, was used to generate and express ECFP-tagged fusion proteins in mammalian cell lines. The vector pECFP-C1 contains a cDNA encoding ECFP. An *NheI* restriction site upstream ECFP cDNA enables the insertion of foreign cDNA thereby yielding a C-terminal ECFP-tagged fusion protein. A multiple cloning site downstream ECFP cDNA allows the insertion of foreign cDNA to yield an N-terminal ECFP-tagged fusion protein. A CMV promotor enables the expression of ECFP or ECFP-tagged protein in mammalian cells. The bacterial origin of replication (ori) enables the plasmid replication in *E. coli*. A kanamycin resistance gene (KAN) allows the selection of transformants on selective media containing kanamycin.
The cloning vector pEYFP-C1 is identical to pECFP-C1 except that it contains a cDNA encoding EYFP instead of ECFP.

Appendix 3.2. Vector maps of pECFP-GRIF-1 and pEYFP-GRIF-1

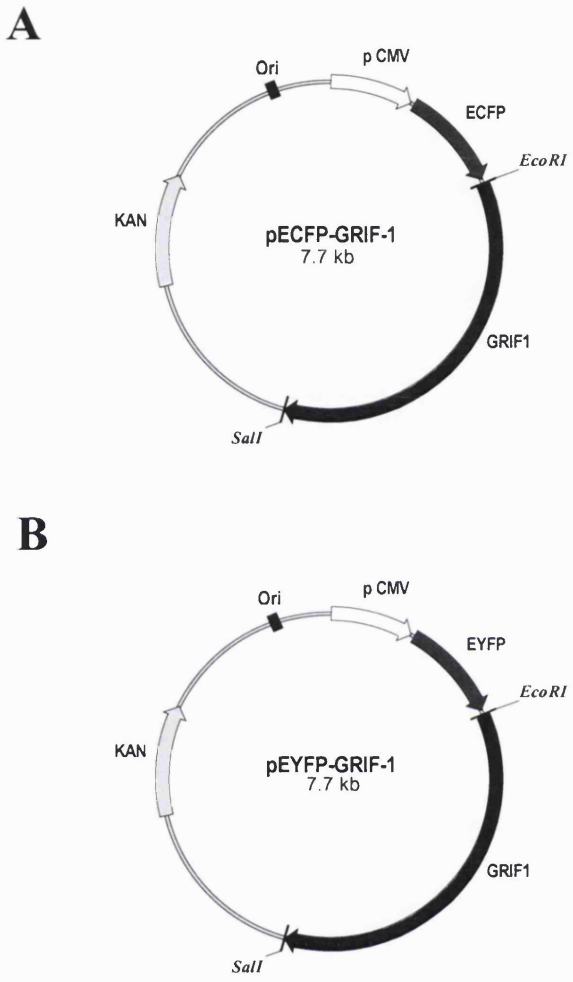

The cDNA encoding GRIF-1 was sub-cloned in frame into the *EcoRI/SalI* restriction sites of A, pECFP-C1 to yield pECFP-GRIF-1 and B, pEYFP-C1 to yield pEYFP-GRIF-1. These constructs were generated by A. M. Salgueiro (University of Algarve, Portugal).

Appendix 3.3. Vector maps of pN-ECFP-KIF5C, pN-EYFP-KIF5C, pC-ECFP-KIF5C and pN-EYFP-KIF5C

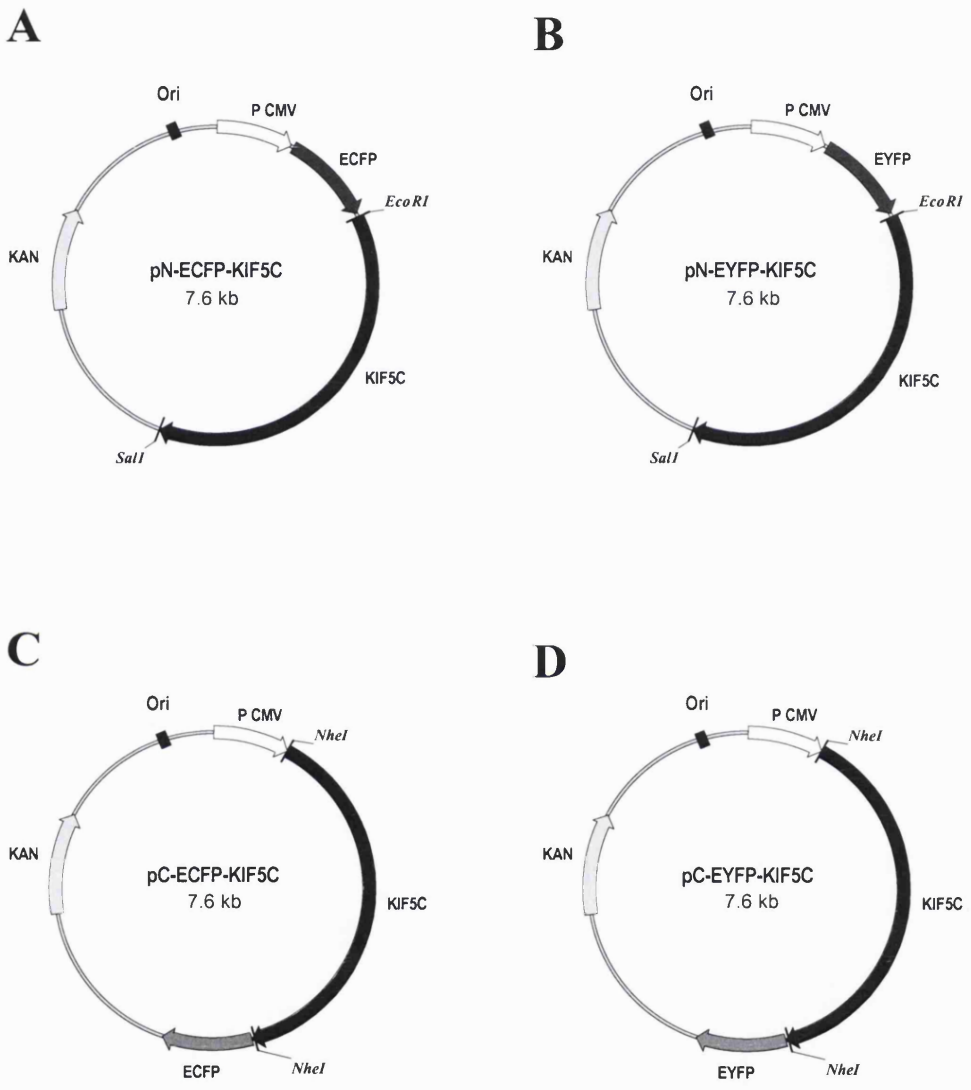

The cDNA encoding KIF5C was sub-cloned in frame into the *EcoRI/SalI* restriction sites of A, pECFP-C1 to yield pN-ECFP-KIF5C (N-terminal ECFP-tagged KIF5C) and B, pEYFP-C1 to yield pN-EYFP-KIF5C (N-terminal EYFP-tagged KIF5C). The cDNA encoding KIF5C was also sub-cloned in frame into the *NheI* restriction site of C, pECFP-C1 to yield pC-ECFP-KIF5C (C-terminal ECFP-tagged KIF5C) and D, pEYFP-C1 to yield pC-EYFP-KIF5C (C-terminal EYFP-tagged KIF5C). pN-EYFP-KIF5C was generated by A. M. Salgueiro (University of Algarve, Portugal).

Appendix 3.4. Vector maps of pEYFP-KIF5C-MD and pEYFP-KIF5C-NMD

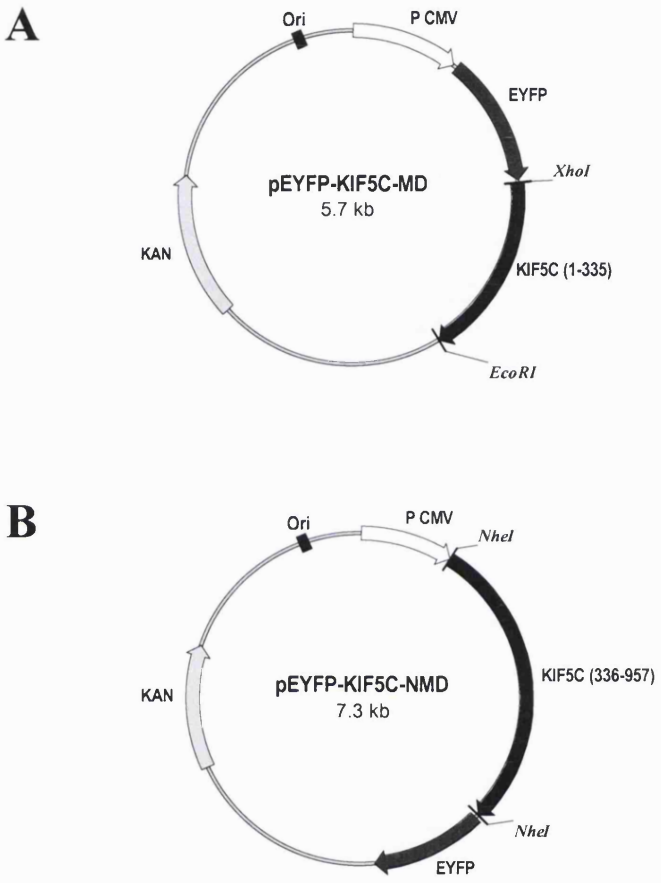

A, the cDNA encoding KIF5C (1-335) was sub-cloned in frame into the *XhoI/EcoRI* restriction sites of pEYFP-C1 to yield pEYFP-KIF5C-MD (N-terminal EYFP-tagged KIF5C-MD). B, the cDNA encoding KIF5C (336-957) was sub-cloned into the *NheI* restriction site of pEYFP-C1 to yield pEYFP-KIF5C-NMD (C-terminal EYFP-tagged KIF5C-NMD).

Appendix 4.1. Vector map of the pCIS-GABA$_A$R-β2^{EYFP} plasmid

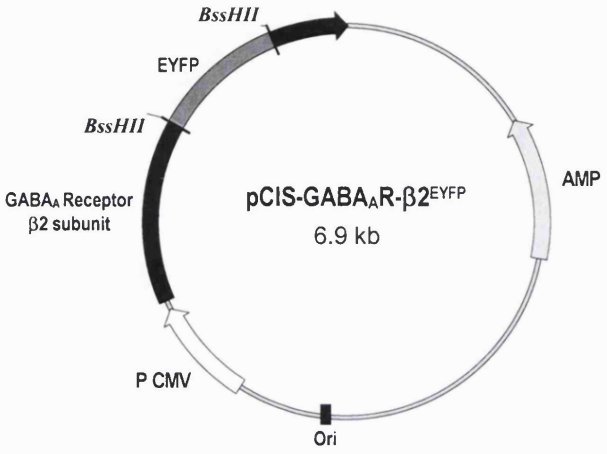

The pCIS-GABA$_A$R-β2^{EYFP} plasmid was used to generate and express EYFP-tagged GABA$_A$ receptor β2 subunits in HEK 293 and COS-7 cells. The plasmid contains a CMV promoter for the expression of EYFP-tagged GABA$_A$ receptor β2 subunit in mammalian cells. The cDNA encoding EYFP was inserted in frame into a unique *BssHII* restriction site. The plasmid contains also a bacterial origin of replication (ori) for efficient replication in *E. coli* and an ampicillin resistance gene (AMP) for the selection of transformants.

Appendix 5.1. Vector map of the yeast two-hybrid cloning vectors, pGBKT7 and pGAD10

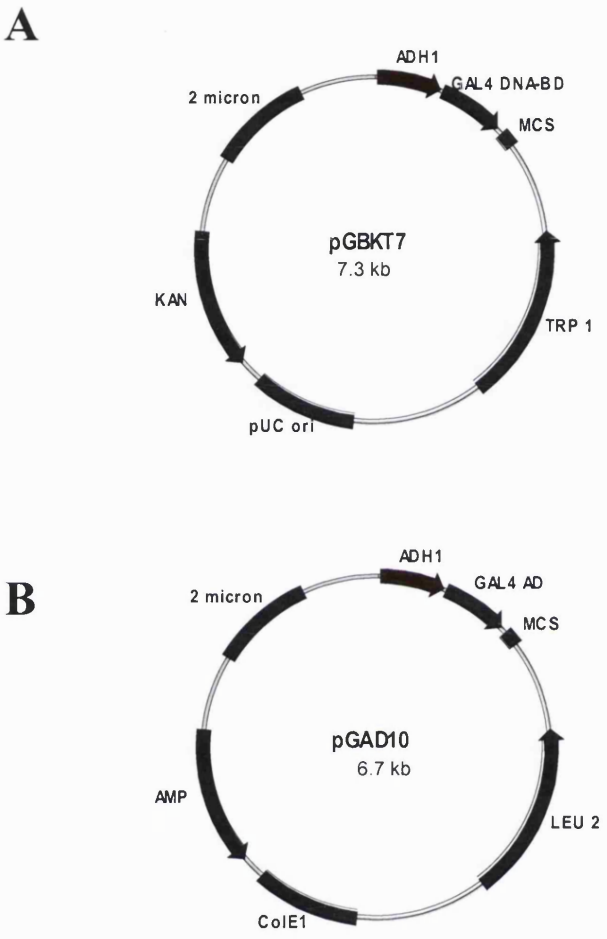

A, the pGBKT7 plasmid vector contains the gene encoding the GAL4 DNA-BD. A multiple-cloning site (MCS) dowstream from the GAL4 DNA-BD allows the insertion of a cDNA encoding a protein of interest. The promoter ADH1 enables the expression of the DNA-BD or DNA-BD fusion protein in yeast cells. A Leu marker allows the plasmid to grow on a media lacking leucine. A pUC ori enables the efficient replication of the plasmid in the bacteria strain *E.coli* and a kanamycin resistance (KAN) gene for growth on media containing kanamycin. B, the pGAD10 plasmid vector contains a gene encoding the GAL4 AD and a MCS dowstream from the GAL4 AD for the insertion of a cDNA encoding a protein of interest. The expression of the GAL4 AD or GAL4 AD fusion protein in yeast cells is controlled by an ADH1 promoter. A Trp marker allows the plasmid to grow on a media lacking tryptophan. An ampicillin (AMP) resistance gene enables the plasmid to grow on a media containing ampicillin.

Appendix 5.2. Procedure for the oligonucleotide sequencing of DNA samples using the ABI PRISM 310 Genetic Analysis system

DNA was sequenced by automated sequencing using the ABI PRISM 310 Genetic Analysis system (Applied Biosystems, Foster city, CA, USA). In this system, fluorescent dyes are coupled to the dideoxynucleoside triphosphates and they are used to detect the DNA fragments separated by capillary electrophoresis. Prior to capillary electrophoresis, the DNA to analyse was amplified by PCR and precipitated.

DNA amplification

The PCR reaction mix was composed of 150-300 ng DNA, 2 µl BigDye Terminator (containing AmpliTaq® DNA polymerase and BigDye terminators), 2 µl sequencing buffer 5X (400 mM Tris-HCl, 10 mM $MgCl_2$, pH 9.0), 0.33 µM primer in a final volume of 10 µl. The DNA was amplified using the following PCR programme: the DNA was denaturated at 95°C for 5 min, then 25 amplification cycles were performed: 95°C for 30 sec, 55°C for 20 sec, 60°C for 4 min. After amplification, the DNA was purified by using the ethanol precipitation method.

DNA precipitation

The precipitation of DNA was carried out by adding 1 µl sodium acetate 3M and 25 µl 100% ethanol to 10 µl amplified DNA. The mixture was incubated for 15 min on ice, and centrifuged at 13000 rpm for 30 min at RT. The supernatant was removed and 100 µl ice-cold 70% (v/v) ethanol was added to the pellet and centrifuged twice at 13000 rpm for 1 min at RT. The supernatant was removed and the pellet was dried at RT for 15 min. The pellet was resuspended in 20 µl template suppression buffer and heated for 2 min at 95°C. The sample was immediately loaded onto the ABI PRISM 310 Genetic Analyser. Nucleotide sequences were visualised using Contig Express (Vector NTI 5.0 package).

Appendix 5.3. Vector map of pcDNAHisMax-mOGT$_{40-374}$

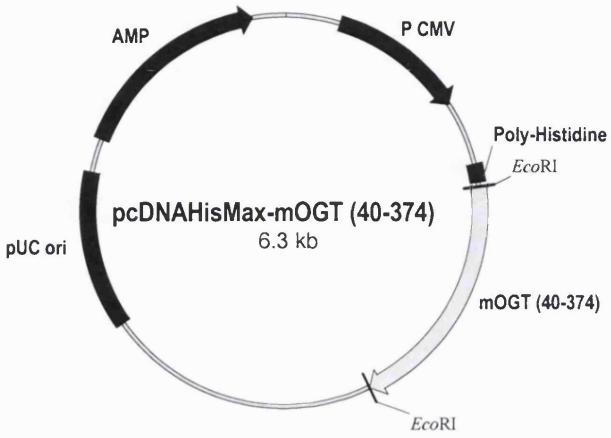

The cDNA encoding mOGT$_{40-374}$ was sub-cloned in frame into the *EcoRI* restriction site of the cloning vector pcDNAHisMax to yield an N-terminal His-tagged mOGT$_{40-374}$. His-tagged mOGT$_{40-374}$ expression in mammalian cell lines is controlled by a CMV promoter. The pcDNAHisMax-mOGT$_{40-374}$ plasmid contains a pUC ori for replication in bacteria and an ampicillin resistance gene (AMP) for growth on media containing ampicillin.

Appendix 5.4. Vector map of pCMVTag4a-OGT

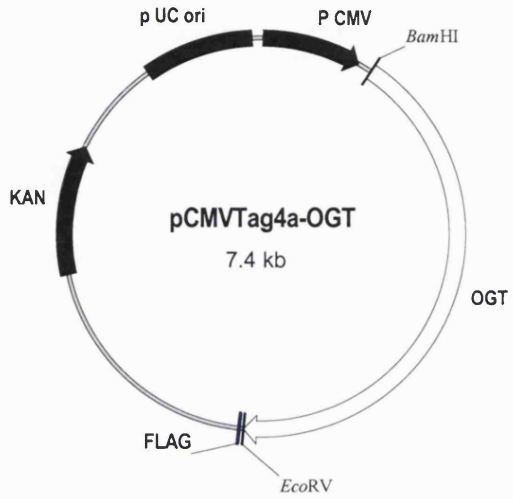

The cDNA encoding ncOGT was sub-cloned in frame into the *BamHI/EcoRV* restriction sites of pCMVTag4a yielding pCMVTag4a-OGT. This construct encodes a C-terminal FLAG-tagged ncOGT. The expression of FLAG-OGT in mammalian cells is controlled by a CMV promoter. The pCMVTag4a-OGT plasmid contains a pUC ori for replication in the bacteria strain *E.coli* and a kanamycin resistance gene (KAN) for growth on selective media containing kanamycin.

Appendix 5.5. Vector map of pEYFP-OGT

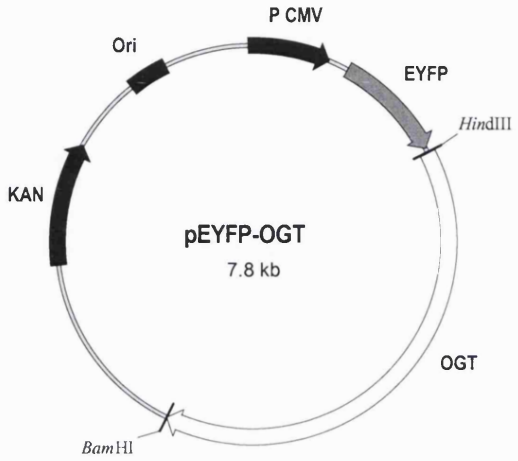

The cDNA encoding ncOGT was sub-cloned in frame into the *HindIII/BamHI* restriction sites of pEYFP-C1 yielding pEYFP-OGT. This construct encodes an N-terminal EYFP-tagged ncOGT, i.e. EYFP-OGT.

Appendix 7.1

CHAPTER 7

CAN THE CYTOTRAP® YEAST TWO-HYBRID SYSTEM BE USED TO FIND NEW GRIF-1 ASSOCIATED PROTEINS?

7.1. INTRODUCTION

7.1.1. Rationale

As explained earlier (Chapter 1), GRIF-1 is a 913 amino acid protein of unknown function that was identified in a yeast two-hybrid rat brain cDNA library screen. A method of understanding GRIF-1 function was to search for new GRIF-1 interacting partners. Yeast two-hybrid technology is a well established technique to find putative interactors (Chapter 5). Initially, the GRIF-1 fragment originally isolated, i.e. GRIF-1_{8-633}, was used as a bait to perform a new screen. However a single interactor was found which was GRIF-1_{8-633} thus showing the ability of GRIF-1 to dimerise. Further attempts to use the full length GRIF-1, i.e. GRIF-1_{1-913}, as a bait failed because GRIF-1_{1-913} was auto-activating the reporter gene activity in the absence of a binding partner (Chapter 5). Thus the C-terminal domain of GRIF-1, i.e. GRIF-$1_{545-913}$, that was the longest GRIF-1 fragment not causing autonomous activation was the bait used in the next yeast two-hybrid screen (Chapter 5). However this approach limited the number of putative GRIF-1 interactors that could be identified to GRIF-1 C-terminal domain associated proteins. Further the spatial conformation of the GRIF-1 C-terminal domain may be different to that found for the full length protein. Therefore, it would be more informative to use GRIF-1_{1-913} as the bait. Since this was not feasible in the conventional yeast two-hybrid system, the newly developed CytoTrap® yeast two-hybrid system was used as a potential alternative to find new GRIF-1 interactors.

7.1.2. The principle of the CytoTrap® yeast two-hybrid system

The CytoTrap® yeast two-hybrid system, or son of sevenless (Sos) recruitment system, was initially developed to identify inhibitors of a transcription factor (Aronheim *et al.*, 1997). It uses cytoplasmic signalling molecules instead of transcription factors for the detection of protein-protein interactions. Interactions are detected in the cytoplasm of the temperature-sensitive yeast strain, cdc25, instead of the nucleus as performed in the conventional yeast two-hybrid system (Chapter 5). The cdc25 yeast strain was mutated in the gene encoding the Ras guanyl nucleotide exchange factor (GEF), Cdc25, thus preventing growth at 37°C but not at 25°C.

The CytoTrap® system is based on the observation that the cdc25 mutant phenotype can be rescued by expressing a myristylated human Ras GEF, Sos, in the mutant yeast strain thereby restoring growth at 37°C. Indeed myristylated Sos was targeted to the

plasma membrane and it activated Ras and the Ras signalling cascade which resulted in cell growth at 37°C.

To carry out a CytoTrap® interaction assay, 2 proteins of interest, i.e. a bait and a fish, are fused to either Sos or to a membrane localisation signal, i.e. a myristylation, sequence respectively and expressed in the yeast strain, cdc25Hα. Following bait-fish protein interaction, Sos is recruited to the cell membrane, activates Ras and its signalling cascade thus promoting growth at 37°C (Figure 7.1).

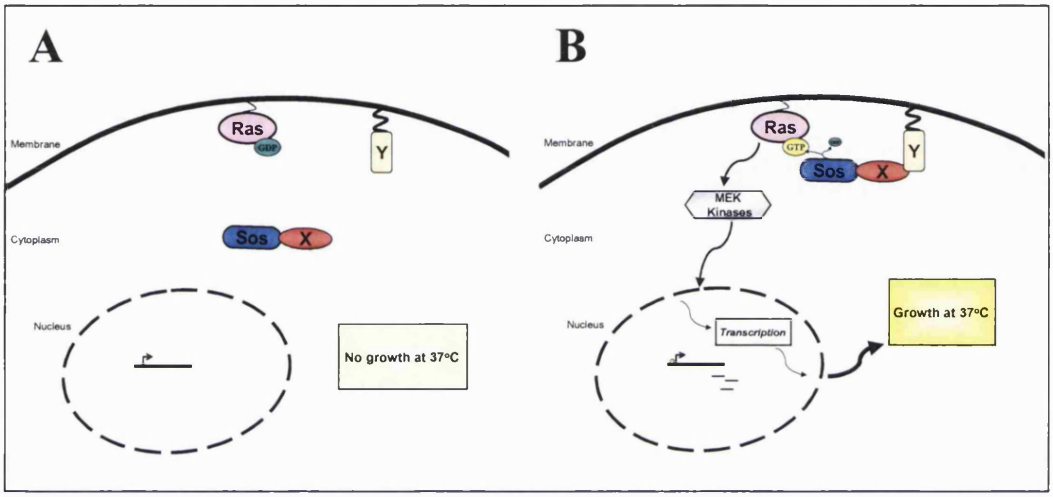

Figure 7.1. A schematic diagram depicting the principle of the CytoTrap® yeast two-hybrid system. Two putative interacting proteins, i.e. X and Y, were fused to the human Sos protein and to the v-Src myristylation sequence to yield Sos-X and Myr-Y and they were co-transformed in the yeast strain, cdc25Hα. A, X and Y do not interact. Sos-X is located in the cytoplasm and Myr-Y is targeted to the membrane. Ras is in a GDP-bound inactive form, no growth is observed at the restrictive temperature of 37°C. B, X and Y interact. Sos-X is targeted to the membrane via its association to Myr-Y, activates Ras and its signalling pathway by promoting the exchange of GDP by GTP, thus resulting in cell growth at 37°C.

Bait and fish fusion proteins are generated by sub-cloning each protein of interest in frame in either the pSos or the pMyr cloning vectors (Table 2.3, Figure 7.2 A-B). The pSos vector encodes the human Sos_{1-1067} protein under the control of an ADH1 promoter and it contains a leucine (L) nutritional selection marker. The pMyr vector encodes the v-Src myristylation sequence under the control of the GAL1 promoter and it contains a uracil (U) nutritional selection marker. Expression of Sos is constitutive whereas expression of the myristylation signal sequence is induced by galactose. Thus, protein-protein interactions are detected by assessing reporter gene activity, i.e. growth at the restrictive temperature of 37°C, on a galactose-selective media lacking leucine and uracil.

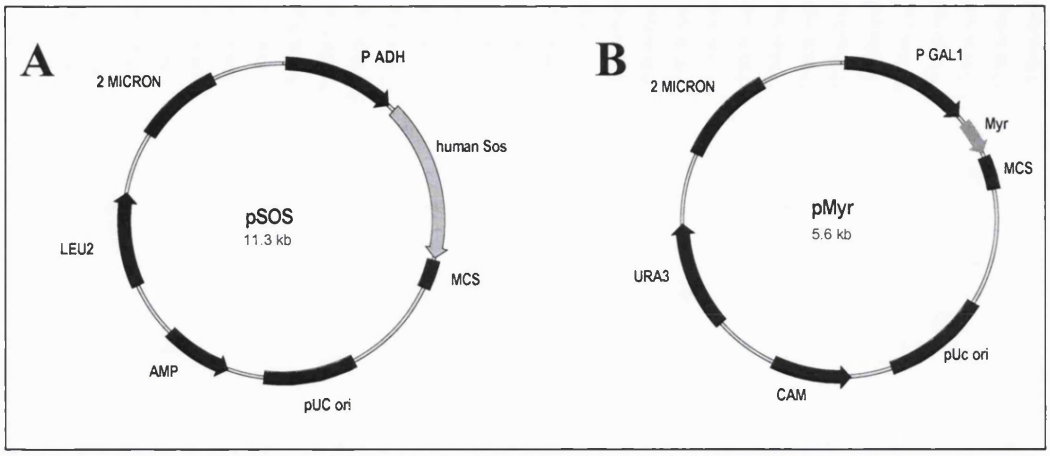

Figure 7.2. Vector map of the CytoTrap® yeast two-hybrid system cloning vectors, pSos and pMyr. A, the pSos plasmid contains the cDNA encoding the human SOS protein followed by a multiple cloning site for the insertion of a cDNA encoding a protein of interest. The expression of Sos or Sos-fusion protein in yeast cells is controlled by an ADH1 promoter. A Leu marker enables the selection on a media lacking leucine. A 2 micron ori and a pUC ori enable the efficient replication in the cdc25Hα yeast strain and in the *E.coli* bacteria strain respectively. An ampicillin resistance (AMP) gene allows growth on media containing ampicillin. B, the pMyr plasmid contains a v-Src myristylation sequence followed by a multiple cloning site for insertion of a cDNA encoding a protein of interest. The Myr fusion protein is controlled by an inducible GAL1 promoter. A Ura marker enables growth on a media lacking uracil. The pMyr plasmid also contains a 2 micron ori and a pUC ori for efficient replication in the cdc25Hα yeast strain and in the *E.coli* bacteria strain respectively and a chloramphenicol resistance gene (CAM) for growth on media containing chloramphenicol.

The advantage of the CytoTrap® yeast two-hybrid system over the traditional systems, e.g. GAL4 yeast two-hybrid (Chapter 7), is that protein-protein interactions are detected within the yeast cytoplasm rather than in the nucleus. Thus the bait and fish proteins used in the assay are post-translationally modified. This is important since many protein-protein interactions are dependent on the post-translationally state of the protein as seen for example for AP2/$GABA_A$ receptor β subunit interactions (Chapter 1; Kittler *et al.*, 2004a).

7.1.3. Aim of this chapter

The aim of this chapter was to investigate whether the CytoTrap® yeast two-hybrid system could be used to search for new GRIF-1 associated proteins thus enabling further insights into GRIF-1 function. This was achieved by (i) assessing the ability of GRIF-1 to auto-activate the reporter gene activity, (ii) testing the known interaction between GRIF-1 and the $GABA_A$ receptor β2 subunit intracellular loop and (iii) testing the ability of GRIF-1 to dimerise in the CytoTrap® yeast two-hybrid system.

7.2. RESULTS

7.2.1. Verification of the authenticity of the CytoTrap® yeast two-hybrid system

Since the CytoTrap® yeast two-hybrid system had never been used before in the laboratory, it was necessary to check the yeast strain, cdc25Hα, phenotype for temperature and nutritional revertancy and to ensure that known protein-protein interactions could be detected using this system.

7.2.1.1. Verification of the yeast strain, cdc25Hα, phenotype

Yeast cells were plated from a glycerol stock onto a glucose-based media (YPAD) and incubated at either 25°C or 37°C for 4 days. Growth was observed at the permissive temperature of 25°C but not at the restrictive temperature of 37°C (Chapter 2). This showed that the cdc25Hα yeast strain was not temperature revertant. Next, yeast cells were plated onto glucose-based selective media lacking either L, U, H or W at 25°C. No growth was observed on any selective media. This demonstrated that the cdc25Hα yeast strain was not revertant for the nutritional selection markers. Thus the cdc25Hα yeast strain had the expected phenotype and it could be used to carry out CytoTrap® interaction assays.

7.2.1.2. Establishment of the CytoTrap® technology

To test whether the CytoTrap® system was working, cdc25Hα yeast cells were co-transformed with different pairs of positive and negative control plasmids that were provided with the CytoTrap® yeast two-hybrid kit (Table 2.3). The positive control combinations were (i) pSos-MAFB + pMyr-MAFB and (ii) pSos-MAFB + pMyr-SB. MAFB is a transcription factor that forms dimers, therefore Sos-MAFB should interact with Myr-MAFB. SB is a Sos binding protein and thus should interact with Sos or Sos fusion proteins. The negative control plasmid pairs were (i) pSos-ColI + pMyr-MAFB, (ii) pSos-MAFB + pMyr-LaminC and (iii) pSos + pMyr. Col I is murine collagenase and it has never been reported to interact with MAFB, therefore no interaction is expected between Sos-ColI and Myr-MAFB. Lamin C is human lamin C and it is not known to associate either with Sos or with MAFB, thus no interaction should be detected between Sos-MAFB and Myr-Lamin C. Finally no interaction should be detected between Sos and the myristylation sequence, Myr.

Co-transformants were grown on glucose and galactose selective media at 25°C and protein-protein interactions were detected as explained in section 2.2.3.5.1. Thus,

cdc25Hα yeast cells were co-transformed with the following combinations: pSos-MAFB + pMyr-MAFB, pSos-MAFB + pMyr-SB, pSos-ColI + pMyr-MAFB, pSos-MAFB + pMyr-LaminC and pSos + pMyr. The results are shown in Table 7.1.

pSos construct	pMyr construct	(-U, -L) Glucose at 25°C	(-U, -L) Galactose at 25°C	(-U, -L) Glucose at 37°C	(-U, -L) Galactose at 37°C
pSos-MAFB	pMyr-MAFB	√	√	-	√
pSos-MAFB	pMyr-SB	√	√	-	√
pSos-MAFB	pMyr-laminC	√	√	-	-
pSos-ColI	pMyr-MAFB	√	√	-	-
pSos	pMyr	√	√	-	-

Table 5.1. The CytoTrap® yeast two-hybrid system can be used to detect known protein-protein interactions. Cdc25Hα yeast cells were co-transformed with different positive and negative control combinations. Protein-protein interactions were detected on (-U, -L) galactose selective media at 37°C. This Table shows that the positive control combinations, i.e. pSos-MAFB + pMyr-MAFB and pSos-MAFB + pMyr-SB, grew on (-U, -L) galactose-based media at 37°C whereas the negative control combinations, i.e. pSos-MAFB + pMyr-LaminC, pSos-ColI + pMyr-MAFB and pSos + pMyr, showed no growth under the same conditions."-U, -L", media lacking uracil and leucine; "-", no growth; "√", growth. These results are representative of n = 3 independent co-transformations.

For each co-transformation, growth was observed on (-U, -L) glucose and (-U, -L) galactose selective media at the permissive temperature of 25°C, thus showing that each plasmid was successfully transformed into the cell. For detection of protein-protein interactions, no co-transformants grew on the (-U, -L) glucose selective media at 37°C. This was expected since activation of the transcription of the Myr fusion construct requires galactose. For the positive control combinations, growth was observed on (-U, -L) galactose selective media at 37°C. No growth was observed under these conditions for the negative control combinations. Thus, the control plasmids behaved as expected thereby showing that the CytoTrap® yeast two-hybrid system worked properly.

7.2.2. Substantiation of the interaction between GRIF-1 and the $GABA_A$ receptor β2 subunit intracellular loop

It was shown that the CytoTrap® yeast two-hybrid system could be used to detect known protein-protein interactions. To investigate whether this system could be used to find new GRIF-1 associated proteins, a full length GRIF-1 bait construct, i.e. pSos-GRIF-$1_{1\text{-}913}$, was generated and tested for its ability to auto-activate reporter gene

activity. Then, prior to performing a yeast two-hybrid screen using Sos-GRIF-$1_{1\text{-}913}$ as a bait, it was checked whether the known interaction between GRIF-1 and the $GABA_A$ receptor β2 subunit intracellular loop could be verified in the CytoTrap® system. Therefore a $GABA_A$ receptor β2 subunit intracellular loop fish construct, i.e. pMyr-β2-$IL_{303\text{-}427}$, was prepared and the interaction between Sos-GRIF-$1_{1\text{-}913}$ and Myr-β2-$IL_{303\text{-}427}$ was assayed in the CytoTrap® system.

7.2.2.1. Preparation of pSos-GRIF-$1_{1\text{-}913}$ and pMyr-β2-$IL_{303\text{-}427}$

GRIF-$1_{1\text{-}913}$ was amplified by PCR from pCIS-GRIF-1 by using the appropriate oligonucleotide primers and sub-cloned in frame into the *BamHI/NotI* restriction site of the pSos cloning vector yielding pSos-GRIF-$1_{1\text{-}913}$ (Figure 7.3 A). The $GABA_A$ receptor β2 subunit $IL_{303\text{-}427}$ was amplified by PCR from pCIS-GABAR-β2 and inserted in frame into the *EcoRI/SalI* restriction sites of the pMyr cloning vector yielding pMyr-β2-$IL_{303\text{-}427}$ (Figure 7.3 B). Each construct was verified by oligonucleotide sequencing using the ABI PRISM 310 Genetic Analyser System (Appendix 2.1).

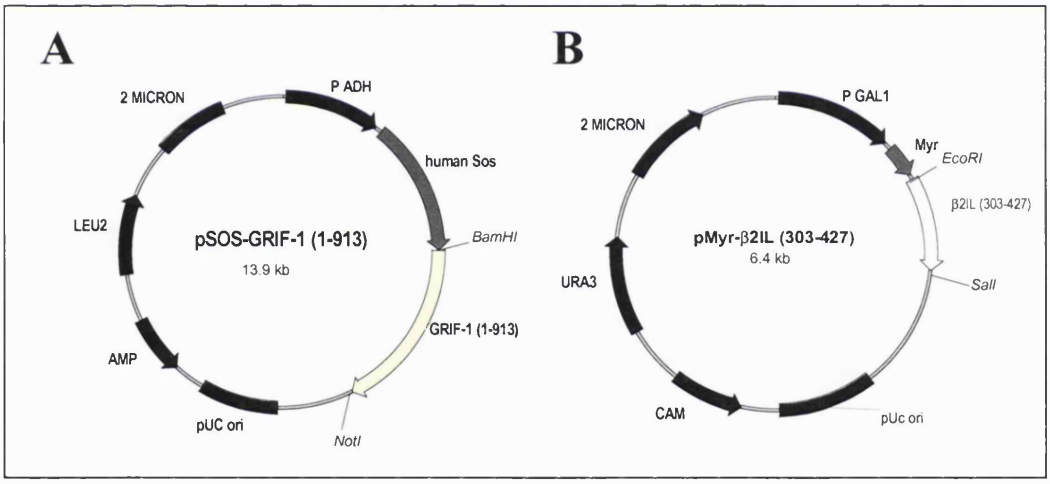

Figure 7.3. Vector map of pSos-GRIF-$1_{1\text{-}913}$ and pMyr-β2-$IL_{303\text{-}427}$. A, the cDNA encoding GRIF-1 was inserted in frame into the *BamHI/EcoRI* restriction sites of the pSos cloning vector to yield the bait construct, pSos-GRIF-$1_{1\text{-}913}$; B, the cDNA encoding $GABA_A$ receptor intracellular loop, i.e. β2-$IL_{303\text{-}427}$, was inserted in frame into *EcoRI/SalI* restriction sites of the pMyr cloning vector to yield the construct, pMyr-β2-$IL_{303\text{-}427}$.

7.2.2.2. Characterisation of Sos-GRIF-$1_{1\text{-}913}$ and Myr-β2-$IL_{303\text{-}427}$ fusion proteins

To test whether Sos-GRIF-$1_{1\text{-}913}$ and Myr-β2-$IL_{303\text{-}427}$ were correctly expressed, cdc25Hα yeast cells were transformed with either pSos-GRIF-$1_{1\text{-}913}$ or pMyr-β2-$IL_{303\text{-}427}$. Protein extracts of transformed cells were prepared and analysed by immunoblotting using anti-GRIF-$1_{8\text{-}633}$ or anti-$GABA_A$ receptor $\beta2_{381\text{-}395}$ polyclonal antibodies. The results are shown in Figures 7.4-7.5.

Sos-GRIF-1$_{1-913}$- Anti-GRIF-1$_{8-633}$ antibodies detected a band with M_r = 217 kDa in protein extracts of cells transformed with pSos-GRIF-1$_{1-913}$ (lane 2, Figure 7.4). This band was consistent with that predicted for pSos-GRIF-1$_{1-913}$. A non-specific band with M_r = 98 kDa was also detected. This band was also recognised in protein extracts of untransformed cells (lane 1, Figure 7.4) thus showing that it was a non-specific band.

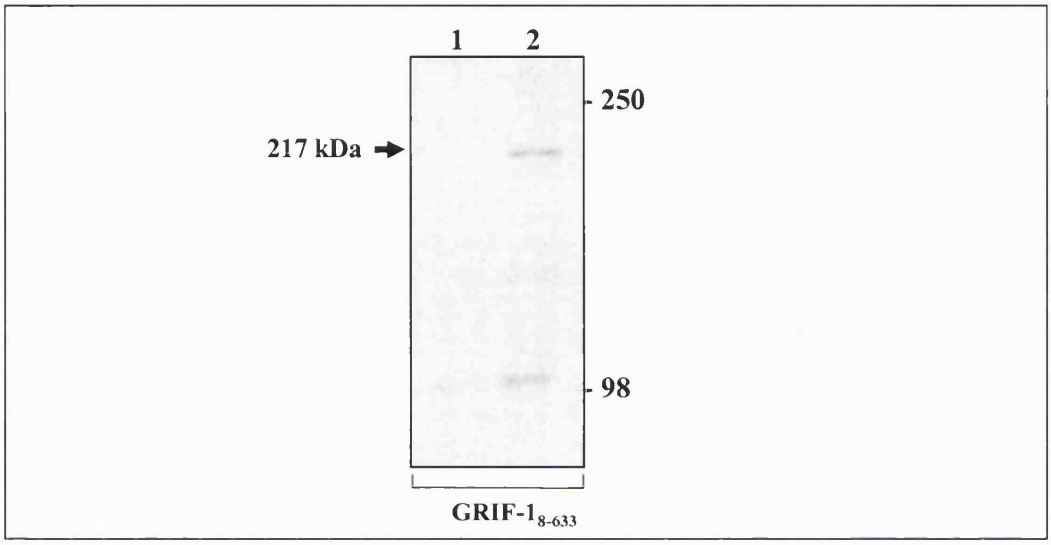

Figure 7.4. Expression of Sos-GRIF-1$_{1-913}$ in the cdc25Hα yeast strain. The yeast strain, cdc25Hα, was transformed with pSos-GRIF-1$_{1-913}$. Proteins were extracted and analysed by immunoblotting using anti-GRIF-1$_{8-633}$ antibodies. Lane 1, untransformed yeast cells; lane 2, protein extract of cells transformed with pSos-GRIF-1$_{1-913}$. The molecular weight standards (kDa) are shown on the right. The immunoreactive band of interest is indicated by an arrow, M_r = 217 kDa. This immunoblot is representative of n = 2 experiments from n = 2 independent transformations.

Myr-β2-IL$_{303-427}$- Anti-GABA$_A$ receptor β2$_{381-395}$ antibodies recognised 2 immunoreactive bands with M_r = 16 kDa and M_r = 80 kDa in protein extracts of cells transformed with pMyr-β2-IL$_{303-427}$ (lane 2, Figure 7.5). The M_r = 16 kDa band corresponded to that predicted for pMyr-β2-IL$_{303-427}$. The band with M_r = 80 kDa was also detected in protein extracts of untransformed cells thus showing that it was not specific (lane 1, Figure 7.5).

These results showed that Sos-GRIF-1$_{1-913}$ and Myr-β2-IL$_{303-427}$ were expressed in cdc25Hα yeast cells and they had a M_r in agreement with those predicted (Figure 7.6).

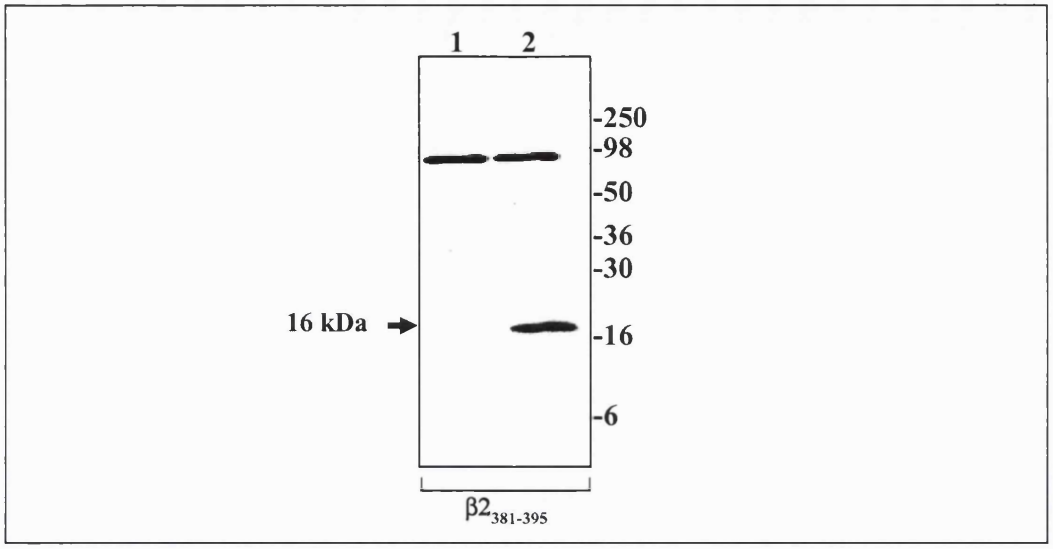

Figure 7.5. Expression of Myr-β2-IL$_{303-427}$ in the cdc25Hα yeast strain. The yeast strain, cdc25Hα, was transformed with pMyr-β2-IL$_{303-427}$. Proteins were extracted and analysed by immunoblotting using anti-β2$_{381-395}$ antibodies. Lane 1, untransformed yeast cells; lane 2, protein extract of cells transformed with pMyr-β2-IL$_{303-427}$. The molecular weight standards (kDa) are shown on the right. The immunoreactive band of interest is indicated by an arrow. M_r = 16 kDa. This immunoblot is representative of n = 2 transformations.

A

Fusion protein	Calculated M_r (kDa)	Experimental M_r (kDa)
SOS-GRIF-1$_{1-913}$	226	217
MYR-GRIF-1$_{1-913}$	139	139
MYR-β2-IL$_{303-427}$	17	16

B

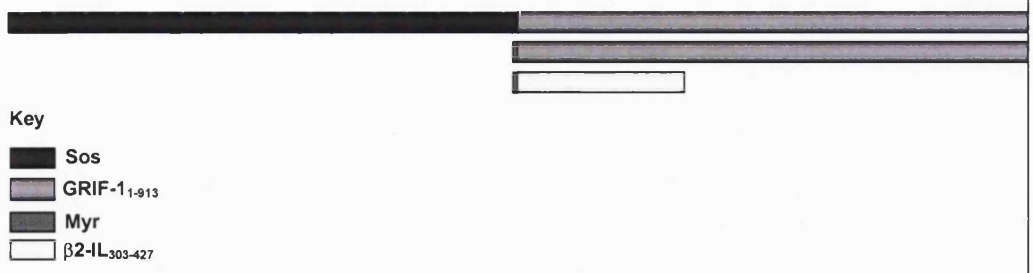

Figure 7.6. A Figure summarising the structure and molecular weight (M_r) of the CytoTrap® fusion proteins. A, a Table summarising the calculated and experimental M_r; B, schematic diagram drawn to scale of Sos- and Myr-fusion constructs.

7.2.2.3. CytoTrap® interaction assays

Sos-GRIF-1_{1-913} and Myr-β2-$IL_{303-427}$ fusion proteins were generated and shown to be expressed in cdc25Hα yeast cells therefore they could be used to carry out yeast two-hybrid interaction assays.

First, it was checked that:

- Sos-GRIF-1_{1-913} was correctly targeted to the cell membrane
- Sos-GRIF-1_{1-913} did not cause autonomous activation of the reporter gene activity.

The membrane localisation was tested by using the combination pSos-GRIF-1_{1-913} + pMyr-SB. The myristylated SB is targeted to the cell membrane and it interacts with Sos or a Sos-fusion protein that is located at the membrane. The auto-activation ability was assessed using the combination pSos-GRIF-1_{1-913} + pMyr. Since no GRIF-1 associated protein is present, no interaction and thus, no growth on (-U, -L) galactose selective media at the permissive temperature of 37°C should be detected. Therefore, cdc25Hα yeast cells were co-transformed with test, positive and negative control combinations, grown on (-U, -L) glucose and (-U, -L) galactose selective media at 25°C and protein-protein interactions were detected as explained in section 2.2.3.5.1. Thus cdc25Hα yeast cells were co-transformed with the following combinations: pSos-GRIF-1_{1-913} + pMyr-SB, pSos-GRIF-1_{1-913} + pMyr, pSos-MAFB + pMyr-MAFB, pSos-MAFB + pMyr-LaminC and pSos + pMyr. The results are shown in Table 7.2. For all co-transformations, growth was observed on (-U, -L) glucose and (-U, -L) galactose selective media at 25°C, thus showing that all plasmids were transformed. For detection of protein-protein interactions, no co-transformants grew on (-U, -L) glucose selective media at 37°C as expected. The positive control combination, i.e. pSos-MAFB + pMyr-MAFB, and the combination pSos-GRIF-1_{1-913} + pMyr-SB grew on (-U, -L) galactose selective media at 37°C, thus showing that Sos-GRIF-1_{1-913} was localised at the membrane via its interaction with Myr-SB. The negative control combinations, i.e. pSos-MAFB + pMyr-LaminC and pSos + pMyr, and the pSos-GRIF-1_{1-913} + pMyr combination showed no growth on (-U, -L) galactose selective media at 37°C. This showed that no interactions were detected and thus that Sos-GRIF-1_{1-913} did not auto-activate the reporter gene activity in absence of a binding partner. To summarise, these assays demonstrated that:

- Sos-GRIF-1_{1-913} was targeted to the membrane
- Sos-GRIF-1_{1-913} did not cause auto-activation of the reporter gene

Therefore Sos-GRIF-$1_{1\text{-}913}$ could be used as a bait in CytoTrap® yeast two-hybrid interaction assays.

pSos construct	pMyr construct	(-U, -L) Glucose at 25°C	(-U, -L) Galactose at 25°C	(-U, -L) Glucose at 37°C	(-U, -L) Galactose at 37°C
pSos-GRIF-$1_{1\text{-}913}$	pMyr-SB	√	√	-	√
pSos-GRIF-$1_{1\text{-}913}$	pMyr	√	√	-	-
pSos-MAFB	pMyr-MAFB	√	√	-	√
pSos-ColI	pMyr-MAFB	√	√	-	-
pSos	pMyr	√	√	-	-

Table 7.2. Demonstration that Sos-GRIF-$1_{1\text{-}913}$ is targeted to the cell membrane in the presence of an interacting partner but it does not activate the receptor gene activity in the CytoTrap® yeast two-hybrid system. Cdc25Hα yeast cells were co-transformed with different pSos and pMyr combinations and protein-protein interactions were detected on galactose selective media at 37°C. An interaction was detected between Sos-GRIF-$1_{1\text{-}913}$ and Myr-SB on galactose selective media at 37°C, thus showing that Sos-GRIF-$1_{1\text{-}913}$ could be targeted to the membrane in presence of an interactor. No interaction was detected in the absence of a Sos-GRIF-$1_{1\text{-}913}$ binding partner, thus showing that Sos-GRIF-$1_{1\text{-}913}$ does not activate reporter gene activity under these conditions. These results are representative of n = 3 independent co-transformations. "-U, -L", media lacking uracil and leucine; "-", no growth; "√", growth.

As described in Chapter 1, GRIF-1 associates specifically with the $GABA_A$ receptor β2 subunit intracellular loop in the GAL4 yeast two-hybrid system (Beck *et al.*, 2002). To check whether this interaction could be detected in the CytoTrap® system, cdc25Hα yeast cells were co-transformed with pSos-GRIF-$1_{1\text{-}913}$ + pMyr-β2-$IL_{303\text{-}427}$ and the positive and negative control combinations and interactions were analysed as before. The results are shown in Table 7.3. All plasmids were co-transformed in yeast cells as shown by transformant growth on (-U, -L) glucose and (-U, -L) galactose selective media at 25°C. For the detection of protein-protein interactions, growth was observed on (-U, -L) galactose selective media at 37°C for the positive controls but not for the negative control, thus showing that the CytoTrap® interaction assay worked and that Sos-GRIF-$1_{1\text{-}913}$ was targeted to the membrane. However, no growth was observed on (-U, -L) galactose selective media at 37°C for the pSos-GRIF-$1_{1\text{-}913}$ + pMyr-β2-$IL_{303\text{-}427}$ combination, thus showing that no interaction was detected between Sos-GRIF-$1_{1\text{-}913}$ and Myr-β2-$IL_{303\text{-}427}$, although Sos-GRIF-$1_{1\text{-}913}$ was expressed and localised to the

membrane. This was not expected since GRIF-$1_{1\text{-}913}$ had been shown previously to interact with β2-$IL_{303\text{-}427}$ in a GAL4-based yeast two-hybrid assay (Beck *et al.*, 2002).

pSos construct	pMyr construct	(-U, -L) Glucose at 25°C	(-U, -L) Galactose at 25°C	(-U, -L) Glucose at 37°C	(-U, -L) Galactose at 37°C
pSos-GRIF-$1_{1\text{-}913}$	pMyr-β2-$IL_{303\text{-}427}$	√	√	-	-
pSos-GRIF-$1_{1\text{-}913}$	pMyr-SB	√	√	-	√
pSos-GRIF-$1_{1\text{-}913}$	pMyr	√	√	-	-
pSos-MAFB	pMyr-MAFB	√	√	-	√
pSos-CollI	pMyr-MAFB	√	√	-	-
pSos	pMyr	√	√	-	-

Table 7.3. Co-transformation of Sos-GRIF-$1_{1\text{-}913}$ and the $GABA_A$ receptor β2 subunit intracellular loop in the CytoTrap® yeast two-hybrid system. Cdc25Hα yeast cells were co-transformed with different pSos and pMyr combinations and protein-protein interactions were detected on galactose selective media at 37°C. This table shows that Sos-GRIF-$1_{1\text{-}913}$ and Myr-β2-$IL_{303\text{-}427}$ do not activate reporter gene activity, i.e. growth at 37°C on galactose-based media, although Sos-GRIF-$1_{1\text{-}913}$ can be targeted to the membrane in the presence of a binding partner as shown by the control pSos-GRIF-$1_{1\text{-}913}$ + pMyr-SB. These results are representative of n = 3 independent co-transformations. "-U, -L", media lacking uracil and leucine; "-", no growth; "√", growth.

7.2.3. Substantiation of GRIF-1-dimers formation in the CytoTrap® yeast two-hybrid system

The interaction between GRIF-$1_{1\text{-}913}$ and β2-$IL_{303\text{-}427}$ could not be detected in a CytoTrap® yeast two-hybrid assay. This could be because this interaction was of low affinity as initially reported (Beck *et al.*, 2002; Chapter 3). Optimisation of the system would be easier if high affinity interacting proteins could be used as bait and fish in a CytoTrap® interaction study. GRIF-1 was shown to form homodimers in GAL4 yeast two-hybrid interaction assays and in immunoprecipitation experiments (M. Beck, G. Ojla, K. Brickley and F.A. Stephenson, unpublished observations). Therefore GRIF-1/GRIF-1 interactions were investigated using the CytoTrap® technology. A Myr-GRIF-$1_{1\text{-}913}$ fusion protein was generated and the Sos-GRIF-$1_{1\text{-}913}$/Myr-GRIF-$1_{1\text{-}913}$ interaction was assessed.

7.2.3.1. Preparation of pMyr-GRIF-$1_{1\text{-}913}$

GRIF-$1_{1\text{-}913}$ was amplified by PCR from pCIS-GRIF-1 by using oligonucleotide primers containing the *EcoRI/SalI* restriction sites at their 5'-ends. The PCR product was sub-cloned in frame into the *EcoRI/SalI* restriction sites of the pMyr cloning vector yielding pMyr-GRIF-$1_{1\text{-}913}$ (Figure 7.7). The construct was verified by oligonucleotide sequencing using the ABI PRISM 310 Genetic Analyser system (Appendix 2.1)

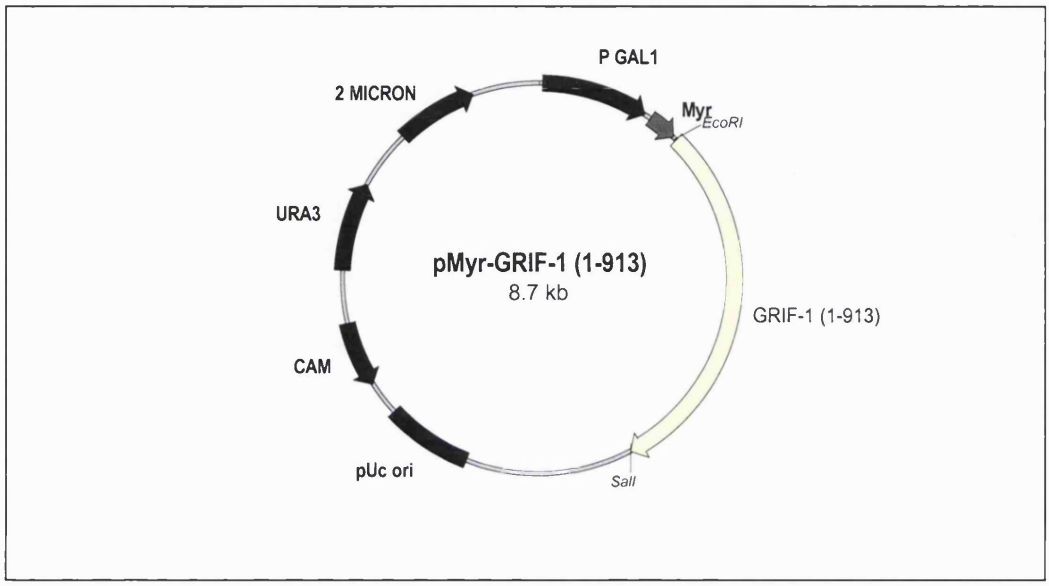

Figure 7.7. Vector map of pMyr-GRIF-$1_{1\text{-}913}$. The cDNA encoding GRIF-1 was inserted in frame into the *EcoRI/SalI* restriction sites of the pMyr cloning vector to yield the construct, pMyr-GRIF-$1_{1\text{-}913}$.

7.2.3.2. Characterisation of Myr-GRIF-$1_{1\text{-}913}$ fusion protein

The expression of Myr-GRIF-$1_{1\text{-}913}$ in cdc25Hα yeast cells was checked by transforming yeast cells with pMyr-GRIF-$1_{1\text{-}913}$ and analysing protein extracts of transformed cells by immunoblotting using anti-GRIF-$1_{8\text{-}633}$ antibodies. The result is shown in Figure 7.8. A single immunoreactive band with M_r = 139 kDa was recognised by anti-GRIF-$1_{8\text{-}633}$ antibodies in protein extracts of transformed cells (Lane 4, Figure 7.8). This band was consistent with that predicted for Myr-GRIF-$1_{1\text{-}913}$ (Figure 7.6), thus showing that Myr-GRIF-$1_{1\text{-}913}$ was expressed in cdc25Hα yeast cells.

7.2.3.3. CytoTrap® interaction assay

Myr-GRIF-$1_{1\text{-}913}$ was shown to be expressed in cdc25Hα yeast cells and therefore it was used to test the Sos-GRIF-$1_{1\text{-}913}$/Myr-GRIF-$1_{1\text{-}913}$ interaction using the CytoTrap® system. Therefore, cdc25Hα yeast cells were co-transformed with the test and control combinations and interactions were detected as explained before. Thus cdc25Hα yeast cells were co-transformed with pSos-GRIF-$1_{1\text{-}913}$ + pMyr-GRIF-$1_{1\text{-}913}$, pSos-GRIF-$1_{1\text{-}913}$

+ pMyr-SB, pSos-MAFB + pMyr-MAFB, pSos-MAFB + pMyr-LaminC and pSos + pMyr. The results are shown in Table 7.4. For all co-transformations, growth was observed on (-U, -L) glucose and (-U, -L) galactose selective media at 25°C, thus showing that all plasmids were transformed. For the detection of protein-protein interactions, growth was observed on (-U, -L) galactose selective media at 37°C for the positive control, including the combination pSos-GRIF-$1_{1\text{-}913}$ + pMyr-SB, but not for the negative control. This showed that the CytoTrap® interaction assay worked and that pSos-GRIF-$1_{1\text{-}913}$ could be targeted to the membrane. However, no growth was observed on (-U, -L) galactose selective media at 37°C for the pSos-GRIF-$1_{1\text{-}913}$ + pMyrGRIF-$1_{1\text{-}913}$ combination, thus showing that the Sos-GRIF-$1_{1\text{-}913}$/Myr-GRIF-$1_{1\text{-}913}$ interaction could not be detected.

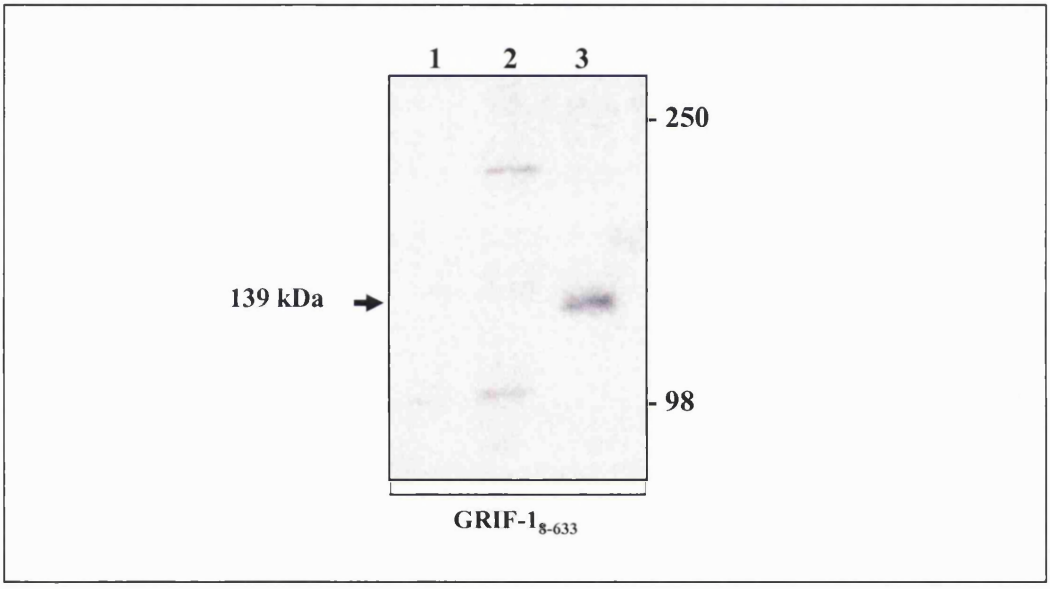

Figure 7.8. Expression of Myr-GRIF-$1_{1\text{-}913}$ in the cdc25Hα yeast strain. The yeast strain, cdc25Hα, was transformed with either pSos-GRIF-$1_{1\text{-}913}$ or pMyr-GRIF-$1_{1\text{-}913}$. Proteins were extracted and analysed by immunoblotting using anti-GRIF-$1_{8\text{-}633}$ antibodies. Lane 1, untransformed yeast cells; lane 2, protein extract of cells transformed with pSos-GRIF-$1_{1\text{-}913}$; lane 3, protein extract of cells transformed with pMyr-GRIF-$1_{1\text{-}913}$. The molecular weight standards (kDa) are shown on the right. Immunoreactive band of interest is indicated by an arrow, M_r (Myr-GRIF-$1_{1\text{-}913}$) = 139 kDa. This immunoblot is representative of n = 2 experiments from n = 2 independent transformations.

pSos construct	pMyr construct	(-U, -L) Glucose at 25°C	(-U, -L) Galactose at 25°C	(-U, -L) Glucose at 37°C	(-U, -L) Galactose at 37°C
pSos-GRIF-$1_{1\text{-}913}$	pMyr- GRIF-$1_{1\text{-}913}$	√	√	-	-
pSos-GRIF-$1_{1\text{-}913}$	pMyr-SB	√	√	-	√
pSos-GRIF-$1_{1\text{-}913}$	pMyr	√	√	-	-
pSos-MAFB	pMyr-MAFB	√	√	-	√
pSos-ColI	pMyr-MAFB	√	√	-	-
pSos	pMyr	√	√	-	-

Table 7.4. Co-transformation of Sos-GRIF-$1_{1\text{-}913}$ and Myr-GRIF-$1_{1\text{-}913}$ in the CytoTrap® yeast two-hybrid system. Cdc25Hα yeast cells were co-transformed with different pSos and pMyr combinations and protein-protein interactions were detected on galactose selective media at 37°C. This table shows that Sos-GRIF-$1_{1\text{-}913}$ and Myr-GRIF-$1_{1\text{-}913}$ do not activate reporter gene activity, i.e. growth at 37°C on (-U, -L) galactose-based media, although Sos-GRIF-$1_{1\text{-}913}$ can be targeted to the membrane in the presence of a binding partner as shown by the control pSos-GRIF-$1_{1\text{-}913}$ + pMyr-SB. These results are representative of n = 3 independent co-transformations. "-U, -L", media lacking uracil and leucine; "-", no growth; "√", growth.

7.2.3.4. Further investigation on the formation of GRIF-1 dimers

The interaction between Sos-GRIF-$1_{1\text{-}913}$ and Myr-GRIF-$1_{1\text{-}913}$ constructs could not be detected in a CytoTrap® yeast two-hybrid interaction assay although the 2 proteins were expressed and Sos-GRIF-$1_{1\text{-}913}$ could be localised at the membrane. This suggested that Sos-GRIF-$1_{1\text{-}913}$/Myr-GRIF-$1_{1\text{-}913}$ dimers could not be formed in cdc25Hα yeast cell cytoplasm.

To test this hypothesis, protein extracts of transformed yeast cells were prepared and analysed in reducing or non-reducing conditions, i.e. with or without addition of DTT. Immunoblotting was carried out using anti-GRIF-$1_{874\text{-}889}$ antibodies. As mentioned in Chapter 1, GRIF-1 exists as disulphide-bridge linked homodimers. In the presence of DTT, disulphide bridges are reduced and Sos-GRIF-$1_{1\text{-}913}$ and Myr-GRIF-$1_{1\text{-}913}$ monomers should be detected. In the absence of DTT, disulphide bridges should persist and Sos-GRIF-$1_{1\text{-}913}$ and Myr-GRIF-$1_{1\text{-}913}$ dimers with $M_r \sim 2$ fold higher that the monomers should be detected. Thus, cdc25Hα yeast cells were co-transformed with pSos-GRIF-$1_{1\text{-}913}$ + pMyr, pMyr-GRIF-$1_{1\text{-}913}$ + pSos, pSos-GRIF-$1_{1\text{-}913}$ + pMyr-GRIF-$1_{1\text{-}913}$. The results are shown in Figure 7.9.

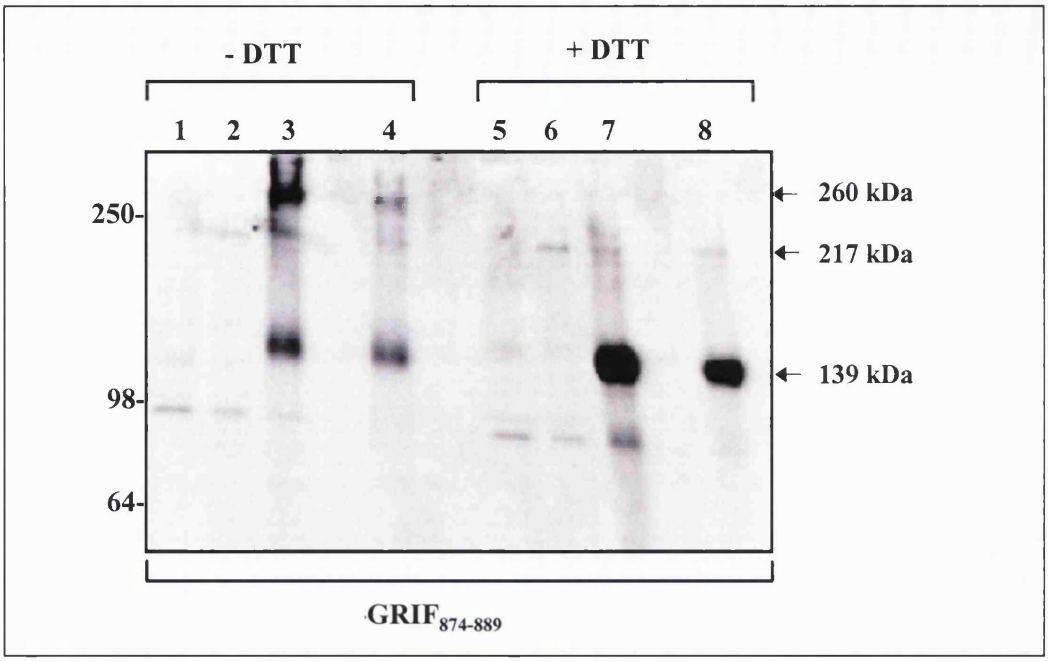

Figure 7.9. Investigation of the formation of Sos-GRIF-$1_{1\text{-}913}$/Myr-GRIF-$1_{1\text{-}913}$ dimer formation in the cdc25Hα yeast strain. The yeast strain, cdc25Hα, was transformed with either pSos-GRIF-$1_{1\text{-}913}$, pMyr-GRIF-$1_{1\text{-}913}$ or pSos-GRIF-$1_{1\text{-}913}$ + pMyr-GRIF-$1_{1\text{-}913}$. Protein extracts were prepared under reducing or non-reducing conditions, i.e. with or without the addition of DTT respectively, and analysed by immunoblotting using anti-GRIF-$1_{874\text{-}889}$ antibodies. Lanes 1-4, non-reducing conditions, lanes 5-8, reducing conditions. Lanes 1, 5, untransformed yeast cells; lanes 2, 6, protein extract of cells transformed with pSos-GRIF-$1_{1\text{-}913}$; lanes 3, 7, protein extract of cells transformed with pMyr-GRIF-$1_{1\text{-}913}$; lanes 4, 8, protein extract of cells co-transformed with pSos-GRIF-$1_{1\text{-}913}$ + pMyr-GRIF-$1_{1\text{-}913}$. The molecular weight standards (kDa) are shown on the left. Immunoreactive bands of interest are indicated by an arrow, M_r (Sos-GRIF-$1_{1\text{-}913}$) = 217 kDa, M_r (Myr-GRIF-$1_{1\text{-}913}$) = 139 kDa, M_r (Myr-GRIF-$1_{1\text{-}913}$ dimers) = 260 kDa. This immunoblot is representative of n = 2 transformations.

Sos-GRIF-$1_{1\text{-}913}$- Under reducing conditions, in protein extracts of cells co-transformed with pSos-GRIF-$1_{1\text{-}913}$ + pMyr, 2 immunoreactive bands with M_r = 217 kDa and with M_r = 98 kDa were detected by anti-GRIF-$1_{874\text{-}889}$ antibodies (lane 6, Figure 7.9). The M_r = 98 kDa band was also detected in protein extracts on untransformed yeast cells and therefore it was a non-specific band. The band with M_r = 217 kDa corresponded to Sos-GRIF-$1_{1\text{-}913}$. In non-reducing conditions the same M_r bands were recognised (lane 2, Figure 7.9). This showed that no Sos-GRIF-$1_{1\text{-}913}$ dimers were formed.

Myr-GRIF-$1_{1\text{-}913}$- Under reducing conditions, 2 immunoreactive bands with M_r = 139 kDa and with M_r = 98 kDa were detected by anti-GRIF-$1_{874\text{-}889}$ antibodies in protein extracts of cells co-transformed with pMyr-GRIF-$1_{1\text{-}913}$ + pSos (lane 7, Figure 7.9). The M_r = 98 kDa band was non-specific as explained before. The band with M_r = 139 kDa had a size corresponding to that of Myr-GRIF-$1_{1\text{-}913}$. Under non-reducing conditions, an additional band with M_r ~ 260 kDa was recognised (lane 3, Figure 7.9). This band had a

size that was ~ 2-fold bigger than that recognised for Myr-GRIF-$1_{1\text{-}913}$ under reducing conditions. Therefore it may correspond to Myr-GRIF-$1_{1\text{-}913}$ dimers. A significant amount of Myr-GRIF-$1_{1\text{-}913}$ monomers were also detected in non-reducing conditions indicating that not all Myr-GRIF-$1_{1\text{-}913}$ proteins were forming dimers.

Sos-GRIF-$1_{1\text{-}913}$ + Myr-GRIF-$1_{1\text{-}913}$- Under reducing conditions, 2 bands with M_r = 217 kDa and with M_r = 139 kDa were recognised by anti-GRIF-$1_{874\text{-}889}$ antibodies in protein extracts of cells co-transformed with pSos-GRIF-$1_{1\text{-}913}$ + pMyr-GRIF-$1_{1\text{-}913}$ (lane 8, Figure 7.9). These bands corresponded to Sos-GRIF-$1_{1\text{-}913}$ and Myr-GRIF-$1_{1\text{-}913}$ respectively. Under non-reducing conditions, an additional band with M_r ~ 260 kDa was recognised (lane 4, Figure 7.9). As mentioned earlier, this band may correspond to Myr-GRIF-$1_{1\text{-}913}$ dimers. However no band corresponding to Sos-GRIF-$1_{1\text{-}913}$ dimers was detected. As observed previously, significant amount of Myr-GRIF-$1_{1\text{-}913}$ monomers were also detected in non-reducing conditions.

These results showed that Myr-GRIF-$1_{1\text{-}913}$ dimers but not Sos-GRIF-$1_{1\text{-}913}$ or Sos-GRIF-$1_{1\text{-}913}$/Myr-GRIF-$1_{1\text{-}913}$ dimers could be formed in cdc25Hα yeast cells. This demonstrates that GRIF-1 dimers *per se* can be formed in the yeast cytoplasm. Only Sos-GRIF-$1_{1\text{-}913}$ and Sos-GRIF-$1_{1\text{-}913}$/Myr-GRIF-$1_{1\text{-}913}$ dimers are prevented from forming. This implies that either the Sos-GRIF-$1_{1\text{-}913}$ fusion protein is misfolded or that the GRIF-1 dimerisation site, i.e. the GRIF-1 N-terminal domain fused to Sos (G. Ojla, K. Brickley and F.A Stephenson, unpublished observations), is sterically hindered by Sos. Thus, the CytoTrap® technology is not optimal for the screening of new GRIF-1 interactors using Sos-GRIF-$1_{1\text{-}913}$ as a bait.

7.3. DISCUSSION

In this chapter, the possibility of using the CytoTrap® yeast two-hybrid system as a tool to identify new GRIF-1 interactors was investigated. The CytoTrap® technology was successfully established in the laboratory using a set of control plasmids provided by the manufacturer. A bait construct, Sos-GRIF-$1_{1\text{-}913}$, was generated and shown to be expressed in the cdc25Hα yeast cells. Importantly Sos-GRIF-$1_{1\text{-}913}$ did not cause auto-activation of the reporter gene activity. This was in contrast with previous GRIF-$1_{1\text{-}913}$ baits to be used in the GAL4 yeast two-hybrid system that auto-activated the reporter gene activity and therefore could not be used as baits (section 7.1.1). Prior to performing a CytoTrap® yeast two-hybrid screen with Sos-GRIF-$1_{1\text{-}913}$ as bait, the ability to detect known GRIF-1 interactions, i.e. GRIF-1/$GABA_A$ receptor β2-IL and GRIF-1/GRIF-1 interactions, was checked. The Myr-GRIF-$1_{1\text{-}913}$ and Myr-β2-$IL_{303\text{-}427}$ constructs were generated and their expression in yeast cells was demonstrated by immunoblotting. However attempts to substantiate the interaction between Sos-GRIF-$1_{1\text{-}913}$ and Myr-β2-$IL_{303\text{-}427}$ and between Sos-GRIF-$1_{1\text{-}913}$ and Myr-GRIF-$1_{1\text{-}913}$ failed. In both cases, the N-terminal domain of GRIF-1 was involved in the interaction. Since the Sos protein was fused to GRIF-1 N-terminal domain to generate Sos-GRIF-$1_{1\text{-}913}$, it was possible that Sos hindered the GRIF-1 N-terminal domain on the fusion protein thereby preventing GRIF-1/$GABA_A$ receptor subunit β2-IL and GRIF-1/GRIF-1 interactions from occurring. Alternatively, the Sos-GRIF-$1_{1\text{-}913}$ fusion protein could be misfolded. The latter hypothesis was verified by the observation that Myr-GRIF-$1_{1\text{-}913}$ dimers but not Sos-GRIF-$1_{1\text{-}913}$ dimers could form under non-reducing conditions. As described in Chapter 1, GRIF-1 contains 3 regions, i.e. 2 N-terminal coiled-coil domains and a C-terminal proline-rich region, all known to be involved in protein-protein interactions (Burkhard *et al.*, 2001; Kay *et al.*, 2000). For example, GRIF-1 coiled-coil domains mediate GRIF-1/β2-IL, GRIF-1/kinesin-1 and GRIF-1/GRIF-1 interactions (section 1.3; Beck *et al.*, 2002; Brickley *et al.*, 2005; G. Ojla, K. Brickley and F.A Stephenson, unpublished observations). It might be possible that the coiled-coil and proline-rich regions interact also with the Sos component of Sos-GRIF-$1_{1\text{-}913}$, thereby resulting in misfolding of the Sos-GRIF-$1_{1\text{-}913}$ fusion protein. In contrast the Myr construct consists of a short myristoylation sequence that may not interfere with the folding of the Myr-fusion protein thus enabling the formation of Myr- GRIF-$1_{1\text{-}913}$ dimers.

The $GABA_A$ receptor γ2 subunit interacting protein, GODZ, was identified in a CytoTrap® yeast two-hybrid screen (section 1.2.2.2; Keller *et al.*, 2004). The bait consisted of a 44 amino acid γ2-IL polypeptide ($\gamma2_{361-404}$) fused to Sos. Although the γ2-IL bait was short, the Sos moietie did not interfere with its binding ability. This suggests that short but not large proteins should be used as Sos-fusion bait in the CytoTrap® system.

The data presented here shows that the CytoTrap® yeast two-hybrid technology cannot be used to search for GRIF-1 interactors using the full length GRIF-1 as a bait. A different methodology should be adopted. For example a proteomic approach could be undertaken. This would allow the identification of proteins associated with GRIF-1 *in vivo*.

REFERENCES

Aizawa, H., Sekine, Y., Takemura, R., Zhang, Z., Nangaku, M. and Hirokawa, N. (1992) *J. Cell. Biol.* **119**, 1287-1296. Kinesin family in murine central nervous system.

Alberts, B., Johnson, A., Lewis, J., Raff, M., Roberts, K. and Walter, P. (2002) *Mol. Biol. Cell* 4th Ed. Garland Science. p678-684.

Altschul, S.F., Madden, T.L., Schaeffer, A.A, Zhang, J., Zhang, Z., Miller, N., and Lipman D.J. (1997) *Nucleic Acid Res.* **25**, 3389-3402. Gapped Blast and psi-Blast: a new generation of protein database search programs.

Angres, B. and Green, G. (1999) *CLONTECHniques* **XIV**, 28-29. Dual labeling using ECFP and EYFP in standard fluorescence microscopy.

Aronheim A., Zandi E., Henneman H., Elledge S.J., Karin M. (1997) *Mol. Cell. Biol.* **17**, 3094-3102. Isolation of an AP-1 repressor by a novel method for detecting protein-protein interactions.

Baas, P.W., Deitch, J.S., Black, M.M. and Banker, G.A. (1988) *Proc. Natl. Acad. Sci. USA* **85**, 8335-8339. Polarity orientation of microtubules in hippocampal neurons: uniformity in the axon and nonuniformity in the dendrites.

Baas, P.W. and Ahmad, F.J. (2001) *Encyclopedia of Life Sciences.* John Wiley & Sons, Ltd. Axonal transport and the neuronal cytoskeleton.

Bannai, H., Inoue, T., Nakayama, T., Hattori, M. and Mikoshiba, K. (2003) *J. Cell Sci.* Kinesin dependent, rapid, bi-directional transport of ER sub-compartment in dendrites of hippocampal neurones.

Bastians, P.I.H. and Squire, A. (1999) *Trends Cell Biol.* **9**, 48-52. Fluorescence lifetime imaging microscopy: spatial resolution of biochemical processes in the cell.

Beck, M., Brickley, K., Wilkinson, H.L., Sharma, S., Smith, M.J., Chazot, P.L., Pollard, S. and Stephenson, F.A. (2002) *J. Biol. Chem.* **277**, 30079-30090. Identification, molecular cloning, and characterization of a novel $GABA_A$ receptor-associated protein, GRIF-1.

Bedford, F.K., Kittler, J.T., Muller, E., Thomas, P., Uren, J.M., Merlo, D., Wisden, W., Triller, A., Smart, T.G. and Moss, S.J. (2001) *Nat. Neurosci.* **4**, 908-916. $GABA_A$ receptor cell surface number and subunit stability are regulated by the ubiquitin-like protein Plic-1.

Blom, N., Gammeltoft, S. and Brunak, S. (1999) *J. Mol. Biol.* **294**, 1351-1362. Sequence- and structure-based prediction of eukaryotic protein phosphorylation sites.

Bollan, K., King, D., Robertson, L.A., Brown, K., Taylor, P.M., Moss, S.J. and Connolly, C.N. (2003) *J. Biol. Chem.* **278**, 4747-4755. $GABA_A$ receptor composition is determined by distinct assembly signals within α and β subunits.

Bolton, E.T. and McCarthy, B.J. (1962) *Proc. Natl. Acad. Sci. USA* **48**, 1390-1397. A general method for the isolation of RNA complementary to DNA.

Brady, S.T. (1985) *Nature* **317**, 73-75. A novel brain ATPase with properties expected for the fast axonal transport motor.

Brandon, N.J., Uren, J.M., Kittler, J.T., Wang, H., Olsen, R., Parker, P.J. and Moss, S.J. (1999) *J. Neurosci.* **19**, 9228-9234. Subunit-specific association of protein kinase C and receptor for activated C kinase with GABA type A receptors.

Brandon, N.J., Jovanovic, J.N., Colledge, M., Kittler, J.T., Brandon, J.M., Scott, J.D. and Moss, S.J. (2003) *Mol. Cell. Neurosci.* **22**, 87-97. A-kinase anchoring protein 79/150 facilitates the phosphorylation of $GABA_A$ receptors by cAMP-dependent protein kinase via selective interaction with receptor β subunits.

Brickley, K., Smith, M.J., Beck, M. and Stephenson, F.A. (2005) *J. Biol. Chem.* **280**, 14723-14732. GRIF-1 and OIP106, members of a novel family of coiled-coil domain proteins.

Burkhard, P., Stetefeld, J. and Strelkov, S.V. (2001) *Trends Cell Biol.* **11**, 82-88. Coiled coils: a highly versatile protein folding motif.

Cai, Q., Gerwin, C. and Sheng, Z.H (2005) *J. Cell Biol.* **170**, 959-969. Syntabulin-mediated anterograde transport of mitochondria along neuronal processes.

Cai, Y., Singh, B.B., Aslanukov, A., Zhao, H. and Ferreira, P.A. (2001) *J. Biol. Chem.* **276**, 41594-41602. The docking of kinesins, KIF5B and KIF5C, to Ran-binding protein 1 (RanBP2) is mediated via a novel RanBP2 domain.

Chada, S.R. and Hollenbeck, P.J. (2004) *Curr. Biol.* **14**, 1272-1276. Nerve growth factor signaling regulates motility and docking of axonal mitochondria.

Chalfie, M., Tu, T., Euskirchen, G., Ward, W.W. and Prasher, D.D. (1994) *Science* **263**, 802-805. Green fluorescent protein as a marker for gene expression.

Chapell, R., Bueno, O.F., Alvarez-Hernandez, X., Robinson, L.C. and Leidenheimer, N.J. (1998) *J. Biol. Chem.* **49**, 32595-32601. Activation of protein kinase C induces γ-aminobutyric acid type A receptor internalisation in Xenopus oocytes.

Charych, E.I., Yu, W., Miralles, C.P., Serwanski, D.R., Li, X., Rubio, M. and De Blas, A.L. (2004) *J. Neurochem.* **90**, 173-179. The brefeldin A-inhibited GDP/GTP exchange factor 2, a protein involved in vesicular trafficking, interacts with the β subunits of the $GABA_A$ receptors.

Chen, L., Wang, H., Vicini, S. and Olsen, R. W. (2000) *Neurobiol.* 97, 11557-11562. The γ-aminobutyric acid type A ($GABA_A$) receptor-associated protein (GABARAP) promotes $GABA_A$ receptor clustering and modulates the channel kinetics.

Chu, P.J., Rivera, J.F. and Arnold, D.B. (2006) *J. Biol. Chem.* **281**, 365-373. A role for KIF17 in transport of Kv4.2.

Colomer, V., Engelender, S., Sharp, A.H., Duan, K., Cooper, J.K., Lanahan, A., Lyford, G., Worley, P. and Ross, C.A. (1997) *Hum. Mol. Genet.* **6**, 1519-1525. Huntingtin-

associated protein 1 (HAP1) binds to a Trio-like polypeptide, with a rac1 guanine nucleotide exchange factor domain.

Connolly, C.N., Wooltorton, J.R.A., Smart, T.G. and Moss, S.J. (1996a) *Proc. Natl. Acad. Sci. USA.* **93**, 9899-9904. Subcellular localisation of γ-aminobutyric acid type A receptors is determined by receptor β subunits.

Connolly, C.N., Krishek, B.J., McDonald, B.J., Smart, T.G. and Moss, S.J. (1996b) *J. Biol. Chem.* **271**, 89-96. Assembly and cell surface expression of heteromeric and homomeric γ-aminobutyric acid type A receptors.

Connolly, C.N., Kittler, J.T., Thomas, P., Uren, J.M., Brandon, N.J. Smart, T.G. and Moss, S.J. (1999) *J. Biol. Chem.* **274**, 36565-36572. Cell surface stability of γ-aminobutyric acid type A receptors.

Connor, J.X., Boileau, A.J. and Cjakowski, C. (1998) *J. Biol. Chem.* **273**, 28906-28911. A $GABA_A$ receptor α1 subunit tagged with green fluorescent protein requires a β subunit for functional surface expression.

Coy, D.L., Hancock, W.O., Wagenbach, M. and Howard, J. (1999) *Nat. Cell Biol.* **1**, 288-292. Kinesin's tail domain is an inhibitory regulator of the motor domain.

Craig, A.M., Banker, G., Chang, W., McGrath, M.E. and Serpinskaya, A.S. (1996) *J. Neurosci.* **16**, 3166-3177. Clustering of gephyrin at GABAergic but not glutamatergic synapses in cultured rat hippocampal neurons.

Cyr, J.L., Pfister, K.K, Bloom, G.S., Slaughter, C.A and Brady, S.T. (1991) *Proc. Natl. Acad. Sci. USA* **88**, 10114-10118. Molecular genetics of kinesin light chains: generation of isoforms by alternative splicing.

Day, R.N., Periasamy, A. and Schaufele, F. (2001) *Methods* **25**, 4-18. Fluorescence resonance energy transfer microscopy of localized proteins interactions in the living cell nucleus.

Dickinson, M.E., Bearman, G., Tille, S., Lansford, R. and Fraser, S.E. (2001) *Biotechniques* **31**, 1272-1278. Multi-spectral imaging and linear unmixing add a whole new dimension to laser scanning fluorescence microscopy.

Diefenbach, R.J., Mackay, J.P., Armati, P.J. and Cunningham, A.L. (1998) *Biochem.* **37**, 16663-16670. The C-terminal region of the stalk domain of ubiquitous human kinesin heavy chain contains the binding site for kinesin light chain.

Dillon, C. and Goda, Y. (2005) *Annu. Rev. Neurosci.* **28**, 25-55. The actin cytoskeleton: integrating form and function at the synapse.

Dong, H., O'Brien, R.J., Fung, E.T., Lanahan, A.A., Worley, P.F. and Huganir, R.L. (1997) *Nature* **386**, 279-284. GRIP: a synaptic PDZ domain-containing protein that interacts with AMPA receptors.

Dotti, C.G., Banker, G.A. and Binder, L.I. (1987) *Neuroscience.* **23**, 121-130 The expression and distribution of the microtubule-associated proteins tau and microtubule-associated protein 2 in hippocampal neurons in the rat in situ and in cell culture.

Duggan, M.J. and Stephenson, F.A. (1989) *J. Neurochem.* **53**, 132-139. Bovine $GABA_A$ receptor sequence-specific antibodies: identification of two epitopes which are recognised in both native and denatured $GABA_A$ receptors.

Elluru, R.G., Bloom, G.S. and Brady, S.T. (1995) *Mol. Biol. Cell* **6**, 21-40. Fast axonal transport of kinesin in the rat visual system: functionality of kinesin heavy chain isoforms.

Engelender, S., Sharp, A.H., Colomer, V., Tokito, M.K., Lanahan, A., Worley, P., Holzbaur, E.L. and Ross, C.A. (1997) *Hum. Mol. Genet.* **6**, 2205-2212. Huntingtin-associated protein 1 (HAP1) interacts with the p150Glued subunit of dynactin.

Essrich, C., Lorez, M., Benson, J.A., Fritschy, J.M. and Lüscher, B. (1998) *Nat. Neurosci.* **1**, 563-571. Postsynaptic clustering of major $GABA_A$ receptor subtypes requires the γ2 subunit and gephyrin.

Farrar, S.J., Whiting, P.J., Bonnert, T.P. and McKernan, R.M. (1999) *J. Biol. Chem.* **274**, 10100-10104. Stoichiometry of a ligand-gated ion channel determined by fluorescence energy transfer.

Fields, S. and Song, O. (1989) *Nature* **340**, 245-246. A novel genetic system to detect protein-protein interactions.

Forster, T. (1948) *Ann. Phys.* **2**, 55-75. Intermolecular energy migration and fluorescence.

Fransson, A., Ruusala, A. and Arpenstrom, P. (2003) *J. Biol. Chem.* **278**, 6495-6502. Atypical Rho GTPases have roles in mitochondrial homeostasis and apoptosis.

Fransson, A., Ruusala, A. and Arpenstrom, P. (2006) *Biochem. Biophys. Res. Commun.* **344**, 500-510. The atypical Rho GTPases Miro-1 and Miro-2 have essential roles in mitochondrial trafficking.

Friedman, D.S. and Vale, R.D. (1999) *Nat. Cell Biol.* **1**, 293-297. Single-molecule analysis of kinesin motility reveals regulation by the cargo-binding tail domain.

Fritschy, J.M., Benke, D., Mertens, S., Oertel, W.H., Bachi, T. and Möhler, H. (1992) *Proc. Natl. Acad. Sci. USA* **89**, 6726-6730. Five subtypes of type A γ-aminobutyric acid receptors identified in neurons by double and triple immunofluorescence staining with subunit-specific antibodies.

Fritschy, J.M. and Brünig, I. (2003). *Pharmcol. Ther.* **98**, 299-323. Formation and plasticity of GABAergic synapses: physiological mechanisms and pathophysiological implications.

Gauger, A.K. and Goldstein, L.S.B. (1993) *J. Biol. Chem.* **268**, 13657-13668. The *Drosophila* kinesin light chain.

Gauthier, L.R., Charrin, B.C., Borrell-Pages, M., Dompierre, J.P., Rangone, H., Cordelieres, F.P., De Mey, J., MacDonald, M.E., Lessmann, V., Humbert, S. and Saudou, F. (2004) *Cell* **118**, 127-138. Huntingtin controls neurotrophic support and survival of neurons by enhancing BDNF vesicular transport along microtubules.

Glater, E.E., Megeath, L.J., Stowers, R.S. and Thomas, T.L. (2006) *J. Cell Biol.* **173**, 545-557. Axonal transport of mitochondria requires milton to recruit kinesin heavy chain and is light chain independent.

Gilbert, S.L., Zhang, L., Forster, M.L., Iwase, T., Soliven, B., Donahue, L.R., Sweet, H.O., Bronson, R.T., Davisson, M., Wollmann, R.L. and Lahn, B.T. (2006) *Nat. Genet.* **38**, 245-250. *Trak*l mutation disrupts $GABA_A$ receptor homeostasis in hypertonic mice.

Gorrie, G.H., Vallis, Y., Stephenson, A., Whitfield, J., Browning, B., Smart, T.G. and Moss, S.J. (1997) *J. Neurosci.* **17**, 6587-6596. Assembly of $GABA_A$ receptors composed of α1 and β2 subunits in both cultures neurons and fibroblasts.

Gorska-Andrzejak, J., Stowers, R.S., Borycz, J., Kostyleva, R., Schwarz, T.L. and Meinertzhagen, I.A. (2003) *J. Comp. Neurol.* **463**, 372-388. Mitochondria are redistributed in *Drosophila* photoreceptors lacking Milton, a kinesin-associated protein.

Grishin, A., Li, H., Levitan, E.S and Zaks-Mahina, E. (2006) *J. B **iol. Chem.*** **281**, 30104-30111. Identification of γ-aminobutyric acid receptor-interacting factor 1 (TRAK2) as a trafficking factor for the K^+ channel Kir2.1.

Gross, S.P., Welte, M.A., Block, S.M. and Wieschaus, E.F. (2002) *J. Cell Biol.* **28**, 715-724. Coordination of opposite-polarity microtubule motors.

Guo, X., Macleod, G.T., Wellington, A., Hu, F., Panchumarthi, S., Schoenfield, M., Marin, L., Charlton, M.P., Atwood, H.L. and Zinsmaier, K.E. (2005) *Neuron* **47**, 379-393. The GTPase dMiro is required for axonal transport of mitochondria to *Drosophila* synapses.

Gutekunst, C.A., Li, S.H., Ferrante, R.J., Li, X.J. and Hersch S. M. (1998) *J. Neurosci.* **18**, 7674-7686. The cellular and subcellular localization of huntingtin-associated protein 1 (HAP1): comparison with huntingtin in rat and human.

Hackney, D.D., Levitt, J.D. and Suhan, J. (1992) *J. Biol. Chem.* **267**, 8696-8701. Kinesin undergoes a 9 S to a 6 S conformational transition.

Hadano, S., Yanagisawa, Y., Skaug, J., Fichter, K., Nasir, J., Martindale, D., Koop, B.F., Sherer, S.W., Nicholson, D.W., Rouleau, G.A., Ikeda, J.E and Hayden, M.R. *Genomics* **71**, 200-213. Cloning and characterisation of three novel genes, ALS2CR1, ALS2CR2 and ALS2CR3, in the juvenile amyotrophic lateral sclerosis (ALS2) critical region at chromosome 2q33-2q34: candidate genes for ALS2.

Hafezparast, M., Klocke, R., Ruhrberg, C., Marquardt, A., Ahmad-Annuar, A., Bowen, S., Lalli, G., Witherden, A.S., Hummerich, H., Nicholson, S., Morgan, P.J., Oozageer, R., Priestley, J.V., Averill. S., King, V.R., Ball, S., Peters, J., Toda, T., Yamamoto, A., Hiraoka, Y., Augustin, M., Korthaus, D., Wattler, S., Wabnitz, P., Dickneite, C., Lampel, S., Boehme, F., Peraus, G., Popp, A., Rudelius, M., Schlegel, J., Fuchs, H., Hrabe de Angelis, M., Schiavo, G., Shima, D.T., Russ, A.P., Stumm, G., Martin, J.E. and Fisher, E.M. (2003) *Science* **300**, 808-812. Mutations in dynein link motor neuron degeneration to defects in retrograde transport.

Haltiwanger, R.S., Blomberg, M.A. and Hart, G.W. (1992) *J. Biol. Chem.* **267**, 9005-9013. Glycosylation of nuclear and cytoplasmic proteins.

Hamori, E., Arndt-Jovin, D.J., Grimwade, B.G. and Jovin, T.M. (1980) *Cytometry* **1**, 132-135. Selection of viable cells with known DNA content.

Hanbook Molecular probes

He, L., Olson, D.P., Wu, X., Karpova, T.S., McNally, J.G. and Lipsky, P.E. (2003) *Cytometry* **55A**, 71-85. A flow cytometric method to detect protein-protein interactions in living cells by directly visualizing donor fluorophore quenching during CFP to YFP fluorescence resonance energy transfer (FRET).

Heim, R., Prasher, D.C. and Tsien, R.Y. (1994) *Proc. Natl. Acad. Sci. USA* **91**, 12501-12504. Wavelength mutations and posttranslational autoxidation of green fluorescent protein.

Heim, R. and Tsien, R.Y. (1996) *Curr. Biol.* **6**, 178-182. Engineering green fluorescence protein for improved brightness, longer wavelengths and fluorescence energy transfer.

Hirokawa, N., Sato-Yoshitake, R., Kobayashi, N., Pfister, K.K., Bloom, G.S. and Brady, T.S. (1991) *J. Cell Biol.* **114**, 295-302. Kinesin associates with anterogradely transported membranous organelles in vivo.

Hirokawa, N. and Takemura, R. (2005) *Nat. Rev. Neurosci.* **6**, 201-214. Molecular motors and mechanisms of directional transport in neurons.

Hoffmann, C., Gaietta, G., Bünnemann, M., Adams, S.R., Oberdorff-Maass, S., Behr, B., Vilardaga, J.P., Tsien, R.Y., Ellisman, M.H. and Lohse, M.J. (2005) *Nat. Methods* **2**, 171-175. A FlAsH-based FRET approach to determine G protein-coupled receptor activation in living cells.

Hollenbeck, P.J. (1989) *J. Cell Biol.* **108**, 2335-2342. The distribution, abundance and subcellular localization of kinesin.

Hollenbeck, P.J. (1993) *J. Neurochem.* **60**, 2265-2275. Phosphorylation of neuronal kinesin heavy and light chains *in vivo*.

Hollenbeck, P.J. and Saxton, W.M. (2005) *J. Cell Sci.* **118**, 5411-5419. The axonal transport of mitochondria.

Hoppe, A., Christensen, K. and Swanson, J.A. (2002) *Biophys. J.* **83**, 3652-3664. Fluorescence resonance energy transfer-based stoichiometry in living cells.

Horiuchi, H., Barkus, R.V., Pilling, A.D., Gassman, A. and Saxton, W.M. (2005) *Curr. Biol.* **15**, 2137-2141. APLIP-1, a kinesin binding JIP1/JNK scaffold protein influences the axonal transport of both vesicles and mitochondria in *Drosophila.*

Huang, J.D, Brady, S.T., Richards, B.W., Stenoien, D., Resau, J.H., Copeland, N.G. and Jenkins, N.A. (1999) *Nature* **397**, 267-270. Direct interaction of microtubule- and actin-based transport motors.

Hurley, J.H. and Erm, S.D. (2006) *Annu. Rev. Biophys. Biomol. Struct.* **35**, 277-298. The ESCRT complexes: structure and mechanism of a membrane-trafficking network.

Iyer, S.P.N., Akimoto, Y. and Hart, G.W. (2003a) *J. Biol. Chem.* **278**, 5399-5409. Identification and cloning of a novel family of coiled-coil domain proteins that interact with *O*-GlcNAc transferase.

Iyer, S.P.N and Hart, G.W. (2003b) *J. Biol. Chem.* **278**, 24608-24616. Roles of the tetratricopeptide repeat domain in *O*-GlcNAc transferase targeting and protein substrate specificity.

Jacobson, C., Schnapp, B. and Banker, G. (2006) *Neuron* **49**, 797-804. A change in the selective translocation of the kinesin-1 motor domain marks the initial specification of the axon.

Kamal, A. and Goldstein, L.S.B. (2002) *Curr. Opin. Cell Biol.* **14**:63-68. Principles of cargo attachment to cytoplasmic motor proteins.

Kanai, Y., Okada, Y., Tanaka, Y., Harada, A., Terada, S. and Hirokawa, N. (2000) *J. Neurosci.* **20**, 6374-6384. KIF5C, a novel neuronal kinesin enriched in motor neurons.

Kanai, Y., Dohmae, N. and Hirokawa, N. (2004) *Neuron* **43**, 513-525. Kinesin transports RNA: isolation and characterization of an RNA-transporting granule.

Kanematsu, T., Jang, I.S., Yamaguchi, T., Nagahama, H., Yoshimura, K., Hidaka, K., Matsuda, M., Takeuchi, H., Misumi, Y., Nakayama, K., Yamamoto, T., Akaike, N., Hirata, M. and Nakayama, K. (2002) *EMBO J.* **21**, 1004-1011. Role of the PLC-related, catalytically inactive protein p130 in $GABA_A$ receptor function.

Kanematsu, T., Yasunaga, A., Mizoguchi, Y., Kuratani, A., Kittler, J.T., Jovanovic, J.N., Takenaka, K., Nakayama, K.I., Fukami, K., Takenawa, T., Moss, S.J., Nabekura, J. and Hirata, M. (2006) *J. Biol. Chem.* **281**, 22180-22189. Modulation of $GABA_A$ receptor phosphorylation and membrane trafficking by phospholipase C-related inactive protein/protein phosphatase 1 and 2A signaling complex underlying BDNF-dependent regulation of GABAergic inhibition.

Karpova, T.S., Baumann, C.T., He, L., Wu, X., Grammer, A., Lipsky, P., Hager, G.L. and McNally, J.G. (2003) *J. Microscopy* **209**, 56-70. Fluorescence resonance energy

transfer from cyan to yellow fluorescent protein detected by acceptor photobleaching using confocal microscopy and a single laser.

Karcher, R.L., Deacon, S.W. and Gelfand, V.I. (2002) *Trends Cell Biol.* **12**, 21-7. Motor-cargo interactions: the key to transport specificity.

Kay, B.K., Williamsom, M.P. and Sudol, M. (2000) *FASEB J.* **14**, 231-241. The importance of being proline: the interaction of proline-rich motifs in signaling proteins with their cognate domains.

Keller, C. A., Yuan, X., Panzanelli, P., Martin, M.L., Alldred, M., Sassoe-Pognetto, M. and Lüscher, B. (2004) *J. Neurosci.* **24**, 5881-5891. The γ2 subunit of $GABA_A$ receptors is a substrate for palmitoylation by GODZ.

Kellogg, D.R., Moritz, M. and Alberts, B.M. (1994) *Annu. Rev. Biochem.* **63**, 639-674. The centrosome and cellular organization.

Khodjakov, A., Lizunova, E.M., Minin, A., Koonce, M.P. and Gyoeva, F.K. (1998) *Mol. Biol. Cell* **9**, 333-343. A specific light chain of kinesin associates with mitochondria in cultured cells.

Kirk, E., Chin, L.S. and Li, L. (2006) *J. Cell Sci.* **119**, 4689-4701. GRIF1 binds Hrs and is a new regulator of endossomal trafficking.

Kittler, J.T., Delmas, P., Jovanovic, J.N., Brown, D.A., Smart, T.G. and Moss, S.J. (2000a) *J. Neurosci.* **20**, 7972-7977. Constitutive endocytosis of $GABA_A$ receptors by an association with the adaptin AP2 complex modulates inhibitory synaptic currents in hippocampal neurons.

Kittler, J.T., Wang, J., Connolly, C.N.,Vicini, S., Smart, T.G and Moss, S.J. (2000b) *Mol. Cell Neurosci.* **16**, 440-452. Analysis of $GABA_A$ receptor assembly in mammalian cell lines and hippocampal neurons using γ2 subunit green fluorescent protein chimeras.

Kittler, J.T., Rostaing, P., Schiavo, G., Fritschy, J.M., Olsen, R., Triller, A. and Moss, J.M. (2001) *Mol. Cell Neurosci.* **18**, 13-25. The subcellular distribution of GABARAP and its ability to interact with NSF suggest a role for this protein in the intracellular transport of $GABA_A$ receptors.

Kittler, J.T. and Moss, S.J. (2003) *Curr. Opin. Neurobiol.* **13**, 1-7. Modulation of $GABA_A$ receptor activity by phosphorylation and receptor trafficking: implications for the efficiency of synaptic inhibition.

Kittler, J.T., Chen, G., Honing, S., Bogdanov, Y., McAinsch, K., Arancibia-Carcamo, I.L., Jovanovic, J.N., Pangalos, M.N., Haucke, V., Yan, Z. and Moss, S.J. (2004a) *Proc. Natl. Acad. Sci. USA* **102**, 14871-14876. Phospho-dependent binding of the clathrin AP2 adaptor complex to $GABA_A$ receptors regulates efficiency of inhibitory synaptic transmission.

Kittler, J.T., Thomas, P., Tretter, V., Bogdanov, Y.D., Haucke, V., Smart, T.G. and Moss S.J. (2004b) *Proc. Natl. Acad. Sci. USA.* **101**, 12736-12741. Huntingtin-

associated protein 1 regulates inhibitory synaptic transmission by modulating gamma-aminobutyric acid type A receptor membrane trafficking.

Kneussel, M., Haverkamp, S., Fuhrmann, J.C., Wang, H., Wassle, H., Olsen, R.W. and Betz, H. (2000) *Proc. Natl. Acad. Sci. USA.* **97**, 8594-8599. The gamma-aminobutyric acid type A receptor ($GABA_AR$)-associated protein GABARAP interacts with gephyrin but is not involved in receptor anchoring at the synapse.

Knuesel, I., Mastrocola, M., Zuellig, R.A., Bornhauser. B., Schaub, M.C. and Fritschy, J.M. (1999) *Eur. J. Neurosci.* **11**, 4457-4462. Altered synaptic clustering of $GABA_A$ receptors in mice lacking dystrophin (mdx mice).

Kuznetsov, S.A. and Gelfand, V.I. (1986) *Proc. Natl. Acad. Sci. USA* **83**, 8530-8534. Bovine brain kinesin is a microtubule-activated ATPase.

Kuznetsov, S.A., Vaisberg, E.A., Shanina, N.A., Magretova, N.N., Chernyak, V.Y. and Gelfand, V.I. (1988) *EMBO J.* **7**, 353-356. The quaternary structure of bovine brain kinesin.

Kuznetsov, S.A., Vaisberg, Rothwell, S.W., Murphy, D.B. and Gelfand, V.I. (1989) *J. Biol. Chem.* **264**, 589-595. Isolation of a 45-kDa fragment from the kinesin heavy chain with enhanced ATPase and microtubule-binding activities.

Kural, C., Kim, H., Syed, S., Goshima, G., Gelfand, V.I. and Selvin, P.R. (2005) *Science* **308**, 1469-1472. Kinesin and dynein move a peroxisome in vivo: a tug-of-war or coordinated movement.

Kreppel, L.K., Blomberg, M.A. and Hart, G.W. (1997) *J. Biol. Chem.* **272**, 9308-9315. Dynamic glycosylation of nuclear and cytosolic proteins.

Kreppel, L.K. and Hart, G.W. (1999) *J. Biol. Chem.* **274**, 32015-32022. Regulation of a cytosolic and nuclear O-GlcNAc transferase.

Lamb, J.R., Tugendreich, S. and Hieter, P. (1995) *Trends Biochem. Sci.* **20**, 257-259. Tetratrico peptide repeat interactions: to TPR or not to TPR?

Laemmli, U.K. (1970) *Nature* **227**, 680-685. Cleavage of structural proteins during the assembly of the head of the bacteriophage T4.

Langford, G.M. (2002) *Traffic* **3**, 859-865. Myosin-V, a versatile motor for short range vesicle transport.

Laschet, J.J., Minier, F., Kurcewicz, I., Bureau, M.H., Trottier, S., Jeanneteau, F., Griffon, N., Samyn, B., Van Beeumen, J., Louvel, J., Solokoff, P. and Pumain, R. (2004) *J. Neurosci.* **24**, 7614-7622. Glyceraldehyde-3-phosphate dehydrogenase is a $GABA_A$ receptor kinase linking glycolysis to neuronal inhibition.

Lawrence, C.J., Dawe, R.K., Christie, K.R., Cleveland, D.W., Dawson, S.C., Endow, S.A., Goldstein, L.S.B., Goodson, H.V., Hirokawa, N., Howard, J., Malmnerg, R.L., McIntosh, J.R., Miki, H., Mitchison, T.J., Okada, Y., Reddy, A.S.N., Saxton, W.M.,

Schliwa, M., Scholey, J.M., Vale, R.D., Walczak, C.E. and Wordeman, L. (2004) *J. Cell. Biol.* **167**, 19-22. A standardized kinesin nomenclature.

Lee, K.D. and Hollenbeck, P.J. (1995). *J. Biol. Chem.* **270**, 5600-5605. Phosphorylation of kinesin *in vivo* correlates with organelle association and neurite outgrowth.

Leil, T.A., Chen, Z.W., Chang, C.S.S. and Olsen, R.W. (2004) *J. Neurosci.* **24**, 11429-11438. $GABA_A$ receptor-associated protein traffics $GABA_A$ receptors to the plasma membrane in neurons.

Lévi, S., Logan, S.M., Tovar, K.R. and Craig, A.M. (2004) *J. Neurosci.* **24**, 207-217. Gephyrin is critical for glycine receptor clustering but not for the formation of functional GABAergic synapses in hippocampal neurons.

Li, X.J., Li, S.H., Sharp, A.H., Nucifora, F.C.Jr., Shilling, G., Lanahan, A., Worley, P., Snyder, S.H. and Ross, C.A. (1995) *Nature* **378**, 398-402. A huntingtin-associated protein enriched in brain with implications for pathology.

Li, Y., Chin, L.S., Levey, A.I. and Li, L. (2002) *J. Biol. Chem.* **277**, 28212-28221. Huntingtin-associated protein 1 interacts with hepatocyte growth factor-regulated tyrosine kinase substrate and functions in endosomal trafficking.

Li, Z., Okamoto, K.I., Hayashi, Y. And Sheng, M. (2004) *Cell* **119**, 873-887. The importance of dendritic mitochondria in the morphogenesis and plasticity of spines and synapses.

Ligon, L.A., Tokito, M., Finklestein, J.M., Grossman, F.E. and Holzbaur, E.L.F. (2004) *J. Biol. Chem.* **279**, 19201-19208. A direct interaction between cytoplasmic dynein and kinesin I may coordinate motor activity.

Lin, R.C. and Scheller, R.H. (1997) *Neuron* **19**, 1087-1094. Structural organization of the synaptic exocytosis core complex.

Lisé, M.F., Wong, T.P., Trinh, A., Hines, R.M., Liu, L., Kang, R., Hines, D.J., Liu, L., Kang, R., Hines, D.J., Lu, J., Goldenring, J.R., Wang, Y.T. and El-Husseini, A. (2006) *J. Biol. Chem.* **281**, 3669-3678. Involvement of myosin Vb in glutamate receptor trafficking.

Liu, F., Wan, Q., Pristupa, Z.B., Yu, X.M., Wang, T.Y. and Niznik, H.B. (2000) *Nature* **403**, 274-280. Direct protein-protein coupling enables cross-talk between dopamine D5 and γ-aminobutyric acid A receptors.

Liu, J., Ernst, S.A., Gladycheva, S.E., Lee, Y.Y.F., Lentz, S.I., Ho., C.S., Li, Q. and Stuenkel, E.L. (2004) *J. Biol. Chem.* **279**, 55924-55936. Fluorescence resonance energy transfer reports properties of syntaxin1A interaction with Munc18-1 *in vivo*.

Love, D.C., Kochran, J., Lamont Cathey, R., Shin, S. and Hanover, J.A. (2003) *J. Cell Sci.* **116**, 647-654. Mitochondrial and nucleocytoplasmic targeting of O-linked GlcNAc transferase.

Lubas, W.A., Frank, D.W., Krause, M. and Hanover, J.A. (1997) *J. Biol. Chem.* **272,** 9316-9324. O-linked GlcNAc transferase is a conserved cytoplasmic protein containing tetratricopeptide repeats.
Lund, A. H., Duch, M. and Pederson, F. S. (1996) *Nucleic Acids Res.* **24,** 800-801. Increased cloning efficiency by temperature-cycle ligation.

Lüscher, B. and Keller, C.A. (2004) *Pharm. Therap.* **102,** 195-221. Regulation of $GABA_A$ receptor trafficking, channel activity, and functional plasticity of inhibitory synapses.

Macioce, P., Gambara, G., Bernassola, M., Gaddini, L., Torreri, P., Macchia, G., Ramoni, C., Ceccarini, M. and Petrucci, T.C. (2003) *J. Cell Sci.* **116,** 4847-4856. Beta-dystrobrevin interacts directly with kinesin heavy chain in brain.
Mahajan, N.P., Linder, K., Berry, G., Gordon, G.W., Heim, R. and Herman, B. (1998) *Nat. Biotechnol.* **16** 547-552. Bcl-2 and Bax interactions in mitochondria probed with green fluorescent protein and fluorescence resonance energy transfer.

Majumbar, G., Wright, J., Markowitz, P., Martinez-Hernandez, A., Raghow, R. and Solomon, S.S. (2004) *Diabetes* **53,** 3184-3192. Insulin stimulates and diabetes inhibits O-linked N-acetylglucosamine transferase and O-glycosylation of Sp1.

Martin, M.A., Iyadurai, S.J., Gassman, A., Gindhart, J.G.Jr., Hays, T.S. and Saxton, W.M. (1999) *Mol. Biol. Cell* **10,** 3717-3728. Cytoplasmic dynein, the dynactin complex, and kinesin are interdependent and essential for fast axonal transport.

Matsuda, S., Matsuda, Y. And D'Adamio, L. (2003) *J. Biol. Chem.* **278,** 38601-38606. Amyloid β protein precursor (AβPP), but not AβPP-like protein 2, is bridged to the kinesin light chain by the scaffold protein JNK-interacting protein-1b.

Matz, M.V., Fradkov, A.F., Labas, Y.A., Savitsky, A.P., Zaraisky, A.G., Markelov, M.N. and Lukyanov, S.A. (1999) *Nat. Biotechno.* **17;** 969-973. Fluorescent proteins from nonbioluminescent Anthozoa species.

McGuire, J.R., Rong, J., Li, S.H. and Li, X.J. (2006) *J. Biol. Chem.* **281,** 3552-3559. Interaction of huntingtin-associated protein-1 with kinesin light chain: implications in intracellular trafficking in neurons.

McKernan, R. M. and Whiting, P.J. (1996) *Trends Neurosci.* **19,** 139-143. Which $GABA_A$-receptor subtypes really occur in brain?

Mekler, V. M. (1994) *Photochemistry and Photobiology* **59,** 615-620. A photochemical technique to enhance sensitivity of detection of fluorescence resonance energy tranfer.

Mermall, V., Post, P.L. and Mooseker, M.S. (1998) *Science* **279,** 527-533. Unconventional myosins in cell movement, membrane traffic and signal transduction.

Miller, K.E., DeProto, J., Kaufmann, N., Patel, B.N., Duckworth, A. and Van Vactor, D. (2005) *Curr. Biol.* **15,** 684-689. Direct observation demonstrates that liprin-α is required for trafficking of synaptic vesicles.

Miyawaki, A., Llopis, J., Heim, R., McCaffery, J.M., Adams, J.A., Ikura, M. and Tsien, R.Y. (1997) *Nature* **388**, 882-887. Fluorescent indicators for Ca^{2+} based on green fluorescent proteins and calmodulin.

Miyawaki, A. and Tsien, R.Y. (2000) *Methods Enzymol.* **327**, 472-500. Monitoring protein conformations and interactions by fluorescence resonance energy transfer between mutants of green fluorescent protein.

Morfini, G., Szebenyi, G., Elluru, R., Ratner, N. and Brady, S.T. (2002) *EMBO J.* **23**, 281-293 Glycogen synthase kinase 3 phosphorylates kinesin light chains and negatively regulates kinesin-based motility.

Morfini, G., Szebenyi, G., Brown, H., Pant, H.C., Pigini, G., DeBoer, S., Beffert, U. and Brady, S.T. (2004) *EMBO J.* **23**, 2235-2245. A novel CDK5-dependent pathway for regulating GSK3 activity and kinesin-driven motility in neurons.

Morise, H., Shimomura, O., Johnson, F.H. and Winant, J. (1974) *Biochemistry* **13**, 2656-2662. Intermolecular energy transfer in the bioluminescent system of *Aequorea.*

Morris, R.L. and Hollenbeck, P.J. (1995) *J. Cell Biol.* **131**, 1315-1326. Axonal transport of mitochondria along microtubules and F-actin in living vertebrate neurons.
Nagai., S., Miyazaki, M., Aoki, R., Zama, T., Inouye, S., Hirose, K., Iino, M. and Hagiwara, M. (2000) *Nat. Biotech.* **18**, 313-316. A fluorescent indicator for vizualising cAMP-induced phosphorylation *in vivo.*

Nagawa, T., Tanaka, Y., Matsuoka, E., Kondo, S., Okada, Y., Noda, Y., Kanai, Y. and Hirokawa, N. (1997) *Proc. Natl. Acad. Sci. USA* **94**, 9654-9659. Identification and classification of 16 new kinesin superfamily (KIF) proteins in mouse genome.

Nakata, T. and Hirokawa, N. (2003) *J. Cell Biol.* **162**, 1045-1055. Microtubules provide directional cues for polarized axonal transport through interaction with kinesin motor head.

Nashmi, R., Dickinson, M.E., McKinney, S., Jareb, M., Labarca, C., Fraser, S.E. and Lester, H.A. (2003) *J. Neurosci.* **23**, 11554-11567. Assembly of $\alpha 4\beta 2$ nicotinic acetylcholine receptors assessed with functional fluorescently labeled subunits: effect of localization, trafficking, and nicotine-induced upregulation in clonal mammalian cells and in cultured midbrain neurons.

Navone, F., Niclas, J., Horn-Booher, N., Sparks, L., Bernstein, H.D. McCaffrey, G and Vale, R.D. (1992) *J. Cell Biol.* **117**, 1263-1275. Cloning and expression of a human kinesin heavy chain gene: interaction of the COOH-terminal domain with cytoplasmic microtubules in transfected CV-1 cells.

Nishimura, A., Morita, M., Nishimura, Y., and Sugino, Y. (1990) *Nucleic Acids res.* **18**, 6169. A rapid and highly efficient method for preparation of competent *Escherichia coli* cells.

Ormo, M., Cubitt, A.B., Kallio, K., Gross, L.A., Tsien, R.Y. and Remington, S.J. (1996) *Science* **273**, 1392-1395. Crystal structure of the Aequorea victoria green fluorescent protein.

Ortells, M.O. and Lunt, G.G. (1995) *Trends Neurosci.* **18**, 121-127. Evolutionary history of the ligand-gated ion-channel superfamily of receptors.

Pastural, E., Barrat, F.J., Dufourcq-Lagelouse, R., Certain, S., Sanal, O., Jabado, N., Seger, R., Griscelli, C., Fischer, A. and de Saint Basile, G. (1997) *Nat. Genet.* **16**, 289-92. Griscelli disease maps to chromosome 15q21 and is associated with mutations in the myosin-Va gene.

Patterson, G.H., Piston, D.W. and Barisas, B.G. (2000) *Anal. Bioch.* **284**, 438-440. Förster distances between green fluorescent protein pairs.

Pilling, A.D., Horiuchi, D., Lively, C.M. and Saxton, W.M. (2006) *Mol. Biol. Cell* **17**, 2057-2068. Kinesin-1 and dynein are the primary motors for fast transport of mitochondria in *Drosophila* motor axons.

Pirker, S., Schwarzer, C., Wieselthaler, A., Sieghart, W. and Sperk, G. (2000) *Neurosci.* **101**, 815-850. $GABA_A$ receptors: immunocytochemical distribution of 13 subunits in the adult rat brain.

Pollard, S., Duggan, M.J. and Stephenson, F.A. (1993) *J. Biol. Chem.* **268**, 3753-3757. Further evidence for the existence of a subunit heterogeneity within discrete $GABA_A$ receptors subpopulations.

Pollard, S. and Stephenson, F.A. (1997) *Biochem. Soc. Trans.* **25**, 547S. Characterisation of novel β2 and β3 γ-amminobutyric $acid_A$ receptor antibodies.

Pozo, K., Beck, M., Brickley, K. and Stephenson, F.A. (2004) *FENS Abstr. 1*, A080.4. Identification of mitochondrial OGT as a GRIF-1 interacting protein.

Pozo, K. And Stephenson, F.A. (2006) *Biochem. Soc. Trans.***34**, 48-50. GRIF-1-kinesin-1 interactions: a confocal microscopy study.

Prasher, D.C., Eckenrode, V.K., Ward, W.W., Prendergast, F.G. and Cormier, M.J. (1992) *Gene* **111**, 229-233. Primary structure of the Aequorea victoria green-fluorescent protein.

Rahman, A., Friedman, D.S. and Goldstein, L.S.B. (1998) *J. Biol. Chem.* **273**, 15395-15403. Two kinesin light chain genes in mice. Identification and characterization of the encoded proteins.

Rathenberg, J., Kittler, J.T. and Moss, S.J. (2004) *Mol. Cell. Neurosci.* **26**, 251-257. Palmitoylation regaulates the clustering and cell surface stability of $GABA_A$ receptors.

Reid, E., Kloos, M., Ashley-Koch, A., Hughes, L., Bevan, S., Svenson, I.K., Graham, F.L., Gaskell, P.C., Dearlove, A., Pericak-Vance, M.A., Rubinsztein, D.C. and

Marchuk, D.A. (2002) *Am. J. Hum. Genet.* **71**, 1189-1194. A kinesin heavy chain (KIF5A) mutation in hereditary spastic paraplegia (SPG10).
Rivera, J.F., Ahmad, S., Quick, M.W., Liman, E.R. and Arnold, D.B. (2003) *Nat. Neurosci.* 6, 243-250. An evolutionarily conserved dileucine motif in Shal K+ channels mediates dendritic targeting.

Rizzuto, R., Brini, M., De Giorgi, F., Rossi, R., Heim, R., Tsien, R.Y. and Poyyan, T. (1996) *Curr. Biol.* **6**, 183-188. Double labelling of subcellular structures with organelle-targeted GFP mutants *in vivo*.

Rong, J., McGuire, J.R., Fang, Z.H., Sheng, G., Shin, J.Y, Li, S.H. and Li, X.J. (2006) *J. Neurosci.* **26**, 6019-6030. Regulation of intracellular trafficking of huntingtin-associated protein-1 is critical for TrkA protein levels and neurite outgrowth.

Schaerer, M.T., Kannenberg, K., Hunziker, P., Baumann, S.W. and Sigel, E. (2001) *J. Biol. Chem.* **276**, 25597-26604. Interaction between the $GABA_A$ receptor β subunits and the multifunctional protein gG1q-R.

Schiestl, R.H. and Gietz, R.D. (1989) *Curr. Genet.* **16**, 339-346. High efficiency transformation of intact yeast cells using single stranded nucleic acids as a carrier.

Schofield, P.R., Darlison, M.G., Fujita, N., Burt, D.R., Stephenson, F.A., Rodriguez, H., Rhee, L.M., Ramachandran, J., Reale, V., Glencorse, T.A., Seeburg, P.H. and Barnard, E.A. (1987) *Nature* **328**, 221-227. Sequence and functional expression of the $GABA_A$ receptor shows a ligand-gated receptor super-family.

Selvin, P.R. (1995) *Methods Enzymol.* **246**, 300-334. Fluorescence resonance energy transfer.

Setou, M., Nakagawa, T., Seog, D.H. and Hirokawa, N. (2000) *Nature* **488**, 1796-1802. Kinesin superfamily motor protein KIF17 and mLin-10 in NMDA receptor-containing vesicle transport.

Setou, M., Seog, D.H., Tanaka, Y., Kanai, Y., Takei, Y., Kawagishi, M. and Hirokawa, N. (2002) *Nature* **417**, 83-86. Glutamate receptor interacting protein GRIP1 directly steers kinesin to dendrites.

Shafi, R., Iyer, S.P., Ellies, L.G., O'Donnell, N., Marek, K.W., Chui, D., Hart, G.W. and Marth, J.D. (2000) *Proc. Natl. Acad. Sci. USA* **97**, 5735-5739. The O-GlcNAc transferase gene resides on the X chromosome and is essential for embryonic stem cell viability and mouse ontogeny.

Shaner, N.C., Steinbach, P.A and Tsien, R.Y. (2005) *Nat. Methods* **2**, 905-909. A guide to choosing fluorescent proteins.

Siegart, W. (2000) *Trends Pharm. Sci.* **21**, 411-413. Unraveling the function of $GABA_A$ receptor subtypes.

Skoufias, D., Cole, D.G., Wedaman, K.P. and Sholey, J.M. (1994) *J. Biol. Chem.* **269**, 1477-1485. The carboxyl-terminal domain of kinesin heavy chain is important for membrane binding.

Smith, M.J., Pozo, K., Brickley, K. and Stephenson, F.A. (2006) *J. Biol. Chem.* **281**, 27216-27228. Mapping the GRIF-1 binding domain of the kinesin, KIF5C, substantiates a role for GRIF-1 as an adaptor protein in the anterograde trafficking of cargoes.

Soldati, T. and Schliwa, M. (2006) *Nat. Rev. Mol. Cell Biol.* **7**, 897-908. Powering membrane trafficking in endocytosis and recycling.

Stephenson, F.A., Duggan, M.J. and Pollard, S. (1990) *J. Biol. Chem.* **265**, 21160-21165. The γ2 polypeptide is integral to the $GABA_A$ receptor oligomer but the α subunit is the principal site of the agonist benzodiazepine photoaffinity labelling reaction.

Stephenson, F.A. (2001) *Encyclopedia of Life Sciences.* John Wiley & Sons, Ltd. $GABA_A$ receptors

Stowers, R.S., Megeath, L.J., Gorska-Andrzejak, Meinertzhagen and Schwarz, T.L. (2002) *Neuron* **36**, 1063-1077. Axonal transport of mitochondria to synapses depends on Milton, a novel *Drosophila* protein.

Su, Q., Cai, C., Gerwin, C., Smith, C.L., and Sheng, Z.H. (2004) *Nat. Cell Biol.* **6**, 941-953. Syntabulin is a microtubule-associated protein implicated in syntaxin transport in neurons.

Suggs, S.V., Wallace, R.B., Hirose, T., Kawashima, E.H. and Itakura, K. (1981) *Proc. Natl. Acad. Sci. USA.* **78**, 6613-6627. Use of synthetic oligonucleotides as hybridization probes: isolation of cloned cDNA sequences for human beta 2-microglobulin.

Tanaka, Y., Kanai, Y., Okada, Y., Nonaka, S., Takeda, S., Harada, A. and Hirokawa, N. (1998) *Cell* **93**, 1147-1158. Targeted disruption of mouse conventional kinesin heavy chain, kif5B, results in abnormal perinuclear clustering of mitochondria.

Tang, T.S., Tu, H., Chan, E.Y., Maximov, A., Wang, Z., Wellington, C.L., Hayden, M.R. and Bezprozvanny, I. (2003) *Neuron* **39**, 227-239. Huntingtin and huntingtin-associated protein 1 influence neuronal calcium signaling mediated by inositol-(1,4,5) triphosphate receptor type 1.

Terunuma, M., Jang, I.S., Ha, S.H., Kittler, J.T., Kanematsu, T., Jovanovic, J.N., Nakayama, K.I., Akaike, N., Ryu, S.H., Moss, S.J. and Hirata, M. (2004) *J. Neurosci.* **24**, 7074-7084. $GABA_A$ receptor phospho-dependent modulation is regulated by phospholipase C-related inactive protein type 1, a novel protein phosphatase 1 anchoring protein.

Thompson, J.D., Higgins, D.D. and Gibson, T.J. (1994) *Nucleic Acids Res.* **22**, 4672-4680. ClustalW: improving the sensitivity of progressive multiple sequence alignment through sequence weighting, position specific gap penalties and weight matrix choice.

Toyoshima, I., Yu, H., Steuer, E.R. and Sheetz, M.P. (1992) *J. Cell Biol.* **118**, 1121-1131. Kinectin, a major kinesin-binding protein in ER.

Tretter, V., Ehya, N., Fuchs, K. and Sieghart, W. (1997) *J. Neurosci.* **17**, 2728-2737. Stoichiometry and assembly of a recombinant $GABA_A$ receptor subtype.

Tsien, R.Y. (1998) *Annu. Rev. Biochem.* **67**, 509-44. The green fluorescent protein.

Vale, R.D., Reese, T.S. and Sheetz, M.P. (1985) *Cell* **42**, 39-50. Identification of a novel force-generating protein, kinesin, involved in microtubule-based motility.

Vale, R.D. (2003) *Cell* **112**, 467-480. The molecular motor toolbox for intracellular transport.

Vallee, R.B. and Sheetz, M.P. (1996) *Science* **271**, 1539-1544. Targeting of motor proteins.

Verveer, P.J., Harpur, A.G. and Bastiaens, P.I.H (2002) Protein-protein interactions, a molecular cloning manual. CSHL Press p181-213. Imaging protein interactions by FRET microscopy.

Verhey, K.J., Lizotte, D.L., Abramson, T., Bareboim, L., Schnapp, B.J. and Rapoport, T.A. (1998) *J. Cell Biol.* **143**, 1053-1066. Light chain-dependent regulation of kinesin's interaction with microtubules.

Verhey, K.J., Meyer, D., Deehan, R., Blenis, J., Schnapp, B.J., Rapoport, T.A. and Margolis, B. (2001) *J. Cell Biol.* **152**, 959-970. Cargo of kinesin identified as JIP scaffolding proteins and associated signaling molecules.

Wan, Q., Xiong, Z.G., Man, H.Y., Ackerley, C.A., Braunton, J., Lu, W.Y., Becker, L.E., MacDonald, J.F. and Wang, Y.T. (1997) *Nature* **388**, 686-690. Recruitment of functional $GABA_A$ receptors to postsynaptic domains by insulin.

Wang, H., Bedford, F.K., Brandon, N.J., Moss, S.J. and Olsen, R.W. (1999) *Nature* **397**, 69-72. $GABA_A$ receptor-associated protein links $GABA_A$ receptors and the cytoskeleton.

Wells, L., Vosseller, K. and Hart, G.W. (2001) *Science* **291**, 2376-2378. Glycosylation of nucleocytoplasmic proteins: signal transduction and O-GlcNAc.

Wells, L., Kreppel, L.K., Comer, F.I., Wadzinski, B.E. and Hart, G.W. (2004) *J. Biol. Chem.* **279**, 38466-38470. O-GlcNAc transferase is in a functional complex with protein phosphatase 1 catalytic subunits.

Welte, M.A. (2004) *Curr. Biol.* **14**, R525-R537. Bidirectional transport along microtubules.

Whiting, P., McKernan, R. and Iversen, L.I. (1990) *Proc. Natl. Acad. Sci. USA* **87**, 9966-9970. Another mechanism for creating diversity in γ-aminobutyrate type A

receptors: RNA splicing directs expression of two forms of γ2 subunit, one of which contains a protein kinase C phosphorylation site.

Wisden, W., Laurie, D.J., Monyer, H. and Seeburg, P.H. (1992) *J. Neurosci.* **12**, 1040-1062. The distribution of 13 $GABA_A$ receptor subunit mRNAs in the rat brain. I. Telencephalon, Diencephalon, Mesencephalon.

Wisniewski, T.P., Tanzi, C.L. and Gindhart, J.G. (2003) *Biol. Cell.* **95**, 595-602. The *Drosophila* kinesin-1 associated protein YETI binds both kinesin subunits.

Wu, X.S., Rao, K., Zhang, H., Wang, F., Sellers, J.R., Matesic, L.E., Copeland, N.G., Jenkins, N.A. and Hammer, J.A. 3rd. (2002) *Nat. Cell Biol.* **4**, 271-278. Identification of an organelle receptor for myosin-Va.

Ymer, S, Schofield, P. R., Draguhn, A., Werner, P., Kohler, M. and Seeburg P.H. (1989) *EMBO J.* **9**, 1668-1670. $GABA_A$ receptor β subunit heterogeneity: functional expression of cloned cDNAs.

Zacharias, D.A., Violin, D.J., Newton, A.C. and Tsien, R.Y. (2002) *Science* **296**, 913-916. Partitioning of lipid-modified monomeric GFPs into membrane microdomains of live cells.

Zhang, J., Campbell, R.E., Ting, A.Y and Tsien, R.Y. (2002) *Nat. Rev. Mol. Cel. Biol.* **3**, 906-918. Creating new fluorescent probes for cell biology.

Zhao, C., Takita, J., Tanaka, Y., Setou, M., Nakagawa, T., Takedam, S., Yang, H.W., Terada, S., Nakata, T., Takei, Y., Saito, M., Tsuji, S., Hayashi, Y. and Hirokawa, N. (2001) *Cell* **105**, 587-597. Charcot-Marie-Tooth disease type 2A caused by mutation in a microtubule motor KIF1Bbeta.

List of publications

Reviewed research article

Pozo, K., Smith, M.J, Brickley, K. and Stephenson, F.A. (2006) *J. Biol. Chem.* In press. Mapping the GRIF-1 binding domain of the kinesin, KIF5C, substantiates a role for GRIF-1 as an adaptor protein in the anterograde trafficking.

Non-reviewed research articles

Pozo, K. and Stephenson, F.A. (2006) *Bioc. Soc. Trans.* **34**, 48-50. GRIF-1/kinesins1 interactions: a confocal microscopy study.

Smith, M.J., **Pozo, K.** and Stephenson, F.A. (2006) *Springer-Verlag Berlin Heidelberg.* Yeast two-hybrid studies.

Abstracts

Pozo, K., Brickley, K., Smith, M.J, and Stephenson, F.A. (2006) *Biochem. Soc. Bioscience 2006 Abs.* 0311. GRIF-1 is a kinesin adaptor forming a ternary complex with kinesin heavy and light chains.

Pozo, K., Smith, M.J, Brickley, K. and Stephenson, F.A. (2005) *Soc. Neurosci. Abs.* 844-815. GRIF-1 is an adaptor protein facilitating kinesin-mediated transport in brain.

Pozo, K. and Stephenson, F.A. (2005) *Biochem. Soc. Focused Meeting. Abs.* GRIF-1/kinesin-1 interactions: a confocal microscopy study.

Pozo, K., Salgueiro, A.M. and Stephenson, F.A. (2005) *British Neurosci. Assoc. Abst.* ISSN 1345-8301, 9.03 Generation of fluorescent tagged probes for confocal microscopy analysis of the interaction between GRIF-1 and kinesin heavy chain, KIF5C.

Pozo, K., Beck, M., Brickley, K. and Stephenson, F.A. (2004) *FENS Abstr.* A080.4 Vol. Identification of mitochondrial OGT as a GRIF-1 interacting protein.

THE JOURNAL OF BIOLOGICAL CHEMISTRY VOL. 281, NO. 37, pp. 27216–27228, September 15, 2006

Mapping the GRIF-1 Binding Domain of the Kinesin, KIF5C, Substantiates a Role for GRIF-1 as an Adaptor Protein in the Anterograde Trafficking of Cargoes*[S]

Received for publication, January 18, 2006, and in revised form, July 10, 2006 Published, JBC Papers in Press, July 11, 2006, DOI 10.1074/jbc.M600522200

Miriam J. Smith[1,2], **Karine Pozo**[1], **Kieran Brickley, and F. Anne Stephenson**[3]

From the Department of Pharmaceutical and Biological Chemistry, School of Pharmacy, University of London, 29/39 Brunswick Square, London WC1N 1AX, United Kingdom

γ-Aminobutyric acid, type A ($GABA_A$) receptor interacting factor-1 (GRIF-1) and *N*-acetylglucosamine transferase interacting protein (OIP) 106 are both members of a newly identified coiled-coil family of proteins. They are kinesin-associated proteins proposed to function as adaptors in the anterograde trafficking of organelles to synapses. Here we have studied in more detail the interaction between the prototypic kinesin heavy chain, KIF5C, kinesin light chain, and GRIF-1. The GRIF-1 binding site of KIF5C was mapped using truncation constructs in yeast two-hybrid interaction assays, co-immunoprecipitations, and co-localization studies following expression in mammalian cells. Using these approaches, it was shown that GRIF-1 and the KIF5C binding domain of GRIF-1, GRIF-1-(124–283), associated with the KIF5C non-motor domain. Refined studies using yeast two-hybrid interactions and co-immunoprecipitations showed that GRIF-1 and GRIF-1-(124–283) associated with the cargo binding region within the KIF5C non-motor domain. Substantiation that the GRIF-1-KIF5C interaction was direct was shown by fluorescence resonance energy transfer analyses using fluorescently tagged GRIF-1 and KIF5C constructs. A significant fluorescence resonance energy transfer value was found between the C-terminal EYFP-tagged KIF5C and ECFP-GRIF-1, the C-terminal EYFP-tagged KIF5C non-motor domain and ECFP-GRIF-1, but not between the N-terminal EYFP-tagged KIF5C nor the EYFP-KIF5C motor domain and ECFP-GRIF-1, thus confirming direct association between the two proteins at the KIF5C C-terminal and GRIF-1 N-terminal regions. Co-immunoprecipitation and confocal imaging strategies further showed that GRIF-1 can bind to the tetrameric kinesin light-chain/kinesin heavy-chain complex. These findings support a role for GRIF-1 as a kinesin adaptor molecule requisite for the anterograde delivery of defined cargoes such as mitochondria and/or vesicles incorporating β2 subunit-containing $GABA_A$ receptors, in the brain.

γ-Aminobutyric acid, type A ($GABA_A$)[4] receptor interacting factor-1 (GRIF-1) was initially identified from rat brain by a yeast two-hybrid screen searching for $GABA_A$ receptor clustering and trafficking proteins (1). It was shown to associate at least *in vitro* with $GABA_A$ receptor β2 subunits. GRIF-1 is highly expressed in excitable tissue, most notably in the brain and in the heart (1). It is the orthologue of the human protein, β-*O*-linked *N*-acetylglucosamine transferase (OGT) interacting protein 98 (OIP98, also termed ALS2CR3, huMilt2, or TRAK2), and it is the homologue of the protein OIP106 (also termed huMilt1 and TRAK1 (2)). GRIF-1 is also probably the orthologue of the *Drosophila* protein, Milton, a kinesin-associated protein that is involved in the transport of mitochondria to the synapses in retina (3, 4). GRIF-1 and OIP106 have also been shown to aggregate mitochondria following overexpression in mammalian cells (5). Recently, the gene encoding OIP106 (TRAK1), *Trak1*, was identified as the mutated gene in *hyrt* mice, an animal model of hypertonia (6). *hyrt* mice were shown to have a deficit of $GABA_A$ receptors; wild-type OIP106 (TRAK1) was shown to co-immunoprecipitate with $GABA_A$ receptor α1 subunits in extracts of mouse brain stem and spinal cord (6). Although the mutant OIP106 was shown to still associate with $GABA_A$ receptors, it was concluded that OIP106 (TRAK1) may play a crucial role in regulating endocytic trafficking of receptors and dysfunction disrupts receptor homeostasis leading to hypertonia (6). Thus, GRIF-1, OIP106, and Milton belong to a newly identified family of coiled-coil proteins putatively involved in the trafficking of organelles and $GABA_A$ receptors to synapses.

Two additional proteins that associate with high affinity with both GRIF-1 and OIP106 have been identified. These proteins are the enzyme, OGT (2),[5] and, consistent with the role in trafficking, the molecular motor protein, kinesin (5). Kinesin was also shown to be immunoprecipitated from detergent extracts of *Drosophila* heads with anti-Milton antibodies, thereby dem-

* This work was funded by the Biotechnology and Biological Sciences Research Council, United Kingdom. The costs of publication of this article were defrayed in part by the payment of page charges. This article must therefore be hereby marked "*advertisement*" in accordance with 18 U.S.C. Section 1734 solely to indicate this fact.

[S] The on-line version of this article (available at http://www.jbc.org) contains supplemental Table S1 and Figs. S1 and S2.

[1] Both authors contributed equally to this work.

[2] Current address: Center for Neurologic Diseases, Brigham and Women's Hospital, Harvard Medical School, Boston, MA 02115.

[3] To whom correspondence should be addressed: Tel.: 44-207-753-5877; Fax: 44-207-753-5964; E-mail: anne.stephenson@pharmacy.ac.uk.

[4] The abbreviations used are: GABA, γ-aminobutyric acid; AMPA, α-amino-3-hydroxy-5-methylisoxazole-4-propionate; APP, amyloid precursor protein; cfu, colony forming units; ECFP, enhanced cyan fluorescent protein; EYFP, enhanced yellow fluorescent protein; FRET, fluorescence resonance energy transfer; GFP, green fluorescent protein; GRIF-1, $GABA_A$ receptor interacting factor-1; GRIP1, glutamate-receptor-interacting protein 1; HAP-1, huntingtin-associated protein; HEK, human embryonic kidney; KHC, kinesin heavy chain; IL, intracellular loop; KIF, kinesin superfamily protein; KLC, kinesin light chain; *N*-methyl-D-aspartate, *N*-methyl-D-aspartate; OGT, *O*-GlcNAc transferase; OIP, OGT interacting protein; JNK, c-Jun N-terminal kinase; CMV, cytomegalovirus; AD, activation domain; SD, synthetic defined media.

[5] K. Pozo, K. Brickley, M. Beck, and F. A. Stephenson, unpublished observations.

Supplemental Material can be found at:
http://www.jbc.org/cgi/content/full/M600522200/DC1

onstrating, albeit reportedly indirect, an association between Milton and kinesin (3). Kinesins belong to the kinesin superfamily, *i.e.* KIFs. KIFs are microtubule-based mechanochemical motors that are involved primarily in the anterograde transport of organelles and protein complexes (reviewed in Refs. 7 and 8). They are particularly important in transport processes in neurons where it is necessary to deliver defined cargoes from the cell body along axons and dendrites to pre- and post-synaptic sites. In brain, GRIF-1 associates predominantly with KIF5A, whereas in heart association is predominantly with KIF5B (5). Following overexpression in human embryonic kidney (HEK) 293 cells, GRIF-1 will co-associate with exogenous KIF5C (5). KIF5A, KIF5B, and KIF5C are members of the kinesin-1 family. KIF5B is ubiquitously expressed, whereas KIF5A and KIF5C are only expressed in neurons (7). They are conventional kinesin heavy chains belonging to the kinesin-1 family, and they share at least 60% amino acid identity. It is probable that each has a binding site for GRIF-1 and that GRIF-1 is promiscuous with regard to association with KIF5 subtypes.

Kinesin-1 proteins are tetramers formed by the association of two kinesin heavy chains (KHC or alternatively KIF5) and two kinesin light chains (KLC). The KHC is formed from an N-terminal motor domain that contains the microtubule and ATP binding sites and a C-terminal non-motor domain. This domain includes a neck, a coiled-coil stalk region, and a cargo binding site in its C-terminal region. The KLC interacts with the KHC via the stalk region. Cargoes bind to either the KLC or to the KHC of kinesin-1 proteins. Increasing evidence suggests that this interaction is mediated by an adaptor protein. For example, mitochondria and syntaxin-1-containing vesicles are attached to the KHC cargo binding domain by the adaptor protein, syntabulin, for their transport to synapses (9); JIP-3, a c-Jun N-terminal kinase (JNK) signaling pathway protein, binds to a six tetratricopeptide motif in KLCs to transport the cargo, amyloid precursor protein (APP; 10); KIF17 forms a complex with mLin10 in the transportation of *N*-methyl-D-aspartate receptor NR2B subunits to the synapse (11, 12); and glutamate receptor interacting protein 1 (GRIP1) is an adaptor protein linking the α-amino-3-hydroxy-5-methylisoxazole-4-propionate (AMPA) subtype of glutamate receptor containing vesicles to KIF5 (13).

In this report, we have studied the interaction between GRIF-1 and the prototypic kinesin-1, KIF5C, and kinesin light chain. The results obtained provide supporting evidence that GRIF-1 is a kinesin adaptor protein involved in motor-dependent trafficking of organelles and/or proteins. Please note a preliminary report of some of these findings (14).

EXPERIMENTAL PROCEDURES

Constructs and Antibodies—pCISGRIF-1, splice form GRIF-1a, hereafter referred to as GRIF-1, pCMVTag4aGRIF-1 (C-terminal FLAG-tagged GRIF-1), pGADT7GRIF-1-(1–913), pGAD10GRIF-1-(8–633), pGADT7GRIF-1-(124–283), and affinity-purified rabbit anti-GRIF-1_{8-633} antibodies were all as previously described (1). pMBL33 $GABA_A$ receptor β2 intracellular loop (303–427; IL), pcDNAHisMaxKIF5C, and affinity-purified sheep anti-GRIF-$1_{874-889}$ were as described in Brickley *et al.* (5). The kinesin heavy-chain KIF5C fragments, corresponding to the motor domain (1–335), the non-motor domain (336–957), coil 1 (336–542), coil 2 (594–804), and the cargo binding domain, coil 3 (827–957), were PCR-amplified from the construct, pBluescriptSKII+KIAA0531 and cloned in-frame into the EcoR1 and SalI restriction sites of the modified mammalian expression vector, pCMVTag4a, to generate the constructs pCMV-KIF5C-(1–335), pCMV-KIF5C-(336–957), pCMV-KIF5C-(336–542), pCMV-KIF5C-(593–804), and pCMV-KIF5C-(827–957) each with an N-terminal c-Myc tag. The same fragments were also cloned into the EcoR1 and SalI restriction sites of the DNA binding domain yeast expression vector, pMBL33, to generate the constructs, pMBL33-KIF5C-(1–335), pMBL33-KIF5C-(336–957), pMBL33-KIF5C-(336–542), pMBL33-KIF5C-(593–804), and pMBL33-KIF5C-(827–957). The kinesin light chain was amplified by PCR from a kinesin light chain cDNA in the pHA vector and subcloned in-frame into pMBL33 using EcoR1/SalI and into pCMVTag4a using EcoR1/SalI to generate an N-terminal c-Myc-tagged KLC. Full-length GRIF-1 was amplified from pCISGRIF-1 by PCR and subcloned in-frame in the EcoRI and SalI restriction sites of pECFP-C1 (BD Biosciences, Clontech, Palo Alto, CA) to generate pECFP-GRIF-1, *i.e.* GRIF-1 with an N-terminal enhanced cyan fluorescent protein (ECFP) tag. KIF5C was amplified from pcDNAHisMaxKIF5C and subcloned into either the EcoRI and SalI restriction sites of pEYFP-C1 (BD Biosciences, Clontech) to generate pEYFP-KIF5C, *i.e.* KIF5C with an N-terminal tag, or into the NheI site of pEYFP to generate pKIF5C-enhanced yellow fluorescent protein (EYFP), *i.e.* KIF5C with a C-terminal EYFP tag. The KIF5C motor domain, KIF5C-(1–335), and KIF5C non-motor domain, KIF5C-(336–957), were amplified by PCR from pcDNAHisMaxKIF5C. KIF5C-(1–335) was subcloned in-frame in the XhoI/EcoRI sites and KIF5C-(336–957) in the NheI site, respectively, of pEYFP to generate pEYFP-KIF5C-(1–335) with an EYFP tag at the N terminus and pEYFP-KIF5C-(336–957) with an EYFP tag at the C-terminal end of KIF5C. All constructs were verified by DNA sequencing (MWG-Biotech AG, Ebersberg, Germany). Further, for all constructs used in yeast two-hybrid interaction assays, the expression of fusion proteins was verified by immunoblotting (data not shown). A schematic of all constructs used is shown in Fig. 1.

Anti-GFP and anti-$KIF5C_{938-957}$ antibodies were from Abcam Ltd. (Cambridge, UK); anti-c-Myc clone 4A6 antibodies were from Upstate (Charlottesville, VA); and anti-mouse-Ig Alexa Fluor 633 antibodies from Invitrogen. Anti-FLAG antibodies were raised in-house against the FLAG amino acid sequence, DYKDDDDK, with an N-terminal cysteine coupled to thyroglobulin and affinity-purified for use using CDYKDDDDK covalently coupled via the cysteine to thiopropyl-activated Sepharose.

Mammalian Cell Transfection and Preparation of Detergent-solubilized Extracts of Transfected Cells—For immunoprecipitation assays, HEK 293 cells were transfected with combinations of FLAG-tagged pCMVGRIF-1-(1–913) together with c-Myc-tagged pCMV-KIF5C-(1–335), pCMV-KIF5C-(336–957), pCMV-KIF5C-(336–542), pCMV-KIF5C-(593–804), or pCMV-KIF5C-(827–957), using the calcium phosphate method using a 1:1 ratio with a total of 10 μg of DNA per

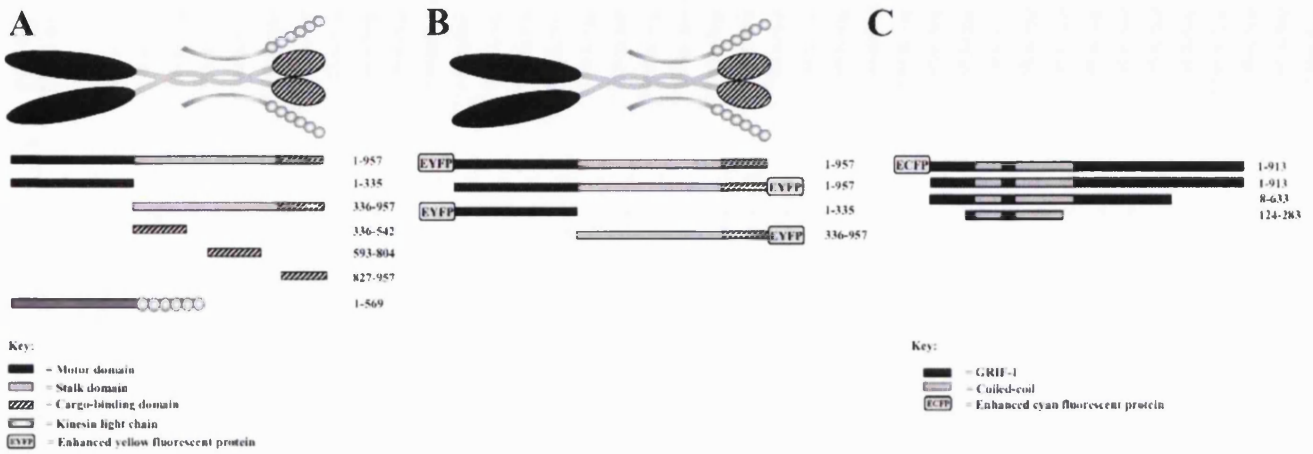

D

Coiled-coil protein 1 : TRAK1 = OIP106 = huMilt1

Coiled-coil protein 2 : TRAK2 = OIP98 = huMilt2 = GRIF-1 = ALS2CR3

FIGURE 1. **A schematic diagram showing the kinesin and GRIF-1 constructs used in this study.** *A*, KIF5C and kinesin light chain constructs used for the yeast two-hybrid and immunoprecipitation studies; *B*, KIF5C-EYFP constructs used for the imaging and FRET studies; *C*, GRIF-1 constructs used for the imaging and FRET studies depicting also, the kinesin binding domain, GRIF-1-(124–283); *D*, a summary of the nomenclatures in the literature for the two proteins encoded by the GRIF-1 coiled-coil gene family.

TABLE 1

GRIF-1 interacts directly with the KIF5C non-motor domain: demonstration by yeast two-hybrid interaction assays

The yeast strain, L40, was co-transformed with bait and fish constructs and transformants grown on −2 SD, *i.e.* −W and −L, and −3 SD, *i.e.* −W, −L, and −H. Colonies from −2 plates were re-streaked onto new plates, and colony growth was determined as described under "Experimental Procedures."

AD vector	DNA-BD vector	Growth on −W and −L dropout media[a]	Growth on −W, −L, and −H dropout media
pGADT7GRIF-1-(1–913)	pMBL33KIF5C-(1–335)	++	−
pGADT7GRIF-1-(1–913)	pMBL33KIF5C-(336–957)	+++	++
pGADT7GRIF-1-(1–913)	pMBL33KLC-(1–569)	+++	−
pGADT7GRIF-1-(8–633)	pMBL33KIF5C-(1–335)	++	−
pGADT7GRIF-1-(8–633)	pMBL33KIF5C-(336–957)	+++	+
pGADT7GRIF-1-(8–633)	pMBL33KLC-(1–569)	+++	−
pGADT7GRIF-1-(124–283)	pMBL33KIF5C-(1–335)	++	−
pGADT7GRIF-1-(124–283)	pMBL33KIF5C-(336–957)	+++	+
pGADT7GRIF-1-(124–283)	pMBL33KLC-(1–569)	+++	−
pGADT7	pMBL33KIF5C-(1–335)	++	−
pGADT7	pMBL33KIF5C-(336–957)	+++	−
pGADT7	pMBL33KLC-(1–569)	+++	−
pGADT7GRIF-1-(1–913)	pMBL33	+++	−
pGADT7GRIF-1-(8–633)	pMBL33	+++	−
pGADT7GRIF-1-(124–283)	pMBL33	+++	−
pGADT7	pMBL33	+++	−
pGAD10GRIF-1-(8–633)	pMBL33β2-IL	+++	++

[a] For colony growth, − = 0 cfu; + = 10–100 cfu; ++ = 100–200 cfu; +++ > 200 cfu. pGAD10GRIF-1-(8–633) and pMBL33β2-IL served as the positive control. The results are representative of $n = 3$ independent co-transformations.

250-ml culture flask. In pCISGRIF-1, pEYFP-KIF5C, and pCMVKLC triple transfections, a ratio of 1:1:3 was used with a total of 10 μg of DNA per 250-ml culture flask. For the characterization of the ECFP- and EYFP-tagged proteins, HEK 293 cells were transfected with either pCISGRIF-1 plus pEYFP-KIF5C; pCISGRIF-1 plus pKIF5C-EYFP; pCISGRIF-1 plus pEYFP-KIF5C-(336–957); pCISGRIF-1 plus pEYFP-KIF5C-(1–335); or pcDNAHismaxKIF5C plus pECFP-GRIF-1 and pECFP-GRIF-1 plus pEYFP-KIF5C or pECFP-GRIF-1 plus pKIF5C-EYFP all using a 1:1 ratio with a total of 10 μg of DNA per 250-ml culture flask. Cells were harvested 24–48 h post-transfection, and cell homogenates were either analyzed by immunoblotting or, alternatively, transfected cell homogenates were solubilized with 10 mM HEPES, pH 7.5, 145 mM NaCl, 1 mM EGTA, 0.1 mM $MgCl_2$, benzamidine (1 μg/ml), bacitracin (1 μg/ml), soybean trypsin inhibitor (1 μg/ml), chicken egg trypsin inhibitor (1 μg/ml), and phenylmethylsulfonyl fluoride (1 mM) and 1% (v/v) Triton X-100 for 60 min at 4 °C. Detergent-solubilized extracts were collected following centrifugation for 40 min at 4 °C at 100 000 × *g* (6). For confocal microscopy studies, HEK 293 cells or COS-7 cells were plated onto poly-D-lysine (0.1 mg/ml)-coated coverslips and transfected using the calcium phosphate method and plasmid DNA ratios as above. Transfections using pDsRed1Mito to visualize mitochondria used a ratio of 1 pDsRed1-Mito:19 ECFP-GRIF-1 for double transfections, and 1 pDsREd1Mito:8 ECFP-GRIF-1:8 EYFP-KIF5C for triples.

Immunoblotting—Immunoblotting was performed as previously described using 25–50 μg of protein/sample precipitated

using the chloroform/methanol method and SDS-PAGE under reducing conditions in either 7.5% or 12.5% polyacrylamide slab minigels (1, 5). Rabbit and mouse horseradish-linked secondary antibodies (Amersham Biosciences) were used at a final dilution of 1:2000, and immunoreactivities were detected using the ECL Western blotting system.

Immunoprecipitation Assays—Detergent-solubilized extracts of transfected HEK 293 cells (diluted to 1 mg of protein/ml with a final Triton X-100 concentration of 0.5% (v/v); 20 ml) were incubated for polyclonal antibodies, with either affinity-purified rabbit anti-FLAG antibodies (10 μg), protein A-purified non-immune rabbit Ig (10 μg) as control or, affinity-purified sheep anti-GRIF-$1_{874-889}$ antibodies (10 μg), protein G-purified non-immune sheep Ig as control for 1.5 h at 37 °C (6). Protein A (rabbit polyclonal antibodies) or protein G (sheep polyclonal antibodies) Sepharose (20 μl) was added, and samples were incubated for 1 h at 37 °C. Immune pellets were collected by centrifugation for 3 s at 10,000 × *g* and washed with 3 × 1.5 ml of 10 mM HEPES, pH 7.5, 145 mM NaCl, 1 mM EGTA, 0.1 mM $MgCl_2$, benzamidine (1 μg/ml), bacitracin (1 μg/ml), soybean trypsin inhibitor (1 μg/ml), chicken egg trypsin inhibitor (1 μg/ml), phenylmethylsulfonyl fluoride (1 mM), and 0.5% (v/v) Triton X-100 and then were analyzed by immunoblotting.

Yeast Two-hybrid Interaction Assays—Yeast two-hybrid assays were carried out using a modified LexA system as described previously (5). The *Saccharomyces cerevisiae* strain, L40 (MATa *his3Δ200 trp1*-901 *leu2–3112 ade2 LYS2*::(4lexAop-*HIS3*) *URA3*::(8lexAop*lacZ*) *GAL4*), was transformed with combinations of GRIF-1 fragments in the activation domain (AD) plasmid, pGADT7, together with each of the KIF5C fragments in the DNA binding domain plasmid, pMBL33. Negative control transformations were carried out using empty AD or DNA binding domain vectors. Positive control transformations were carried out using AD-GRIF-1-(8–633) with pMBL33β2-IL, *i.e.* the DNA binding domain vector containing the residues 303–427 of the intracellular loop of the $GABA_A$ receptor β2 subunit. Resulting colonies were assessed for reporter gene activation by growth on nutritional selection agar lacking tryptophan, leucine, and histidine.

Confocal Microscopy and FRET Efficiency Determinations—Transfected cells 20–40 h post-transfection were rinsed three times with ice-cold phosphate-buffered saline followed by fixation for 10 min with 4% (w/v) ice-cold paraformaldehyde. Coverslips were rinsed three times with phosphate-buffered saline and mounted onto a microscope slide using 10 μl of mounting solution containing an anti-fading agent (Citifluor, Citifluor Ltd., Leicester, UK). The coverslips were sealed and kept at 4 °C until analysis. For visualization of cells transfected with pCMVKLC, post-fixation coverslips were incubated with anti-c-Myc antibodies (1:4000) overnight at 37 °C, washed as described (1), and incubated with anti-mouse-Ig Alexa Fluor 633, and again washed as previously described (1). Cells were imaged using an inverted LSM510 META Zeiss confocal microscope in the multitrack mode. EYFP was excited with the λ = 514 nm laser line, and emitted light was collected with a long pass filter LP530. ECFP was excited at λ = 458 nm, and light was collected with a band-pass filter BP 475–525. The absence of bleed-through was checked prior to each experiment by using the Meta software of the microscope. This software enables the decomposition of the mixed emission spectra (*i.e.* generated from cells co-transfected with both ECFP and EYFP) into the emission of the single fluorescent dyes, *i.e.* ECFP and EYFP, according to reference spectra generated from cells transfected with either ECFP or EYFP alone. Images were analyzed using the Image Browser software (Zeiss) available with the microscope.

For FRET analyses, again the Meta software mode of the LSM510 META Zeiss confocal microscope was used. FRET efficiency was measured by acceptor photobleaching as described previously by Liu *et al.* (15) and Nashmi *et al.* (16). That is, co-transfected HEK 293 cells were firstly imaged with the λ = 458 nm laser to visualize ECFP-tagged proteins. A defined area of co-localization within one cell was selected, and EYFP was photobleached for ~30 s using the λ = 514 nm laser at full power. Cells were imaged post-photobleaching with the λ = 458 nm laser. FRET was measured as the increase of ECFP fluorescence after photobleaching where values were taken at t = 1.6 s prior to photobleaching and t = ~32 s post-photobleaching and were corrected for background fluorescence (usually of the order of ~10%) determined by the imaging of untransfected HEK 293 cells. The relative FRET efficiency was calculated by the following: (1 − [pre-bleached intensity of ECFP/

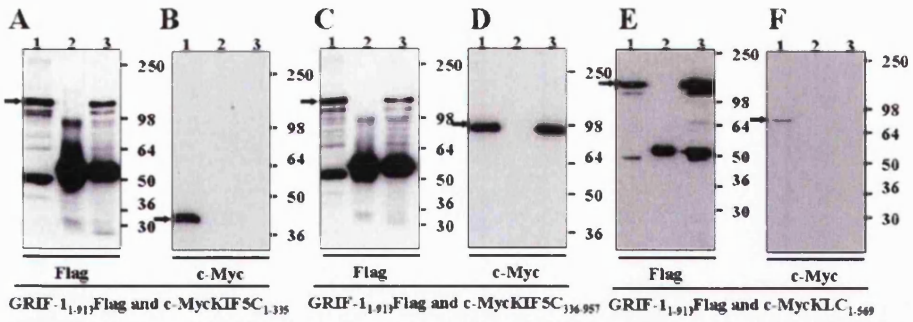

FIGURE 2. **GRIF-1 associates with the non-motor domain of KIF5C: demonstration by immunoprecipitation following co-expression of GRIF-1 and KIF5 constructs in HEK 293 cells.** HEK 293 cells were transfected with pCISGRIF-1-FLAG and either pCMV-KIF5C-(1–335), pCMV-KIF5C-(336–957), or pCMVKLC, detergent extracts of cell homogenates were prepared 48 h post-transfection, and immunoprecipitation assays were carried out using either affinity-purified anti-FLAG antibodies or non-immune Ig and immune pellets analyzed by immunoblotting using anti-FLAG (20% of immune pellet) and anti-c-Myc (80% of immune pellet) antibodies all as described under "Experimental Procedures." *A* and *B*, immunoprecipitation from HEK 293 cells transfected with pCISGRIF-1_{FLAG} and pCMV-KIF5C-(1–335); *C* and *D*, immunoprecipitation from HEK 293 cells transfected with pCISGRIF-1_{FLAG} and pCMV-KIF5C-(336–957); and *E* and *F*, pCISGRIF-1_{FLAG} and pCMVKLC. In *A*, *C*, and *E*, immunoblots were probed with anti-FLAG antibodies, and in *B*, *D*, and *F* immunoblots were probed with anti-c-Myc antibodies. Gel lanes are: *1*, detergent-solubilized transfected HEK 293 cell homogenate; *2*, non-immune pellet; *3*, anti-FLAG pellet. *Arrows* denote: *A*, *C*, and *E*, GRIF-1-FLAG, 115 kDa; *B*, c-Myc-tagged KIF5C-(1–335), 43 kDa; *D*, c-Myc-tagged KIF5C-(336–957), 98 kDa; and *F*, c-Myc-tagged KLC, 70 kDa. The positions of molecular mass standards (kDa) are shown on the *right*. The immunoblots are representative of at least n = 3 immunoprecipitations from n = 3 independent transfections.

TABLE 2

GRIF-1 interacts directly with the KIF5C cargo binding domain coil 3: demonstration by yeast two-hybrid interaction assays

The yeast strain, L40, was co-transformed with bait and fish constructs and transformants grown on −2 SD, *i.e.* −W and −L and −3 SD, *i.e.* −W, −L, and −H. Colonies from −2 plates were re-streaked onto new plates and colony growth was determined as described under "Experimental Procedures."

AD vector	DNA-BD vector	Growth on −W and −L dropout media[a]	Growth on −W, −L, and −H dropout media
pGADT7GRIF-1-(1–913)	pMBL33KIF5C-(336–542)	+++	−
pGADT7GRIF-1-(1–913)	pMBL33KIF5C-(593–804)	++	−
pGADT7GRIF-1-(1–913)	pMBL33KIF5C-(827–957)	+	+
pGADT7GRIF-1-(8–633)	pMBL33KIF5C-(336–542)	+++	−
pGADT7GRIF-1-(8–633)	pMBL33KIF5C-(593–804)	++	−
pGADT7GRIF-1-(8–633)	pMBL33KIF5C-(827–957)	+	+
pGADT7GRIF-1-(124–283)	pMBL33KIF5C-(336–542)	+++	−
pGADT7GRIF-1-(124–283)	pMBL33KIF5C-(593–804)	++	−
pGADT7GRIF-1-(124–283)	pMBL33KIF5C-(827–957)	+	+
pGADT7	pMBL33KIF5C-(336–542)	+++	−
pGADT7	pMBL33KIF5C-(593–804)	++	−
pGADT7	pMBL33KIF5C-(827–957)	+	−
pGADT7GRIF-1-(1–913)	pMBL33	+++	−
pGADT7GRIF-1-(8–633)	pMBL33	+++	−
pGADT7GRIF-1-(124–283)	pMBL33	+++	−
pGADT7	pMBL33	+++	−
PGAF10GRIF-1-(8–633)	pMBL33β2-IL	+++	++

[a] For colony growth, − = 0 cfu; + = 10–100 cfu; ++ = 100–200 cfu; +++ > 200 cfu. As for Table I, pGAD10GRIF-1-(8–633) and pMBL33β2-IL served as the positive control. The results are representative of $n = 3$ independent co-transformations.

post-bleached intensity of ECFP]) × 100% (14). For each FRET experiment, pseudo-FRET was always determined by applying the photobleaching protocol to cells transfected with pECFP alone. Pseudo-FRET values (typically ~2.9%) were always subtracted from the calculated FRET efficiencies of the test samples. As a further control, an area of the cell that was not photobleached was also analyzed in parallel for FRET to ensure that the FRET efficiency values determined were not artifacts due to the photobleaching protocol. A positive control, an ECFP-EYFP tandem construct linked by two amino acids (17), and a negative control, co-transfection of the separate clones pECFP and pEYFP, were both used to validate the system.

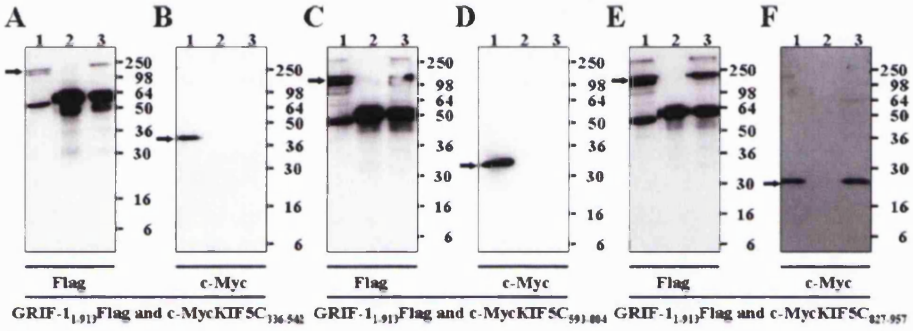

FIGURE 3. **GRIF-1 associates with the KIF5C cargo binding domain: demonstration by immunoprecipitation following co-expression of GRIF-1 and KIF5C truncation constructs in HEK 293 cells.** HEK 293 cells were transfected with pCISGRIF-1-FLAG and either pCMV-KIF5C C1-(336–542), pCMV-KIF5C C2-(593–804), or pCMV-KIF5C C3-(827–957), detergent extracts of cell homogenates were prepared 48 h post-transfection, and immunoprecipitation assays were carried out using either affinity-purified anti-FLAG antibodies or non-immune Ig and immune pellets analyzed by immunoblotting using anti-FLAG (20% of immune pellet) and anti-c-Myc (80% of immune pellet) antibodies, all as described under "Experimental Procedures." *A* and *B*, immunoprecipitation from HEK 293 cells transfected with pCISGRIF-1_{FLAG} and pCMV-KIF5C-(336–542); *C* and *D*, immunoprecipitation from HEK 293 cells transfected with pCISGRIF-1_{FLAG} and pCMV-KIF5C-(593–8-4); *E* and *F*, pCISGRIF-1_{FLAG} and pCMV-KIF5C-(827–957). In *A*, *C*, and *E*, immunoblots were probed with anti-FLAG antibodies and in *B*, *D*, and *F*, immunoblots were probed with anti-c-Myc antibodies. Gel lanes are: *1*, detergent-solubilized transfected HEK 293 cell homogenate; *2*, non-immune pellet; *3*, anti-FLAG pellet. *Arrows* denote: *A*, GRIF-1-FLAG, 115 kDa; *B*, c-Myc-tagged KIF5C-(336–542), 37 kDa; *C*, GRIF-1-FLAG, 115 kDa; *D*, c-Myc-tagged KIF5C-(593–804), 31 kDa; *E*, GRIF-1-FLAG, 115 kDa; and *F*, c-Myc-tagged KIF5C-(827–957), 20 kDa. The positions of molecular mass standards (kDa) are shown on the *right*. The immunoblots are representative of at least $n = 3$ immunoprecipitations from $n = 3$ independent transfections.

RESULTS

GRIF-1 Associates with the KIF5C Non-motor Domain: Demonstration by Both Yeast Two-hybrid Interaction Assays and Immunoprecipitation Strategies

We have previously shown that GRIF-1 associates with endogenous kinesin in the brain and in the heart by co-immunoprecipitation of GRIF-1 and kinesin using anti-GRIF-$1_{874-889}$ antibodies. Association was also demonstrated, again by co-immunoprecipitation, between exogenous GRIF-1 and exogenous KIF5C both co-expressed in HEK 293 cells. Further, yeast two-hybrid interaction assays using GRIF-1 and KIF5C as fish and bait, respectively, suggested that association between the two proteins is probably direct and involves the first coiled-coil domain of GRIF-1, GRIF-1-(124–283) (5). To delineate the GRIF-1 binding domain of KIF5C initially, the KIF5C motor domain, *i.e.* KIF5C-(1–335), and KIF5C non-motor domain, *i.e.* KIF5C-(336–957), were subcloned in-frame into either the yeast two-hybrid DNA binding domain vector, pMBL33, or the modified mammalian expression vector, pCMVTag4a, to yield N-terminally c-Myc-tagged fusion proteins. The association between GRIF-1 and KIF5C was then studied by both yeast two-hybrid interaction assays and immunoprecipitation strategies following the co-expression of GRIF-1 and KIF5C in HEK 293 cells. The results are summarized in Table 1 and Fig. 2.

Co-transformation of yeast with pGADT7GRIF-1-(1–913) with pMBL33KIF5C-(336–957) revealed a significant interaction between the two proteins as determined by nutritional selection on SD media −W, −L, and −H media (Table 1). An

interaction was also found between both GRIF-1-(8–633) and GRIF-1-(124–283) and KIF5C-(336–957). This was in contrast to yeast co-transformed with KIF5C-(1–335) and either full-length or truncated GRIF-1 constructs where no evidence for protein-protein association was found (Table 1). The same results were obtained in immunoprecipitation studies. FLAG-tagged GRIF-1 was co-expressed in HEK 293 cells with either c-Myc-tagged KIF5C-(1–335) (43 kDa) or KIF5C-(336–957) (98 kDa), detergent extracts prepared and immunoprecipitation carried out using anti-FLAG antibodies. In each case, anti-FLAG immunoreactivity with ~114 kDa was detected in the immune pellets (Fig. 2). Anti-c-Myc antibody immunoreactivity was, however, only present for GRIF-1/KIF5C-(336–957) transfectants further demonstrating an association between GRIF-1 and the C-terminal KIF5C non-motor domain.

The above experiments were also repeated for KLC (70 kDa). No association between GRIF-1 and KLC was detected by either yeast two-hybrid or co-immunoprecipitation assays (Table 1 and Fig. 2).

GRIF-1 Associates with the KIF5C C3 Cargo Binding Domain: Demonstration by Both Yeast Two-hybrid Interaction Assays and Immunoprecipitation Strategies

The GRIF-1 binding domain was further refined by generating three truncation constructs, KIF5C-(336–542), KIF5C-(593–804), and KIF5C-(827–957), of the KIF5C non-motor domain in both yeast DNA binding domain and mammalian expression vectors. These corresponded to three predicted coiled-coil domains in the non-motor domain where KIF5C-(336–542) and KIF5C-(593–804) encompassed the KIF5C stalk region and KIF5C-(827–957) the cargo binding domain. All three constructs were used, as above, in both yeast two-hybrid interaction assays and immunoprecipitation experiments following the co-expression of GRIF-1 and KIF5C-(336–542) (37 kDa), KIF5C-(593–804) (31 kDa), or KIF5C-(827–957) (20 kDa) truncated constructs in HEK 293 cells. The results are summarized in Table 2 and Fig. 3. Both experimental paradigms demonstrate that it is only the KIF5C-(827–957) cargo binding domain that associates with GRIF-1. This domain associates with full-length GRIF-1 and the GRIF-1-(8–633) and GRIF-1-(124–283) fragments.

Confocal Microscopy Studies of the Association between GRIF-1 and KIF5C

Characterization of ECFP-GRIF-1 and EYFP-KIF5C Constructs—The following in-frame constructs were generated by molecular cloning: full-length N- and C-terminally tagged KIF5C-EYFP, an N-terminal EYFP-tagged KIF5C-(1–335) motor domain, a C-terminal EYFP-tagged KIF5C-(336–957) non-motor domain, and an N-terminal ECFP-GRIF-1 (Fig. 1). Each was characterized with respect to molecular size by immunoblotting following expression in HEK 293 cells using anti-GFP antibodies and anti-GRIF-1 or anti-KIF5C antibodies. This was to ensure that the respective EYFP- or ECFP-tagged proteins did not undergo proteolytic digestion, thus the fluorescent moieties remained attached to the target proteins. The results for the full-length KIF5C constructs and GRIF-1 are shown in Fig. 4 and for the KIF5C-(1–335) motor domain and KIF5C-(336–957) non-motor domains in Fig. 5. In all cases, an increase in molecular weight for the tagged proteins was observed consistent with the addition of ECFP or EYFP. Further, a single band was found for all constructs in immunoblots using anti-GFP antibodies. The molecular masses of the tagged proteins were: GRIF-1, 115 kDa; ECFP-GRIF-1, 143 kDa; KIF5C, 115 kDa; EYFP-KIF5C, 143 kDa; c-Myc-tagged KIF5C-(1–335), 39 kDa; EYFP-KIF5C-(1–335), 66 kDa; c-Myc-tagged KIF5C-(336–957), 98 kDa; and EYFP-KIF5C-(336–957), 139 kDa.

It was also requisite to demonstrate that the tagged proteins

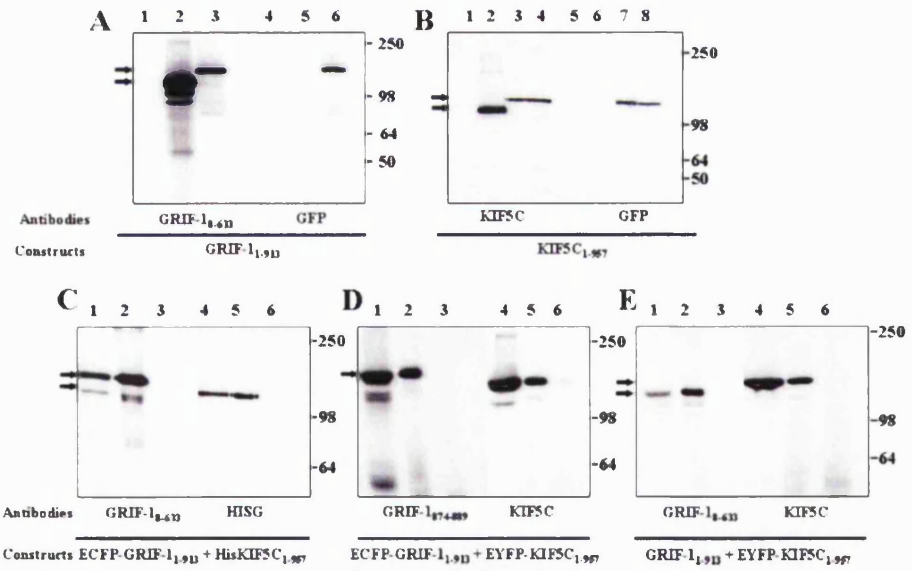

FIGURE 4. **Characterization of ECFP-GRIF-1 and EYFP-KIF5C: molecular size determination and co-association properties.** In *A* and *B*, HEK 293 cells were transfected with either pCISGRIF-1, pECFP-GRIF-1, pcDNAHisMAXKIF5C, pEYFP-KIF5C, or pKIF5C-EYFP, cell homogenates were prepared 24 h post-transfection, and samples were analyzed by immunoblotting with antibody specificities as shown in the abscissae. *A*, lanes are: *1* and *4*, untransfected cells; *2* and *5*, cells transfected with pCISGRIF-1; *3* and *6*, cells transfected with pECFP-GRIF-1. *B*, lanes are: *1* and *5*, untransfected cells; *2* and *6*, cells transfected with pcDNAHisMAXKIF5C; *3* and *7*, cells transfected with pEYFP-KIF5C; and *4* and *8*, cells transfected with pKIF5C-EYFP. In *C–E*, HEK 293 cells were co-transfected with either pECFP-GRIF-1 plus pcDNAHisMAXKIF5C (*C*), pECFP-GRIF-1 plus pEYFP-KIF5C (*D*), or pCISGRIF-1 plus pEYFP-KIF5C (*E*), homogenates were collected 24 h post-transfection, and immunoprecipitations were carried out using either sheep anti-GRIF-$1_{874-889}$ antibodies or non-immune Ig and immune pellets analyzed by immunoblotting using antibody specificities as shown in the abscissae, all as described under "Experimental Procedures." The lane layout is identical with: *lanes 1* and *4*, detergent-soluble fraction; *2* and *5*, immune pellet; and *3* and *6*, control pellet. *Arrows* denote: *A*, GRIF-1, 115 kDa; *B*, KIF5C, 115 kDa; EYFP-KIF5C, 143 kDa; *C*, ECFP-GRIF-1, 143 kDa; KIF5C, 115 kDa; *D*, ECFP-GRIF-1, 143 kDa; EYFP-KIF5C, 143 kDa; and *E*, GRIF-1, 115 kDa; EYFP-KIF5C, 143 kDa. The positions of molecular mass standards (kDa) are shown on the *right*. The immunoblots are representative of at least $n = 3$ immunoprecipitations from $n = 3$ independent transfections.

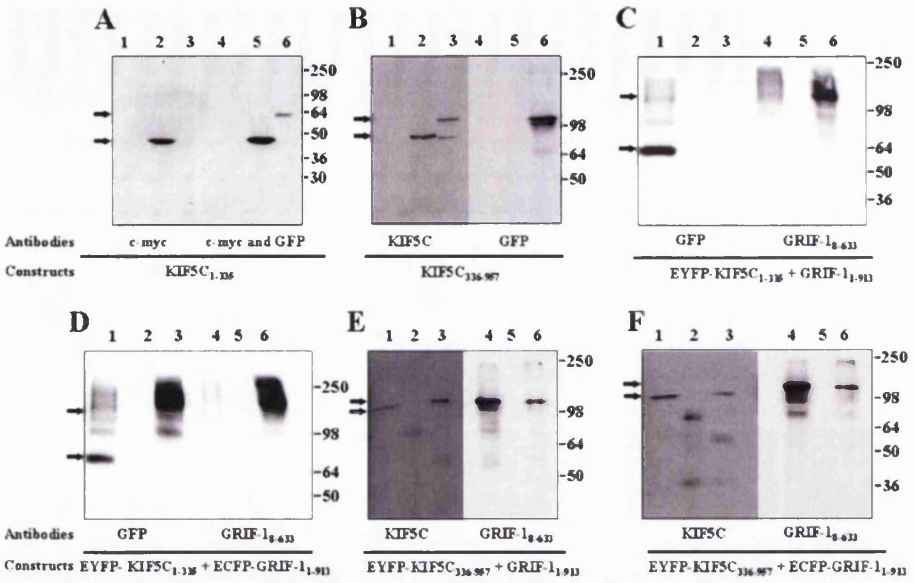

FIGURE 5. **Characterization of EYFP-KIF5C-(1–335) and EYFP-KIF5C-(336–957): molecular size determination and co-association properties.** In *A* and *B*, HEK 293 cells were transfected with either pCMV-KIF5C-(1–335), pEYFP-KIF5C-(1–335), pCMV-KIF5C-(336–957), or pEYFP-KIF5C-(336–957), cell homogenates were prepared 24 h post-transfection, and samples were analyzed by immunoblotting with antibody specificities as shown in the abscissae. *A*, lanes are: *1* and *4*, untransfected cells; *2* and *5*, cells transfected with pCMV-KIF5C-(1–335); *3* and *6*, cells transfected with pEYFP-KIF5C-(336–957). *B*, lanes are: *1* and *4*, untransfected cells; *2* and *5*, cells transfected with pCMV-KIF5C-(336–957); and *3* and *6*, cells transfected with pEYFP-KIF5C-(336–957). In *C–F*, HEK 293 cells were co-transfected with either pCISGRIF-1 plus pEYFP-KIF5C-(1–335) (*C*), pECFP-GRIF-1 plus pEYFP-KIF5C-(1–335) (*D*), pCISGRIF-1 plus pEYFP-KIF5C-(336–957) (*E*), or pECFP-GRIF-1 plus pEYFPKIF5C-(336–957) (*F*), homogenates were collected 24 h post-transfection, and immunoprecipitations were carried out using either sheep anti-GRIF-$1_{874-889}$ antibodies or non-immune Ig and immune pellets analyzed by immunoblotting using antibody specificities as shown in the abscissae all as described under "Experimental Procedures." The lane layout is identical with: *1* and *4*, detergent-soluble fraction; *2* and *5*, control pellet; and *3* and *6*, immune pellet. *Arrows* denote: *A*, c-Myc-tagged KIF5C-(1–335), 39 kDa; EYFP-KIF5C-(1–335), 66 kDa; *B*, c-Myc-tagged KIF5C-(336–957), 98 kDa; EYFP-KIF5C-(336–957), 139 kDa; *C*, EYFP-KIF5C-(1–335), 66 kDa; ECFP-GRIF-1, 143 kDa; *D*, EYFP-KIF5C-(1–335), 66 kDa; ECFP-GRIF-1, 143 kDa; *E*, EYFP-KIF5C-(336–957), 139 kDa; GRIF-1, 115 kDa; and *F*, EYFP-KIF5C-(336–957), 139 kDa; ECFP-GRIF-1 143 kDa. The positions of molecular mass standards (kDa) are shown on the *right*. The immunoblots are representative of at least $n = 3$ immunoprecipitations from $n = 3$ independent transfections.

behaved as wild type. This was demonstrated here by the ability of the tagged protein to co-associate with the non-tagged or tagged binding partner. Thus the following pairwise combinations were co-expressed in HEK 293 cells, immunoprecipitations carried out with anti-GRIF-$1_{874-889}$ antibodies, and immune pellets analyzed by anti-GRIF-1, anti-KIF5C, and anti-GFP antibodies: ECFP-GRIF-1 plus KIF5C; ECFP-GRIF-1 plus EYFP-KIF5C; GRIF-1 plus EYFP-KIF5C; ECFP-GRIF-1 plus KIF5C-EYFP; GRIF-1 plus KIF5C-EYFP; GRIF-1 plus EYFP-KIF5C-(1–335); ECFP-GRIF-1 plus EYFP-KIF5C-(1–335); GRIF-1 plus EYFP-KIF5C-(336–957); and ECFP-GRIF-1 plus EYFP-KIF5C-(336–957). The results are shown for full-length constructs in Fig. 4 (*E–G*) and for the KIF5C motor and non-motor domains in Fig. 5 (*C–F*). In all cases except as expected for the KIF5C-(1–335) and GRIF-1 double transfectants, a specific association was found between the tagged-untagged or tagged-tagged GRIF-1/KIF5C combinations. Note that the results for the immunoprecipitations for the C-terminal-tagged KIF5C constructs, *i.e.* KIF5C-EYFP, are not shown, because they gave identical results to those found for the immunoprecipitations of N-terminal-tagged KIF5C and GRIF-1/ECFP-GRIF-1.

Co-localization Studies—In transfected COS-7 cells, ECFP-GRIF-1 was found to be distributed throughout the cell cytoplasm with some areas showing notable enrichment at sites close to the nucleus (Fig. 6, *B* and *C*). This localization pattern is similar to that reported for the expression of GRIF-1 in HEK 293 cells (1) where the enriched areas were shown to co-localize with aggregated mitochondria (5). EYFP-KIF5C and KIF5C-EYFP expressed alone in COS-7 cells showed the same distribution profile with fluorescence visible throughout the cell cytoplasm, and, when they are present, EYFP-KIF5C was concentrated at the ends of cellular extensions (Fig. 6*E*). When ECFP-GRIF-1 plus EYFP-KIF5C or KIF5C-EYFP was co-expressed, the distribution of ECFP-GRIF-1 was changed. In all cells imaged ($n = 35$), the majority of ECFP-GRIF-1 was recruited to KIF5C-enriched areas, which were particularly apparent at the end of cellular extensions. In cells where no processes were evident, co-localization was seen adjacent to the cell membrane (supplemental Fig. S1). In some co-transfected cells (19 out of 35 cells; 54%), some ECFP-GRIF-1 was still found in the cell cytoplasm where it was not associated with EYFP-KIF5C (Fig. 6, *G* and *H*). This may be a result of overexpression of ECFP-GRIF-1 in those particular cells. Fig. 6 also shows the distribution of mitochondria in COS-7 cells transfected with either ECFP-GRIF-1 (*L–P*), ECFP-KIF5C (*Q–U*), or ECFP-GRIF-1 plus EYFP-KIF5C (*V–AA*). Aggregated mitochondria are only seen in cells when ECFP-GRIF-1 was overexpressed; *i.e.* compare Fig. 6*N* (ECFP-GRIF-1 transfectant) with Fig. 6*S* (EYFP-KIF5C transfectant).

EYFP-KIF5C-(1–335) expressed alone showed a diffuse distribution throughout the whole cell, including in 55% of transfected cells (16 of 29 cells), and the cell nucleus (Fig. 7*B*). In addition, in ~24% of transfected cells (7 of 29 cells), KIF5C-(1–335) was associated with filamentous structures thought to be the microtubules, consistent with the existence of a microtubule binding site within the KIF5C-(1–335) (supplemental Fig. S2). This distribution pattern was not changed by co-expression of EYFP-KIF5C-(1–335) with ECFP-GRIF-1 (Fig. 7, *E–G*). EYFP-KIF5C-(336–957) expressed alone was localized as filamentous structures in the cell cytoplasm (Fig. 7*J*). This distribution was similar to that reported by Navone *et al.* (18) following overexpression in CV-1 monkey kidney endothelial cells of a vesicular stomatitis virus-tagged KHC construct that contained the KHC C-terminal portion of the α-helical coiled-coil rod and the C-terminal tail. The filamentous labeling found by Navone *et al.* (18) co-localized with microtubules and a micro-

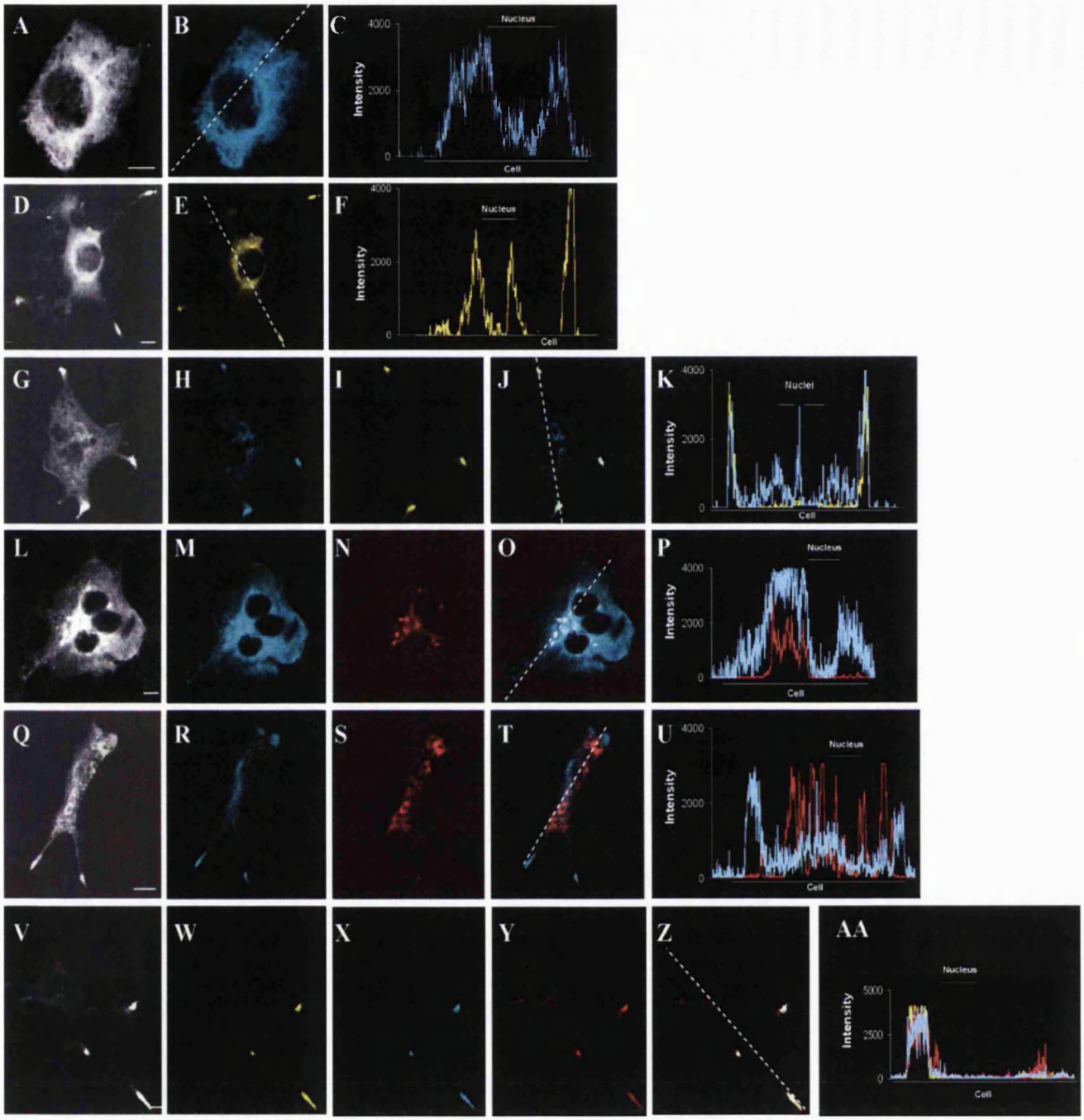

FIGURE 6. **Confocal microscopy imaging of ECFP-GRIF-1 and EYFP-KIF5C expressed in COS-7 cells.** ECFP-GRIF-1 and/or EYFP-KIF5C and/or DsRed1-Mito were co-expressed in COS-7 cells, cells were fixed 24–40 h post-transfection and imaged by confocal microscopy all as described under "Experimental Procedures." *A–C*, ECFP-GRIF-1; *D–F*, EYFP-KIF5C and *G-K*, co-expression of ECFP-GRIF-1 plus KIF5C-EYFP; *L–P*, ECFP-GRIF-1 plus DsRed1-Mito; *Q–U*, ECFP-KIF5C plus DsRed1-Mito; *V–AA*, ECFP-GRIF-1 plus EYFP-KIF5C plus DsRed1-Mito. *A*, *D*, *G*, *L*, *Q*, and *V* are images with saturated fluorescence intensity to show the complete cell outline; *B*, *E*, *H*, *I*, *J*, *M*, *N*, *O*, *R*, *S*, *T*, *W*, *X*, *Y*, and *Z* are a single confocal section of a selected transfected cell; *C*, *F*, *K*, *P*, *U*, and *AA* are pixel intensity profiles of the line scans shown in *B*, *E*, *J*, *O*, *T*, and *Z*, respectively; *J*, *O*, *T*, and *Z* are the merged images of (*H* plus *I*), (*M* plus *N*), (*R* plus *S*), and (*W* plus *X* plus *Y*), respectively, to show the co-localization. Note that in *G–J* and *L–O*, the transfected cell is multinucleated. It has been previously reported that there is a higher percentage of multinucleated cells when cells transfected with KHC clones are compared with untransfected cells (18). However, multinucleate and uninucleate transfected cells showed the same distribution of KIF5C in single transfections and co-distribution of KIF5C and GRIF-1 in co-transfected cells. Images are representative of $n = 35$ cells from at least $n = 3$ independent transfections. *Scale bars* are 10 μm.

tubule binding site within the non-motor domain was identified (18). In the presence of ECFP-GRIF-1 the distribution pattern of EYFP-KIF5C-(336–957) was changed. It was always co-localized with ECFP-GRIF-1-rich regions close to the nucleus (Fig. 7, *M* and *O*). This pattern is reminiscent of the localization of GRIF-1 with aggregated mitochondria as reported for GRIF-1-transfected HEK 293 cells (5). Indeed, when COS-7 cells were transfected with pECFP-GRIF-1,

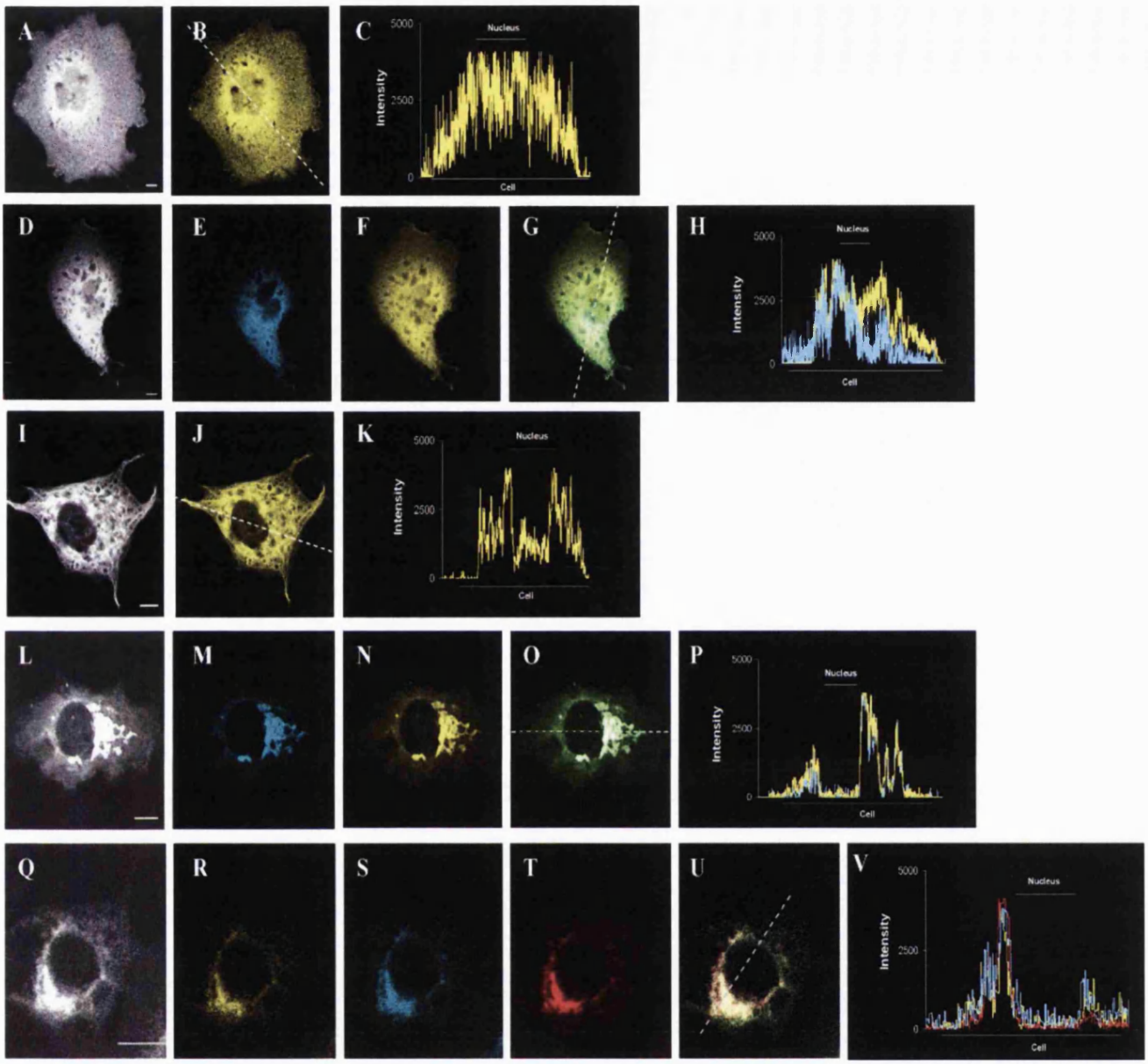

FIGURE 7. **Confocal microscopy imaging of ECFP-GRIF-1 and EYFP-tagged KIF5C-(1–335) and KIF5C-(336–957) expressed in COS-7 cells.** ECFP-GRIF-1 and/or EYFP-KIF5C-(1–335), EYFP-KIF5C-(336–957), and/or DsRed1-Mito were co-expressed in COS-7 cells, cells were fixed 24–40 h post-transfection and imaged by confocal microscopy all as described under "Experimental Procedures." *A–C*, EYFP-KIF5C-(1–335); *D–H*, EYFP-KIF5C-(1–335) plus ECFP-GRIF-1; *I–K*, EYFP-KIF5C-(336–957); *L–P*, EYFP-KIF5C-(336–957) plus ECFP-GRIF-1; and *Q–V*, ECFP-GRIF-1 plus EYFP-KIF5C-(336–957) plus DsRed1-Mito. *A*, *D*, *I*, *L*, and *Q* are images with saturated fluorescence intensity to show the complete cell outline; *B*, *E*, *F*, *G*, *J*, *M*, *N*, *O*, *R*, *S*, *T*, and *U* are a single confocal section of a selected transfected cell; *C*, *H*, *K*, *P*, and *V*, pixel intensity profile of the line scans shown in *B*, *G*, *J*, *O*, and *U*, respectively; *G*, merged *E* and *F*; *O*, merged *M* and *N*; and *U* is merged *R*, *S*, and *T* to show areas of co-localization. Images are representative of at least $n = 25$ cells from $n = 3$ independent transfections. *Scale bars* are 10 μm.

pEYFP-KIF5C-(336–957), and pDsRed1Mito to label mitochondria, all three fluorescent moieties were co-localized close to the cell nucleus (Fig. 7, *Q–V*).

FRET Measurements—To test whether ECFP-GRIF-1 associated directly with fluorescently tagged KIF5C, FRET studies were carried out in transfected HEK 293 cells. FRET efficiencies were measured by acceptor photobleaching. It was necessary to carry out these measurements in HEK 293 cells rather than COS-7 cells, because in the latter, the expression level of the fluorescent constructs was relatively low thus exposure to the appropriate laser for cell imaging resulted in the photobleaching of either EYFP or ECFP. In HEK 293 cells, the expression of the constructs was higher due to both a higher transfection efficiency and greater protein expression thus circumventing problems due to the photobleaching. Note that similar subcellular distribution profiles were found for the expression of single and pairwise GRIF-1/KIF5C combinations for both COS-7 cells and HEK 293 cells, *i.e.* GRIF-1/KIF5C and GRIF-1/KIF5C-(336–957) both co-localized.

In initial studies, optimum conditions were established for the measurement of FRET efficiency by acceptor photobleaching

using positive and negative ECFP/EYFP controls (Fig. 8). A FRET efficiency of 24.6% ± 2.0 (n = 22 cells) was determined for the positive control (ECFP-EYFP tandem construct) and a FRET efficiency of 3.8% ± 0.5 (n = 18 cells) was measured for the negative control (pECFP and pEYFP). The percentages of FRET efficiency for the GRIF-1/KIF5C constructs were: 5.6% ± 0.5 for ECFP-GRIF-1/N-EYFP-KIF5C (n = 15 cells); 10.3% ± 0.7 for ECFP-GRIF-1/KIF5C-EYFP (n = 20 cells); 4.0% ± 0.4 for ECFP-GRIF-1/EYFP- KIF5C-(1–335) (n = 11 cells); and 12.5% ± 0.5 for ECFP-GRIF-1/EYFP-KIF5C-(336–957) (n = 16 cells). Thus, a significant FRET value was only found for the ECFP-GRIF-1/KIF5C-EYFP and ECFP-GRIF-1/EYFP-KIF5C-(336–957) pairs showing a direct association between GRIF-1 and the C-terminal, non-motor domain of the kinesin-1 molecule, KIF5C.

GRIF-1, KIF5C, and KLC Interactions

To investigate whether GRIF-1 associates with the assembled heavy chain plus light chain tetrameric kinesin complex, immunoprecipitation and confocal imaging experiments were carried out on cells co-transfected with GRIF-1, KIF5C, and KLC clones. The results are shown in Fig. 9.

Co-immunoprecipitation Studies—In the following experiments, it was necessary to use the EYFP-tagged form of KIF5C, because pcDNAHisMaxKIF5C generates a His-tagged protein that is recognized by anti-GRIF-1_{8-633} antibodies (anti-GRIF-1_{8-633} antibodies were raised to poly-His tagged GRIF-1_{8-633} (5)). In GRIF-1/EYFP-KIF5C double transfectants, GRIF-1 and EYFP-KIF5C co-immunoprecipitated (Fig. 4*E*); in KIF5C and KLC double transfectants, KIF5C and KLC co-immunoprecipitated (Fig. 9*B*), but in GRIF-1 and KLC double transfectants, no association between the two proteins was detected (Figs. 1*E*, 1*F*, and 9*A*). When HEK 293 cells were transfected with GRIF-1 plus EYFP-KIF5C plus KLC clones, detergent extracts were prepared and samples were immunoprecipitated with anti-GRIF-1_{8-633} antibodies, and GRIF-1, KIF5C, *and* KLC immunoreactivities were then all found in the test but not control pellets (Fig. 9*C*). Because KLC did not associate with GRIF-1 in the absence of KIF5C, this must mean that GRIF-1 associates with the KHC, KLC tetrameric complex.

Co-localization Studies—The same combinations of clones as described for the co-immunoprecipitation studies were used for the transfection of COS-7 cells. Representative confocal microscopy images are shown in Fig. 9. Points to note are: (i) overexpression of GRIF-1 did not change the distribution pattern of KLC and no areas of co-localization were found (Fig. 9, *D–H*); (ii) EYFP-KIF5C and KLC mostly co-localized within the cell cytoplasm (Fig. 9, *I–M*); (iii) it was noted that in the majority of the EYFP-KIF5C plus KLC double transfectants, no fluorescence was detected at the tips of cell extensions such as seen in Fig. 6*E*; (iv) in the triple transfections, co-localization of EYFP-KIF5C, KLC, and ECFP-GRIF-1 was seen both in the cell cytoplasm and later, as for both EYFP-KIF5C alone and EYFP-KIF5C plus ECFP-GRIF-1, concentrated at focal points at the tips of cell processes (Fig. 9, *N–S*).

DISCUSSION

We have previously shown that GRIF-1 associates with the molecular motor, kinesin (5). In this report, we have used four experimental approaches to map the GRIF-1 binding domain of the prototypic kinesin-1, KIF5C. Immunoprecipitations and yeast two-hybrid studies both mapped the GRIF-1 binding region of KIF5C to the C3 cargo binding domain. Further, in the yeast two-hybrid interaction assays it was found that the C3 cargo binding domain specifically associated with GRIF-1-(124–283) in agreement with the previous mapping of the kinesin binding domain of GRIF-1 (5). Overexpression of EYFP- and ECFP-tagged KIF5C and GRIF-1, respectively, in either HEK 293 cells or COS-7 cells showed that GRIF-1 co-localized with KIF5C (Fig. 6, *H–J*) and in refined studies, with the KIF5C non-motor domain, KIF5C-(336–957). FRET experiments established that the interaction between the two proteins was direct. The fact that a significant FRET value was found between the C-terminal-tagged KIF5C and ECFP-GRIF-1, the C-terminal-tagged KIF5C-(336–957) and GRIF-1, but not between the N-terminal-tagged KIF5C nor the motor domain, EYFP-KIF5C-(1–335), confirmed the direct association between the two proteins at the KIF5C C-terminal and GRIF-1 N-ter-

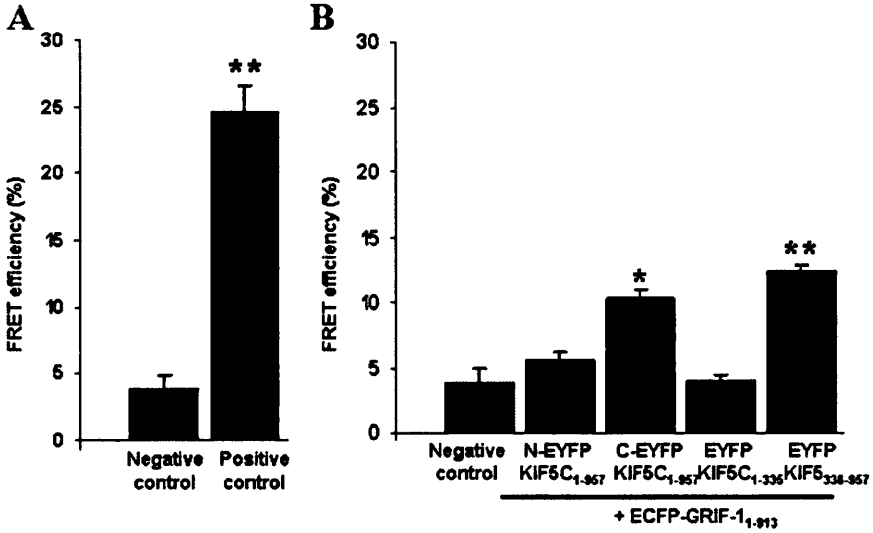

FIGURE 8. **Measurement of FRET efficiencies between ECFP-GRIF-1 and EYFP-tagged KIF5C constructs by acceptor photobleaching.** ECFP-GRIF-1 and either EYFP-KIF5C, KIF5C-EYFP, EYFP-KIF5C-(1–335), EYFP-KIF5C-(336–957) combinations were co-expressed in HEK 293 cells and FRET efficiencies by acceptor photobleaching were measured exactly as described under "Experimental Procedures." *A*, the FRET efficiencies for the negative control, *i.e.* HEK 293 cells transfected with pECFP plus pEYFP and the positive control, *i.e.* the pECFP-EYFP tandem construct. *B*, the FRET efficiencies for the negative control and each GRIF-1/KIF5C combination as labeled. The results are the means for at least n = 8 individual cells from n = 3 independent transfections for each pairwise combination. Each FRET efficiency was compared with the FRET efficiency obtained for the negative control using an unpaired Student t test. *, $p < 0.025$; **, $p < 0.0005$.

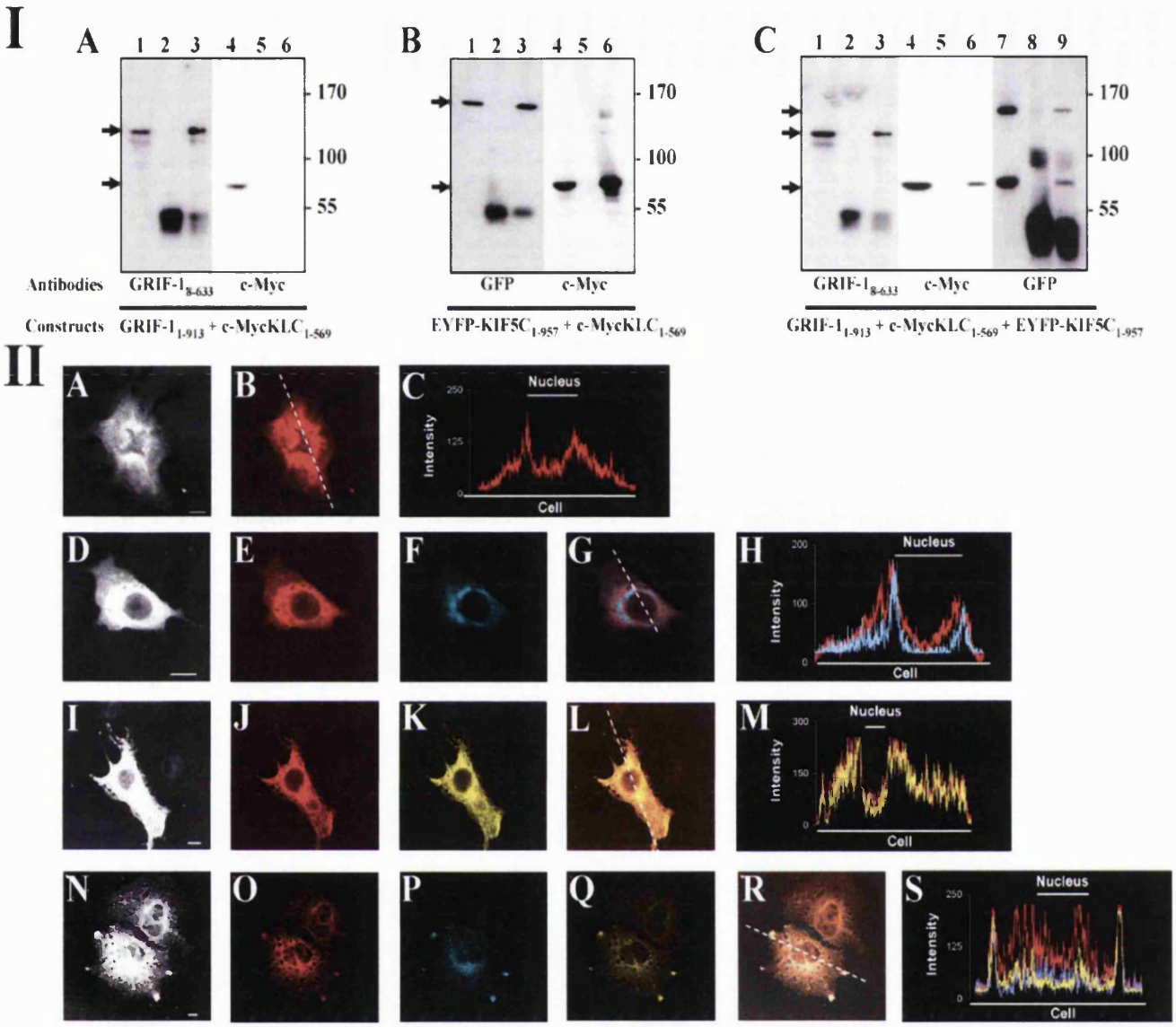

FIGURE 9. **GRIF-1 associates with the KHC/KLC tetrameric complex: demonstration by co-immunoprecipitation studies and confocal microscopy imaging.** *I*, immunoprecipitation experiments where HEK 293 cells were transfected with either pCISGRIF-1 plus pCMVKLC (*A*); pEYFP-KIF5C plus pCMVKLC (*B*), or pCISGRIF-1 plus pEYFP-KIF5C plus pCMVKLC (*C*), detergent extracts of cell homogenates were prepared 48 h post-transfection, immunoprecipitation assays were carried out using either affinity-purified anti-GRIF-1$_{8-633}$ (*A* and *C*), anti-KIF5C$_{938-957}$ antibodies (*B*), or non-immune Ig (*A–C*), and immune pellets were analyzed by immunoblotting using antibodies as shown in the abscissae, all as described under "Experimental Procedures." The gel layout has the same format for each immunoprecipitation as follows: *lanes 1*, *4*, and *7*, detergent-solubilized transfected HEK 293 cell homogenate; *lanes 2*, *5*, and *8*, non-immune pellet; and *lanes 3*, *6*, and *9*, immune pellet. Note that 10% of the immune pellet was analyzed for the detection of the immunoprecipitating antibody protein, whereas 90% of the immune pellets were analyzed for the detection of co-associating proteins. The positions of molecular mass standards (kDa) are shown on the *right*. The immunoblots are representative of at least $n = 3$ immunoprecipitations from $n = 3$ independent transfections. *II*, confocal microscopy imaging experiments. COS-7 cells were transfected with either *A–C*, pCMVKLC; *D–H*, pCMVKLC plus pECFP-GRIF-1; *I–M*, pCMVKLC plus pEYFP-KIF5C; and *N–S*, pCMVKLC plus pECFP-GRIF-1 plus pEYFP-KIF5C. Cells were fixed 24–40 h post-transfection, stained with anti-c-Myc antibodies, and imaged by confocal microscopy all as described under "Experimental Procedures." *A*, *D*, *I*, and *N* are images with saturated fluorescence intensity to show the complete cell outline; *B*, *E*, *J*, and *O*, are each a single confocal section of a selected transfected cell showing the distribution of c-Myc-tagged KLC; *F* and *P*, are each a single confocal section of a selected transfected cell showing the distribution of ECFP-GRIF-1; *K* and *Q*, are each a single confocal section of a selected transfected cell showing the distribution of EYFP-KIF5C; *G*, *L*, and *R*, are merged to show the co-localization; *H*, *M*, and *S*, pixel intensity profile of the line scans shown in *G*, *L*, and *R*, respectively. Images are representative of at least $n = 10$ cells from $n = 3$ independent transfections for all combinations. *Scale bars* are 10 μm.

minal regions. Finally, GRIF-1 was shown to form a ternary complex with KHC and KLC. These findings substantiate a role for GRIF-1 as an adaptor protein linking kinesin to its cargo in the anterograde trafficking processes in neurons. A schematic model summarizing the possible interactions between GRIF-1 and kinesin is shown in Fig. 10.

The concept of the selective transport of proteins and/or organelles via adaptor proteins linking kinesin motor proteins to their cargoes is an emerging feature of trafficking mechanisms in neurons. As described in the introduction, there are now several examples of such kinesin-associated adaptors and their cargoes, *i.e.* mitochondria and syntaxin-1-containing vesicles are attached to the KHC cargo binding domain by the adaptor protein, syntabulin, for their transport to synapses (9);

JIP-3, a JNK signaling pathway protein, binds to a six tetratricopeptide motif in KLCs to transport the cargo, APP (10); KIF17 forms a complex with mLin10 in the transportation of *N*-methyl-D-aspartate receptor NR2B subunits to the synapse (11, 12); and GRIP1 is an adaptor protein linking the AMPA subtype of glutamate receptor-containing vesicles to KIF5 (13). In all these examples, the KHC or the KLC were studied in isolation, whereas, here it is clearly shown that GRIF-1 binds to the KHC when assembled with the KLC. Further, it was noted that the distribution pattern of EYFP-KIF5C is affected by co-expression of KLCs. This observation agrees with that reported by Verhey *et al.* (19). Here it was shown that association of KHCs with KLCs inhibits the binding of KHC to microtubules by inducing the formation of a folded KHC conformation. In the presence of GRIF-1, KHCs and KLCs are co-associated with GRIF-1 in the cell cytoplasm *and* at the tips of transfected COS-7 cell processes as observed for cells transfected with EYFP-KIF5C alone but not for the majority of cells for EYFP-KIF5C plus KLC transfectants. This suggests that, perhaps, GRIF-1 mediates conformational changes of KHC/KLC complexes such as unfolding. This then permits binding of the complex to microtubules, and active motor transport can now occur as has been shown in kinesin motility assays *in vitro* (20, 21).

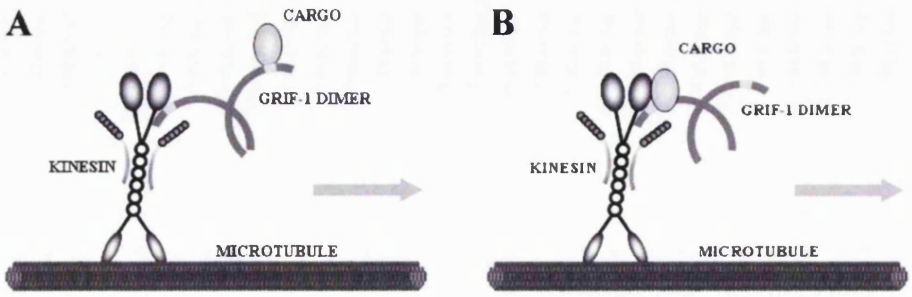

FIGURE 10. **A schematic diagram depicting putative GRIF-1-kinesin-cargo interactions for the anterograde trafficking of defined cargoes to synapses.** Kinesin is depicted as a tetramer with two copies of the KHC and two copies of the KLC. For the heavy chain, the motor domain is shown associated with microtubules and contains, additionally, the stalk and cargo binding regions. GRIF-1 is depicted as a dimer (G. Ojla, M. Beck, K. Brickley, and F. A. Stephenson, manuscript in preparation) forming a ternary complex with the cargo binding domain of the KHC and the cargo. Yeast two-hybrid interaction assays using GRIF-1 deletion constructs previously showed that $GABA_A$ receptor $\beta 2$ subunits and KIF5C share the same coiled-coil binding domain of GRIF-1, *i.e.* GRIF-1-(124–283) (*1* and *5*) that is depicted in the figure by the *lighter shading*. *A* is a model where the KHC and the cargo bind separately to each of the GRIF-1 polypeptides; *B* is an alternative model whereby the KHC, GRIF-1, and the cargo associate with the same GRIF-1 subunit.

A further example of kinesin adaptor proteins are the α and β isoforms of dystrobrevin (22). Like GRIP1 (13) and now, GRIF-1, β-dystrobrevin was shown to bind to the C-terminal KHC cargo binding domain (23). Both GRIP-1 and α- and β-dystrobrevins bind to the cargo binding domain with similar affinities as determined by surface plasmon resonance analysis, *i.e.* GRIP-1, $K_D = 1.9 \times 10^{-8}$ M (13); β-dystrobrevin, $K_D = 4 \times 10^{-8}$ M (23). Moreover and interestingly, Ceccarini *et al.* (23) showed that two distinct regions of β-dystrobrevin contribute to the binding to KHC and that *in vitro* phosphorylation of a glutathione-β-dystrobrevin construct resulted in a decreased binding to KHC (23). This suggests that both tertiary structure and post-translational modification may modulate β-dystrophin-KHC or, more generally, adaptor-kinesin interactions.

The one or more cargoes transported by GRIF-1 (and the homologous protein, OIP106) have yet to be ascertained. The first description of GRIF-1 identified it as a $GABA_A$ receptor $\beta 2$ subunit-associated protein (1). This suggested that the cargo may be assembled, $\beta 2$ subunit-containing $GABA_A$ receptors, but *in vivo* evidence to support this function is still lacking. However, Gilbert *et al.* (6) recently showed that OIP106 (TRAK1) co-associated with $GABA_A$ receptor $\alpha 1$ subunits, thus corroborating a role for the GRIF-1/OIP106 family in transporting $GABA_A$ receptors. Additionally, both GRIF-1 and OIP106, like the *Drosophila* orthologue Milton, have been shown to aggregate mitochondria following their respective overexpression in mammalian cells (3, 5). Further, without Milton, *Drosophila* are blind and mitochondria accumulated in neuronal cell bodies, whereas synaptic terminals and axons were depleted of mitochondria (3). However, if the cargo is a mitochondrion, it is unclear with which mitochondrial protein GRIF-1 or OIP106 associates. It is unlikely that $GABA_A$ receptors are expressed in mitochondria. GRIF-1 and OIP106 have, however, both been shown to associate with the enzyme, OGT (2). There are two forms of OGT, a mitochondrial (m) and a nucleocytoplasmic (nc) variant. The GRIF-1 or OIP106 binding domain of OGT is conserved between both forms mapping to mOGT-(51–100) and ncOGT-(167–283) (2, 5).[6] mOGT has been reported to localize within the mitochondrial inner membrane (24) and would not therefore be accessible for binding to soluble GRIF-1-KHC or OIP106-KHC complexes. It is thus more likely that GRIF-1 and OIP106 associate with ncOGT.

Other candidate proteins that mediate the association between GRIF-1 and mitochondria include syntabulin (25) and the mitochondrial GTPase, Miro (26). Both have both been implicated in anterograde mitochondrial trafficking in neurons. Indeed, it was recently demonstrated that Miro forms complexes with both GRIF-1 and OIP106 (27) and in *Drosophila*, Milton with Miro (28).

GRIF-1 is found within the brain in both neurons and glial cells.[7] Furthermore, it is also expressed in the heart and at lower levels in skeletal muscle (1). It is possible that the cargo transported by GRIF-1-KHC complexes may be cell type-specific depending on the repertoire of KHCs expressed by the host cell and that the formation of such complexes may possibly be regulated by post-translational modifications such as that recently described for α- and β-dystrobrevin. The enzyme, OGT, with which GRIF-1 and OIP106 are known to be associated, catalyzes the addition of *N*-acetylglucosamine onto serine and

[6] M. Beck, K. Pozo, and F. A. Stephenson, unpublished results.
[7] K. Brickley, G. S. Ojla, M. J. Smith, and F. A. Stephenson, unpublished observations.

threonine residues of protein substrates. This *O*-glycosylation post-translational modification occurs in the cell cytoplasm, and it is thought to regulate protein function and to have a reciprocal relationship with post-translational modification and regulation via phosphorylation, the so-called "YinOYang" relationship (29). The YingOYang neural network predictions for *O*-β-GlcNAc attachment sites in eukaryotic protein sequences (www.cbs.dtu.dk/services/YinOYang) predicts several sites for *O*-glycosylation within the non-kinesin binding GRIF-1 C-terminal domain. It is known that GRIF-1 and OIP106 are *O*-glycosylated *in vivo* (2), although the residues that are actually *O*-glycosylated have not been identified. Thus perhaps the association of GRIF-1 and OIP106 with OGT is to regulate GRIF-1-KHC interactions rather than OGT *per se* being a cargo.

In summary, the work described herein maps the GRIF-1 binding domain of KIF5C and shows that GRIF-1 forms a ternary complex with KIF5C and KLC that results in the aggregation of mitochondria. These findings consolidate the role of GRIF-1 as an adaptor protein involved in motor-dependent anterograde transport. Defects in these transport mechanisms, especially in the transport of mitochondria and $GABA_A$ receptors, purported to be GRIF-1 cargoes, may contribute to the pathology of neurodegenerative diseases such as Alzheimer disease, amyotrophic lateral sclerosis, hypertonia, and hereditary spastic paraplegia (30).

Acknowledgments—We thank Dr. T. Nagase and colleagues (Kazusa DNA Research Institute, Chiba, Japan) for the gift of the clone KIAA0531 (KIF5C) and Dr. L. B. Lachman (M.D. Andersen Cancer Center, Houston, TX) for the gift of the kinesin light chain clone, Dr. J. G. McNally and Dr. L. He (Johns Hopkins University) for the gift of pEYFP-ECFP, Dr. J. McIlhinney (University of Oxford) for initial help with the FRET studies, Ana Salgueiro (Universidade do Algarve, Portugal) for the preparation of pECFP-GRIF-1 and pEYFP-KIF5C, and Dr. R. J. Harvey (School of Pharmacy, University of London) for the gift of pDsRed1-Mito.

REFERENCES

1. Beck, M., Brickley, K., Wilkinson, H., Sharma, S., Smith, M., Chazot, P. L., Pollard, S., and Stephenson, F. A. (2002) *J. Biol. Chem.* **277,** 30079–30090
2. Iyer, S. P. N., Akimoto, Y., and Hart, G. W. (2003) *J. Biol. Chem.* **278,** 5399–5409
3. Stowers, R. S., Megeath, L. J., Gorska-Andrzejak, J., Meinertzhagen, I. A., and Schwarz, T. L. (2002) *Neuron* **36,** 1063–1077
4. Gorska-Andrzejak, J., Stowers, R. S., Borycz, J., Kostyleva, R., Schwarz, T. L., and Meinertzhagen, I. A., (2003) *J. Comp. Neurol.* **463,** 372–388
5. Brickley, K., Smith, M. J., Beck, M., and Stephenson, F. A. (2005) *J. Biol. Chem.* **280,** 14723–14732
6. Gilbert, S. L., Zhang, L., Forster, M. L., Anderson, J. R., Iwase, T., Soliven, B., Donahue, L. R., Sweet, H. O., Bronson, R. T., Davisson, M. T., Wollman, R. L., and Lahn, B. T. (2006) *Nat. Genet.* **38,** 245–250
7. Hirokawa, N., and Takemura, R. (2005) *Nat. Rev. Neurosci.* **6,** 201–214
8. Miki, H., Okada, Y., and Hirokawa, N. (2005) *Trends Cell Biol.* **15,** 467–476
9. Su, Q., Cai, Q., Gerwin, C., Smith, C. L., and Sheng, Z. H. (2004) *Nat. Cell Biol.* **6,** 941–953
10. Kamal, A., Stokin, G. B., Yang, Z., Xia, C. H., and Goldstein, L. S. (2000) *Neuron* **28,** 449–459
11. Setou, M., Nakagawa, T., Seog, D. H., and Hirokawa, N. (2000) *Science* **288,** 1796–1802
12. Guillaud, L., Setou, M., and Hirokawa, N. (2003) *J. Neurosci.* **23,** 131–140
13. Setou, M., Seog, D. H., Tanaka, Y., Kanai, Y., Takei, Y., Kawagishi, M., and Hirokawa, N. (2002) *Nature* **417,** 83–87
14. Pozo, K., and Stephenson, F. A. (2006) *Biochem. Soc. Transact.* **34,** 48–50
15. Liu, J., Ernst, S. A., Gladycheva, S. E., Lee, F. Y. Y., Lentz, S. I., Ho, C. S., Li, Q., and Stuenkel, E. L. (2004) *J. Biol. Chem.* **279,** 55924–55936
16. Nashmi, R., Dickinson, M. E., McKinney, S., Jareb, M., Labarca, C., Fraser, S. E., and Lester, H. (2003) *J. Neurosci.* **23,** 11554–11567
17. He, L., Bradrick, T. D., Karpova, T. S., Wu, X., Fox, M. H., Fischer, R., McNally, J. G., Knutson, J. R., Grammer, A. C., and Lipsky, P. E. (2003) *Cytometry* **53A,** 39–54
18. Navone, F., Niclas, J., Hom-Booher, N., Sparks, L., Bernstein, H. D., McCaffrey, G., and Vale, R. D. (1992) *J. Cell Biol.* **117,** 1263–1275
19. Verhey, K. J., Lizotte, D. L., Abramson, T., Barenboim, L., Schapp, B. J., and Rapoport, T. A. (1998) *J. Cell Biol.* **143,** 1053–1066
20. Coy, D. L., Hancock, W. O., Wagenbach, M., and Howard, J. (1999) *Nat. Cell Biol.* **1,** 288–292
21. Hackney, D. D., and Stock, M. F. (2000) *Nat. Cell Biol.* **2,** 257–260
22. Macioce, P., Gambara, G., Bernassola, M., Gaddini, L., Torreri, P., Macchia, G., Ramoni, C., Ceccarini, M., and Petrucci, T. C. (2003) *J. Cell Sci.* **116,** 4847–4856
23. Ceccarini, M., Torreri, P., Lombardi, D. G., Macchia, G., Macioce, P., and Petrucci, T. C. (2005) *J. Mol. Biol.* **354,** 872–882
24. Love, D. C., Kochran, J., Cathey, R. L., Shin, S.-H., and Hanover, J. A. (2003) *J. Cell Sci.* **116,** 647–654
25. Cai, Q., Gerwin, C., and Sheng, Z.-H. (2005) *J. Cell Biol.* **170,** 959–969
26. Guo, X., Macleod, G. T., Wellington, A., Hu, F., Panchumarthi, S., Schoenfield, M., Marin, L., Charlton, M. P., Atwood, H. L., and Zinsmaier, K. E. (2005) *Neuron* **47,** 379–393
27. Fransson, A., Ruusala, A., and Aspenstrom, P. (2006) *Biochem. Biophys. Res. Commun.* **344,** 500–510
28. Glater, E. E., Megeath, L. J., Stowers, R. S., and Schwarz, T. L. (2006) *J. Cell Biol.* **173,** 545–557
29. Wells, L., Vosseller, K., and Hart, G. W. (2001) *Science* **291,** 2376–2378
30. Goldstein, L. S. B. (2003) *Neuron* **40,** 415–425

GRIF-1–kinesin-1 interactions: a confocal microscopy study

K. Pozo and F.A. Stephenson[1]
School of Pharmacy, University of London, 29/39 Brunswick Square, London WC1N 1AX, U.K.

Abstract

GRIF-1 [$GABA_A$ (γ-aminobutyric $acid_A$) receptor interacting factor-1] is a member of a coiled-coil family of proteins thought to function as adaptors in the anterograde trafficking of organelles utilizing the kinesin-1 motor proteins to synapses. To study in more detail the molecular interaction between GRIF-1 and the kinesin-1 family member KIF5C, fluorescent yellow- and fluorescent cyan-tagged GRIF-1, KIF5C, the KIF5C MD (motor domain) and the KIF5C NMD (non-motor domain) fusion proteins were generated. Each was characterized with respect to size and ability to co-associate by immunoprecipitation following expression in HEK-293 (human embryonic kidney 293) cells. Further, their distribution in transfected HEK-293 and transformed African green monkey kidney (COS-7) cells was analysed by confocal microscopy. The fluorescent GRIF-1 and KIF5C fusion proteins were all found to behave as wild-type. Double GRIF-1/KIF5C transfectants revealed co-localization. The GRIF-1/KIF5C and GRIF-1/KIF5C NMD double transfectants showed different subcellular distributions compared with single GRIF-1, KIF5C or KIF5C NMD transfections. These studies confirm the association between GRIF-1 and kinesin-1 NMDs. Fluorescence resonance energy transfer studies are ongoing to characterize this interaction in more detail.

Introduction

GRIF-1 [$GABA_A$ (γ-aminobutyric $acid_A$) receptor interacting factor-1] was initially identified from rat brain by a yeast two-hybrid screen searching for $GABA_A$ receptor clustering and trafficking proteins [1]. GRIF-1 is the orthologue of the human protein, OIP98 [OGT (β-O-linked *N*-acetylglucosamine transferase) interacting protein 98], and it is the homologue of the protein OIP106. GRIF-1 is also probably the orthologue of the *Drosophila* protein Milton, a kinesin-associated protein that is involved in the transport of mitochondria to the synapses in retina [2]. GRIF-1, OIP106 and Milton belong to a newly identified family of coiled-coil proteins. Although their function is not definitively established, GRIF-1 interacting proteins have been identified, which gives insight into their possible role in neurons. These proteins include the enzymes OGT [3,4] and kinesin [2,5]. OGT catalyses the addition of *N*-acetylglucosamine on to serine and threonine residues of protein substrates. This O-glycosylation post-translational modification occurs in the cell cytoplasm. It is thought to regulate protein function and to have a reciprocal relationship with post-translational modification and regulation via phosphorylation, the so-called 'YinOYang' relationship [6]. Cytoplasmic O-glycosylated proteins are particularly abundant in the central nervous system [7].

Kinesin-1 proteins are plus-end-directed microtubule motors. They transport specific cargoes, e.g. synaptic vesicle precursors, lysosomes and mitochondria, anterogradely along the microtubules. The kinesin-1 family members are conventional kinesins that include KIF5A, KIF5B and KIF5C. KIF5B is ubiquitously expressed, whereas KIF5A and KIF5C are only present in neurons [8]. Kinesin-1 proteins are tetramers formed by the association of two KHCs (kinesin heavy chains) and two KLCs (kinesin light chains). The KHC is formed from an N-terminal MD (motor domain) that contains the microtubule- and ATP-binding sites, and a C-terminal NMD (non-motor domain). This domain includes a neck, a coiled-coil stalk region and a cargo-binding site in its C-terminal region. The KLC interacts with the KHC via the stalk region. Cargoes bind to either the KLC or the KHC of kinesin-1 proteins. This interaction is mediated by an adaptor protein. For example, mitochondria and syntaxin-1-containing vesicles are attached to the KHC cargo-binding domain by the adaptor protein, syntabulin, for their transport to synapses [9,10]. JIP-3, a c-Jun N-terminal kinase signalling pathway protein, binds to a six-tetratricopeptide motif in KLCs to transport the cargo, APP (amyloid precursor protein) [11]. Defects in these transport mechanisms may contribute to the pathology of neurodegenerative diseases such as Alzheimer's disease, amyotrophic lateral sclerosis and hereditary spastic paraplegia (for a review, see [12]).

In the present study, we provide supporting evidence suggesting that GRIF-1 is another example of an adaptor protein involved in motor-dependent trafficking of proteins.

Key words: adaptor protein, confocal microscopy, γ-aminobutyric $acid_A$ ($GABA_A$), γ-aminobutyric $acid_A$ receptor interacting factor-1 (GRIF-1), kinesin, non-motor domain, trafficking.

Abbreviations used: ECFP, enhanced cyan fluorescent protein; EYFP, enhanced yellow fluorescent protein; FRET, fluorescence resonance energy transfer; $GABA_A$, γ-aminobutyric $acid_A$; GRIF-1, $GABA_A$ receptor interacting factor-1; HEK-293 cells, human embryonic kidney 293 cells; KHC, kinesin heavy chain; KLC, kinesin light chain; MD, motor domain; NMD, non-motor domain; OGT, β-O-linked *N*-acetylglucosamine transferase; OIP98, OGT interacting protein 98.

[1]To whom correspondence should be addressed (email anne.stephenson@ulsop.ac.uk).

Figure 1 | Confocal microscopy imaging of ECFP GRIF-1, EYFP KIF5C, KIF5C-NMD EYFP and EYFP KIF5C-MD in COS-7 cells
(**A**) Single-protein expression; (**B**) GRIF-1/KIF5C pairwise combinations. Images are representative of at least $n = 20$ cells from $n = 3$ independent transfections for all combinations. Scale bars, 10 μm.

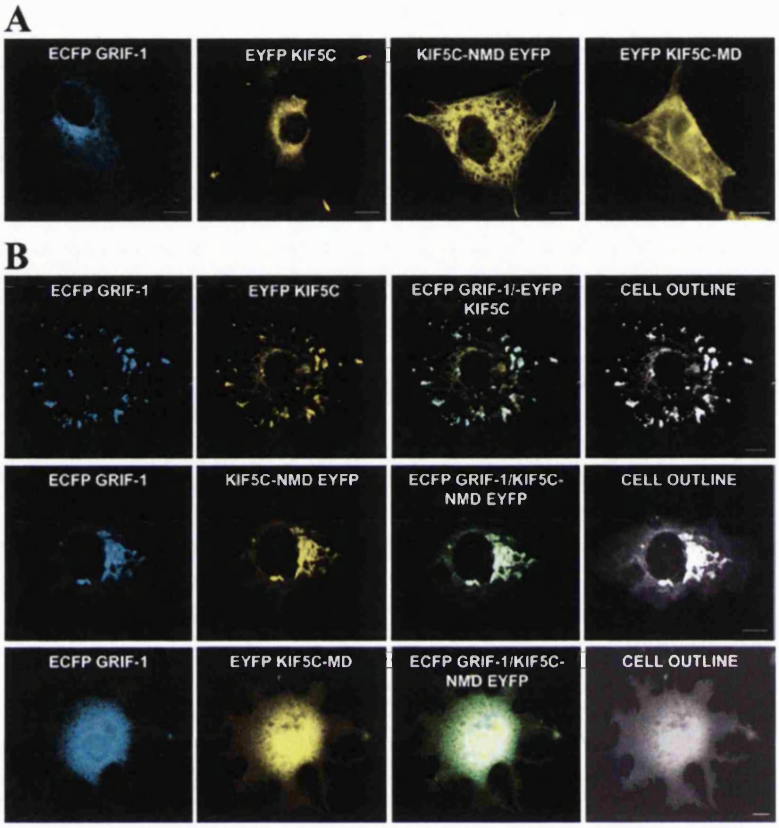

Confocal microscopy imaging of GRIF-1–kinesin-1 interactions

The following fluorescent constructs were generated by subcloning: ECFP (enhanced cyan fluorescent protein) GRIF-1; EYFP (enhanced yellow fluorescent protein) KIF5C-(1–957) (N- and C-terminally tagged); the EYFP KIF5C MD, KIF5C-(1–335) (referred to as EYFP KIF5C-MD); and the KIF5C-NMD EYFP, KIF5C-(336–957) (referred to as KIF5C-NMD EYFP). Each construct was expressed alone or in GRIF-1/KIF5C pairwise combinations in either HEK-293 (human embryonic kidney 293) cells or COS-7 cells, and the localization of the fluorescent proteins was imaged by confocal microscopy. Representative results are shown in Figure 1.

In COS-7 cells, ECFP GRIF-1 expressed alone was found to be localized in cytoplasmic perinuclear regions (Figure 1A), whereas EYFP KIF5C or KIF5C ECYP expressed alone in these cells was distributed throughout the cell cytoplasm (Figure 1A). When ECFP GRIF-1 and EYFP KIF5C constructs were co-expressed, the distribution of both proteins was distinct from that observed for single-protein transfections. ECFP GRIF-1 and EYFP KIF5C (or KIF5C EYFP) were found to co-localize, forming small clusters in the cell cytoplasm and also in cell processes (Figure 1B, top panels). KIF5C-NMD EYFP expressed alone was localized to filamentous, tubular structures in the cell cytoplasm (Figure 1A). In the presence of ECFP GRIF-1, however, the distribution pattern was changed such that it was recruited to EYFP GRIF-1-rich regions where co-localization of the two proteins was observed (Figure 1B, middle panels). EYFP KIF5C-MD expressed alone showed a diffuse distribution throughout the whole cell (Figure 1A). This distribution pattern was not changed by co-expression of EYFP KIF5C-MD with ECFP GRIF-1 (Figure 1B, bottom panels).

To test whether ECFP GRIF-1 associated directly with fluorescently tagged KIF5C, FRET (fluorescence resonance energy transfer) studies were carried out in transfected HEK-293 cells. FRET efficiencies were measured by acceptor photobleaching using appropriate ECFP and EYFP positive and negative controls [13,14]. A significant FRET efficiency (~10%) was measured only for the ECFP GRIF-1/C-terminal-tagged KIF5C EYFP and ECFP GRIF-1/KIF5C-NMD EYFP combinations.

Figure 2 | Schematic diagram showing the proposed function of GRIF-1 as an adaptor protein linking kinesin-1 to its cargo
GRIF-1 dimers attach a $GABA_A$ receptor-containing vesicle to kinesin. GRIF-1 is also attached to OGT trimers that have also been shown to be part of the transport complex [3,4].

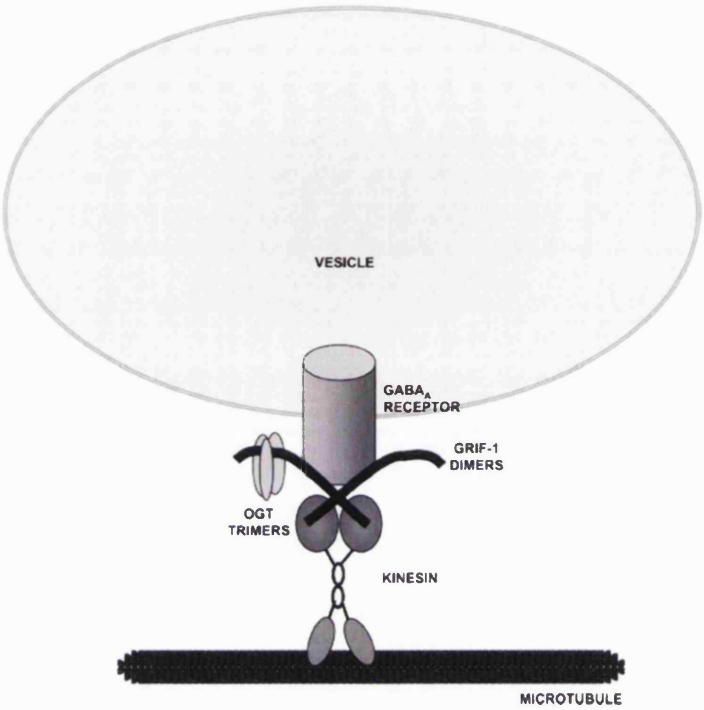

Concluding remarks

Functional fluorescent GRIF-1 and KIF5C chimaeras were generated and used in immunofluorescence imaging studies to show that GRIF-1 associated directly with KIF5C and, more specifically, the KIF5C-NMD. This is in agreement with [15], in which the GRIF-1-binding site was mapped to the KIF5C cargo-binding site by yeast two-hybrid interaction assays and co-immunoprecipitation experiments. These findings substantiate a role for GRIF-1 as an adaptor protein linking kinesin-1 to its cargo in anterograde trafficking mechanisms in neurons (Figure 2).

This work was funded by the Biotechnology and Biological Sciences Research Council (U.K.). We thank Professor T. Nagase (The Kazusa DNA Research Institute, Chiba, Japan) for the gift of pBlueScriptSII(+)KIF5C, Dr J.G. McNally and Dr L. He (NCI, National Institutes of Health, Bethesda, MD, U.S.A.) for the gift of pECFP-EYFP and Ana Marisa Salgueiro for the generation of pECFP-GRIF-1 and pEYFP-KIF5C.

References

1 Beck, M., Brickley, K., Wilkinson, H.L., Sharma, S., Smith, M., Chazot, P.L., Pollard, S. and Stephenson, F.A. (2002) J. Biol. Chem. **277**, 30079–30090
2 Stowers, R.S., Megeath, L.J., Gorska-Andrzejak, J., Meinertzhagen, I.A. and Schwarz, T.L. (2002) Neuron **36**, 1063–1077
3 Iyer, S.P.N., Akimoto, Y. and Hart, G.W. (2003) J. Biol. Chem. **278**, 5399–5409
4 Pozo, K., Brickley, K., Beck, M. and Stephenson, F.A. (2004) FENS Abstr. **2**, A080.4
5 Brickley, K., Smith, M.J., Beck, M. and Stephenson, F.A. (2005) J. Biol. Chem. **280**, 14723–14732
6 Wells, L., Vosseler, K. and Hart, G.W. (2001) Science **291**, 2376–2378
7 Cole, R.N. and Hart, G.W. (2001) J. Neurochem. **79**, 1080–1089
8 Hirokawa, N. and Takemura, R. (2005) Nat. Rev. Neurosci. **6**, 201–214
9 Su, Q., Cai, Q., Gerwin, C., Smith, C.L. and Sheng, Z.H. (2004) Nat. Cell Biol. **6**, 941–953
10 Cai, Q., Gerwin, C. and Sheng, Z.H. (2005) J. Cell Biol. **170**, 959–969
11 Kamal, A., Stokin, G.B., Yang, Z., Xia, C.H. and Goldstein, L.S. (2000) Neuron **28**, 449–459
12 Goldstein, L.S.B. (2003) Neuron **40**, 415–425
13 Nashmi, R., Dickinson, M.E., McKinney, S., Jareb, M., Labarca, C., Fraser, S.E. and Lester, H. (2003) J. Neurosci. **23**, 11554–11567
14 Liu, J., Ernst, S.A., Gladycheva, S.E., Lee, F.Y.Y., Lentz, S.I., Ho, C.S., Li, Q. and Stuenkel, E.L. (2004) J. Biol. Chem. **279**, 55924–55936
15 Smith, M.J., Brickley, K. and Stephenson, F.A. (2005) Br. Neurosci. Assoc. Abstr. **18**, P9.05

Received 19 September 2005